Functional implications of Bone Morphogenetic Protein 10 (BMP10) expression in pathological hearts

Inauguraldissertation
zur Erlangung des Grades einesDoctors der Humanbiologie
Des Fachbereichs Medizin
Der Justus-Liebig-Universität Gieβen

vorgelegt von Izabela Piotrowska
aus Poznań, Polen

Gieβen 2006

Aus dem Max-Planck-Institute für Hertz und Lungen Forschung
In Bad Nauheim
Direktor: Prof. Dr. Thomas Braun

Gutachter: Prof. Dr. T. Braun

Gutachter: Prof. Dr. G. Euler

Tag der Disputation**: 2 July 2007**

1. Introduction

1.1. Bone Morphogenetic Proteins as members of Transforming Growth Factor β Superfamily

Transforming growth factor β (TGFβ) and related molecules are members of the polypeptide growth factor superfamily. Based on sequence homology over 50 evolutionary conserved members were identified and grouped into the following subfamilies: TGFβs, activins and inhibins, bone morphogenetic proteins (BMPs) and growth/differentiation factors (GDFs) (reviewed by Mehra et al., 2002). In addition proteins with a lower degree of similarity such as Műllerian inhibitory substance (MIS) and glial cell line-derived neurotropic factor (GDNF) have been considered as members of the TGFβ family (Kingsley et al., 1994). Originally in the 1960s, only the activity of BMPs to induce bone formation, as their name suggests, was identified (Urist, 1965). More than two decades later this activity has been assigned to specific factors, when bovine osteogenin (BMP3) (Luyten et al., 1989), and human BMP2 and 4 (Wozney et al., 1988) were sequenced and purified. Later on, a number of GDFs has been also recognized as bone morphogenetic proteins, raising the number of BMPs to around 20 (Yamashita et al., 1996). The BMPs/GDFs have been further grouped into six subsets based on amino acid sequence homology (Miyazono et al., 2005), as follows:

1. BMP2 and BMP4 (BMP2b).
2. BMP3 (Osteogenin) and BMP3b (GDF10).
3. BMP5, BMP6 (Vg-1 related, Vgr-1), BMP7 (osteogenic protein-1, Op-1) and BMP8 (Op-2).
4. BMP9 (GDF2) and BMP10.
5. BMP12 (GDF7 or cartilage-derived morphogenetic protein-3, CDMP3), BMP13 (GDF6 or CDMP2) and BMP14 (GDF5 or CDMP1).
6. BMP11 (GDF11) and GDF8 (Myostatin).

Since the TGFβ superfamily comprises so many protein families, it is obvious that sequence and percentage of homology among families, subsets and even between members of the same group varies significantly. However, there are common and consistent features that allow to classify them as TGFβ related proteins (i.e. synthesis as precursor, conserved tertiary structure etc.), as described below.

Members of the TGFβ superfamily, including BMPs, are synthesized as pre-pro-protein precursors (of approximately 400-525 amino acids in case of BMPs), containing leader secretion sequence, pro-region and carboxy-terminal mature region (Gentry et al., 1988). The pro-region facilitates proper dimerization of pro-proteins, and dimers are subsequently cleaved by endoproteases at conserved RXXR amino acid sequence (Mehra et al., 2002). Furin-like proteases are generally believed to convert the precursors into biologically active, mature forms (Matthews et al., 1994) prior to secretion. Mature peptides form a cystein knot which contains most ofen six cystein residues (Reddi, 1998), however, there may be additional one to three cysteines included in the sequence (Neuhaus et al., 1999). As for TGFβ1, the cleaved, disulfide-linked pro-region has been shown to remain non-covalently associated with the mature peptide to form a “latent complex” (Lawrence, 1996) followed by secretion and further processing. The ability of other BMPs to create such a complex has not yet been shown.

A cystein knot, common for all mature TGFβ ligands, including BMPs, was also found in a number of other growth factors, as for example platelet-derived growth factor (PDGF) and glycol-protein hormone. These factors share no other sequence homology/similarity to TGFβ, but they are together defined by some authors as members of cystein-knot growth factor superfamily (Sun et al., 1995).

1.2. BMPs receptors

The physiological effect of BMPs is achieved by binding of the secreted form to specific receptors. There are three known types of TGFβ receptors, type I, type II and type III, named according to the their mobility on SDS-PAGE gels (Cheifetz et al., 1986). Type I of molecular mass of approximately 55 kDa, and a 70-85 kDa type II are transmembrane serine/threonine (Ser-Thr) receptor kinases, while 200-400 kDa type III receptors contain two distinct members, a proteoglycan (betaglycan) and a glycoprotein (endoglin) (Massague et al., 1994, Cheifetz et al., 1988). It is believed, that BMPs signal only through type I and II receptors (Liu et al., 1995). Type I receptors were firstly identified as activin receptor-like kinases 1-4 or ALK1-ALK4 (ten Dijke et al., 1993). At the same time, other groups cloned these and others type I receptors and named them according to their specificity of ligand binding. Because of this reason each receptor has at minimum of 2 names. ALK-2 is also known as ActR I or Acvr1 (activin receptor type

I), ALK-3 and ALK-6 as BMPR IA and IB (BMP receptor IA and IB), respectively, ALK-4 – ActR IB (activin receptor type IB) and finally ALK-5, based on its specificity to TGFβ, is also called TGFβ RI (reviewed by Mehra and Wrana, 2002). Four members of type II receptors have been identified and three of them preferentially bind activins (ActR II and ActR IIB) and TGFβ1 (TβR II) (Lin et al., 1992), while BMPs have a higher affinity to BMPRII, although they were shown to interact with ActR IIA as well (Mathews et al., 1991, Mathews et al., 1992). Known TGFβ/Activin/BMP receptors, are summarized in table 1. Receptors, which have been identified to bind BMP10, will be described separately in the chapter 1.4.

Type I Receptors	**Type II Receptors**			
	TGFβR II	**BMPR II**	**ActR II**	**ActR IIB**
ALK-1	🟦 **TGFβ-1**	🔴 **TGFβ-1** 🔴 **Act A** 🔴 **BMP7**	🟢 **Act A**	🟢 **Act A**
ALK-2	🟢 **TGFβ-1**	🔴 **TGFβ-1** 🔴 **Act A** 🔵 **BMP2** 🔵 **BMP7** 🔵 **BMP6**	🔵 **Act A** 🔵 **BMP7** 🔴 **GDF5** 🔴 **GDF6** 🔵 **BMP6**	🔵 **Act A** 🟦 **BMP7** 🟥 **GDF5** 🔴 **GDF6**
ALK-3	🟢 **TGFβ-1**	🔴 **TGFβ-1** 🔴 **Act A** 🟢 **BMP2** 🟢 **BMP7** 🔴 **GDF5** 🔵 **GDF6**	🔴 **Act A**	🔵 **BMP2** 🟦 **BMP7** 🟢 **GDF5**
ALK-4	🟢 **TGFβ-1**	🔴 **TGFβ-1** 🔴 **Act A** 🔴 **BMP7**	🔴 **BMP7** 🔵 **Act A** 🟦 **GDF5**	🔵 **Act A**
ALK-5	🔵 **TGFβ-1**	🔴 **TGFβ-1** 🔴 **Act A** 🔴 **BMP7**	🟢 **Act A**	
ALK-6	🟢 **TGFβ-1**	🔴 **TGFβ-1** 🔴 **Act A** 🔵 **BMP2** 🔵 **BMP4** 🔵 **BMP7** 🔵 **GDF5** 🔵 **GDF6** 🔵 **BMP6**	🟢 **Act A** 🔵 **BMP7** 🔵 **GDF5**	🟦 **BMP2** 🔵 **BMP7**

KEY
🔵 **binding/signal transduction**
🔴 **no binding**
🟢 **binding/no signal transduction**
🟦 **binding/signal transduction uncertain**
🟥 **binding uncertain/no signal transduction**

Tab. 1. TGFβ/BMP receptors and their putative ligands (modified from Cytokine Mini-reviews, R&D Systems', 2004)

The serine/threonine kinase domain of type II receptors is constitutively active, and upon a ligand binding, phosphorylate glycine-serine domain (GS domain) of type I receptor, which results in induction of their kinase activity (Miyazono et al., 2005) and initiates downstream Smad-dependent or -independent signaling. Hence, specificity of induction is mainly achieved by type I receptor. BMPs bind to ALK-2, ALK-3 and ALK-6 type I receptors (ten Dijke et al., 1994, Chen et al., 1998, Macias-Silva et al., 1998), although an interaction with ALK-1 cannot be excluded (Mazerbourg et al., 2005). Some BMPs were also shown to bind to type II and I receptors in a cooperative, rather than in a stepwise manner (Knaus et al., 2001, Gilboa et al., 2000, Mehra et al., 2002). It was also suggested that receptors of both types can constitutively form homodimers or can even heterotetramized, because the autophosphorylated type II naturally recruits type I receptor (Derynck et al., 1997, Cho et al., 1998). The precise mechanism of ligand-dependent receptor recruitment and action remains unknown. It is known that type I receptors are negatively regulated by various receptor-associated molecules, like FK506-binding protein 12 (FKBP12) (Wang et al., 1996), BMP and activin membrane bound inhibitor (BAMBI), and BMP receptor associated molecule 1 (BRAM1). For instance, FKBP12 binds to type I receptor and possibly prevents its premature activation (reviewed by Massague et al., 2000).

In the signaling cascade, upon ligand binding, receptors are internalized and can be either recycled to the membrane or can be downregulated through endocytosis. Internalization of receptors is implicated as a mechanism of limitation or additional negative regulation of TGFβ/BMPs signaling (Mellman et al., 1996).

1.3. Smad-dependent and Smad-independent signaling pathways

As mentioned before, both type I and II receptors are necessary for BMPs signal transduction. After ligand binding they form a heterotetrameric-activated receptor complex, that transmits BMP signal through either Smad-dependent or Smad-independent pathways. In addition to the canonical Smad-mediated pathway, BMPs activate also a number of mitogen activated protein kinases (MAPKs), like extra-cellular signal-regulated kinases (ERKs), p38 MAP kinase (Iwasaki et al., 1999) or protein kinase C-dependent pathway (Hay et al., 2001). It was shown, that the mode of receptor oligomerization/recruitment prior to the ligand binding mainly determines downstream signal transduction pathway (Hassel et al., 2003). A schematic representation of BMPs induced Smad-dependent signaling is shown in Fig. 1.1.

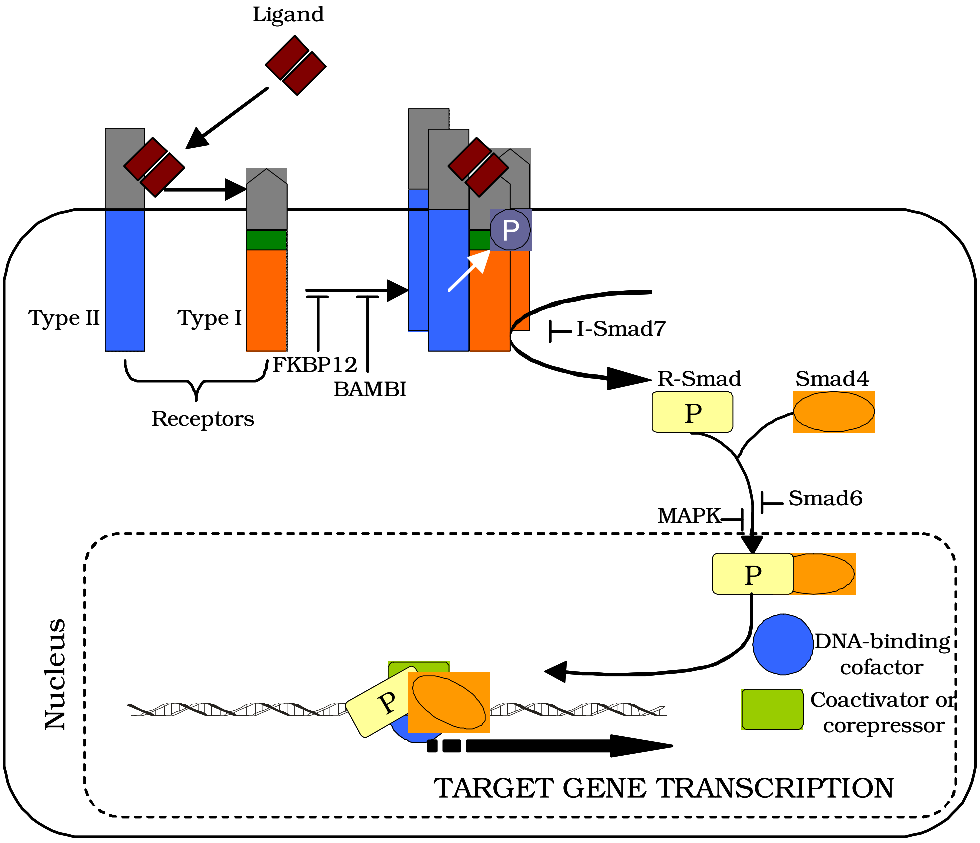

Fig. 1.1. Schematic representation of the TGFβ/BMP induced Smad signaling pathway (modified from Massague et al., 2000).

Smads are considered, however, as the major transducers for the serine/threonine kinase receptors. Eight Smad proteins have been identified so far in mammals and have been grouped into three classes, based on their function (Goumans et al., 2000):

1. Receptor-regulated Smads (R-Smads). They can be further subdivided in 2 groups: activated by TGFβ and activins (Smad2 and Smad3 – AR-Smads). The second group is activated by BMP receptors (Smad1,-5,-8 – BR-Smads) (Miyazono et al., 2005). Interaction of the R-Smads with a defined type I receptor determines the specificity of the TGFβ family members (ten Dijke et al., 2000). Unique c-terminal phosphorylation site is typical only for members of R-Smads.
2. Common-partner Smads (co-Smads). This subgroup is represented only by Smad4 in mammals, but others might also exist, as two Smad4 homologues have

been found in *Xenopus laevis*. Smad4 is utilized in both BMP and TGFβ/activin signaling pathways (Masuyama et al., 1999).

3. Inhibitory Smads (I-Smads). Smad6 and Smad7 have been recognized as inhibitors of BMP and TGFβ/activin signaling and their expression is induced by mature ligand binding (Christian et al., 1999). The inhibitory effect can be achieved by stable interaction with the activated type I receptor, thus preventing phosphorylation of R-Smads, or by competition for binding of co-Smad, thereby preventing the formation of R/co-Smads complex. The first mechanism applies to both I-Smads, while the later is unique for Smad6 and its inhibition of Smad1/Smad4 interaction (Hata et al., 1998).

Upon ligand binding and activation by type II receptor, type I receptors phosphorylate R-Smads at their C-terminal SSXS sequence and oligomerize with a co-Smad (Heldin et al., 1997). This complex is translocated into the nucleus, where it regulates transcription of target genes by direct binding to specific DNA sequences, interacting with other DNA-binding proteins, and recruiting transcriptional co-activators or co-repressors (Fig. 1.1) (Miyazono et al., 2000).

1.4. Role of BMP signaling in heart development and angiogenesis

At least six BMPs have been found to be expressed in the heart, i.e. BMP2, BMP4, BMP5, BMP6, BMP7 and BMP10, with distinct but partially overlapping distribution (reviewed by Schneider et al., 2003).

Among the BMPs, the BMP2 expression patterns and function were the most intensively studied. BMP2 is widely expressed during mouse embryonic development as well as in the adult heart has dynamic expression pattern (Lyons et al., 1989, 1990). BMP2 was noted in cardiac crescent at E7.5 (Ma et al., 2005), and at E8.5 BMP2 transcripts are detectable by in situ hybridization in the promyocardium and surrounding mesodermal cells, while the protein is localized in the atrioventricular (AV) myocardium and the dorsal wall of future atria as well (Sugi et al., 2004). One day later at E9.5, transcripts of BMP2 were observed in the region, where protein was found one day before (i.e. AV myocardium) and at a lower levels in the outflow tract. At E10.5 BMP2 protein was diminished in myocardial cells, but was detectable in cushion AV mesenchyme and epicardium. This pattern of protein localization was preserved during later stages of development- E13.5- E16.5, i.e. during valvulogenesis. By in situ hybridization, BMP2 expression in the AV canal was extinguished at E10.5 (Sugi et al., 2004). On the other hand BMP2 transcripts were found in and ventricular myocardium by another group (Ma et al., 2005). In adult mouse heart, protein expression persisted in cardiac valve tissue (Sugi et al., 2004).

BMP2 is implicated in multiple developmental and physiological processes. A homozygous null mutation of BMP2 causes, in addition to the amnion/chorion defects, abnormal development of the heart in the exocoelomic cavity, but the specification of the cardiac mesoderm occurs normally (Zhang et al., 1996). Conditional inactivation of BMP2 in the myocardium led to cardiac jelly loss and at later developmental stages resulted in failure in endocardial endothelial-mesenchymal transition (EMT) (Ma et al., 2005). *In vitro* studies proved that BMP2 is required for myocardial segmental regulation of AV endocardial cushion mesenchymal cells formation (Sugi et al., 2004). Moreover BMP2 can direct regionalized myocardial patterning (Ma et al., 2005). In addition to cardiac development, BMP2 has been reported to exert both pro- and anti-apoptotic effects, depending on cell type and circumstances (Yokouchi et al., 1996; Iwasaki et al., 1999; Bhatia et al., 1999). In neonatal cardiomyocytes in culture the inhibition of apoptosis by BMP2 was shown to occur through activation of Smad-1 and induction of anti-apoptotic gene Bclx expression (Izumi et al., 2001). Elevated levels of BMP2 expression in tumors, suggesting the possible role of this cytokine in promotion of tumor angiogenesis were recently reported. The authors found that BMP2 had no significant effect on proliferation, but promoted tube formation of human dermal microvascular endothelial cells *in vitro* (Raida et al., 2005).

BMP4 is the most widely expressed BMP gene throughout mouse developmental stages and in adult tissues. During embryonic heart development BMP4 was found in the outflow tract at E8.5. In addition, BMP4 transcripts were found in muscular layer of the OFT and its derivatives (aorta and pulmonary trunk) and this expression is maintained until birth (Jiao et al., 2003). In the inflow region, BMP4 was first noticed in the sinus venosus at E8.5. At E9.0 expression was detected in the dorsal midline of common atrium and in the AV cushion, regions where the atrial septum primum is initiated (Jiao et al., 2003). Another report proved additionally the expression of BMP4 in parietal pericardium (Stottmann et al., 2004). In adult heart, in addition to expression in muscle layers of aorta and pulmonary trunk, BMP4 was found in valves and the annulus of mitral and tricuspid valves (Jiao et al., 2003).

Conditional inactivation of BMP4 in mouse hearts leads to atrioventricular canal defects (AVCD), and a single AV junction with a common valve. In the outflow region of developing heart, BMP4 deficient embryos display a double-outlet right ventricle. Initiation of cushion formation and endothelial-mesenchymal transition was not affected, probably due to compensatory effects of other BMPs. However, after the cushion was formed BMP4 was required for the proper septation of the AVC (Jiao et al., 2003). Using the micro-bead delivery technique, BMP4 was shown to significantly induce programmed cell death in surrounding embryonic tissue explants *in vitro*. The highest induction of apoptosis by BMP4 was observed in the conotruncal cushion, while in myocardial and AV cushion explants the number of apoptotic cells was approximately two fold lower (Zhao et al., 2000).

BMP5, BMP6 and BMP7 belong to the same subgroup of BMPs, with an almost 90% homology within the mature, active region (Solloway et al., 1999). BMP5 and BMP7 are strongly expressed in developing myocardium, whereas BMP6 is expressed in both the OFT myocardium and atrioventricular cushion (Dudley et al., 1997). Surprisingly, mice lacking BMP5 (Kingsley et al., 1992), BMP6 (Solloway et al., 1998), or BMP7 (Dudley et al., 1995) do not exhibit cardiac abnormalities. Double mutations, i.e. BMP5/BMP7 (Solloway et al., 1999) or BMP6/BMP7 (Kim et al., 2001) resulted in severe heart development retardation indicating that these closely related factors are interchangeable. In double BMP5/BMP7 knock-outs (Solloway et al., 1999) the general morphology of the heart was disorganized with reduced cell density and trabeculation. The authors explained the lack of endocardial cushion formation as a secondary effect of overall growth/development retardation.

BMP6 and BMP7 share 87% amino acid identity in the C-terminal mature domain (Kim et al., 2001). BMP6 expression in the heart was restricted to the AV cushion and OFT at E9.5 with its decrease on the right side of the OFT at E10.5 and was absent by E11.5. At later developmental stages BMP6 transcripts were also found in endothelium lining dorsal aorta and pulmonary trunk and valve leaflets. Asymmetric expression of BMP7 in myocardium of developing heart was also noted, with its down-regulation in the left atrium and ventricles. Deletion of both BMP6 and BMP7 caused mouse embryonic lethality between E10.5- E12.5, a period when significant overlap in the BMP6 and BMP7 expression occur (Kim et al., 2001). Double BMP6/BMP7 knock-outs had underdeveloped endocardial cushions of , reduced ventricular trabeculation and displaced venous valves within the heart. Additionally, both atrial chambers and cardiac veins were dilated. However this edema might be secondary to heart failure and valvular malformation (Kim et al., 2001).

Since BMPs act through receptors, their localization and mutational analysis can provide valuable functional information. Activin receptor like kinase 1 (ALK-1) is able to bind TGFβ1 or activins in the presence of either TβR II or activin type II receptors, respectively. However preliminary data showed that it does not induce transcriptional activity (Kretzschmar et al., 1998, Bassing et al., 1994). Thus ALK-1 was considered as an orphan receptor. Expression of this receptor in arterial endothelium during embryogenesis (Roelen et al., 1997) and in adult tissues (Panchenko et al., 1996) suggested its potential role in the regulation of angiogenesis. Mice lacking ALK-1 exhibit dilation of major vessels and fusion of capillaries (Oh et al., 2000). Similar phenotypes were observed in TGFβ1 (Dickson et al., 1995), TβR II (Oshima et al., 1996), endoglin (Li et al., 1999) and Smad5 (Sankar et al., 1996) deficient mice. It is generally believed, that BMPs activate Smad 1/5/8 whereas TGFβs induce Smad 2/3 pathway. Although ALK-1 has been identified to bind TGFβ1, the signal is most probably mediated through a BMPs Smad1/5 dependent pathway (Oh et al., 2000). Additionally, ALK-1 signaling was shown to be required for differentiation and proper localization of vascular smooth muscle cells to the perivascular region during embryogenesis (Oh et al., 2000). The most extensively studied cytokine in angiogenesis was TGFβ1 and its receptors, i.e. ALK-1 and ALK-5 (reviewed by Goumans et al., 2003). It is proposed that two TGFβ signaling pathways (via ALK-1 and ALK-5) may play a balancing role in vascular development (Seki et al., 2006). As already mentioned, ALK-1 is expressed in the endothelial layer of arteries, while ALK-5 transcripts were found in vascular smooth muscle cells in medial and adventitial layers of blood vessels, but they were undetectable in the intimal layer in embryos. Some groups however, found ALK-5 expression in endothelial cell lines (reviewed by Goumans et al., 2003). ALK-5 was shown to exert its function via the Smad2/3, but not the Smad1/5/8 pathway (Lebrin et al., 2005). Moreover ALK-5 knock-outs exhibit defects in the formation of the smooth muscle layer, but no dilation of blood vessels, as in case of ALK-1, was observed. During embryonic heart development, ALK-5 was found to be expressed by trabecular muscle cells (Seki et al., 2006). Based on these data, the authors proposed that TGFβ signaling is involved in vascular morphogenesis utilizing two distinct type I receptors: ALK-1 in endothelial cells and ALK-5 in vascular smooth muscle cells. As shown by the example of TGFβ1, one ligand might exhibit different functions depending on the binding to particular receptors in various cell types.

Activin receptor like kinase 2 (ALK-2) has been shown to play a role in rightward looping of the primary heart tube in *Xenopus leavis* (Ramsdell et al., 1999). During mouse embryogenesis ALK-2 was found to be expressed at low levels in the myocardium, whereas an abundant expression was detected in endocardial cells and the underlying mesenchyma of AV canal (Wang et al., 2005). Interestingly, mice with a deficiency of ALK-2 in cardiomyocytes did not develop an obvious cardiac phenotype while severe septal and valvular defects were observed, when ALK-2 was ablated in endothelial cells, as a result of disturbed endothelial to mesenchyme transdifferentiation (Wang et al., 2005).

It has been already mentioned, that BMPs act mainly through ALK-3 and ALK-6 of type I receptor. ALK-3 is ubiquitously expressed throughout development, whereas ALK-6 is absent in the developing heart from midgestation (Dewulf et al., 1995). Cardiac specific ALK3 deletion results in many heart defects (Gaussin et al., 2002). Ablation of ALK-3 leads to increased apoptosis rate of cardiomyocytes, thus the ALK-3 mediated pathway is required for myocyte survival. Additionally, ALK-3 expression in myocytes is necessary at mid-gestation for proper intraventricular septation, development of normal trabeculae, compact myocardium and endocardial cushion. Interestingly, in mutant embryos, BMP10 expression in trabeculae was unchanged, but precocious expression in atria was found (Gaussin et al., 2002). When ALK-3 expression was abolished in the subset of cardiac myocytes of AVC, anomalies in mitral septal leaflets and tricuspid mural leaflets were found in adult animals. Downward displacement and disruption of the annulus fibrosus resulted in direct myocytic connection between atrium and ventricle that led to ventricular preexcitation (Gaussin et al., 2005). Surprising results were obtained when ALK-3 expression was ablated in neural crest cells (Stottmann et al., 2004). Most aspects of neural crest development occurred normally, but the mutant embryos died at midgestation due to acute heart failure. Mutants display a shortened with defective septation, lack of endocardial cushion and reduced rate of ventricular myocardial proliferation leading to little expansion of trabeculae and thinned compact myocardium. Ablation of ALK-3 in Isl1 expressing cells (believed to be undifferentiated cardiac progenitors) leads to aberrant morphology of and right ventricle at E9.5. At E11.5 a thinner ventricular wall and reduced trabeculation was observed. At E13.5 severe defects in formation with persistent truncus arteriosus and underdeveloped valves were noted. Thinner ventricular wall and septation defects appeared due to disturbed proliferation and apoptosis, respectively (Yang et al., 2006).

Developmental events are also sensitive not only to complete absence but also to reduced BMP signaling (Délot et al., 2003). Mice lacking half of the ligand-binding domain in the BMP type II receptor die at midgestation as a result of severe cardiovascular defects. Mutants exhibit a very restricted phenotype, limited specifically to the outflow tract (OFT). The main defects of BMP signaling limitation are absence of septation in the developing heart with interruption of the aortic arch as well as lack of the semilunar valve, which prevents the backflow from aorta and pulmonary trunk into the ventricles (Délot et al., 2003).

1.5. BMP10 as a heart specific member of the TGFβ superfamily

BMP10 starts to be expressed during mouse embryogenesis exclusively in heart at E9.0. Its transcripts were found to be restricted to the trabeculated part of common ventricles and bulbus cordis, but to be absent in endocardial cells (Neuhaus et al., 1999). During later stages (E14.5), the signal also appears in the trabeculated inner atrial wall. The sequence of BMP10 displays all characteristic features of a bone morphogenetic protein family member, such as RRIR cleavage site, that divides 421 amino acid precursors into a pro-region with a hydrophobic leader sequence and the mature ligand with conserved cysteine residues. On the basis of sequence homology, BMP10 together with BMP9 and chicken *dorsalin*, constitute a new BMP subgroup (Neuhaus et al., 1999). The closest relative to BMP10 is BMP9, which is not expressed in the heart. In adult tissues, northern blot analysis revealed that BMP10 transcripts are restricted to the right atrium of the healthy human heart (Neuhaus et al., 1999), and such kind of expression pattern was further confirmed in the mouse by another group (Chen et al., 2004). Recently, studies concerning BMP10 ablation in the mouse have been published as well. Absence of BMP10 caused embryonic lethality, between E9.5 and E10.5. BMP10 deficient mice exhibit severe cardiac abnormalities with a profound hypoplastic ventricular wall, absence of ventricular trabeculation and halted at acellular stage the development of endocardial cushions in both and the atrioventricular canal (AVC) (Chen et al., 2004). The authors found that lack of trabeculated myocardial layers in mutants was caused by a defect in myocyte proliferation and ectopic expression of negative cell-cycle regulator p57^{kip2}. Moreover, BMP10 expression was found to be upregulated in FKBP12- deficient mouse, which exhibit hypertrabeculation (Shou et al., 1998). High ectopic levels of BMP10 expression were also found in adult hearts of ventricular cardiomyocyte restricted knock-out of Nkx2.5 (Pashmforoush et al., 2004). Hearts of Nkx2.5 deficient mice are hypertrabeculated due to persistent myocyte mitosis leading to complete heart block. Additionally, ventricular myocardium shows noncompaction and a disorganized conduction system with progressive fibrosis. Proliferative function of BMP10 was further confirmed by generation of transgenic mouse strains overexpressing the gene under the ANF promoter, which led to a similar phenotype of myocardial hypertrabeculation and noncompaction (Pashmforoush et al., 2004).

Receptor binding studies revealed that BMP10 can interact with type I receptors ALK-3 and ALK-6 and both type II receptors (BMPR II and ActR IIA) and activates Smad1/5/8 pathway. However the design of this study and results are questionable and more work is needed to clarify the details of BMP10 signal transduction (Mazerbourg et al., 2005).

1.6. Aim of the project

The general purpose of the present work was to investigate the role of BMP10 in the adult heart. A thorough knowledge of the expression and localization studies of BMP10 is a prerequisite for any further work. As BMP10 undergoes secretion from the cells where it is expressed, it was necessary to generate an antibody specific to the processed, mature secreted form of the protein to investigate the localization of BMP10. I was also interested to study the qualitative and quantitative changes of BMP10 expression in genetic and drug induced models of dilated and hypertrophic cardiomyopathy. Additionally, in the work presented here I attempt to unveil the function of BMP10. Overexpression of active BMP10 in mammalian cells allowed to study the effects of this protein on cells of various origins *in vitro*.

2. Experimental procedures

2.1. Materials

2.1.1. Basic materials

MATERIALS	COMPANY
Biodyne® Nylon Membrane	Pall (Dreieich, Germany)
Bio-Traces® Nitrocelulose	Pall (Dreieich, Germany)
Blotting Paper 3MM	Whatman International (Maidstone, England)
Chamber slide w/cover permanox slide	Nunc (Roskilde, Denmark)
Cell culture plates	Nunc (Roskilde, Denmark)
Filters	Schleicher & Schüll (Hannover, Germany)
Filters Minisart NML (0.2 und 0.45 µm)	Sartorius (Göttingen, Germany)
Glass slides and cover slides	Roth (Karlsruhe, Germany)
Glassware	Schütt (Göttingen, Germany)
Mini osmotic-pump 2002	Alzet (USA)
NAP-5™ columns (Sephadex® G-25)	Pharmacia Biotech (Sweden)
Nitrocellulose membrane	Invitrogen (Karlsruhe)
Plastic ware	Nunc (Wiesbaden, Germany)
Pro-Bond Ni-chelating Resins	Invitrogen (Karlsruhe, Germany)
Round cover slides	Roth (Karlsruhe, Germany)
X-ray developer	Kodak (Frankfurt/Main, Germany)
X-ray Film	Kodak (Frankfurt/Main, Germany)
Ni-NTA agarose	Qiagen

2.1.2. Chemicals

Basic chemicals were purchased from the following companies: Boehringer Mannheim (Mannheim), Invitrogen (Karlsruhe, Germany), Merck (Darmstadt), Molecular Probes (Goettingen), New England Biolabs (Schwalbach), Pharmacia (Freiburg), Promega (Mannheim), Roth (Hamburg/Karlsruhe, Germany), Serva

Feinbiochemika (Heidelberg), Sigma-Aldrich (Deisenhofen), Stratagene (Heidelberg), Quiagen (Hilden).

2.1.3. Radiochemicals

Radioactive labelled nucleotides were purchased from Amerscham Buchler (Braunschweig) or PerkinElmer (Boston):

- [α-^{32}P] dCTP (6000 Ci/ml)

2.1.4. Reagents

Avertin® 2,2,2-Tribromoethyl Alkohol	Boehringer (Mannheim)
Agar plaque plus agarose	BD Clontech (USA)
BaculoGold TNM-FH insect medium	BD Clontech (USA)
BCIP(5-Bromo-4-chloro-3-indolylphosphat)	Boehringer (Mannheim)
BMP-2	Sigma-Aldrich(Deisenhofen)
Chloroquine	Sigma-Aldrich(Deisenhofen)
DAB (3,3'-diaminobenzidine)	Sigma-Aldrich(Deisenhofen)
DAPI (4',6-diamidino-2-phenylindole)	Invitrogen (Karlsruhe)
Dimethylsulfoxid	Sigma-Aldrich(Deisenhofen)
Dil-Ac-LDL	Cell Systems (Frankfurt)
Digoxigenin-UTP	Boehringer (Mannheim)
Dithyotreithol (DTT)	Promega (Mannheim)
Doxorubicine	Sigma-Aldrich(Deisenhofen)
Draq5™	(Alexis)
Dubelcco's Modified Eagle Medium (D-MEM) 1.000 mg0/ml D-glucose, L-glutamine and sodium pyruvate	Invitrogen (Karlsruhe)
Dubelcco's Modified Eagle Medium (D-MEM) 4.500 mg0/ml D-glucose, L-glutamine and sodium pyruvate	Invitrogen (Karlsruhe)
Eosin	Division Chroma
Fetal Bovine Serum	Invitrogen (Karlsruhe)

Geneticin G-418	Invitrogen (Karlsruhe)
Grace’s insect medium	Invitrogen (Karlsruhe)
Gradient acrylamide 4-12% gels	Invitrogen (Karlsruhe)
Gradient acrylamide 8-20% gels	Anamed
Heparin	Sigma-Aldrich(Deisenhofen)
Haemalaun sauer	Division Chroma
IPTG (Isopropyl-β-D-tiogalactopyranosidase)	Roth (Karlsruhe)
Isoflurane	Forene (Germany)
Isoproterenol	Sigma-Aldrich(Deisenhofen)
Levamisole	Sigma-Aldrich(Deisenhofen)
Matrigel	BD Clontech (USA)
NBT (4-Nitro-Blue-Tetrazoliumchlorid)	Boehringer (Mannheim)
Neutral red	Sigma-Aldrich(Deisenhofen)
NP-40	Roth (Karlsruhe)
NuPAGE 4-12% Bis-Tris Gel	Invitrogen (Karlsruhe)
Mowiol	Merck (Darmstadt)
Opti-MEM® with GlutaMAX™-I	Invitrogen (Karlsruhe)
PageRuler™ Prestained Protein Ladder	Fermentas (Lithuania)
Penicillin-Streptamycin-Glutamine	Invitrogen (Karlsruhe)
PFA (paraformaldehyde)	Merck (Darmstadt)
Phalloidin-TRITC conjugated	Sigma-Aldrich(Deisenhofen)
Phalloidin-FITC conjugated	Sigma-Aldrich(Deisenhofen)
Polyfreeze™ tissue freezing medium™	Polysciences Inc. (USA)
Prestained Protein Ladder 10-180 kDa	Fermentas
Probond™ Resin	Invitrogen (Karlsruhe)
Protease inhibitor coctail EDTA-free	Roche (Karlsruhe)
RNasin®	Invitrogen (Karlsruhe)
Serum free insect medium	Sigma-Aldrich(Deisenhofen)
Sheep serum	Sigma-Aldrich(Deisenhofen)
Triton X-100	Roche (Karlsruhe)
Trizol®	Invitrogen (Karlsruhe)
Trypan blue	Sigma-Aldrich(Deisenhofen)

• Trypsin 2,5%	Invitrogen (Karlsruhe)
• Tween-20	Roche (Karlsruhe)
• Vectabond^{TM}	Vector Laboratories
• X-Gal (5-bromo-4-chloro-3-indolyl β-D-galactopyranoside)	Roth (Karlsruhe)
• Yeast tRNA	Boehringer (Mannheim)

2.1.5. Enzymes

Restriction endonucleases were obtained from Jena Bioscience, New England Biolabs and Fermentas.

DNA Polymerase I Large Klenov	Promega
Expand High Fidelity Polymerase	Roche
RQ1 RNase Free DNase	Promega
RNA Polymerases (T7, T3, SP6)	Promega
SuperScript^{TM} II Reverse Transcriptase	Invitrogen
Taq DNA Polymerase	Eppendorf
T4 Polynucleotide Kinase	Promega
T4 DNA Ligase	Promega

2.1.6. Kits

BaculoGold transfection kit	BD Clontech
Baculovirus kit	BD Clontech
BrDu Immunohistochemistry system	Oncogene
Comassie Plus^{TM} Protein Assay Kit	Pierce
ECL developing system	Amersham, Pierce
FUGENE 6 transfection reagent	Roche
In situ cell death detection kit	Roche
JetQuick PCR purification kit	Genomed

JetQuick Gel extraction kit	Genomed
JetStar Maxi plasmid purification kit	Genomed
JetStar Mega plasmid/cosmid purification kit	Genomed
Micro-Fast Track 2.0™ mRNA isolation kit	Invitrogen
Ne-Per nuclear and cytoplasm extraction kit	Pierce
Rapid Ligation Kit	Fermentas
TOPO®TA Cloning Kit	Invitrogen
Femto WB detection system	Pierce

2.1.7. Oligonucleotides

All oligonucleotides were obtained from Roth, Invitrogen.

Primer	Sequence 5’→3’
T7	TAATACGACTCACTATAGGG
T3	ATTAACCCTCACTAAAGGGA
Sp6	ATTAGGTGACACTATAG
M13 Forward	GTAAAACGACGGCCAG
M13 Reverse	CAGGAAACAGCTATGAC
5`-mouse-HPRT	GCTGGTGAAAAGGACCTCT
3`-mouse-HPRT	CACAGGACTAGAACACCTGC
5’-mouse-GAPDH	GTGGCAAAGTGGAGATTGTTGCC
3’-mouse-GAPDH	GATGATGACCCGTTTGGCCC
5’-mouse-BMPRII	ATGACTTCCTCGCTGCATCGGCCA
3’-mouse-BMPRII	CAGCTAACACAGAAACTGATGCCAAAG
5’-pRSET-BMP10	CGGATCAGCTCGAGCGCCAAGGGGAACTAC
3’-pRSET-BMP10	GCCTCTGGTACCCTATCTACAGCCACACTC
5’-3’arm-BMP10-ApaI-ko	GGAGAGGAGAGGGGGCCCATGGC
3’-3’arm-BMP10-ApaI-ko	CAAGGCTGATTTCAGGGCCCAAGCTC
5’-5’ex2-BMP10-	CATACTGCAAGTCTGGTACCTCATAAGTATC

KpnI-ko	
3’-5’ex2-BMP10-KpnI-ko	GCCACACTCAGACGGTACCATCCCTTC
5’-PVL-BMP10-NotI	GCGGCCGCATGGGGTCTCTGGTTCTGC
3’-PVL-BMP10-XbaI	TCTAGACTATCTACAGCCACACTCAGACAC
5’-IRES-GFP-BMP10-PstI	CTCGCTGCAGGCCATGGGCTCTCTGGTCCTG
3’-IRES-GFP-BMP10-XmaI	GGGCCCGGGCTTTGTGGGCACACAGCAG
5’-5’arm-BMP10-ko	GGAAGGATCCATGGCCGCGGAGCTGAGC
3’-5’arm-BMP10-ko	CCAGACTTGCCGCGGGCTTCATAATATAGC
5’-mouse-BNP	GTTACAGGAGCAGCGCAACC
3’-mouse-BNP	AGGCCACTGGAGGAGCTGAT
5’-mouse-ANF	CTCCTTCTCCATCACCAAGG
5’-mouse-ANF	CTCTGGGCTCCAATCCTGTC
5’-mouse-pDGFRß	GGCAGGTCATACCATGAT
5’-mouse-pDGFRß	TCGAGGTGGTCTTGAGCT
5’-mouse-SM-actin	GAGAAGCCCAGCCAGTCG
3’-mouse-SM-actin	CTCTTGCTCTGGGCTTCA
5’mouse-calponin	GAAATACGACCATCAGCGGG
3’mouse-calponin	CCAGTTTGGGATCATAGAGG
5’ mouse-BMP10	GGA AAC TAC TGT AAG AGG ACC CC
3’ mouse-BMP10	CTA TCT ACA GCC ACA TTC GGA GAC
5’ mouse-PECAM	AGGGGACCAGCTGCACATTAGG
3’ mouse-PECAM	AGGCCGCTTCTCTTGACCACTT
5’mouse-POD1	GGCAAGCAGGTCCAGCGCAAC
3’mouse-POD1	CAAGCGGTTGGCGGTCACCAC
5’mouse-ALK1	CCTTGGGGAGCTTCAGAAGGGGC
3’mouse-ALK1	GGGCCACCAGGACCGGCAAG
5’mouse-ALK2	GCCGCCCGGGCCACCCGCCCGCGG
3’mouse-ALK2	CTGCTGGCCTTCACAGTGGTCCTCGTTCC
5’mouse-ALK3	GCTATACACTTACATCAGATTACTGGG

3’mouse-ALK3	CCATGGAAATGAGCACAACCAG
5’mouse-ALK5	CTGCTCCCGGGGGCGAAGGCATTACAG
3’mouse-ALK5	GGTGGTGCCCTCTGAAATGAAAGGGCG
5’mouse-ALK6	GGAGGATGGAGAGAGTACAGCCCC
3’mouse-ALK6	CAGCCCAATGCTGTACCGAGGTCG
5’mouse-ALK7	GGTAAGCCTGCTATTGCTCACCGA
3’mouse-ALK7	GCCACTGGTTTGGGAGATTTGGTC
5’mouse-Mef2C	GCGTGCTGTGCGACTGTGAGATTGC
3’mouse-Mef2C	CCGCCCATCAGACCGCCTGTGTTACC
5’mouse-p57	AGTCTGTGCCCGCCTTCTAC
3’mouse-p57	CTCAGTTCCCAGCTCATCACCC
5’mouse-CHISEL	GGGAGCCTTTCGTCCGGGAGCTGG
3’mouse-CHISEL	CATCTCCTGATTCTAAGCATCCAATG
5’mouse-dHAND	CCCGTGCACCATGAGGGCTACCC
3’mouse-dHAND	CTTCACTGCTTGAGCTCCAGGGCCCAG
5’mouse-Nkx-2.5	TTCAAGCCCGAGGCCTACTCTG
5’mouse-Nkx-2.5	TGAATCCCCTCCTTCCGCATT

2.1.8. Vectors and Plasmids

pGEM T-Vector	Promega	Contains TA cloning ends for PCR products.
pCR TOPO 2.1	Invitrogen	Contains TA cloning ends for PCR products.
pCR TOPO II	Invitrogen	Contains TA cloning ends for PCR products.
pEGFP-C2	Clontech	Contains CMV the promoter and GFP coding sequence at C-terminal end; constructed for production of fused protein.
pRSET A	Invitrogen	Contains 6 copies of Histidine tag which is recognized by the monoclonal antibody; constructed for production of the epitope-tagged protein which can be overexpressed in *E.coli*.
pVL1392	Clontech	For protein over-expression in baculovirus
pIRES2-GFP	Clontech	Contains CMV promoter and GFP coding sequence at C-terminal end; constructed for production of fused protein

pHTOP-BMP10	Generous gift from Dr. Neuhaus	Contains the full length cDNA of human BMP10
BMP10-gen2-BamHI/HindIII	Generous gift from Dr. Neuhaus	Conteins flanking region of the genomic BMP10 locus. Used as probe for ES screening
BMP10pro	Generous gift from Dr. Neuhaus	Contains exon 1 and 2 of the human BMP10.
BMP10-gen10	Generous gift from Dr. Neuhaus	Contains part of the BMP10 genomic locus.
pBlusescript-BMP10-gen-locus	Generous gift from Dr. Neuhaus	Contains fragment of the BMP-10 genomic locus.

2.1.8.1. Plasmids for riboprobes synthesis

GENE	**INSERT**	**SIZE (kb)**	**VECTOR**	**Antisense probe**	
				Enzyme	**Pol.**
BMP10	BMP10 pro region	1,8kb	pBluscript	BamH1	T7
ANF	ANF	0,8 kb	pGEM-T-Vector	HindIII	T7
FHL2	FHL2	0,5 kb	pBluscript	EcoRI	T7

2.1.9. Bacterial strains

Bacterial strain	**Company**	**Brief destription**
TOP10F\` E.coli	(Invitrogen)	*[F\`[lacI*^{q}*,Tn10(Tet*^{R}*)]], mercA,* Δ(mrr-hsdRMS-mcrBC), φ80lacZΔM15, ΔlacX74, deoR, recA1, araD139 Δ(ara-leu)7697, galK, rpsL(StrR), endA1, nupG,
XL1-Blue E. coli	(Stratagene)	*rec*A1, *end*A1, *gyr*A96, *thi-1*, *hsd*R17(r_K^-,m_K^+), *sup*E44, *rel*A1, l^-, *lac*$^-$, [F' *pro*AB, *lac*I^{q}ZD *M15*, Tn10(Tet^r)]
Stbl2 E. coli	(Invitrogen)	F$^-$ *mcr*A Δ(*mrr-hsd*RMS-*mcr*BC) *rec*A1 *end*A1 *lon gyr*A96 *thi*-1 *sup*E44 *rel*A1 λ$^-$ Δ(*lac-pro*AB)

BL21(DE3)pLysE E. Coli	(Stratagene)	*B,F, dcm, ompT,* $hsdS_B(r_B^- m_B^-)gal(DE3)$ *[pLysS Cam*^{r}*, T7 lysozyme, T7 RNA polymerase inhibitor*

2.1.10. Cell lines

BM-MASC	Belema Bedada et al., 2005
COS-1	ATCC No: CRL-1650
C3H10T1/2	ATCC No: CCL-226; murine mesenchymal fibroblasts
C2C12	ATCC No: CRL-1722; murine myoblastoma cell line
SF9	ATCC No: CRL-1711
293T	ATCC No: CRL-11268; human kidney cell line, contains Adeno and SV-40 viral DNA sequence

2.1.11. Antibodies

- Alexa Fluor 488 labelled chicken anti-rabbit IgG, (Molecular Probes)
- Alexa Fluor 488 labelled goat anti-mouse IgG, (Molecular Probes)
- Alexa Fluor 594 labelled chicken anti-mouse IgG, (Molecular Probes)
- Alexa Fluor 594 labelled chicken anti-rabbit IgG, (Molecular Probes)
- Digoxygenin FAB Fragment (Roche)
- Donkey Anti- rabbit IgG horse radish peroxidase linked (Amersham)
- Donkey anti-goat IgG Cy2 (Jackson Immnunoresearch)
- Donkey anti-goat IgG Cy3 (Chemicon)
- Donkey anti-mouse IgG Cy2 (Jackson Immnunoresearch)
- Donkey anti-rabbit IgG Cy3 (Chemicon)
- Goat anti-mouse FAB fragment (Chemicon)
- Goat anti-mouse whole antibody (Chemicon)
- Goat anti-rabbit IgG (H+L) Biotin SP-conjugated (Jackson Immnunoresearch)
- Goat polyclonal anti- Nkx-2.5 antibody (Santa Cruz)
- Goat polyclonal anti- PDGFRß antibody (Santa Cruz)
- Goat polyclonal anti- PECAM antibody (Santa Cruz)
- Goat polyclonal anti- POD1 antibody (Santa Cruz)
- MF-20: Mouse monoclonal antibody anti myosin heavy chain, (Schafer et al. 1999)

- Mouse monoclonal Anti HisG antibody (Invitrogen)
- Mouse monoclonal anti- NCL-CCC9 antibody (Novocastra)
- Mouse monoclonal anti SM-actin clone 1A4 Cy3 conjugated antibody (Sigma)
- Mouse monoclonal anti SM-actin clone 1A4 FITC conjugated antibody (Sigma)
- Mouse monoclonal anti-calponin antibody (Sigma)
- Mouse monoclonal anti-desmoplakin antibody (Labgen)
- Mouse monoclonal anti-plakoglobin antibody clone 15F11 (Sigma)
- Mouse monoclonal anti-vimentin antibody clone V9 Cy3 conjugated (Sigma)
- Mouse monoclonal anti-vinculin antibody clone VIN 11-5 (Sigma)
- Peroxidase conjugated streptavidin antibody (Rockland)
- Polyclonal rabbit anti-GFP (Invitrogen)
- Rabbit affinity purified anti-collagen VI antibody (Rockland)
- Rabbit polyclonal anti phospho-histone 3 antibody (Upstate)
- Rabbit polyclonal anti-Aurora B antibody (Abcam)
- Rabbit polyclonal anti-BMP10 antibody (Abgent)
- Rabbit polyclonal anti-BMP10 antibody (Acris)
- Rabbit polyclonal anti-dystrophin antibody (H300) (Santa Cruz)
- Rat monoclonal anti-ScaI (D7) antibody (BD Clontech)
- Sheep Anti- mouse IgG horse radish peroxidase linked (Amersham)
- Streptavidin-Cy2 conjugated (Chemicon)
- Streptavidin-Cy3 conjugated (Chemicon)
- Texas Red dye conjugated streptavidin antibody (Jackson Immnunoresearch)

2.1.12. Mouse strains

- ICR (CD31) – albino inbred strain used as wild type in the present study.
- BL6C/57 –inbred strain commonly used for the generation of transgenic mice.
- MnSOD knock-out (kind gift from Dr. T. Loch)
- Desmin-LacZ (generous gift from Prof. Braun)
- Sca1-GFP (generous gift from Prof. Braun)

2.1.13. Buffers and solutions

All buffers and solutions were prepared in accordance with standard protocols included in “Molecular Cloning” (Sambrook et al., 1989) or “Current Protocols in Molecular Biology” (Ausubel et al., 1992). All solutions were made in double-distilled water or demineralized MilliQ water. Solutions were either autoclaved or filter-sterilized.

2.2. Methods

2.2.1. Standard molecular biology methods

All molecular biology procedures were used according to the standard protocols of "Molecular Cloning" (Sambrook at al. 1989) and "Current Protocols in Molecular Biology" (Ausubel et al. 1992). Procedures used during current study are described below only if they differ from the manufacture's instructions.

2.2.2. Cloning methods

All plasmids, during the current studies, were prepared as follows. Inserts of interests were amplified using Taq Polymerase (Eppendorf) or Expand High Fidelity Polymerase (Roche) with specific primers (2.1.7). PCR amplified fragments were cloned into the pGEM-T-vector (Promega) or pCR TOPO II (Invitrogen). Plasmid DNA was isolated according to the protocol (Sambrook at al. 1989). Clones were verified by digesting with restriction endonuclease enzymes, followed by sequencing of positive clones. Typically, a standard sequencing reaction contained around 50-100 ng of plasmid DNA, 3.2 pmol of the indicated sequencing primer (2.1.7) supplemented with buffers from DNA Cycle Sequencing Kit (Abi, Weiterstadt). Sequencing reactions were prepared using the ABI 310 Genetic Analyzer sequencer (Perkin Elmer). Sequences and their alignments were validated using the following data bases: www.ncbi.nih.gov. BLAST, www.ensembl.org and DNA-Star, Lasergene 99 software. Clones with proper sequences were used for further studies. Fragments were cut out with restriction enzymes and subcloned into the target vectors (2.1.8).

2.2.3. Plasmids generated during the studies

Plasmids generated during the presented work were prepared as described in the chapter 2.2.2 and summarized in the table. The table contains: primers' pairs used for PCR amplification (2.1.7) as well as their applications for further studies.

Plasmid name	Primers names	Cloning sites	Applications
pCRII-TOPO-GAPDH	5’-m-GAPDH 3’-m-GAPDH	-	320 bp GAPDH fragment obtained using RT-PCR for qRT-PCR.
pRSET-B-mature-BMP10	5’-pRSET-BMP10 3’-pRSET-BMP10	KpnI XhoI	Over-expression of the fused mature region of the BMP10 protein to the N-terminal 6×His- tag. in *E.coli.*
pVL1392-BMP10	5’pvl-BMP10 3’pvl-BMP10	NotI XbaI	Over-expression of the full length BMP10 in insect cells. Transfer plasmid.
pCRII-TOPO-ANF	5’-m-ANF 3’-m-ANF	-	The ANF fragment obtained using RT-PCR for qRT-PCR.
pIRES2-GFP-BMP10	5’pIRES-BMP10 3’pIRES-BMP10	PstI XmaI	Expression of the full length of the human BMP10 protein in eukaryotic cell lines.
pCRII-TOPO-3’flanking-arm-BMP10	5’-3’arm-BMP10 3’-3’arm-BMP10	ApaI	Construct for the conditional inactivation of BMP10.
pCRII-TOPO-5’flanking-arm-BMP10	5’-5’arm-BMP10 3’-5’arm-BMP10	SacII	Construct for the conditional inactivation of BMP10.
pCRII-TOPO-Exon2-BMP10	5’-ex2-BMP10 3’-ex2-BMP10	KpnI	Construct for the conditional inactivation of BMP10.
pK11-loxP-BMP10-loxP	-	-	Construct for the conditional inactivation of BMP10.
pCRII-TOPO-BNP	5’-m-BNP 3’-m-BNP	-	The BNP fragment obtained using RT-PCR.
pCRII-TOPO-FHL2	5’-m-FHL2 3’-m-FHL2	-	The FHL2 fragment obtained using RT-PCR.
pCRII-TOPO-BMPRII	5’-m-BMPRII 3’-m-BMPRII	-	The BMPRII fragment obtained using RT-PCR.
pCRII-TOPO-PDGFRß	5’-m-PDGFRß 3’-m-PDGFRß	-	The PDGFRß fragment obtained using RT-PCR.
pCRII-TOPO-PECAM	5’-m-PECAM 3’-m-PECAM	-	The PECAM fragment obtained using RT-PCR.
pCRII-TOPO-calponin	5’-m-calponin 3’-m-calponin	-	The calponin fragment obtained using RT-PCR.
pCRII-TOPO-POD1	5’-m-POD1 3’-m-POD1	-	The POD1 fragment obtained using RT-PCR.

Plasmids used for riboprobes synthesis were generated by cloning of RT-PCR amplified fragments into the pCR TOPO II (Invitrogen) and are listed in the chapter 2.1.8.1.

2.2.4. Conditional inactivation of BMP10 gene

The plasmid containing the genomic locus of the BMP10 gene was kindly provided by Dr. Herbert Neuhaus (2.1.8). Flanking arms (5’ and 3’) as well as exon 2 of the BMP10 gene were amplified by PCR using Expand High Fidelity polymerase (Roche) and specific primers (2.1.7). All fragments were cloned into the pCRII-TOPO vector (Invitrogen) and verified by sequencing including also internal set of primers. Next, 3’ flanking region (1.6 kb) was inserted into the pK11 vector with the ApaI site followed by cloning exon2 of BMP10 using the KpnI site. Finally, the 5’ flanking arm (4.8 kb) was subcloned into the pK11-3’-arm-exon2 plasmid with the SacII site. A schematic overview of the construct for the conditional BMP-10 ablation in mice is shown in Fig. 2.1.

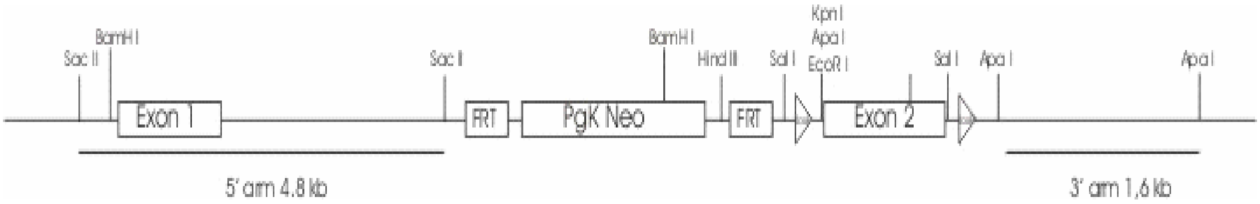

Fig. 2.1. The organization of the BMP-10 modified locus including major restriction sites is shown.

The targeting vector contains also a neomycin resistance gene (neo) under the control of the phosphoglycerol kinase (PGK) promoter flanked by two FRT sites. The pK11-BMP-10-ko plasmid was linearized with the PvuI restriction enzyme for ES cells transfection. Culture plates used for embryonic stem (ES) cells growth were covered with 0.2% gelatine. ES cells were cultivated on a monolayer of feeder cells treated with mitomycin C (kind gift from Dr. T. Loch). Usually, feeder cells were plated one day prior to ES cells seeding. The culture of ES cells was propagated in ES-medium in a humidified atmosphere containing 10% CO_2 at $37^{O}C$. The medium was changed daily. ES cells before trypsinization were washed with HEPES/EDTA buffer and detached using 0.25% trypsin in HEPES/EDTA buffer. The target construct was introduced into ES cells by electroporation methods. Briefly, cells were harvested and around 14×10^{6} cells were suspended in 600µl of OPTI-MEM medium and 25µg of the linearized plasmid DNA was added. Electroporation was done using 4 mm gap electroporation cuvettes (Peqlab) at the following conditions: low voltage mode, 250 V and 1 millisecond pulse. Then cells (2×4×10^6 and 2×7×10^5) were plated in 10-cm dishes. One day later, the medium was replaced by selection medium (ES-medium supplemented with G418 at 400 µg/ml). Transfected ES cells were grown in selection medium for 14 days and the medium was replaced daily. After 10 days single colonies were picked and propagated in 96 well plates followed by their growth in 24 well plates. Only around 80-100 clones were obtained after a single electroporation. A part of the ES culture was prepared for DNA isolation. These clones were grown in 24 well plates for 7-8 days until they reached confluence. Genomic DNA was isolated from around 100 clones using the proteinase K extraction method, and southern blot analysis was done using specific probe. None of the screened clones were positive for a mutated allele (data not shown).

2.2.5. In situ hybridization

2.2.5.1. Embryos preparation

Isolated embryos at the different stages were immediately washed with ice-cold 1×PBS and fixed in 4%PFA over night. Next, samples were dehydrated in 25%, 50%, and 75% methanol in PBT and 2 times in 100% methanol -10 minutes each at room temperature. Dehydrated embryos were stored in -20^{O}C in 100% methanol.

2.2.5.2. Tissue preparation for paraffin embedding

Dissected tissues samples were immediately washed in ice-cold 1×PBS, followed by fixation in 4% PFA over night. Next, tissues were dehydrated in ethanol (25%, 50%, 75%, 96% for 60 minutes each step and twice in 99.8% ethanol for 10 minutes followed by 99,8% EtOH at -20^{o}C over night). Next day, tissues samples were treated twice with 99.8% ethanol/xylol (1:1) for 1 hour, twice per 1 hour with xylol at room temperature and incubated for 2 hours at 60^{o}C with a mixture of Xylol/ Paraffin (1:1), followed by two changes of pure paraffin at 60^{o}C. Finally, tissues were embedded in paraffin. Sections 7-13 µm thick were prepared using a microtome (Leica). Samples were attached to glass slides coated prior to use with Vectabond^{TM} solution according to the manufacture's instruction.

2.2.5.3. In vitro transcription

An antisense and sense riboprobes were synthesized using linearized plasmid DNA with RNA polymerases (T7, T3, SP6), depending on the plasmid (2.1.8.1). The typical reaction mixture contains:

✓ Linearized plasmid	1 µg
✓ 5 transcription buffer	4 µl
✓ 0.1M DTT	2 µl
✓ Dig-Mix	2 µl
✓ RNA polymerase	1 µl
✓ RNasin	2.5 µl
✓ H_2O	ad 20 µl

The reaction was done for 2 hours at 37°C. A plasmid DNA was enzymatically digested using DNase I for 30 minutes at 37°C followed by DNase heat inactivation at 65°C for 15 minutes. Synthesized riboprobes were purified by precipitation with ethanol supplemented with lithium chloride. Next, probes were redissolved in water supplemented with RNase inhibitor. The quality of RNA was checked by electrophoresis on 1% agarose gel.

2.2.5.4. Whole mount in situ hybridization

Embryos at E10.5 were prepared as described in 2.2.5.1. Digoxigenin labeled anti-sense and sense probes were synthesized as described in 5.2.5.3. Whole amount in situ hybridization was done according to Wilkinson. The following steps were applied:

I. Pre-hybrydization washes:

❖ 100% Methanol	5 min.	RT
❖ 75% Methanol/PBT	5 min.	RT
❖ 50% Methanol/PBT	5 min.	RT
❖ 25% Methanol/PBT	5 min.	RT
❖ 2×PBT	5 min.	RT
❖ 6% H_2O_2	45 min.	RT
❖ 3×PBT	5 min.	RT
❖ Proteinase K (10µg/ml)/PBT	11 min.	RT
❖ Glycine (2mg/ml)/PBT	5 min.	RT
❖ 2×PBT	5 min.	RT
❖ 0.2% glutaraldehyde/4% PFA	20 min.	RT
❖ 3×PBT	5 min.	RT
❖ Prehybridization Buffer	120 min.	65°C
❖ Hybridization Buffer	o.n.	65°C

II. Post-hybridization washes:

❖ 2 x Solution 1	30 min.	70°C
❖ Solution 1:Solution 2 (1:1)	10 min.	70°C
❖ 3x Solution 2	5 min.	RT
❖ RNase A (1 mg/ml)/ Solution 2	30 min.	37°C
❖ Solution 2	5 min.	RT
❖ Solution 3	5 min.	RT
❖ 2 x Solution 3	30 min.	65°C
❖ 3 x TBST	5 min.	RT
❖ 10% Sheep serum/TBST	70 min.	RT
❖ Anti-digoxigenin antibody 1:2000 in 1% sheep serum/TBST	o.n.	+4°C

III. Alkaline Phosphatase staining

❖ 6 x TBST	60 min.	RT
❖ 3 x NTMT	10 min.	RT
❖ NBT/BCIP in NTMT		RT

The alkaline phosphate staining of the samples was stopped with PBT at room temperature followed by overnight fixation in 4% PFA at 4^{o}C. Embryos were documented.

2.2.5.5. In situ hybridization in paraffin embedded tissue slides

Tissues samples were prepared as described in 2.2.5.2. Digoxigenin labeled anti-sense and sense probes were synthesized as described in 2.2.5.3. In situ hybridization was done in the following steps:

I. Pre-hybrydization washes:

❖ 2 x 99.8% Ethanol	2 min.	RT
❖ 96% Ethanol	1 min.	RT
❖ 70% Ethanol	1 min.	RT
❖ 50% Ethanol	1 min.	RT
❖ 30% Ethanol	1 min.	RT
❖ PBS	5 min.	RT
❖ 4% PFA	15 min.	RT
❖ PBS	5 min.	RT
❖ Proteinase K (10µg/ml)/PBS	5 min.	RT
❖ Glycine (2mg/ml)/PBS	5 min.	RT
❖ PBS	5 min.	RT
❖ 4% PFA	15 min.	RT
❖ Acetic Anhydrate/0.25% TEA/H_2O	10 min.	RT
❖ 2 x PBS	5 min.	RT
❖ Pre-hybridization buffer	15 min.	65^{O}C
❖ Hybridization buffer	o.n.	65^{O}C

II. Posthybridization wash.

❖ 3 x Solution I	15 min.	65^{O}C
❖ 3 x Solution III	15 min.	65^{O}C

❖ 3 x TBST	10 min.	RT
❖ 10% Sheep serum/TBST	30 min.	RT
❖ Anti-digoxigenin antibody 1:2000 in 1% sheep serum/TBST	o.n.	+4^{O}C

III. Alkaline Phosphatase Staining.

❖ 3 x TBST	15 min.	RT
❖ 3 x NTMT	10 min.	RT
❖ NBT/BCIP in NTMT		RT

The alkaline phosphate staining of the samples was stopped with PBS at room temperature followed by fixation in 4% PFA for 60 minutes. Next, sections were stained with eosin (2.2.5.6) followed by dehydratation. Finally tissues samples were embedded in Entelan and documented.

2.2.5.5.1. In situ hybridization solutions and buffers

✓ **Solution 1**	50% Formamide 5 x SSC pH 4.5 1% SDS
✓ **Solution 2**	0.5 M NaCl 10 mM Tris-HCl pH 7.5 0.1% Tween-20
✓ **Solution 3**	50 % Formamide 2 x SSC pH 4.5
✓ **NTMT**	100 mM Tris-HCl pH 9.5 100 mM NaCl 0.05 M $MgCl_2$ 0.1% Tween-20/levamisole

2.2.5.6. Hematoxylin/eosin staining

After completing the in situ hybridization procedure, sections were stained with 2% eosin solution (Division Chroma) for 5 minutes and washed several times with water.

Cryosections were fixed in 4% PFA for 10 minutes, washed with PBS followed by nuclear staining with hematoxylin (Division Chroma) for 10 minutes and washed with water. The cytoplasm was visualized by eosin staining. Next, sections were dehydrated in increasing concentrations of ethanol and finally in xylol followed by embedding in Entelan.

2.2.6. Basic cell culture methods

2.2.6.1. Maintenance of cell lines

C3H10T1/2, 293T, C2C12 and COS-1 cell lines were grown in D-MEM medium containing 1.000 mg/ml and 4.500 mg/ml glucose respectively, supplemented with 10% FBS, 100 U/ml of penicillin, 100 µg/ml of streptomycin and 0.292 mg/ml L-glutamine. Cells were grown for 2 days to reach around 80% confluence in a humidified atmosphere containing 10% CO_2 at 37°C. Cells were harvested with trypsin solution (PAA Laboratories) and split in different ratios, depending on the cell line. Stocks of cells were made in DMEM medium containing: 20% FBS and 10% DMSO.

2.2.6.2. Transient transfections

2.2.6.2.1. Calcium phosphate method

The calcium phosphate method was used to transiently transfect 293T and COS-1 cell lines. Cells were seeded 24 hours prior to transfection on 6 cm plates (if applicable, containing sterile glass cover slides (Roth)). Cells were plated with a density of approximately 5×10^4 cells per 6cm plate. Approximately 10 minutes before transfection, the medium was replaced with fresh growth medium supplemented with 50 μM chloroquine (Sigma). Next, 1-30 μg of total plasmid DNA was mixed with 500 μl of 2xHBS buffer (100 mM NaCl; 6.5 mM KCl; 0.8 M $Na_2HPO_4 \cdot 2H_2O$; 210 mM HEPES pH 7.05) followed by addition of 62 μl of 2 M $CaCl_2$. The transfection cocktail was immediately mixed by pipeting and added to a plate in dropwise fashion. Usually, 3-4 hours later medium was replaced and fresh medium was applied.

2.2.6.2.2. Fugene 6 transfection reagent

The Fugene 6 transfection reagent was used to transiently transfect the 10T1/2 cell line according to the published protocol (Roche).

2.2.6.3. Overexpression of BMP10 in the 293T cell line, preparation of conditioned medium

The 293T cell line was transiently transfected using the calcium method (2.2.6.2.1) or the Fugene 6 reagent (2.2.6.2.2) with pBMP10-IRES2-GFP plasmid or pEGFP-C2 vector. Twenty-four hours after transfection, the medium was replaced by serum free medium D-MEM containing 1.000 mg/ml glucose supplemented with 100 U/ml of penicillin, 100 μg/ml of streptomycin and 0.292 mg/ml L-glutamine. Seventy-two hours after transfection, its efficiency was proved by fluorescence microscopy and the medium enriched in BMP10 protein as well as control medium were collected, filtrated and used in further experiments. In addition, cells were homogenized in TRIZOL and total RNA was isolated followed by RT-PCR examination. BMP10 conditioned medium and control medium were examined by western blot and the activity of the BMP10 protein to induce alkaline phosphatase (2.6.7) in C2C12 cells was tested.

2.6.7. Alkaline Phosphatase detection

The activity of the BMP10 protein in conditioned medium was analysed by its ability to induce alkaline phosphatase activity in C2C12 cells. Briefly, 1x10^4 C2C12 cells were seeded per 1 well using 96 well plates. The next day, conditioned medium containing secreted BMP10 protein and BMP-2 (Sigma) as positive control were applied. As negative control serum free medium collected from 293T cells transfected with the pEGFP-C2 vector as well as standard GM were applied. Different concentrations of BMP-2 in the range 200 ng, 150 ng, 100 ng, 75 ng, 50 ng, 25 ng per ml were used. In the case of BMP10 conditioned medium and control serum free medium 100%, 75%, 50%, 10%, 5% were used. All tested conditions were done in triplicate. After 48 hours cells were washed a few times in PBS, followed by fixation in 4% PFA for 10 min. Next, cells were washed three times with buffer containing 100 mM Tris-HCl pH 9.5, 0.1% Triton X-100, 0.5 mM $MgCl_2$. Finally, cells were incubated with the NBT/BCIP staining solution at 37^OC for 10-15 minutes followed by washing 4-5 times with PBS and fixation in 4% PFA for 10 minutes. Cells were documented by photographing using a digital camera (Canon).

2.2.8. Mouse adult heart non-cardiomyocyte isolation

Non-cardiomyocyte populations were isolated from BL6C/57 or Sca-1-GFP mice strains. Animals were anesthetized with pentobarbital sodium. The murine hearts were quickly removed and perfused by the aorta with Ca^{2+} free buffer containing: 113 mM NaCl, 4.7 mM KCl, 0.6 mM KH_2PO_4, 1.2 mM $MgSO_4 \times 7H_2O$, 12 mM $NaHCO_3$, 10 mM HEPES, 30 mM Taurin, 10 mM 2,3-butanedione monoxime, 5.5 mM glucose. The enzymatic digestion was initiated by applying Liberase Blendzyme and Trypsin. Next, hearts were gently minced and enzymatic digestion was stopped by supplying bovine calf serum. The suspension was filtered via a 100µM cells strainer. Cells were adjusted with $CaCl_2$ solution to the final 1 mM concentration of Ca^{2+} in four steps and counted for viability. The cell suspension was centrifuged at 300 rpm for 1 minute. The supernatant contained the fraction of non-cardiomyocytes cell, which were seeded on standard cell culture plates. Non-cardiomyocytes were grown in D-MEM medium containing 1.000 mg/ml glucose, supplemented with, 100 U/ml of penicillin, 100 µg/ml of streptomycin and 0.292 mg/ml L-glutamine and 10% FBS in a humidified atmosphere containing 10% CO_2 at 37°C. Isolation of murine adult non-cardiomyocytes were done together with Marion Winslet. The culture purity was checked by immucytochemistry (Fig. 2.2).

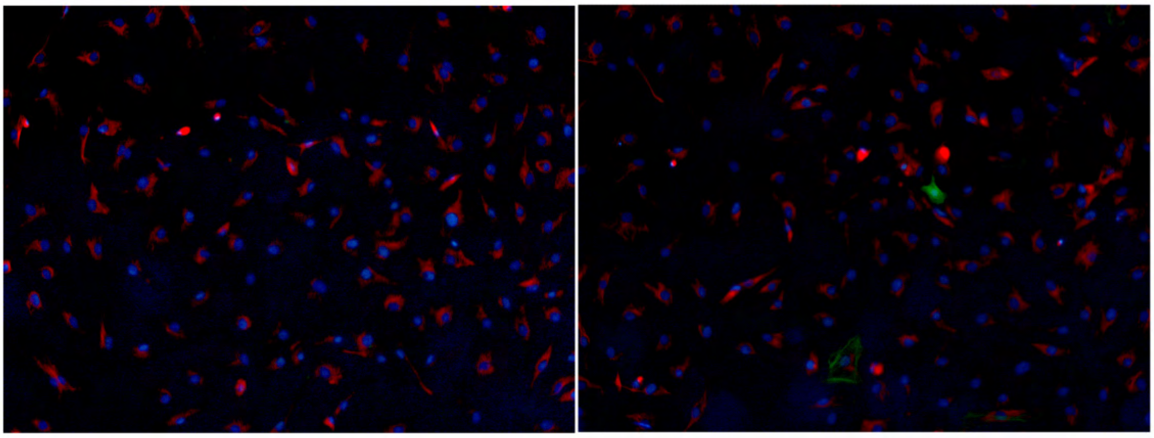

Fig. 2.2. Immunocytochemistry of non-cardiomyocytes isolated from the murine adult heart. Cells were stained with SM-actin conjugated FITC antibody (green) and vimentin conjugated TRITC antibody (red) to quantify the number of fibroblasts (vimentin positive), smooth muscle cells (SMA positive) and myofibroblasts (SMA and vimentin positive). Nuclei were visualized by DAPI staining (blue).

2.2.9. Terminal dUTP deoxynucleotidyl transferase nick end-labeling (TUNEL) assay

The TUNEL assay was performed on mouse heart cryosections. Cryosections were prepared from at least three animals from each of the tested model of CMP and compared to age and strain matched control animals. As a positive control ischemic dog heart was used (Kindly provided by Dr. Sawa Kostin). The In situ Cell Death detection kit (Roche) was used according to supplier's manual.

2.2.10. Immunocytochemistry

Cells after culture were washed several times with PBS, fixed in 4% PFA for 10-20 minutes followed by incubation with PBS/0.1% Triton-X100 solution and blocked with 5% horse serum in PBS/0.1% Triton-X100 solution. Cells were incubated with the primary antibody at 4^{o}C over night or for 1 hour at room temperature, washed with PBS and incubated with secondary, fluorochrom-conjugated antibody for 45 minutes. After three washes with PBS, the cells were embedded in Mowiol (6g of glycerol was mixed with 2,4 g of Mowiol and 6 ml H_2O, followed by incubation for 4 hours at room temperature, mixed with 12 ml of 0.2 M Tris-HCl pH 8.5, heated for 10 minutes at 50^{O}C and aliquoted).

2.2.11. Immunohistochemistry

Depending on the aim of the study and/or primary antibody, different staining protocols and detection systems were used.

Cryosections were washed with PBS, fixed in 4% PFA for 10-20 minutes followed by incubation with PBS solution and blocked with 0.1% BSA in PBS. Cryosections were incubated with the primary antibody at 4^{o}C, washed with PBS and incubated with secondary, fluorochrom-conjugated antibody for 45-60 minutes. After three washes with PBS, sections were embedded in Mowiol. When the signal had to be amplified the two step detection of the primary antibody with the biotin-streptavidin system was used.

2.2.12. β-galactosidase staining

Tissues samples were fixed in PFA solution followed by preparation of the cryosections. Sections were washed with PBS and treated with the staining solution (5 mM potassium ferricyjanide, 5 mM potassium ferrocyjanide, 1 mM magnesium chloride, 0.002% NP-40, 0.05% Na-deoxycholate) containing 0.1% X-Gal for 5-30 minutes. Reaction was stopped by washing with PBS. Cryosections were embedded in Mowiol.

2.2.13. Total RNA isolation from tissues and cells

Total RNA was isolated using the Trizol^{TM} reagent according to the manufacture's instructions (Invitrogene). All equipments for RNA isolation were sterilized by treating with 0.5 M NaOH for 30 minutes at room temperature followed by washing with DEPC water. Tissue samples were homogenized using the Ultra Turrax homogenizer (IKA Works, Wilmington, USA). Solutions used during the RNA isolation procedure were prepared on the base of RNAse free water. Typically 1 ml of Trizol^{TM} reagent was applied to 100 mg of tissue or per 10^6 cells.

2.2.14. Reverse transcription reaction

The reverse transcription reaction was performed on the template total RNA extracted with the TRIzol^{TM} reagent (2.2.13). Total RNA concentration was estimated with the Eppendorf BioPhotometer by measuring absorbance at 260 nm in triplicate. Firstly, due to the possibility of DNA contamination, RNA was treated with RQ1 RNase-free DNase (1 U of DNase per 1 μg of RNA) followed by DNase heat inactivation (65^{O}C, 10 minutes). DNA free samples were used for first stranded cDNA synthesis. Reverse transcription reactions were carried out using SuperscriptII reverse transcriptase (Invitrogen) and oligodT$_{(15)}$ (Promega) according to the manufacture's protocol. Reaction was done at 42^{O}C for 60 minutes followed by heat inactivation of Superscript II at 70^{O}C for 10 minutes. cDNAs obtained were freshly used for PCR reaction or stored in -20^{O}C for further experiments.

2.2.15. PCR reaction

PCR conditions were optimized experimentally for each primer pair according to the manufacturer's instructions (Eppendorf). Usually, the template DNA was used in the range 1-10 ng in the case of plasmid DNA or 2-4 μl of cDNA after the RT reaction. The amount of cDNA used for the PCR reaction depended on the level of gene expression in the samples. The typical reaction mixture contained: 10 x buffer, 5 x Enhancer buffer, 0.2 pmol of each primer, 5U of Taq polymerase (Eppendorf) and when necessary supplemented with $MgCl_2$. Thermal cycling conditions were optimized empirically.

2.2.16. Semi-quantitative and quantitative Real Time PCR reactions

The semi-quantitative PCR analysis was performed using 2-4 µl of cDNA as a template for the PCR reaction. Expression of each of the examined genes was tested individually with a decreasing number of cycles, and repeated in triple. As a reference, the level of the housekeeping genes GAPDH or HPRT was used.

The quantitative Real Time analysis was done using the iCycler iQ Multi Colour Real Time PCR thermocycler (Biorad Laboratories). The typical reaction mixture is described in 2.2.15. It was supplemented by SYBR green and fluorescein according to the published protocol. A standard curve was determined by the expression level of the housekeeping gene GAPDH.

2.2.17. P^{32} labeling probe preparation

Plasmid DNA was digested with specific restriction endonucleases, followed by electrophoresis on the agarose gel. Inserts were cut out and purified with the JetQuick Gel extraction kit (Genomed). Typically, 25-50 ng of purified DNA was mixed together with random hexanucleotides as primers and denatured at $95^{O}C$ for 5 minutes followed by cooling down on ice. These components were mixed with: dNTPs, BSA, Klenow enzyme, 5 µl of $[\alpha\text{-}^{32}P]$ dCTP (6000 Ci/ml) and incubated at $37^{O}C$ for 2 hours. A random primed labeled probe was purified from not nucleotides incorporated using NAP-5^{TM} columns (Sephadex® G-25) (Pharmacia Biotech).

2.2.18. Southern blot analysis

Southern blot analysis was performed according to Sambrook et al. 1989. The genomic DNA was obtained from the ES cells clones (2.2.4). To screen the ES clones, genomic DNA was digested with KpnI and separated on 1% agarose gel followed by

DNA depurination (incubation in 0.25% HCl for 15-20 minutes at room temperature). The transfer was done in alkaline conditions (0.4 M NaOH), over night. More than 12 hours later, the membrane was washed in 2xSSC pH 7.5 for 10 minutes and air-dried. The membrane with bound DNA was hybridized with radioactively labeled DNA probe. In the first step, the membrane was pre-hybridized at 65^{O}C for 2-3 hours in Church and Gilbert hybridization buffer (0.5M Na_2HPO_4, 1 mM EDTA, 7% SDS) containing 0.2 mg/ml denaturated herring sperm DNA. Hybridization was carried out in Church and Gilbert hybridization buffer containing a reduced amount of denaturated herring sperm DNA to 0.1 mg/ml and 3 x 10^6 cpm/ml of labeled probe. The reaction was done at 65^{O}C with rolling over night. Typically, the next day the membrane was washed three times with solution containing 1xSSC pH 7.0, 1% SDS at 65^{O}C. The results were visualized using X-ray films (Kodak).

2.2.19. Western blot analysis

Typically, proteins were separated on standard denaturing SDS-PAGE gels. However, depending on the aim of the experiment, different types of gels were used. The first type of gels was performed according to Sambrook et al. 1989, and was composed of 5% stacking gel and separating gel in the range of 6% to 15%. This type of gels was used for detection of higher amount of proteins. Gradient gels were bought from Invitrogen and Anamed. Upon completion of electrophoresis, proteins were transferred onto nitrocellulose membranes using two systems: semi-dry electroblotting method (Fastblot B 43, Biometra) or the so called wet system according to the manual (Invitrogen). In the case of semi-dry blotting, 4 pieces of Whatman 3MM paper and 1 piece of BioTrace® Nitrocellulose Membrane were cut to the size of the gel and together with the gel soaked for a few minutes in electroblotting buffer. Two layers of 3MM paper were placed on an anode. On the top of that, the nylon membrane was placed. Gels were laid on the membrane and covered with 2 additional layers of 3MM paper. The whole stack was covered with the cathode. Electroblotting was run at a current of 5 mA per cm^2 of the blot for 45-60 minutes. The membrane was stained with Ponceau S for a few minutes to visualize the transferred protein bands followed by blocking in 5% non-fat dry milk powder (Roth) in TBST solution for 60 minutes at room temperature. The membrane was incubated at 4°C over night with the primary antibody in blocking buffer containing 3% non-fat dry milk powder in TBST buffer. Next, three 5 min. washings in TBST buffer preceded 45 min. incubation (room temperature) with the secondary antibody in TBST with 1% non-fat dry milk. All incubations were done on the rotating platform.

Depending on the type of experiment and the level of proteins, different detection systems were used. When highly expressed proteins were monitored, the system based on DAB staining was used. After 3 washings (5 min. each) in TBST, the membrane was incubated with ABC solution (2 drops of 'label A' and 2 drops of 'label B' in 5 ml TBST prepared 30 min. in advance, Vector Laboratories) for 30 min. After that the membrane was washed three times with TBST buffer. Detection was done with DAB (2.5 mg/ml) in 10 ml of 0.1 M Tris·HCl pH 7.2 with 5 µl 30% H_2O_2. Staining was stopped by rinsing in water. When the proteins were not abundant or isolated from different cell lines and tissues, the ECL detection (Amersham) or Femto WB detection system (Pierce) were used according to published manuals.

2.2.20. Protein isolation

Tissues samples after isolation were sonicated in the extraction buffer (0.1 M Tris-HCl pH 8.0, 0.01 M EDTA, 0.04 M DTT, 10% SDS supplemented with proteases inhibitor). After sonication, protein crude was incubated for 2 min. at $99^{O}C$ followed by centrifugation at room temperature with maximum speed. Specific fractions of protein were isolated using NE-PER extraction kit (Pierce) according to the manual. Protein concentration was determined using BioRad Dc assay according to the protocol.

2.2.21. Overexpression and purification of the His-tagged mature region of BMP10

In order to overexpress BMP10 in bacteria, the pRSET vector (Invitrogen) was used which contains N-terminal 6HisG tag. The his tag not only facilitates affinity chromatography purification on a Ni $^{2+}$-NTA column but also the detection of the overexpressed protein, since a specific anti-HisG antibody (Invitrogen) is available. Additionally, as the main aim of the study was the generation of a BMP10 antibody, the His tag is believed to be the least immunogenic. The mature region of BMP10 was PCR amplified with specific primers, containing in-frame XhoI and KpnI restriction sites and the product was cloned into the pCR2.1-Topo vector (Invitrogen) followed by sequencing. After sequence verification, the XhoI/KpnI fragment was subcloned into the pRSET-B vector. The Bl21DE3 bacterial strain (Invitrogen) was used for protein overexpression. The conditions for BMP10 overexpression were estimated empirically. After transformation of Bl21DE3, colonies were picked from plates and then grown in the suspension culture at 37 ^{O}C, with shaking of 250 rpm in 50 ml culture volume. After over night culture, bacterial cells were placed into the fresh culture medium with dilution 1:50 and grown at 37^{O}C or 30^{O}C or RT in various culture volumes (25-150ml). Overexpression was induced by applying 1 mM IPTG. 1ml samples were collected every hour. The level of protein overexpression was monitored by SDS-PAGE gel electrophoresis followed by staining with Coomassie blue solution. The mature region of the BMP10 fused to His tag was efficiently overexpressed at all tested conditions, but unfortunately the test of solubility revealed that it is insoluble independent on culture/overexpression conditions in phosphate buffer, in the pH range compatible for protein binding to Ni^{2+} resins (Fig. 2.3). Hence Mat-BMP10 was overexpressed at 37^{O}C and bacteria were collected 4 hours after induction with IPTG (Figs. 2.3, 2.4). In addition Western blot was done to verify the identity of the protein band. Overexpressed protein was purified under denaturing conditions on a Ni^{2+} chelating column (Figs. 2.4, 2.5) as described in the manufacture's instructions (Qiagen). Fractions (approximately 3 mg) with the highest degree of purity were subjected to separation on SDS-PAGE on standard 15% preparative gels. Proteins were visualized with the ethanol Coomasie solution, appropriate bands were cut out and in this form sent for immunization of rabbits, that was carried out by Dabio (Regensburg, Germany).

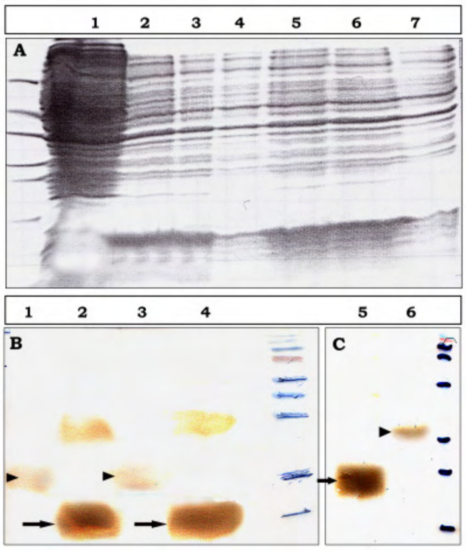

Fig. 2.3. Overexpression of the 6His-tagged BMP10 in *E.coli* (A). Lane 1- negative control; 2 and 5- 4 hours after IPTG induction in 30°C and 37 °C, respectively; 3 and 6- 2 hours after IPTG induction in 30°C and 37 °C; 4and 7 before induction with IPTG. Overexpression of the expected 17 kDa mature region of BMP10 fused to His-tag was apparent (A). The test of solubility in phosphate buffer (B,C) shows that in all tested conditions majority of the overexpressed protein remains insoluble. Overexpression in 30°C (B), with various oxygen accessibility, i.e. culture volume (1 and 2- 50 ml culture, 3 and 4- 20 ml culture) did not improve solubility compared with overexpression in 37°C (C). Lanes 2, 4, 5 show the protein detected with specific anti HisG antibody His-BMP10 in insoluble fractions (arrow), lanes 1,3,6- protein detected in soluble fractions (arrowhead).

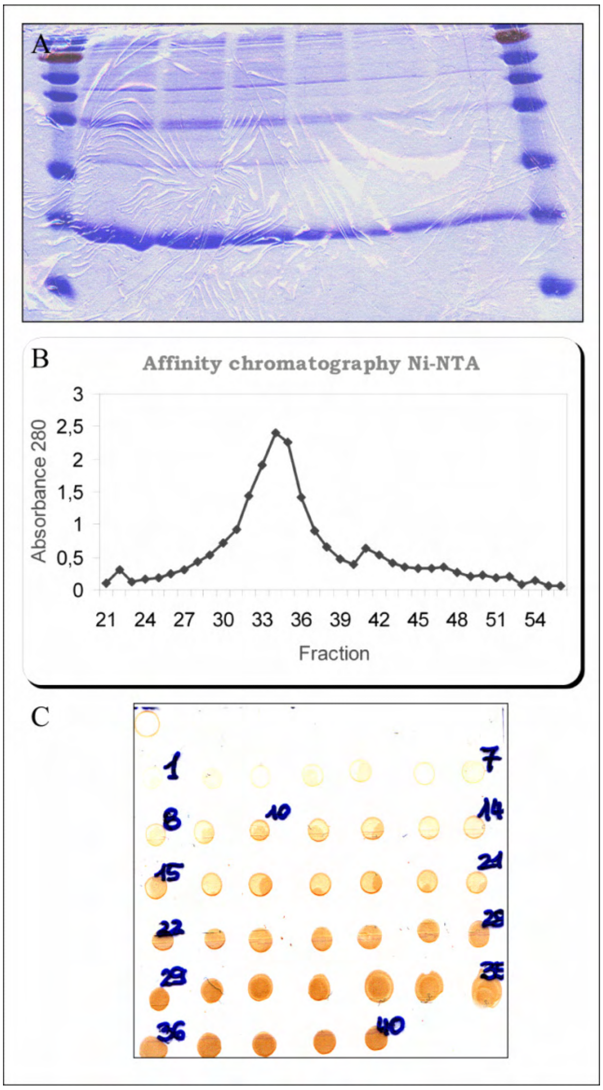

Fig. 2.4. Purification of His-tagged mature region of BMP10. Panel A shows SDS-PAGE of collected fractions eluted with 8M urea at pH 4.5 with the highest protein content as judged on the basis of the elution profile (B) followed by dot blot analysis with anti-HisG antibody of enriched in BMP10 fractions (C).

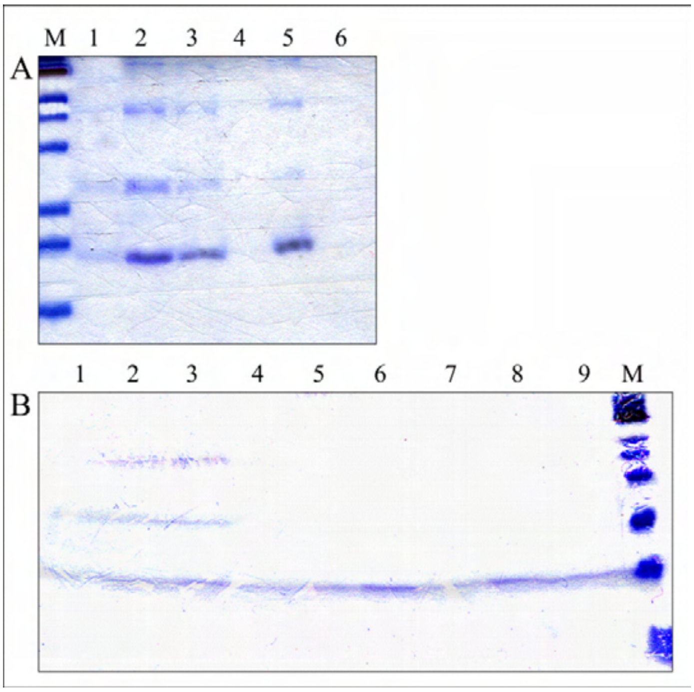

Fig. 2.5. Purification of the His-tagged mature region of BMP10. Panels A and B show different tested conditions to obtain the native mature region of BMP10. Panel A: lanes -1-3: buffer containing 10 mM HEPES, 10µM $Zn(CH_3COO)_2$, 50 mM NaCl supplemented with 5 mM ß-mercaptoethanol (line 1), 20 mM ß-mercaptoethanol (line 2), 1mM DTT (line 3), lane 4 – 50 mM Tris-HCl pH 7.5, lane 5 – 50 mM Tris-HCl pH 8.0, lane 6 – PBS. Panel B, phosphate buffer supplemented with: 0.1%, 0.2% and 0.5% Tween-20 (lines 1-3 respectively), 0.1%, 0.2% and 0.5% Triton X-100 (lines 4-6 respectively), 0.1%, 0.2% and 0.5% NP-40 (lines 7-9 respectively).

2.2.22. Osmotic mini-pump implantation

To induce heart hypertrophy/CMP doxorubicin (15µg/g) and isoproterenol (225µg/g) were administrated in the ICR mouse strain by surgical implantation of the mini-osmotic pump model 2002 according to supply instructions (Alzet). In all experiments both male and female mice were used. Mice were anesthetized with Avertin injection or by Isoflurane together with oxygen inhalation followed by subcutaneous pump implantation. The skin incision was closed with wound clips. Using this pump model, drugs were administrated at 0.5µl per hour for 14 days.

2.2.23. Magnetic Resonance Imaging

MRI measurements and data evaluation were done by Dr. Astrid Wietelmann and Ursula Hoffmann. The study was carried out on 11 C57bl/6 and 7 ICR animals (both genders) of varying ages and weight (22 - 30 g). Animals were anaesthesed by using 2.5% isoflurane (Forene, Abbott, Germany) in air and oxygen and then maintained during the whole MR experiment with 1.5 to 2.5% (v/v) isoflurane at 0.5 l/min air and 0.5 l/min oxygen flow, delivered via a nose-cone (surgivit/Anesco, Hugo Sachs Elektronik-Harvard, Germany). The gaseous mixture was bubbled through water to prevent damage of the mucous membrane of the mouse from the dry gaseous mixture. For electrocardiogram (ECG) triggering ECG leads (Neonatel Monitoring Electrode, Red Dot, 3M Health Care, Germany) were attached to both front paws and the tail. The leads were attached to a preamplifier (ESS ECG Transducer Box, Bruker BioSpin MRI, Germany) to amplify the ECG signal for detection on the magnetic resonance system. The mice were positioned supine on a cradle and then placed into the MRI receiving coil. The temperature of the probe assembly was maintained at 37°C by running heated water through the water channels of the probe assembly to maintain the body temperature of the mouse.

MR acquisitions were performed on a 7.05 T horizontal-bore (16 cm) MR scanner (Bruker, Germany) equipped with a 300mT/m gradient system and with 300.51 MHz for isotope ^{1}H. A 2.6 cm usable diameter quadrature low-pass birdcage coil constructed as described previously (Wagener et al. 2004) was used in all experiments. MRI experiments were conducted by applying an ECG-triggered gradient-echo sequence with the following imaging parameters: echo time (TE) = 2.2ms; repetition time (TR) = 12.11ms; field of view (FOV) = 3.00cm^2; acquisition matrix = 129 x 129; maximal in-plane resolution = 233µm^2; slice thickness = 1.0mm.

At a heart rate of 450 beats/min, the corresponding cardiac cycle length was ms, allowing for acquisition of frames within each cardiac cycle with the given temporal resolution of ms. A sufficient number of dummy scans (5 scans within 2 s) were run to bring the magnetization to steady state prior to imaging data readout. Four accumulations were made to obtain a sufficient signal to noise ratio.

2.2.24. Confocal microscopy and three-dimensional (3D) reconstructions

Sections and cells were examined by laser scanning confocal microscopy (Leica TCS SP2, AOBS). After data acquisition, the images were transferred to Silicon Graphics Indy workstation (Silicon Graphics) for three-dimensional (3D) reconstruction using Imaris, the 3D multichanel image processing software (Bitplane, Zürich, Switzerland) as desribed by Kostin (Kostin et al., 1999). All confocal images and 3D images were done by or in cooperation with Dr. Sawa Kostin.

2.2.25. Embryonic heart cultures

Embryonic hearts were isolated from mouse ICR embryos at stage E9.5 – E11.5. Hearts were grown in D-MEM medium containing 1.000 mg/ml glucose, supplemented with 100 U/ml of penicillin, 100 μg/ml of streptomycin and 0.292 mg/ml L-glutamine as well as with 2.5%, 5% and 10% FBS or in serum free medium. Hearts were maintained in a humidified atmosphere containing 10% CO_2 at 37°C for 48 – 96 hours after isolation (Fig. 2.6).

Due to the fact that embryonic hearts are able to survive in serum free medium the next obvious question was whether they still express typical markers during *in vitro* culture. mRNA was isolated from collected embryonic hearts from *in vitro* cultures and compared to hearts isolated from E9.5 – E11.5. Markers like Nkx-2.5, MEF2C, CHISEL, dHAND, ANF were unchanged. The only p57 transcripts have shown differences in expression level (Fig. 2.7).

In addition to RT-PCR analysis the proliferation test was performed. Embryonic hearts were grown in the presence of Bromo-deoxy-Uridine (BrdU) for 6 – 8 hours. Next, hearts were embedded in OCT medium and 7μM sections were prepared. Cryosections of embryonic hearts were fixed with Methanol/Acetone for 10 minutes in -20^{O}C followed by immuno-detection using the BrdU kit (Oncogene) accordingly to the manufacture's instructions.

As shown in Fig. 2.8, there were no drastic differences between in vitro cultivated hearts in cells proliferation. Taken together, established methods can be useful tools in further studies.

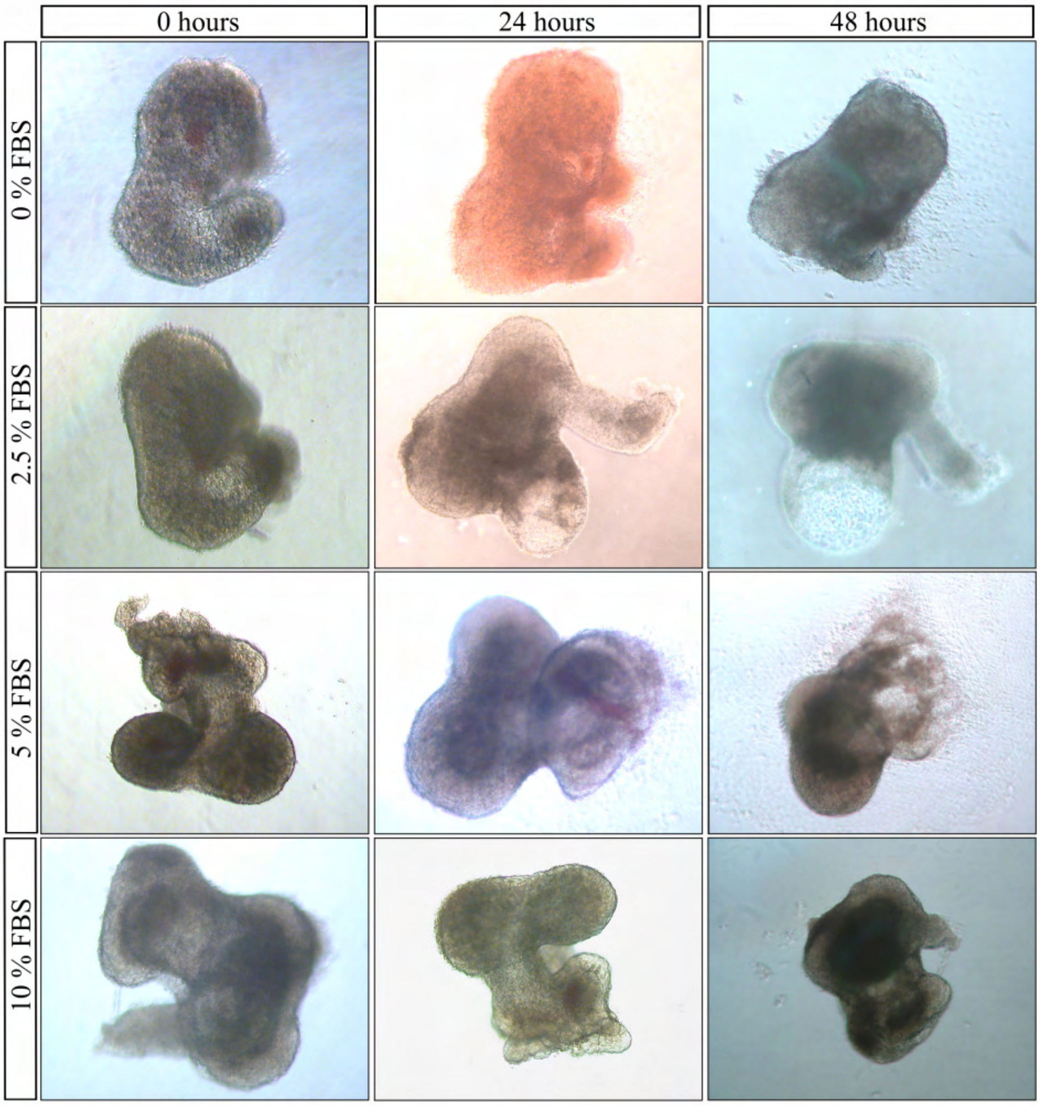

Fig. 2.6. Embryonic hearts isolated from mouse embryos at E 9.5 immediately after isolation, 24 and 48 hours in culture in medium containing different amounts of serum as well as in serum free medium.

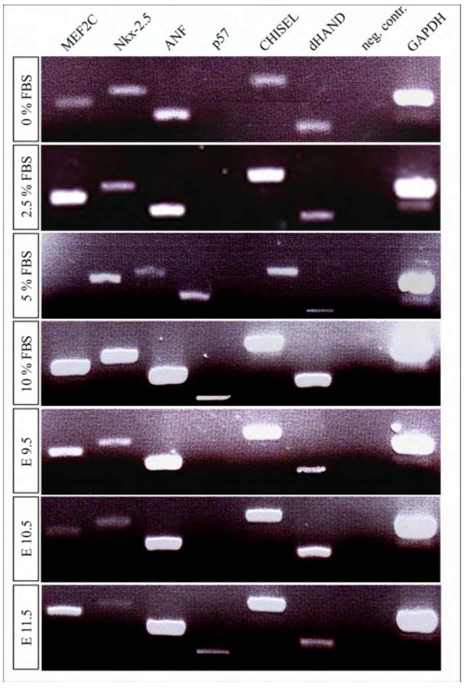

Fig. 2.7. RT-PCR analysis of E11.5 heart cultured *in vitro* in comparison to freshly isolated embryonic hearts at different stages.

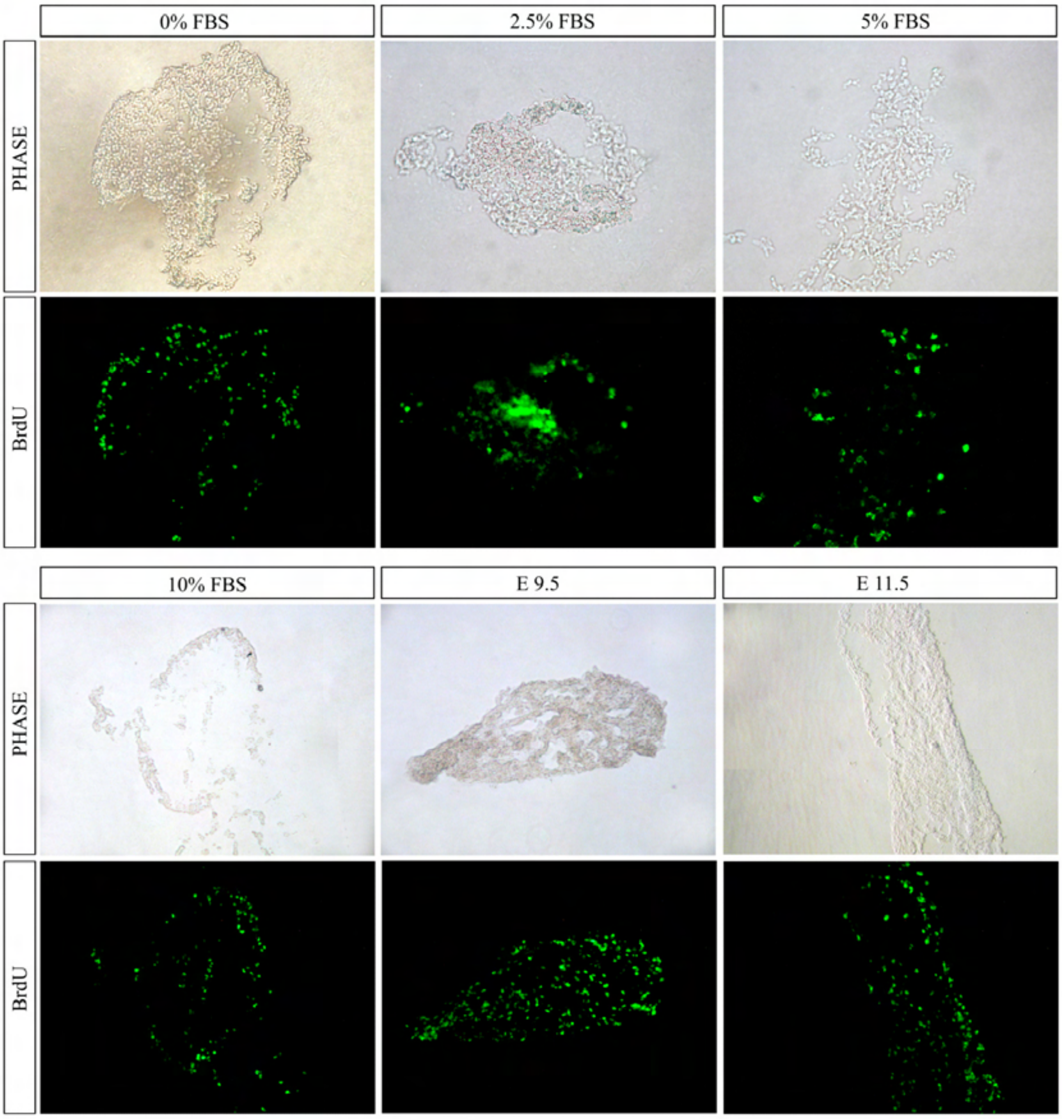

Fig. 2.8. Comparison of BrdU incorporation between in vitro cultured embryonic hearts and in vivo injected BrdU followed by embryonic heart isolation, sectioning and signal detection. Similar rate of proliferation was observed.

In addition, embryonic hearts were infected with adenovirus carrying the GFP cassette to label the epicardial layer (kindly provided by Dr. H. Ebelt). Twenty-four hours after infection expression of GFP was monitored by fluorescence microscopy (Fig. 2.9A). Next, infected embryonic hearts were embedded in the agarose type IX-A (Sigma) followed by cutting into 30-40µm thick sections using a Vibratom (Leica). Sections of embryonic hearts were placed onto cell culture plates coated with growth factors reduced Matrigel^{TM} (BD Clontech) and grown in the same conditions like whole embryonic hearts. Embryonic heart slices were documented daily as shown in Fig.2.9B-D and the culture was carried up to 10 days.

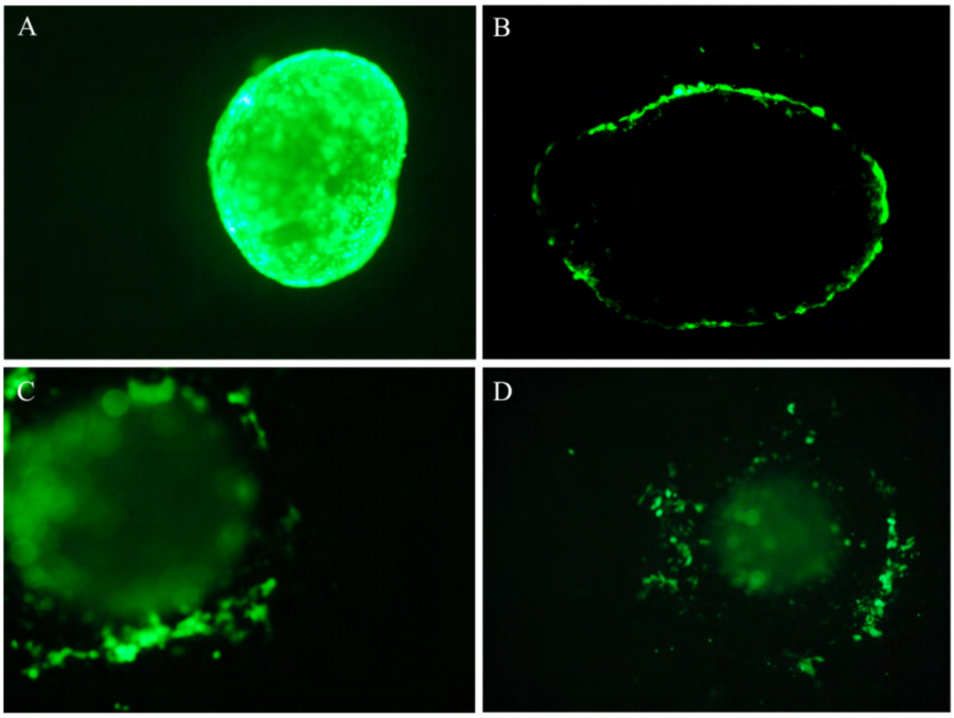

Fig. 2.9. Panel A- *in vitro* labeling of E11.5 embryonic heart epicardium with GFP expressing adenovirus (green). Panel B illustrates the infected epicardial layer directly after sectioning, panels C and D spreading of infected cells after 48 and 72 hours pi (24 and 48 hours after sectioning), respectively. Note discontinuous green layer and increased in the number of GFP positive cells.

2.2.26. Overexpression of BMP10 using the baculovirus/insect cell system

All methods used and described below are a combination of published baculovirus/insect cells protocols (O´Reilly et al, 1992; King et al., 1992; BD Pharmingen Baculovirus Procedures and Methods Manual).

2.2.26.1. Generation of the expression construct

Full length human BMP10 cDNA was PCR amplified with specific primers including Pst I/XmaI restriction sites and cloned into the pCR2.1-Topo vector (Invitrogen) followed by sequencing. After sequence verification, BMP10 cDNA was subcloned into the pVL1392 transfer vector. The pVL1392 vector contains the polyhedrin gene locus of the *Autographa californica* nuclear polyhedrosis virus (AcNPV), but lacks part of the polyhedron gene coding sequence. Although the polyhedron is not essential for virus replication in cell culture, it is responsible for a visible plaque characteristic-the presence of polyhedral occlusion bodies in the nucleus of infected cells (O'Reilly et al, 1992).

2.2.26.2. Routine sub-culturing of the Sf9 cell line in monolayer culture

The Sf9 cell line derived from *Spodoptera frugiperda* (Fall army worm) was cultured in monolayer in 10% FCS supplemented TNF-FH medium (BD Pharmingen) with gentamycine (50µg/ml) in a humidified incubator at 27°C until cells reached confluence, without CO_2 supplementation. For sub-culturing, cells were dislodged by rapidly pipetting medium over the cells. Cells were counted and dependent on the assay Sf9 cells were plated at particular densities as indicated below.

Assay	Plate size	Number of cells per assay	% Confluent
Transfection	60 mm	2.0×10^6	~60%
End-point Dilution Assay	96 well plate	1.0×10^4	~30%
Plaque Assay	100 mm 35 mm	6.2×10^6 1.0×10^6	~70% ~70%
Viral Amplification	100 mm	5.0×10^6	~70%
Protein Overexpression	100 mm	5.0×10^6	~70%

2.2.26.3. Co-Transfection of Sf9 cells

Insertion of the BMP10 gene into a baculovirus genome was achieved by homologous recombination between BMP10-pVL1392 transfer plasmid and viral DNA in Sf9 cells. The liposome mediated co-transfection method of BMP10-pVL1392 and linearized BaculoGold AcNPV viral DNA was carried according to the manufacture's instructions. Linearized viral DNA contains lethal deletion in the polyhedrine gene that can be complemented by recombination with the transfer plasmid, thus only recombinant viruses form plaques (O'Reilly et al, 1992). Simultaneously, co-transfection of control transfer plasmid XylE-pVL1392 (positive control) with BaculoGold DNA and infection with wild-type AcNPV virus was performed. Medium containing virus was harvested 4 days post transfection.

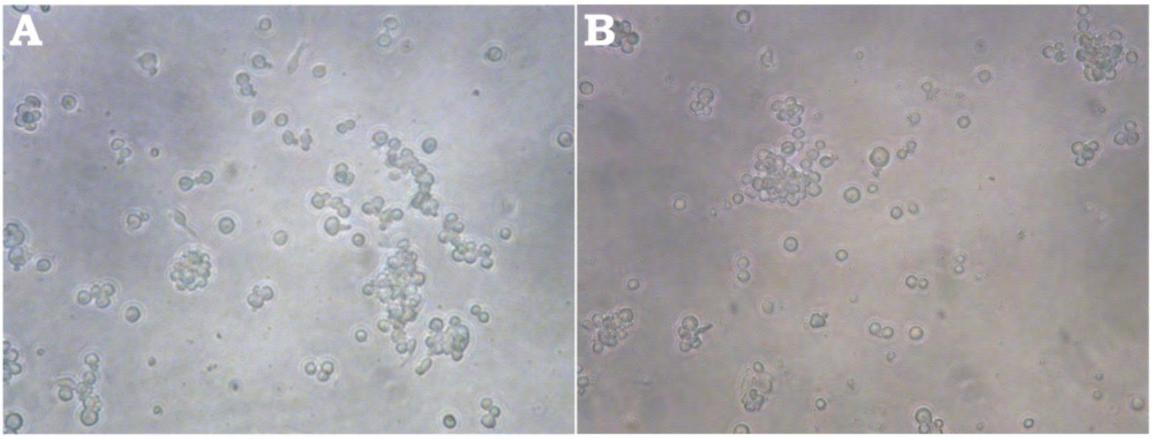

Fig. 2.10. Representative images of Sf9 cells co-transfected with BMP10-pVL1392 (A) or control XylE-pVL1392 (B)..

2.2.26.4. Plaque assay

The plaque assay was performed to titer, separate and purifies individual recombinant viruses. Usually, 1.0 x 10^6 cells were seeded on a 35 mm dish and grown overnight at 28°C. The log (1 in 10) dilution series in the range 10^3 to 10^8 of co-transfection supernatant (medium containing virus) were prepared. TNM-FH growth medium was removed from the cells and cells were overlaid with 100µl at the appropriate dilution. Plates were rocked gently for 1 hour at room temperature. Next, the inoculum was removed and cells were covered with agarose overlay (5% low melting agarose in 2x Grace's medium). Cells were incubated at 28°C for 4-5 days until plaques developed. Plaques were more easily visualized by staining the monolayer with neutral red (Sigma) solution (0.025% w/v in PBS). The staining solution was applied on the agarose overlay followed by incubation at 28°C for 1 hour. Then, the staining solution was removed and dishes were inverted upside-down and stored at room temperature for 2 hours in the dark. Plaques appeared as clear patches in a background of red, living cells. Individual plaques were picked for the further the virus amplification. Usually 10-50 plaques were picked. Plaque of agarose was taken up with Pasteur pipette and placed in 0.5ml TNM-FH growth medium. Virus particles were released from the plaque by vortexing followed by overnight incubation at 4°C with gentle shaking.

2.2.26.5. Amplification of virus and preparation of high-titer working stock

Sf9 cells were seeded on 150mm plates at $5x10^6$ and incubated 2 hours to attach. Next 250µl of virus inoculum from purified agarose plaque was applied to growth medium. Infected cells were grown for four days. Then supernatant was harvested followed by centrifugation to remove cellular debris and the next round of amplification was performed until a high titer stock, i.e. $1x10^8$ pfu/ml was obtained. After each step of amplification the virus titer was determined by plaque assay and end-point dilution method.

2.2.26.6. End-point dilution assay

Sf9 cells were diluted to a final concentration of $1x10^4$ and 100µl aliquots of the cells were seeded into a 96 well plate. Tenfold serial dilution of the amplified virus stock was prepared (10^{-3} to 10^{-8}) and 10µl of each dilution was added per well. The end-point dilution assay was always performed in triplicates, and each dilution was applied to ten wells. Additionally, uninfected controls were included in the experiment. Cells were incubated at 28°C in humidified environment. After 5-7 days each well was examined for virus infection. The total number of positive and negative wells for each virus dilution was counted and the virus titer was calculated using the method of Reed and Muench, as described by King and Possee (King and Possee, 1992).

2.2.26.7. Detection of recombinant virus and overexpressed BMP10 protein

To prove that recombination between BMP10-pVL1392 transfer plasmid and linearized baculovirus DNA had occurred and BMP10 was transcribed in infected Sf9 cells. The RT-PCR reaction on RNA isolated from 10 clones separated by plaque assay was performed. RNA was isolated from transfected Sf9 cells using the TRizol reagent and RT-PCR was done as already described with specific primers. The same clones were used for protein isolation to check protein expression by Western Blot. Additionally, as the secretion sequence was included in BMP10 cDNA cloned into the transfer vector, the supernatant of cells infected with high titer virus for BMP10 overexpression was collected and the presence of the secreted protein was monitored by Western Blot. Fig. 2.11 illustrates the results of RT-PCR analysis of BMP10 transcription on example of the 7 clones selected plaques/clones as well negative and positive controls. The lower panels in Fig. 2.11 show that BMP10 protein is efficiently expressed in Sf9 cells, however, it is not secreted to the medium (supernatant). This phenomenon of ignoring the secretion leader sequence is well known and described (reviewed by O’Reilly et al., 1992).

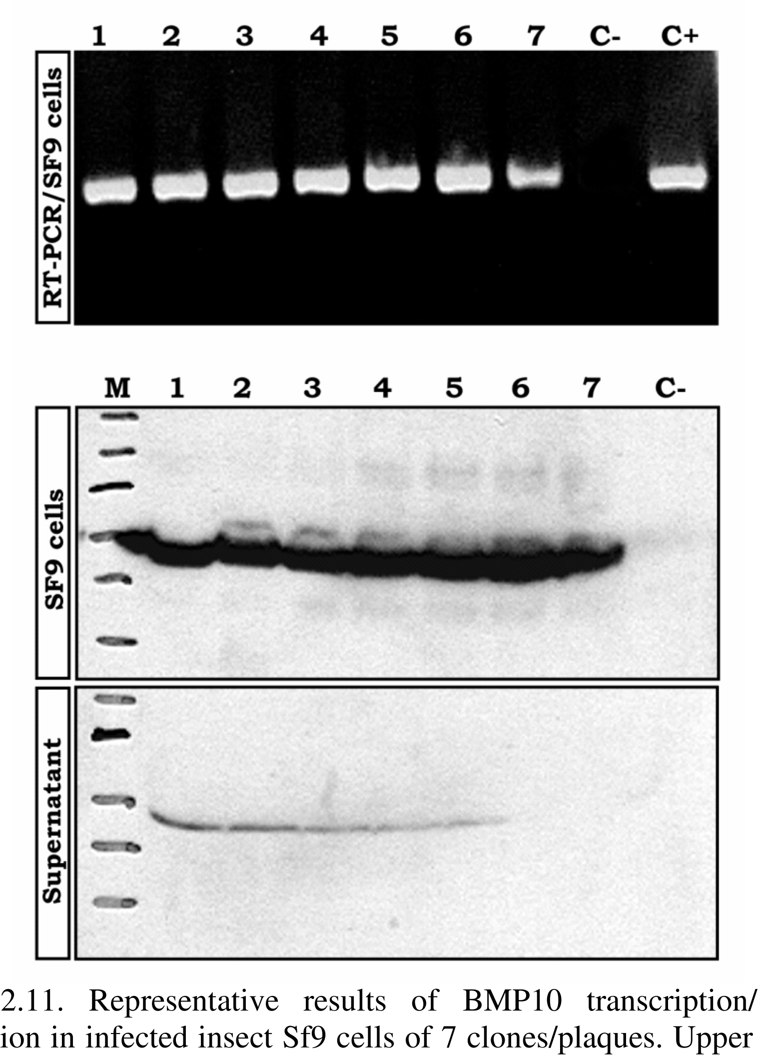

Fig. 2.11. Representative results of BMP10 transcription/expression and secretion in infected insect Sf9 cells of 7 clones/plaques. Upper panel- RT-PCR analysis with BMP10 specific primers proved transcription of the foreign gene. C+ positive control, i.e. PCR on the BMP10-pVL1392 plasmid. C- negative control, RNA and proteins isolated from SSf9 cells infected with wild-type AcNPV virus. Lower panels- Western Blot analysis of BMP10 expression and secretion in BMP10-baculovirus infected Sf9 cells. Proteins and supernatant

were prepared from the same clones as for RT-PCR analysis. The marginal signal in the supernatant in case of 4 clones is most probably a result of BMP10 protein release from dead cells and not due to recognition of the secretion sequence.

2.2.27. Microscopy

Stained sections and cells were documented using Leica system: DFC300Fx camera connected to DMRB microscope.

2.2.28. Statistics

Unless otherwise stated all data are means ± SD. Statistical analysis was performed using Exel software (Microsoft). Student's t tests were used. Data were considered significant when $p<0.05$.

3. Results

3.1. BMP10 expression during mouse embryonic development and in the adult heart

Detailed and careful analysis of BMP10 expression was a prerequisite for further experiments, hence in situ hybridization was performed. Antisense and sense riboprobes were synthetised on the plasmid containing pro-region of BMP10 (generous gift from Dr. H. Neuhaus) linearized with BamHI and EcoRI, respectively and specificity was confirmed by whole mount in situ hybridization on mouse embryos at E10.5.

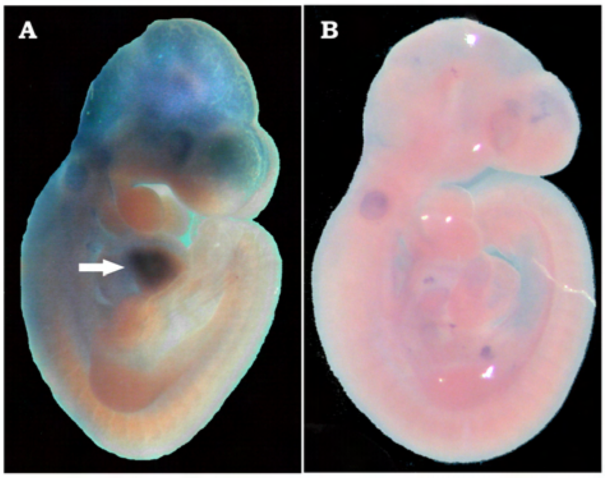

Fig. 3.1. Whole-mount in situ hybridization with antisense (A) and sense probe for BMP10 (B). Expression is detectable only with the antisense riboprobe in the developing heart (arrow, blue label).

As shown in Fig.3.1, the antisense probe detects BMP10 transcripts only in the developing heart, while the sense probe gives no signal. In adult tissues, RT-PCRs results (Fig. 3.2A) revealed the BMP10 transcript only in the heart. To further investigate the localization of BMP10 transcripts within the adult murine heart, in situ hybridization analysis on paraffin embedded tissue slides was used. Twelve µm thick sections were hybridized with the antisense digoxygenin labeled BMP10 probe. A strong and obvious expression of BMP10 was identified in the right atrium. The majority of the cells in the trabeculated wall of entire right atrial appendage were positive for BMP10. Both atrial cardiomyocytes and interstitial cells in this part of the heart expressed BMP10. Transcripts were also detectable in the region neighboring the interatrial septum. The detailed analysis revealed lack of BMP10 expression in the ventricular part of the heart, left atrium and left atrial appendage.

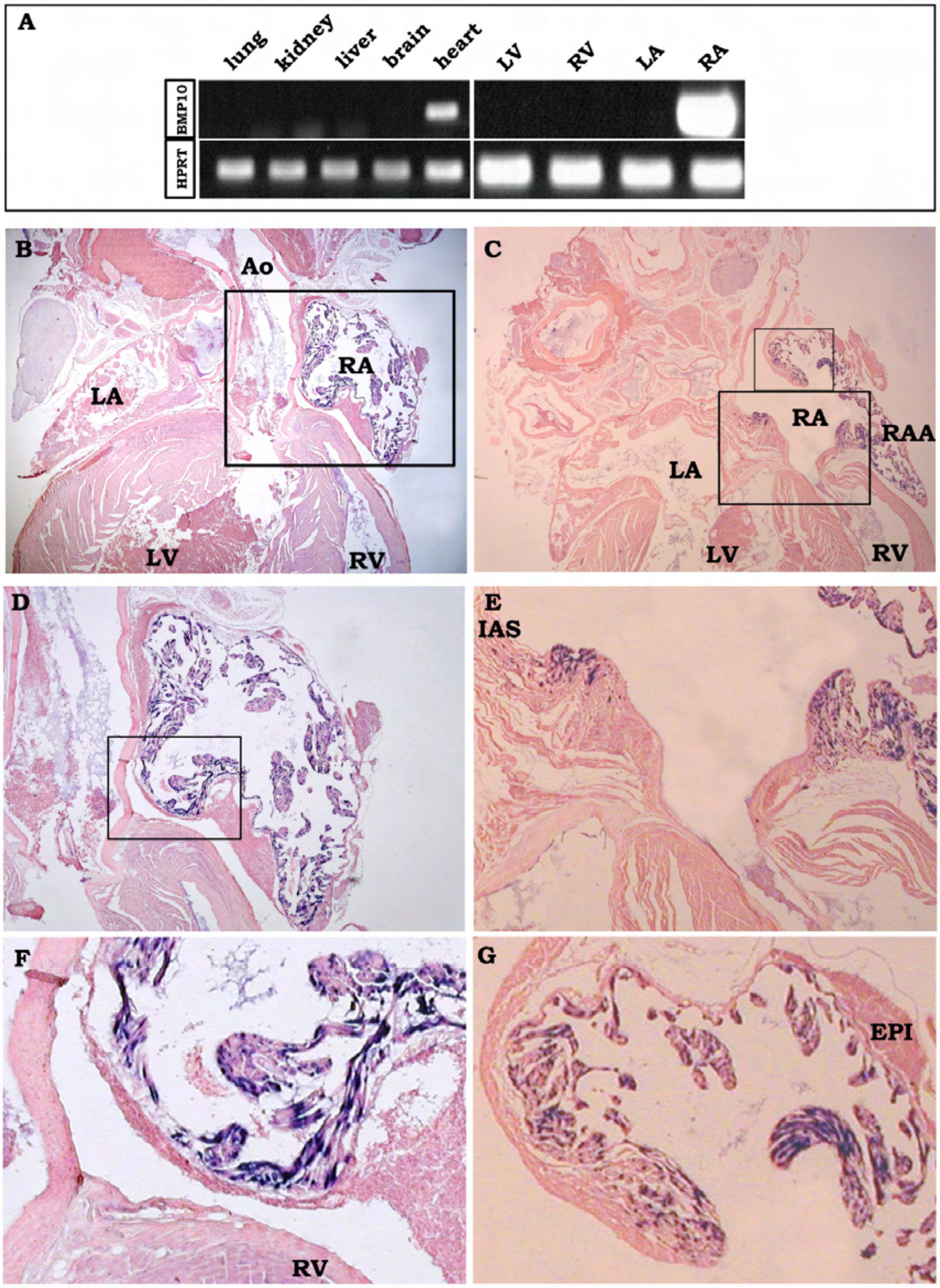

Fig. 3.2. (A) Expression of BMP10 in adult mouse tissues is confined to the heart as revealed by the RT-PCR analysis. Within the heart the PCR product is exclusively localized in the right atrium. (B-G) In situ hybridization of the BMP10 riboprobe on paraffin embedded heart tissue sections (blue label) confirms the RT-PCR results. Transcripts are detectable in the right atrium (RA), right atrial appendage (RAA) and interatrial septum (IAS). LA, left atrium; LAA, left atrial appendage; LV, left ventricle; RV, right ventricle; EPI, epicardial leyer; Ao, aorta.

Experiments that will be presented in next chapters of this work required BMP10 expression analysis in different knock-out mice at various age and with different backgrounds. In order to verify possible age and strain dependent changes of BMP10 expression, the level of transcripts was analyzed by semi-quantitative RT-PCR. RNA was isolated from 6 weeks and 6 months old ICR and C57Bl6 mice hearts and a RT-PCR analysis with BMP10 specific primers was performed. BMP10 expression was normalized to control GAPDH PCR product (22 cycles), as shown in Fig. 3.3. The obtained results indicate a higher level of BMP10 expression in ICR than the C57Bl6 strain and additionally, an age dependent decrease was noted. However, the localization of BMP10 transcripts remains unchanged and restricted to the right atrium and seems to be not age and strain dependent as judged by the in situ hybridization results (data not shown).

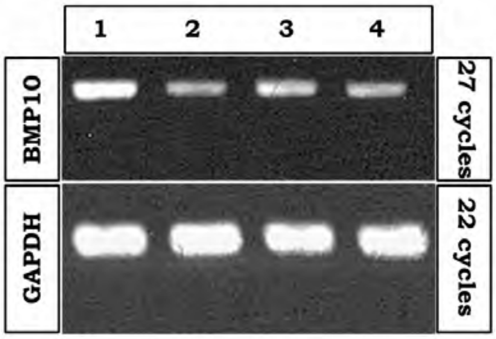

Fig. 3.3. Semi-quantitative RT-PCR analysis of BMP10 expression in 6 weeks (lanes 1 and 3) and 6 months (lanes 2 and 4) old ICR (1,3) and C57Bl6 (2,4). An equal amount of RNA was controlled by the level of the GAPDH PCR product.

3.2. A polyclonal anti-matBMP10 antibody specifically recognizes the processed mature region of BMP10

As was already mentioned, BMP10 has a leader secretion sequence. BMP10 is synthesized as pre-pro-protein followed by its secretion to the extracellular matrix and processing. In this case, cells expressing BMP10, identified by in situ hybridization might, but do not have to overlap with the localization of the active, mature protein and its target cells. As there are no commercially available antibodies against BMP10 it was necessary to generate such an antibody. Overexpression of the mature region of BMP10 fused to His tag in *E.coli* and purification of the protein were prerequisites for further experiments.

3.2.1. Test of antibody specificity

Detailed and careful verification of the specificity of the generated antibody was necessary to avoid artifacts in further experiments. The next chapters describe experimental approaches that were used to verify specificity and applications of the generated antibody.

3.2.1.1. Western Blot analysis

The first step of analysis required to test whether the antibody specifically recognizes BMP10, but not the His-tag fused to protein. For this reason, unrelated to BMP10 protein - 6HisG-ΔVITO1 (kindly provided by Dr. M. Mielcarek), cloned to pRSET-A vector and overexpressed under the same conditions as His-tagged BMP10 was selected. Fig. 3.4 shows the detection of 6HisG-BMP10, but not the tagged ΔVITO1 by obtained antibody.

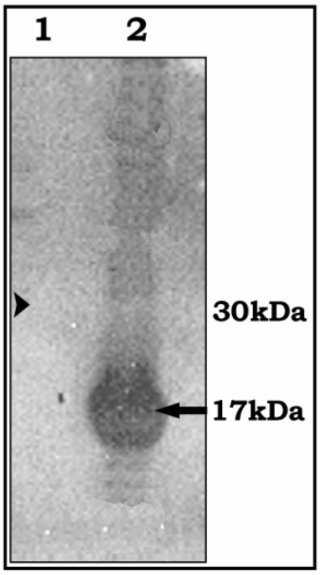

Fig. 3.4. Western Blot analysis of His-tagged VITO1 and BMP10. Polyclonal anti-BMP10 antibody specifically recognized 17kDa 6HisG-BMP10 (lane 2, arrow), but not 30kDa 6HisG-ΔVITO1 (lane 1, arrowhead).

Next, the ability of the antibody to recognize the mature region of mouse BMP10 was investigated. Proteins were extracted from the left and right atrium and nuclear, cytosolic and membrane fractions were separated. BMP10 was immunodetected with a commercially available (Abgent, Orbigen) and the newly generated antibody. The preimmune serum was used as a negative control. Western blotting of protein extracts revealed 2 bands. The approximately 40kDa band corresponds to the full length BMP10 precursor while the second band corresponds to the mature monomer with the predicted molecular mass of 12 kDa. As shown in Fig. 3.5, the generated anti-mat-BMP10 antibody was specific for the processed form of BMP10 and did not recognize the full length propeptide.

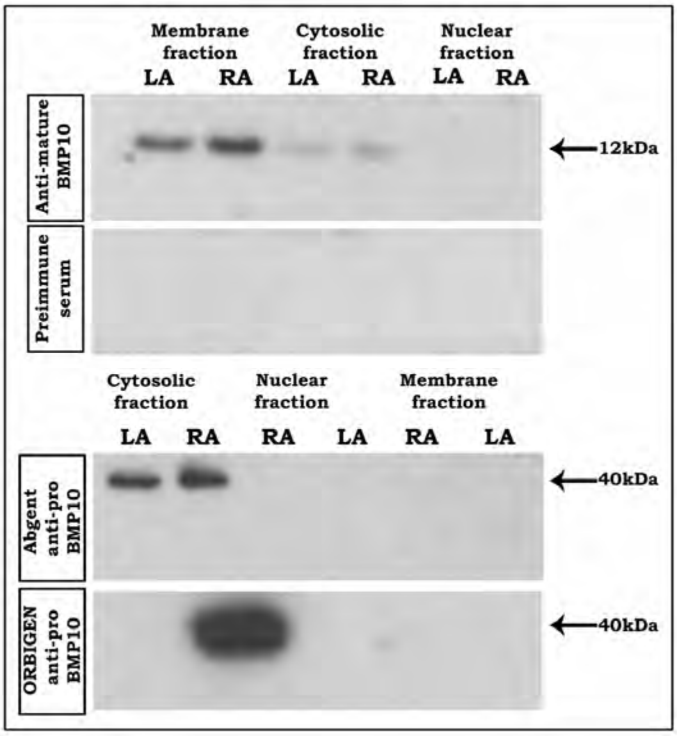

Fig. 3.5. Western Blot analysis of membrane, cytosolic and nuclear protein fraction isolated from mouse atria. The generated anti-matBMP10, control preimmune serum and two commercially available antibodies were used to detect BMP10. The mature form of the protein of predicted 12kDa was detected by the newly generated antibody (but not by preimmune serum). The Abgent antibody gave a signal of 40kDa in right and left atrium, whereas The Orbigen antibody showed the highest specificity to BMP10 precursor of approximately 40 kDa in the cytosolic fraction isolated from right atrium.

Commercially available antibodies detected only the propeptide form of BMP10. All antibodies detected the strongest signal in protein extracts isolated from right atrium.

The Orbigen antibody showed the highest specificity as indicated by the cytoplasmic detection of the BMP10 precursor in the fraction isolated from right atrium.

3.2.1.2. Immunocytochemistry

The unspecific bands, which were observed by Western Blot analysis suggested cross-reactivity of the newly generated anti-BMP10 antibody with other proteins. To test the ability of the newly generated antibody to detect BMP10 by immunohistochemistry, an in situ staining of cells overexpressing BMP10 was performed. COS1 and 293T cells were transiently transfected with the BMP10-IRES-GFP expression plasmid or empty pEGFP vector. Forty-eight hours later, cells were fixed and immunostained with anti-BMP10 antibodies and preimmune serum. Both commercially available antibodies did not detect BMP10 (data not shown) and seem to be not useful for immunohistochemistry. Preimmune serum gave also only marginal, background signal while the new anti-BMP10 antibody showed a strong staining in cells transfected with BMP10-IRES-GFP (Fig. 3.6).

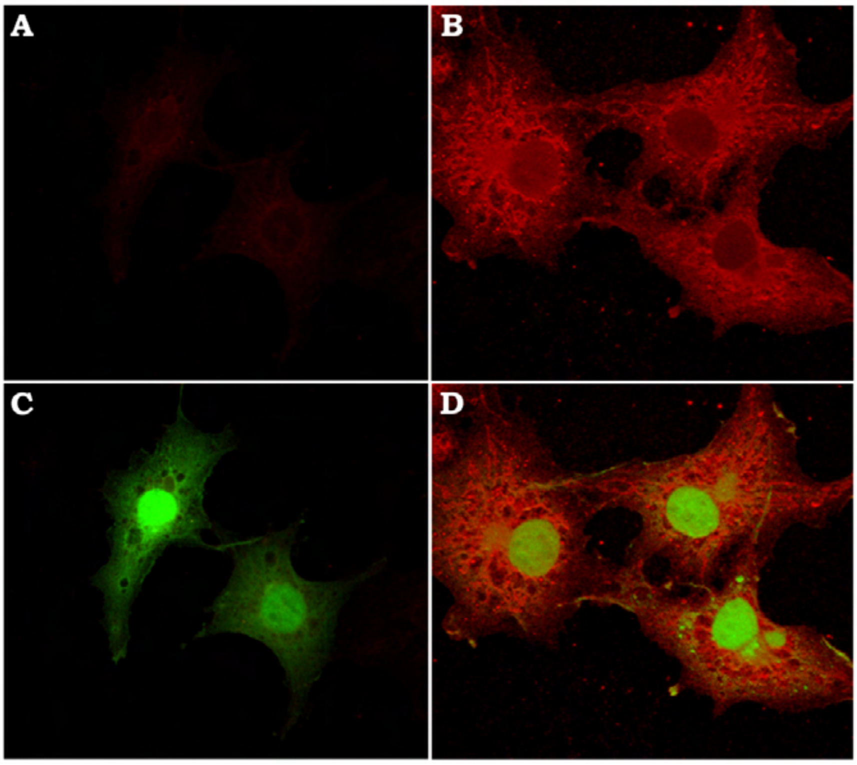

Fig. 3.6. COS1 cells transfected with BMP10-IRES-GFP (green) and immunostained (red) with control preimmune serum (A, merged C) or anti-

BMP10 antibody (B, merged D). Only the generated anti-BMP10 antibody gave a strong staining in cells transfected with BMP10-IRES-GFP (B,D).

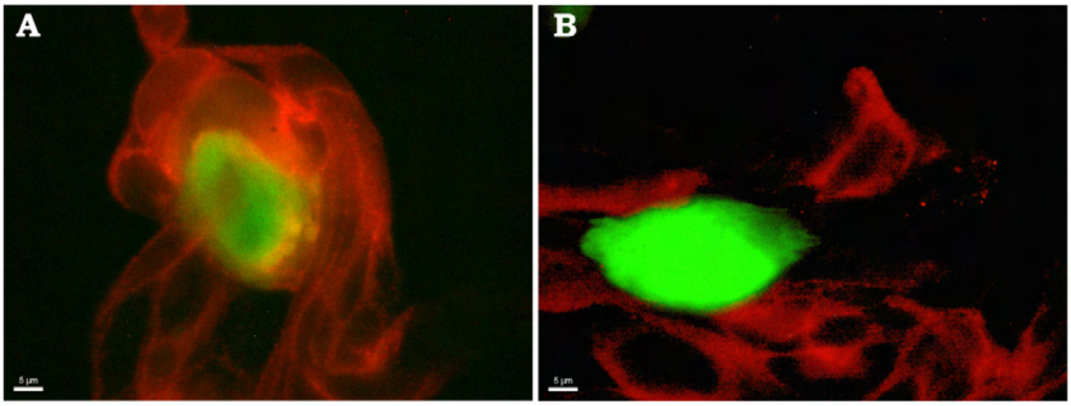

Fig. 3.7. The Anti-BMP10 antibody specifically recognizes the BMP10 protein. 293T cells transfected with the expression construct BMP10-IRES-GFP (green) and immunostained with the anti-BMP10 antibody (red) (A,B).

Interesingly, immunodetection of BMP10 in 293T cells showed a strong signal not only in transfected cells, as judged on the basis of GFP expression, but also in neighboring cells (Fig. 3.7). This might be explained by the efficient release from trensfected cell and subsequent binding to adjacent cells.

3.2.1.3. Immunohistochemistry

Since the tested antibody gave satisfactory results in transfected cells, the determination of the ability to detect the native BMP10 in tissue sections was the last and most important test to prove its specificity. Fig. 3.8 shows representative confocal images of BMP10 detection in mouse heart. A membrane localization of BMP10 in the right atrium and the right atrial appendage (Fig. 3.8 A and B, respectively) is apparent. Using the same laser set up, the left atrium and ventricles (Fig. 3.8 C and D) were examined for a signal. The relative differences in signal intensity between the examined parts were clearly visible. Since the antibody staining of BMP10 matched the in situ hybridization data it seems likely that the antibody generated against the mature region of BMP10 works reliably and specifically.

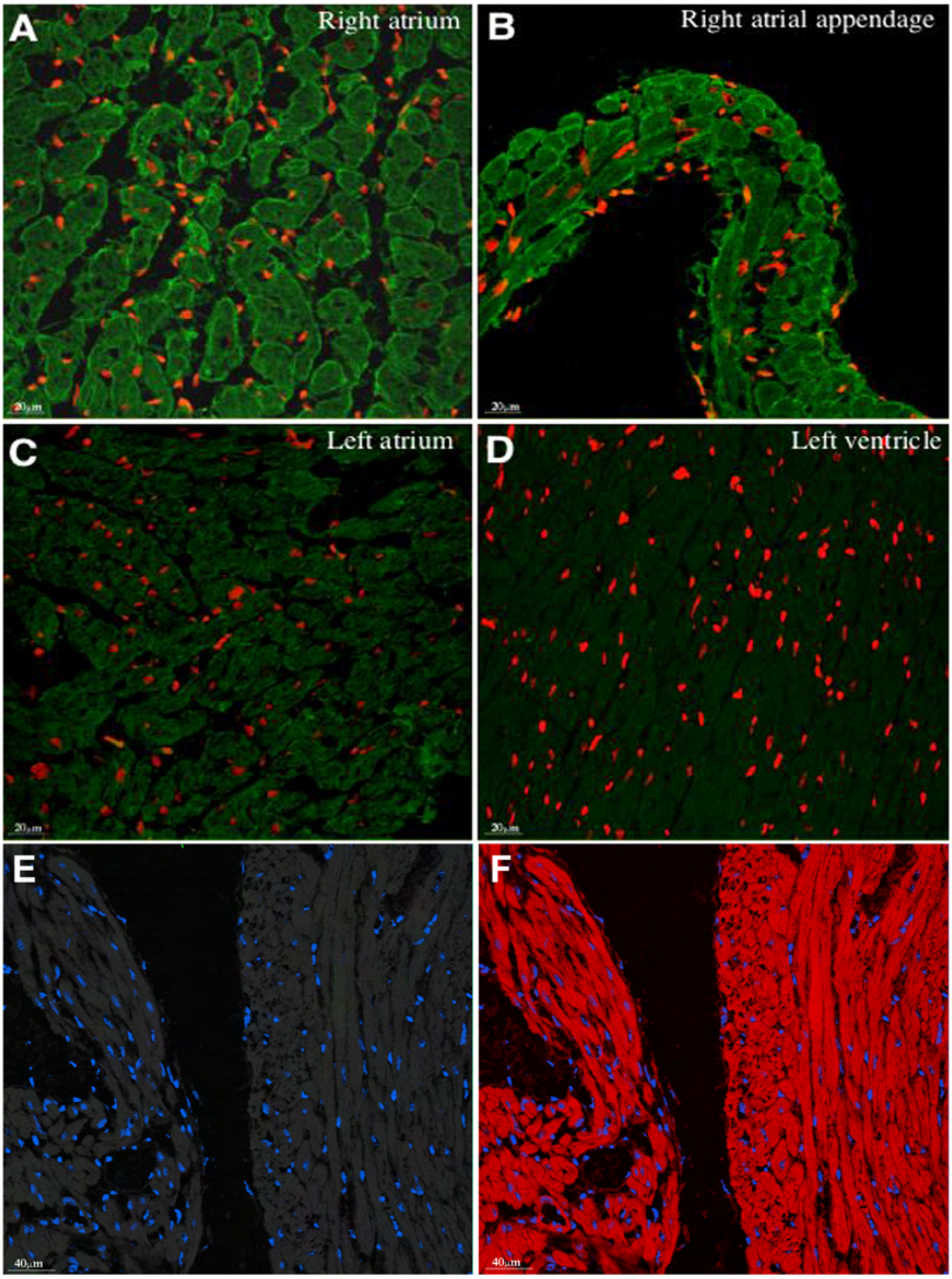

Fig. 3.8. Confocal images of mouse heart immunolabeled with anti BMP10 antibody (A-D) or preimmune serum (E) followed by detection and signal amplification using the biotin-streptavidin system (green). Staining was confined to the right atrium and the right atrial appendage and membrane localization of BMP10 is apparent (A and B). Only a marginal signal was noted in the left atrium (C) and no BMP10 positive cells were found in the ventricular part of the heart (D). Preimmune serum gives no signal (E). Panel F represents the same section like in E counterstained with phalloidin-TRITC (red). Nuclei were visualized with Draq5 (A-D red; E and F blue).

3.3. Localization versus expression of BMP10

Since the newly generated anti-BMP10 antibody allowed specific detection of the BMP10 protein, the comparison of BMP10 expression with its targeted localization became possible.

In situ hybridization with the BMP10 specific probe had already revealed that during mouse embryogenesis BMP10 expression is restricted to the trabeculated part of the developing heart. The immunohistochemical analysis of BMP10 location in mouse embryos is presented in Figs. 3.9 and 3.10.

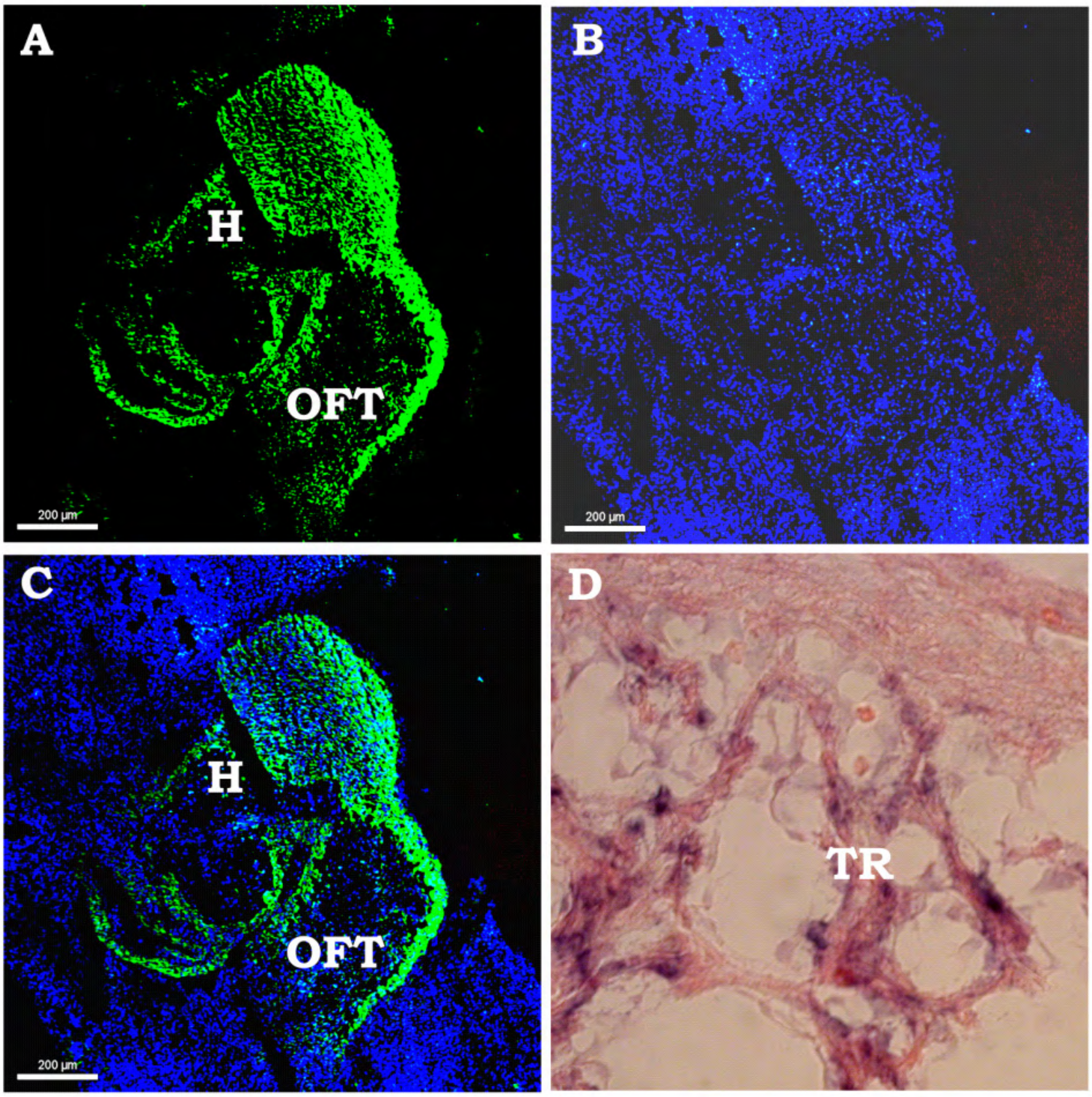

Fig. 3.9. Low magnification images showing BMP10 localization (green fluorescence, panel A) in the developing mouse embryonic heart at E11.5; (B) nuclear staining (blue); (C) merge. The signal was apparent in the trabeculated

part, but also in the non-compacted myocardium and outflow tract. Panel D- higher magnification of in situ hybridization with the BMP10 specific probe at E11.5. BMP10 transcripts (dark blue label) are detectable exclusively in trabeculae but not in other structures of the developing heart. H, heart; OFT, outflow tract; TR, trabeculae.

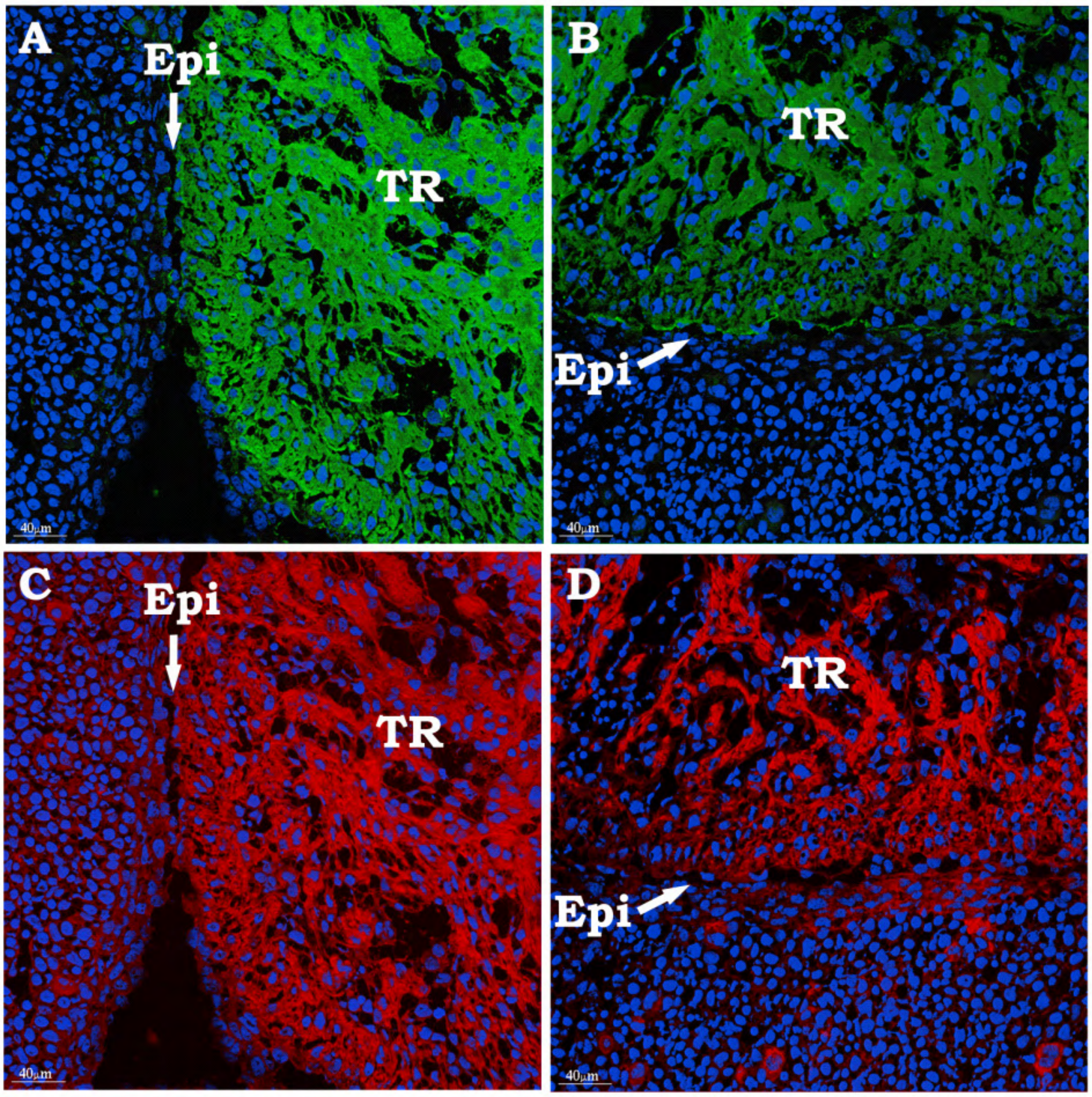

Fig. 3.10. Higher magnification of BMP10 localization (green) in embryonic heart at E11.5 (A, B). BMP10 was detected in a subpopulation of trabeculae a with gradual decrease of staining intensity in non-compacted myocardium. Note, that epicardial cells are positive for BMP10 (arrow). Nuclei were visualized by Dapi (blue) and sections were counterstained with phalloidin-TRITC (red in C and D). TR, trabeculae; Epi, epicardium.

In contrast to in situ hybridization, accumulation of BMP10 positive cells was also found in the outflow tract (Fig. 3.9). BMP10 in embryonic heart was found in trabeculated myocardium and showed the highest staining intensity compared with other cardiac structures (Fig. 3.10). At higher magnification, a gradual decrease of the staining intensity in non-compacted myocardium was clearly visible. At E11.5 of mouse embryonic development, the epicardium is apparent and also cells that constitute the fine epicardial layer were positive for BMP10.

In the neonatal mouse heart, BMP10 transcripts were no longer detectable in the ventricular part and the expression was restricted to the right atrium (Fig. 3.11 C). A fibrous layer separating atria from ventricles limits BMP10 expression within the right atrium. However, by immunostaining of BMP10, a vestigial amount of protein was detectable in ventricles (Fig. 3.11 A). The signal was also partially observed in the epicardial layer. In the right atrium, in addition to the expected membrane location, a cytoplasmic accumulation of BMP10 was found.

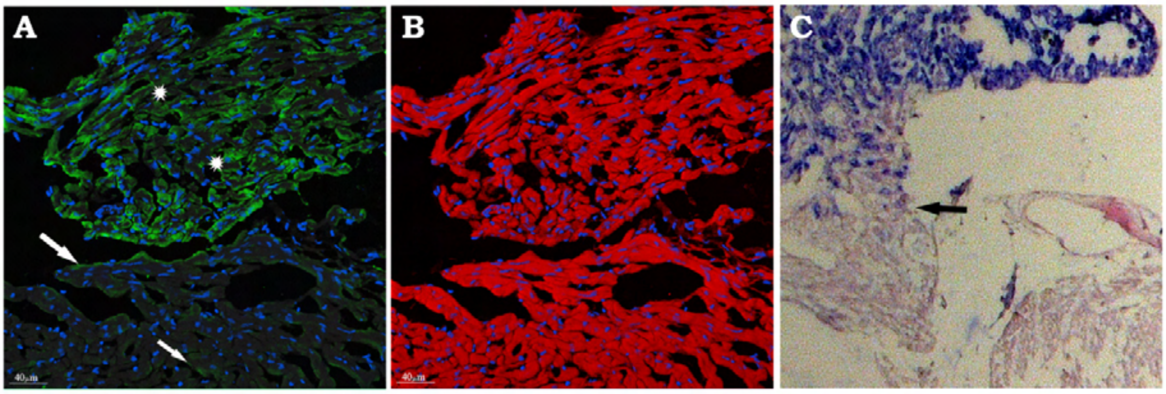

Fig. 3.11. Detection of BMP10 protein (A- green) and transcripts (C- blue) in the neonatal mouse heart. BMP10 was predominantly localized in cells of the right atrium. Asterisks indicate two types of pattern: cytoplasmic accumulation and membrane location (A). Arrows point to vestigial amount of BMP10 in the right ventricle. Nuclei were stained with Dapi (A and B- blue). Panel B represents the same section counterstained with phalloidin (red). C- In situ hybridization of paraffin embedded neonatal heart sections showed the restriction of BMP10 expression to the right atrium (blue label). The arrow indicates the fibrous ring separating atrium from ventricle.

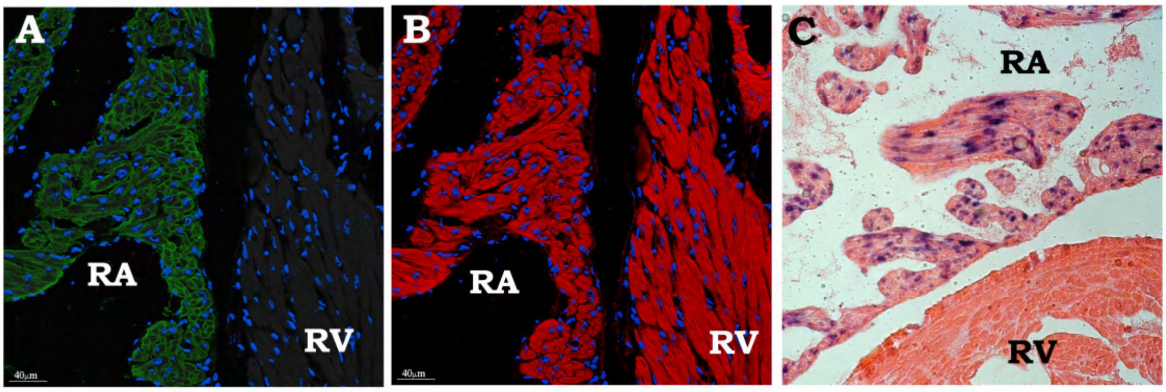

Fig. 3.12. Immunostaining of BMP10 (A-green) and localization of BMP10 transcripts (C- blue) in the adult mouse heart. Expression and localization were

restricted to the right atrium. Panel B represents the same section as A, counterstained with phalloidin-TRITC (red), nuclei were stained with Dapi (A and B- blue).

In adult mice, BMP10 protein was detectable neither in ventricles nor in the epicardium (Fig. 3.12). Additional signals were found in the tricuspid valve and in single cells around big vessels in the atrial area, which initially were not detected by in situ hybridization (Fig. 3.13).

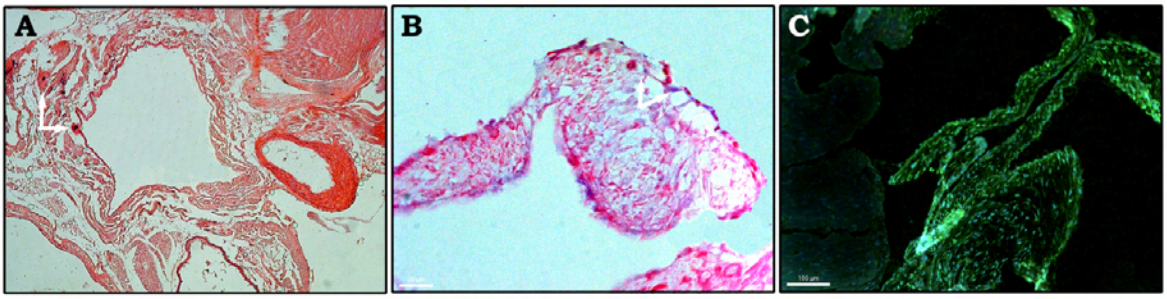

Fig. 3.13. Specific BMP10 expression and localization was found around big vessels in the atrial area (A- blue, arrows) and in the tricuspid valve (arrows in B- blue; C- green). A,B- in situ hybridization, C- immunodetection of BMP10 (green).

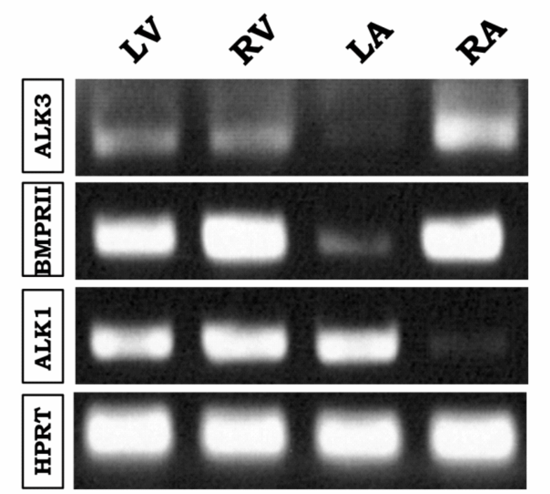

Fig. 3.14. RT-PCR analysis of selected BMPs receptors in different parts of the adult murine heart. Equal amounts of RNA used for reverse transcription were monitored by the HPRT PCR product.

BMP10, as other members of the TGFβ family, acts via receptors and for this reason the expression of bone morphogenetic proteins receptors (type I and II) in adult and embryonic heart was analyzed. RT-PCR analysis revealed comparable expression levels of Alk1 and BMPRII in the adult and embryonic heart. The ALK4 PCR product was weaker in the adult than in the embryonic heart and the opposite situation was observed in the case of ALK3. Expression of ALK6 was restricted to embryonic heart, but this receptor is not expressed in adult myocardium (data not shown). Next, the expression of selected receptors was examined in atria and ventricles of the adult heart (Fig. 3.14). RT-PCR analysis revealed higher expression levels of ALK3 and BMPRII in the right atrium, while the ALK1 PCR product was barely visible in this heart chamber.

3.4. Murine models of cardiomyopathies

The primary aim of this work was the characterization of changes of BMP10 expression in pathological hearts. Two genetic models of cardiomyopathy, i.e. Desmin knock-out (Desmin LacZ strain; generous gift from Prof. T. Braun) and 10 months old MnSOD (SOD2) heterozygous mice (generous gift from Dr. T. Loch; laboratory collection) as well two drug-induced (doxorubicin and isoproterenol) models of cardiomyopathy were investigated. The degree of pathological changes was estimated on the basis of Magnetic Resonance Imaging (MRI) analysis as well as detailed histological examination.

3.4.1. Magnetic Resonance Imaging (MRI)

Cardiovascular MRI allows the accurate evaluation of ventricular function and determination of myocardial volumes and ejection fraction (EF). In this study, Desmin knock-outs, doxorubicin and isoproterenol treated mice as well as PBS treated age and strain matched controls were measured. Fig. 3.15 shows an example of Desmin knock-out and control in coronal plane for anatomical imaging of apparent heart hypertrophy in the knock-out mouse. End-systolic and end-diastolic frames at the papillary muscle level are presented to demonstrate chamber dilation with increase of myocardial thickness.

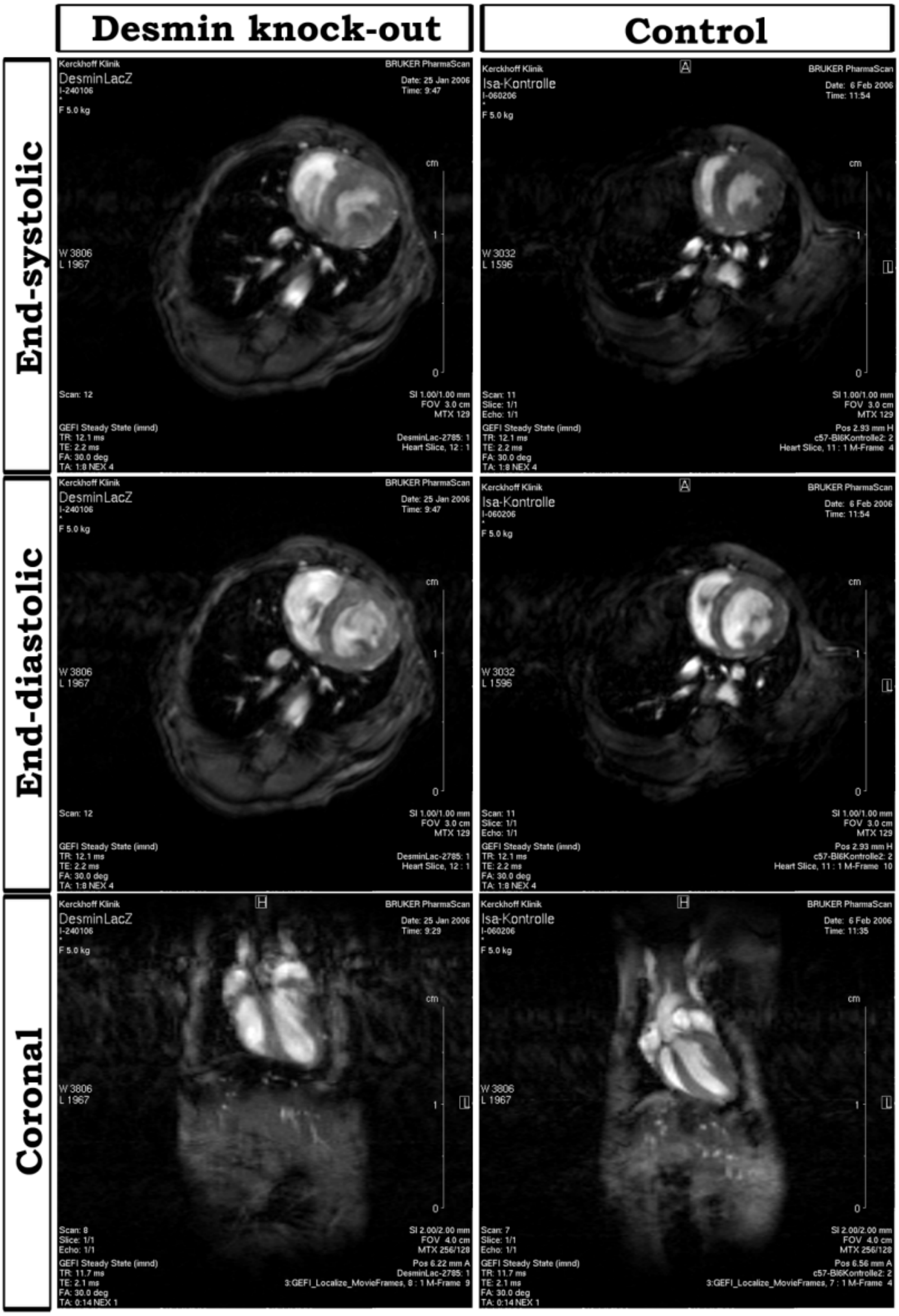

Fig. 3.15. Representative transversal and coronal MRI images of Desmin knock-out (left panel) and control (age and strain matched) mouse. Heart hypertrophy and chambers dilatation are evident in the knock-out.

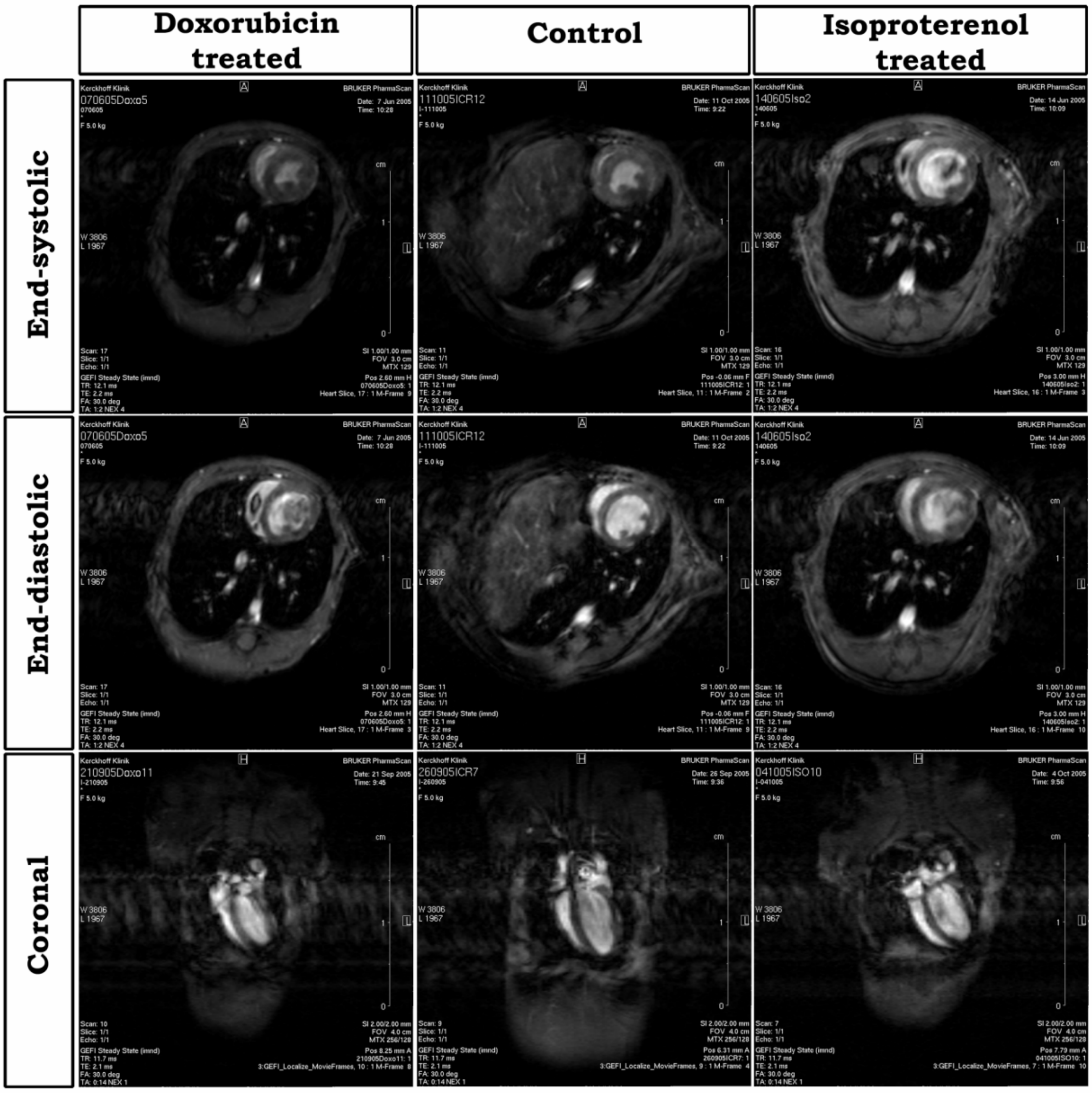

Fig. 3.16. Examples of MRI analysis of doxorubicin (left panel) and isoproterenol (right panel) treated mice. In the centre a representative control for both drugs is presented. See text for the details.

Similar sets of images of doxorubicin and isoproterenol treated and control mice are shown in Fig. 3.16. Heart hypertrophy, chamber dilation and impaired systolic function in isoproterenol induced cardiomyopathy are clearly visible.

Administration of doxorubicin did not cause a degree of heart failure as severe as treatment with isoproterenol (Fig. 3.16, left panel). However, as seen in humans, chronic cardiotoxic effects might develop even after several weeks or months after doxorubicin administration (Singal et al., 1987). To obtain a more severe cardiomyopathy, higher concentrations of adriamycin were applied. Since the higher dose was lethal for the animals, only the modest cardiomyopathy, caused by the low doxorubicin concentration was analyzed further.

A characteristic feature of dilated cardiomyopathy is the enlargement of the ventricles with impaired systolic function. In the present study, changes in ejection fraction (EF) and myocardial volumes were used as main parameters to determine heart failure. All examined models showed a decrease of ejection fraction. Desmin knock-outs (n=5) exhibited 11% reduction compared with controls (47.8%±3.34 and 53.6%±3.75, respectively). The most pronounced decrease was noted in isoproterenol treated mice. The average value of ejection fraction from five measurements was calculated as 17.3%±1.21, whereas it was 61.6%±4.15 in ICR control mice. Doxorubicin administration caused a reduction of ejection fraction by 13% in comparison to controls. A graphic illustration of changes in ejection fraction and myocardial volumes is depicted in Fig. 3.17.

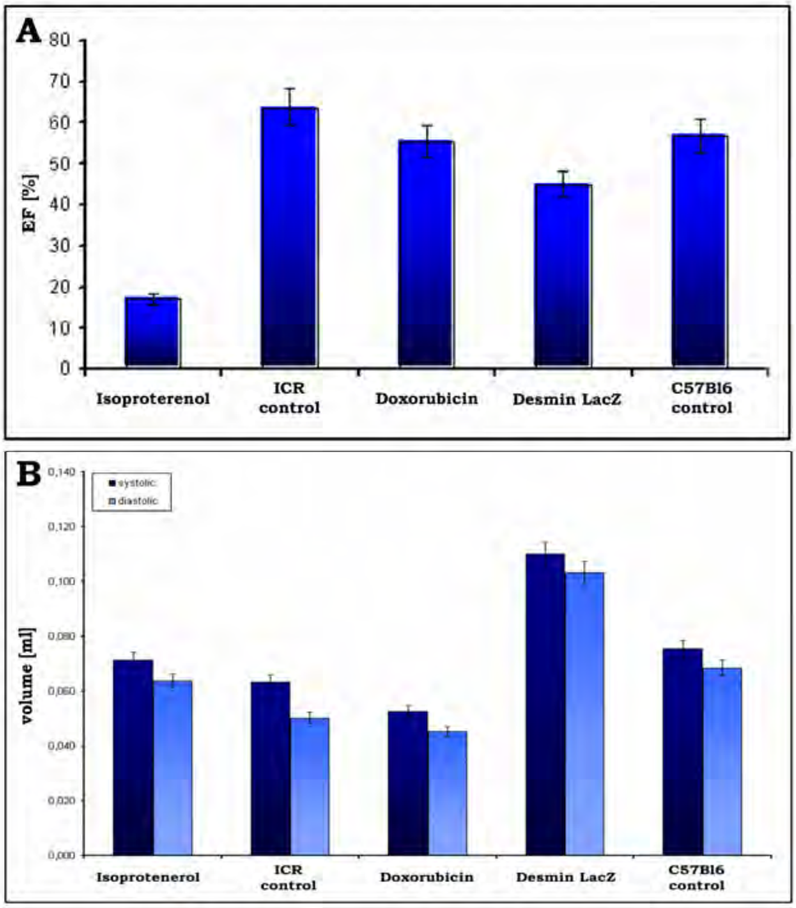

Fig. 3.17. Graphic presentation of average values of ejection fractions (EF) – panel A and myocardial volumes (B) in representative groups of all examined models.

The myocardial volumes were estimated in both systole and diastole as illustrated in Fig. 3.17 B. An increase of the myocardial volume was apparent in Desmin LacZ strain and was calculated in systole (0.110ml) and in diastole (0.103ml).

The same parameters were also determined in control C57Bl6 mice (systole: 0.075ml, diastole: 0.069ml). A comparison between both strains revealed an increase of 46% in systole and 49% in diastole in Desmin knock-out mice. In isoproterenol treated mice the changes in myocardial volume were less pronounced (increase of 11% in systole and 28% in diastole compared with ICR controls). Induction of cardiomyopathy with doxorubicin resulted in reduction of myocardial volume of 17% and 10% (0.053ml and 0.045ml, controls- 0.064ml and 0.050ml) in systole and diastole, respectively. An additional parameter, which indicates heart failure, was the heart weight (mg) to body weight (g) ratio. As shown in Fig. 3.18 this ratio was elevated in all models compared to control mice.

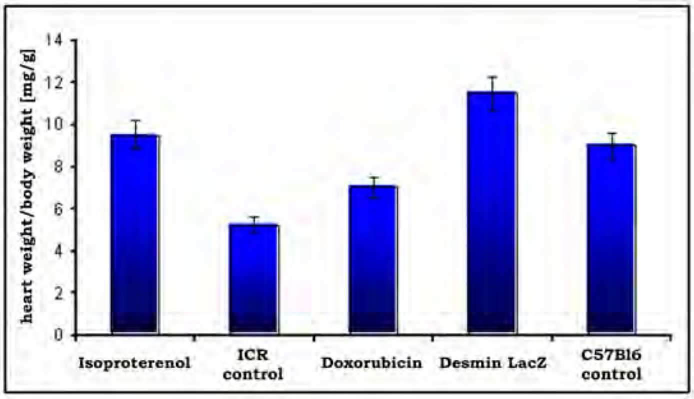

Fig. 3.18. Heart weight to body weight ratio.

3.4.2. Pathomorphological analysis of murine models of cardiomyopathy

The histopathological analysis of murine models of cardiomyopathies included the following features:

- Myofiber disarray
- Replacement fibrosis
- Cardiomyocyte hypertrophy
- Cell death

Originally, a disarray of hypertrophied and disorganized myocytes was described in humans as a unique feature of hypertrophic cardiomyopathy. However, identical histological abnormalities have been reported in the absence of myocardial thickening (Shapiro et al., 1996). A striking and consistent feature of cardiomyopathy in Desmin knock-out was myofiber disarray, which is characterized by severe disarrangement of the myocardial architecture resulting in bizzarely shaped myocytes (Fig. 3.19). A milder degree of disarray developed after doxorubicin administration. Neither SOD2 heterozygous nor isoproterenol treated mice exhibited this feature (data not shown).

Another typical pathological feature in cardiomyopathic hearts is the formation of focal fibrosis. The extracellular matrix to which cardiomyocytes are attached plays a vital role in cardiac contraction (McKenna et al., 1996). In the healthy heart collagen VI is localized around myocytes as a fine, thin sheet (Fig. 3.20).

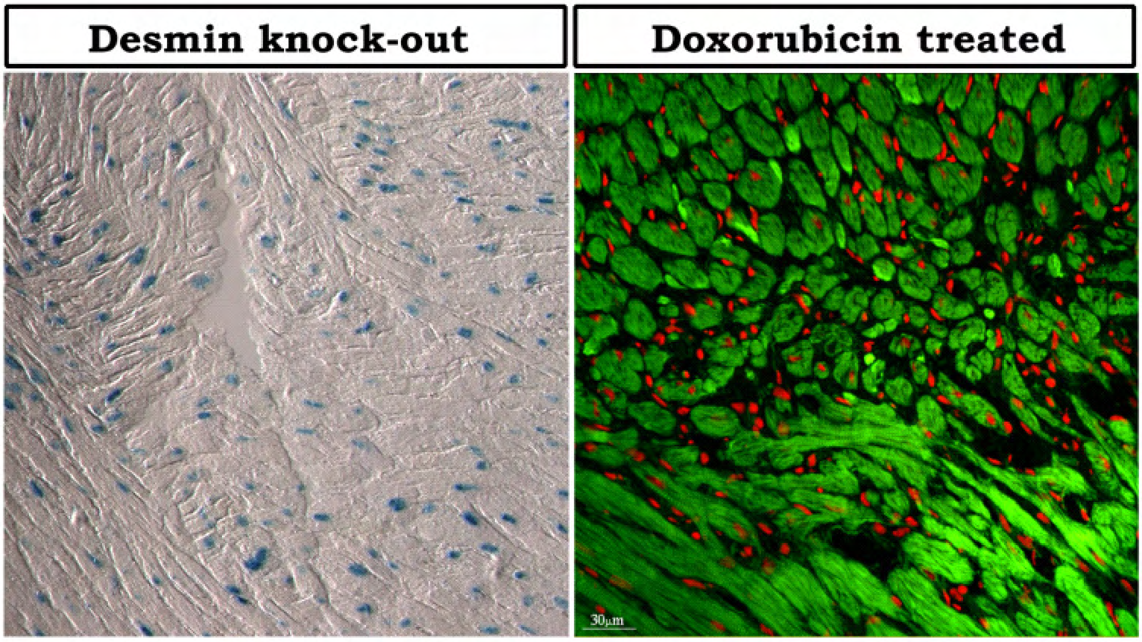

Fig. 3.19. Representative images of myocyte disarray in Desmin knock-out and doxorubicin treated mice. The left panel shows detection of LacZ in Desmin knock out. Disarray in Doxorubicin treated mice is visualized by phalloidin-FITC staining, nuclei are shown in red.

In pathological hearts an increased collagen deposition was clearly visible (as shown in Desmin knock-out and doxorubicin treated mice). Especially, the Desmin knock-out hearts showed an abundant accumulation of collagen VI in areas of replacement fibrosis. In MnSOD heterozygous and isoproterenol treated mice collagen deposits were not as pronounced as in Desmin LacZ, and resembled a modest fibrosis as seen after adriamycin administration (data not shown).

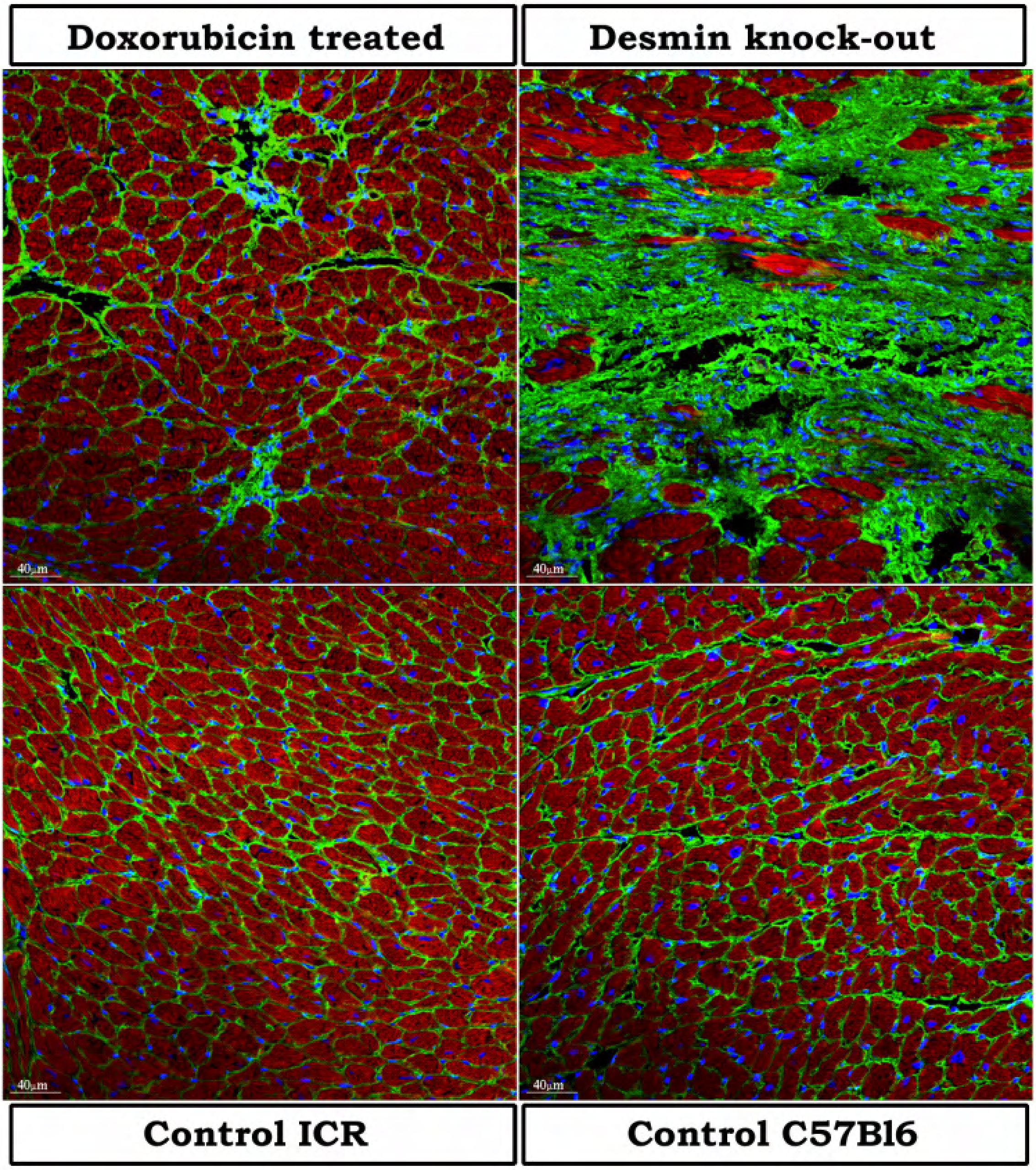

Fig. 3.20. Different degrees of increased collagen VI (green) deposition in Desmin knock-out and doxorubicin treated mice and adequate controls. Sections were counterstained with phalloidin-TRITC (red) and nuclei were visualized by DAPI staining (blue).

Basically, hypertrophy is defined as an increase in the size of the cardiac myocytes in response to pathological stimuli. As shown in Fig. 3.21, mice treated with isoproterenol showed an increase in myocyte size. Immunostaining for intercalated disk and/or membrane associated proteins is exceptionally helpful to clearly illustrate hypertrophic cardiomyocytes. Detection of plakoglobin in MnSOD heterozygous (left panel) and desmoplakin in isoproterenol treated mice (right panel- higher magnification) demonstrates moderate and severe increase in myocytes size, respectively. Induction of cardiomyopathy by doxorubicin treatmentdid not result in cellular hypertrophy, as shown in Fig. 3.22 by vinculin staining. Desmin knock-out mice exhibited the highest degree of hypertrophy among all models tested.

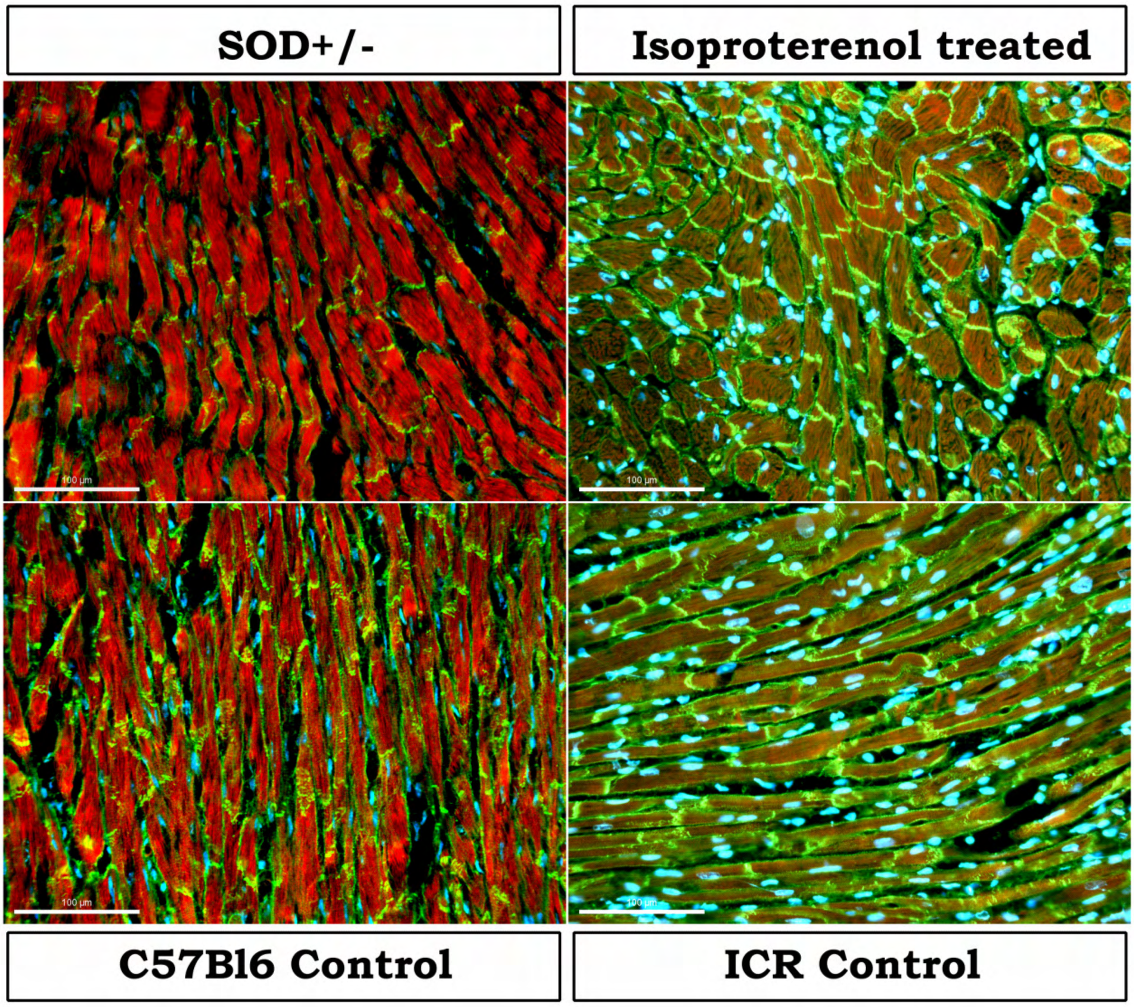

Fig. 3.21. Immunodetection of plakoglobin (green) in SOD2 heterozygous (left panel) and vinculin in isoproterenol treated mice (right panel -green) illustrates different degrees of myocyte hypertrophy in both models in comparison to adequate controls. Sections were counterstained with phalloidin-TRITC (red). Nuclei are visualized in blue by DAPI.

Numerous experimental and clinical studies have demonstrated that myocyte death is a critical determinant of cardiac remodeling and heart failure in different pathological settings, including cardiomyopathies. Two distinct types of cell death are known and recognized, namely necrosis and apoptosis (reviewed by Kostin, 2005). Necrosis is defined as an accidental type of cell death caused by ischemia, inflammatory reaction or toxic agents. In contrast, apoptosis is a pre-programmed cell suicide. To distinguish between both types of cell death tissue sections were stained for Complement9 - a part of membrane-attack complex (Homeister et al., 1992), which is a marker of necrosis and TUNEL protocol was used to detect apoptotic DNA fragmentation.

Examples of necrotic and apoptotic cells are shown in Fig. 3.23.

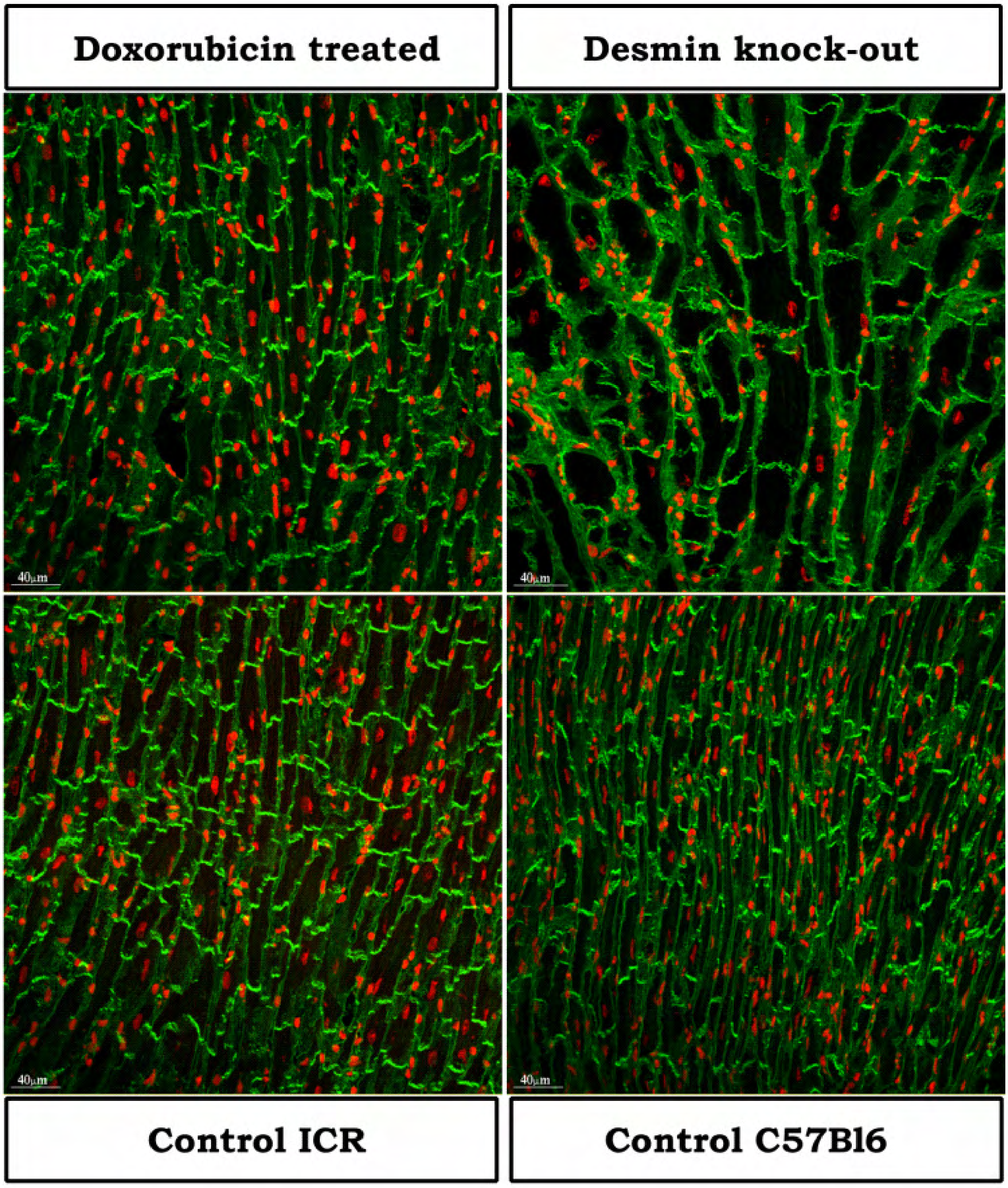
Doxorubicin treated

Desmin knock-out

Control ICR

Control C57Bl6

Fig. 3.22. Doxorubicin treated mice did not exhibit cardiomyocyte hypertrophy (left panel) as demonstrated by vinculin detection (green), while in Desmin

knock-out mice an increase in myocytes size is apparent. Nuclei are visualized in red by Draq5.

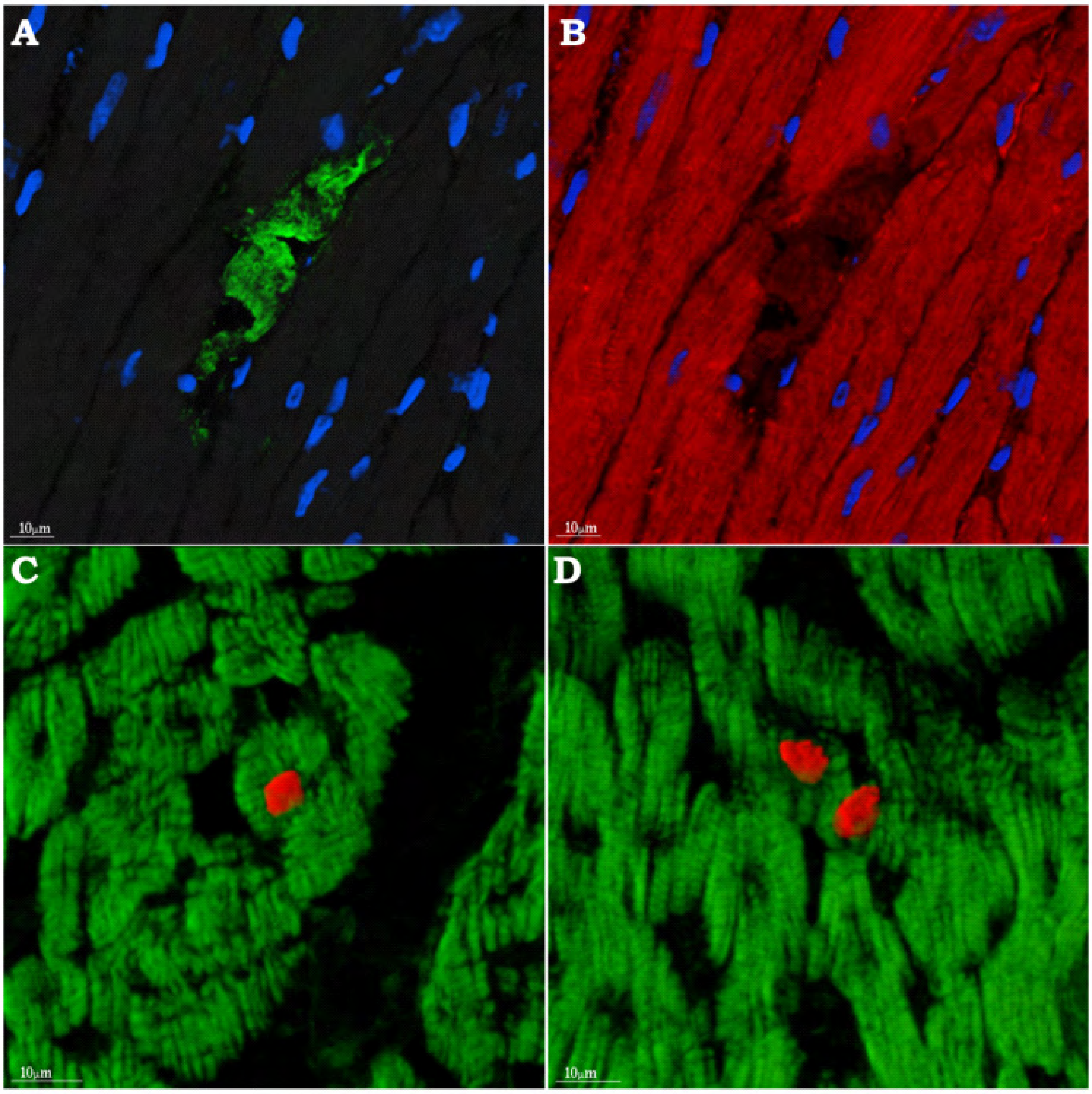

Fig. 3.23. Example of a Complement9 positive myocyte (A-green). Panel B represents the same section as in A counterstained with phalloidin-TRITC (red). Nuclei were visualized with Draq5 (blue). Apoptotic cells (C and D- red) in isoproterenol (A-C) and doxorubicin (D) treated mice. Sections C and D were counterstained with phalloidin-FITC (green).

Desmin knock-out displays the most severe cardiac phenotype among the models examined, albeit neither necrotic nor apoptotic cells were detectable (data not shown). In MnSOD heterozygous only necrosis was noted (data not shown) while isoproterenol and doxorubicin administration was inducing both types of cell death.

Many studies showed that dystrophin cleavage is associated with advanced heart failure (Kawada et al., 2005). In the healthy heart, a continuous dystrophin distribution covers the cytoplasmic face of the peripheral plasma membrane, as described by Kaprielian (Kaprielian et al., 2000) and illustrated in examples of control mouse heart in Fig. 3.24. Cells lacking this membrane-associated protein were found in doxorubicin induced DCM, but not in the other tested models. Results of the histopathological analysis are summarized in table 3.1.

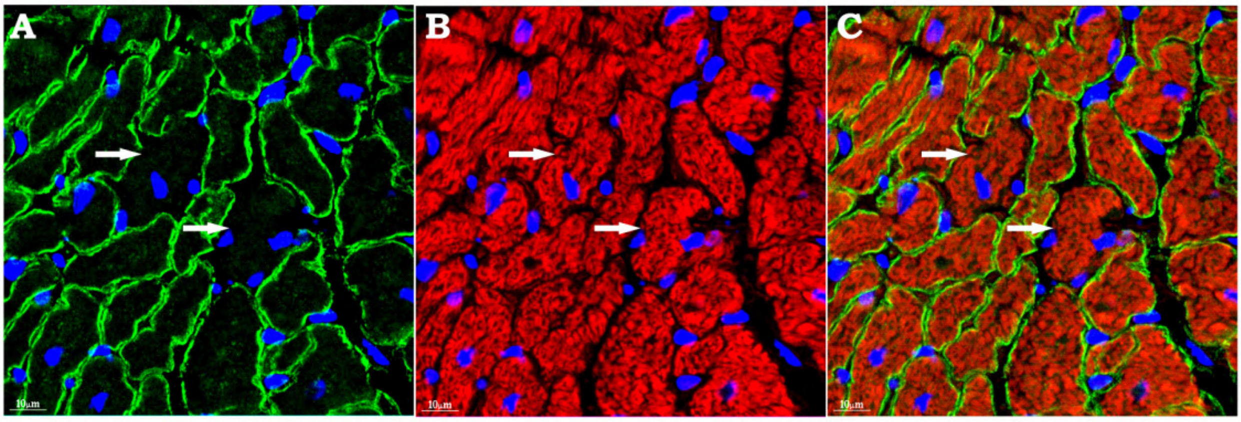

Fig. 3.24. Immunolabelling of dystrophin (A-green) in doxorubicin treated mouse heart. Arrows indicate cardiomyocytes lacking dystrophin. Panel B represents the same section counterstained with phalloidin-TRITC (red), panel C- merged images. Nuclei were visualized with Draq5 (blue).

Summary of histopathological analysis.

	Disarray	**Fibrosis**	**Myocyte Hypertrophy**	**Dystrophin lost**	**Cell Death**	
					Necrosis	**Apoptosis**
Desmin -/-	+	+	+	-	-	-
MnSOD+/-	-	+	+	-	+	-
Isoproterenol	-	+	+	-	+	+
Doxorubicin	+	+	-	+	+	+

Tab. 3.1. Results of pathomorphological analysis.

3.5. BMP10 expression in Cardiomyopathies

The main aim of the study was the determination of BMP10 expression under pathological conditions. Changes in the expression level were assessed by in situ hybridization and immunohistochemistry. To estimate the deregulation of BMP10 on the RNA level semi-quantitative RT-PCR analysis was performed and followed by Western Blot analysis for protein quantification.

3.5.1. BMP10 is ectopically expressed in ventricles of Desmin knock-out mice

As described in the previous chapter, mice lacking desmin exhibit the most severe cardiac phenotype among the tested murine models of cardiomyopathy. Detection of BMP10 transcripts by in situ hybridization revealed an ectopic expression in the ventricular myocardium of Desmin knock-out mice (Fig. 3.25). Based on the in situ hybridization result it is difficult to decide, whether this BMP10 expression occurs in cardiomyocytes or in other types of cells

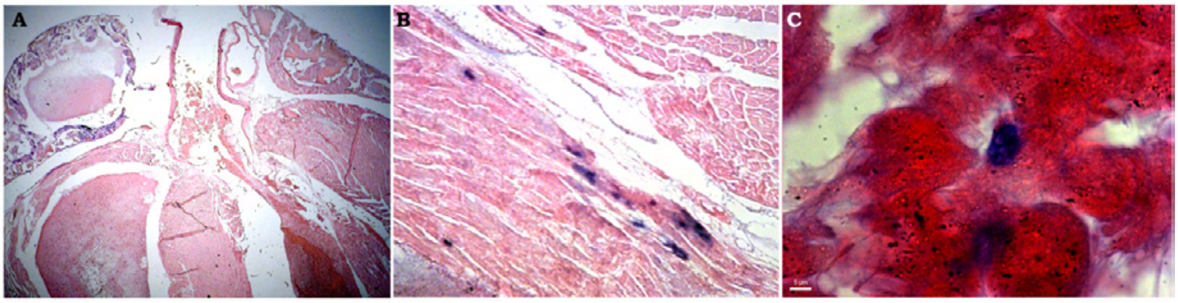

Fig. 3.25. In situ hybridization (blue label) on paraffin embedded Desmin knock-out heart slides. Panel A- low magnification; B- concentration of BMP10 expressing cells in the left ventricle; C- high magnification of BMP10 positive cells in the myocardium indicate expression in interstitial cells. Sections were counterstained with eosin.

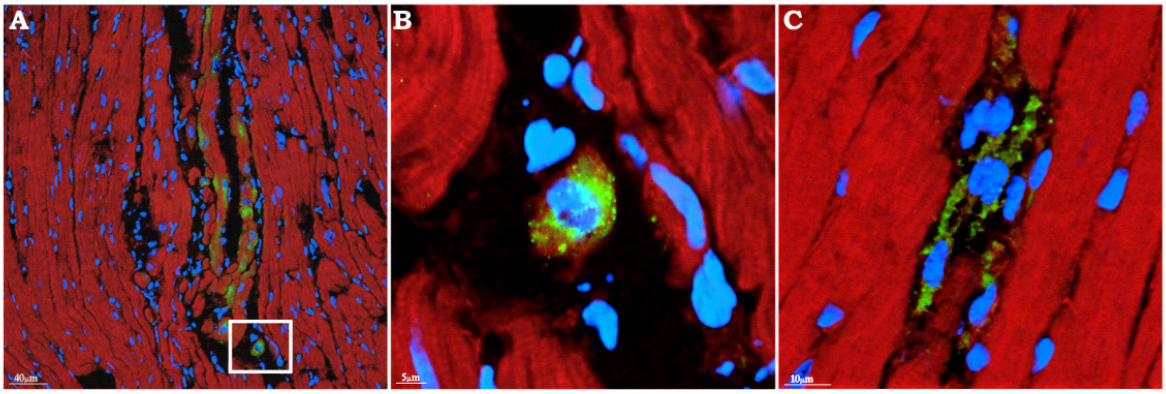

Fig. 3.26. Immunostaining of BMP10 in cryosections of Desmin knock-out heart. Panel A- BMP10 positive cells were found in or in the vicinity of vessels. B- Higher magnification of (A) showing small cell nearby an artery. Note, that the appearance of the nucleus might indicate cell division, or there are two cells close to each other. Panel C- cluster of BMP10 positive cells localized between cardiomyocytes.

To increase the level of resolution and to determine the identity of BMP10 expressing cells in the ventricular myocardium immunofluorescent stainings were employed. In addition to the right atrium, some labeling was also noted in ventricular cells (Fig. 3.26). BMP10 positive cells were found often, but not exclusively, in the proximity of vessels or even as incorporated cells in walls of coronary arteries. In Desmin knock-out mice, ventricular cells positive for BMP10 often appeared as clusters of interstitial cells. In some cases it was difficult to identify individual cells since the nuclei seemed not to be separated completely. Qualitative and quantitative changes of BMP10 protein were also found in right atrium (Fig. 3.27). An increase in the amount of BMP10 and its cellular redistribution from membrane to cytosolic accumulation was apparent. This pattern resembled the protein distribution in the neonatal atrium. The upregulation of BMP10 expression in Desmin knock-out, as judged by immunohistochemistry was also confirmed by semi-quantitative RT-PCR (Fig. 3.28) and Western Blot analysis (data not shown).

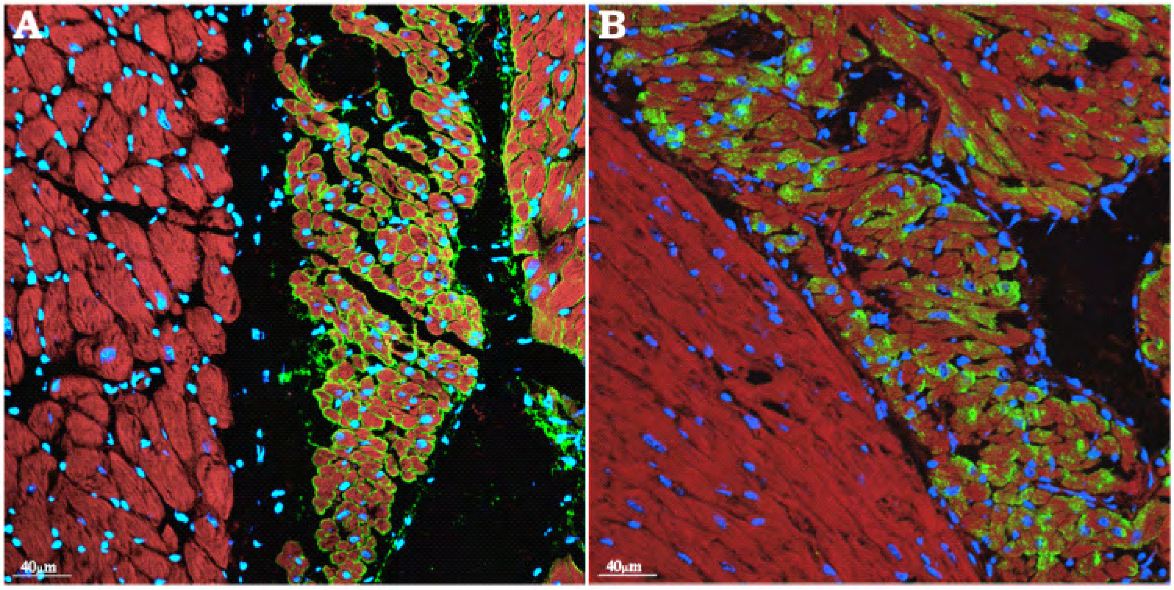

Fig. 3.27. BMP10 localization in the right atrium of WT (A) and Desmin knock-out mice (B). Note increased amount of BMP10 protein accumulated in the cytoplasm (green) in the knock-outs right atrium. Cryosections were counterstained with F-actin (red) and nuclei were visualized by Draq5 (blue).

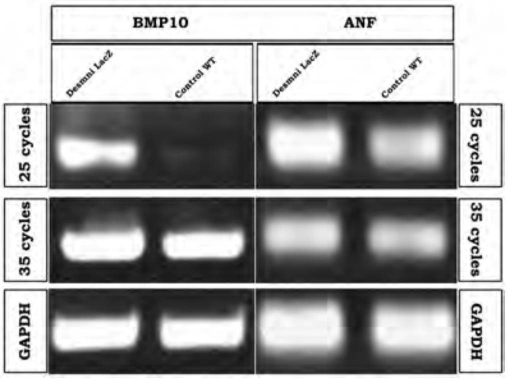

Fig. 3.28. Semi-quantitative RT-PCR analysis of BMP10 (left panel) and ANF expression (right panel) in Desmin knock-out and control WT mice. Up-regulation of BMP10 expression is apparent.

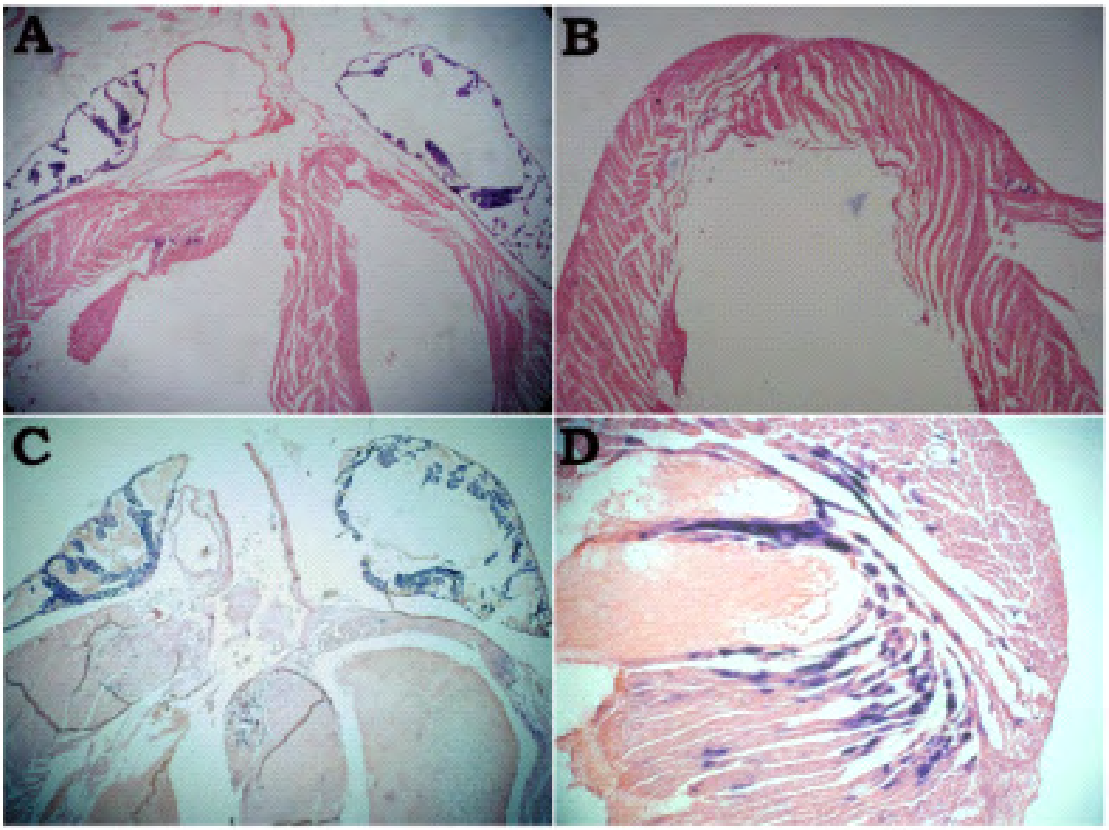

Fig. 3.29. In situ hybridization with an ANF specific antisense probe (blue label) in control (A,B) and Desmin knock-out (C,D) mouse heart. Upregulation of ANF expression in septum (A,C) and apex (B,D) of knock-out, but not in WT.

An upregulation of BMP10 expression on both, RNA and protein levels were found in Desmin knock-outs in comparison to wild type controls. Changes in ANF transcript levels, a well known marker of cardiomyopathy were also checked. As expected, higher expression of this gene was also found. This observation was confirmed by in situ hybridization with an ANF specific riboprobe (Fig. 3.29). Strong signals in the septum and apex as well as small foci in the ventricular free wall were apparent.

3.5.2. Qualitative and quantitative changes of BMP10 expression in the heterozygous MnSOD knock-out mice

The second genetic model examined for BMP10 expression was MnSOD heterozygous. Six months old mice exhibit impaired systolic function and reduced ejection fraction (data kindly provided by Dr. T. Loch, personal communication). In situ hybridization with the BMP10 antisense probe revealed a significant reduction of BMP10 expression in right atrium (Fig. 3.30) yielding a population of cells that was negative for BMP10. Furthermore, an ectopic expression of BMP10 was scored in some ventricular cells of MnSOD heterozygous mice (data not shown), but not in age and strain matched controls.

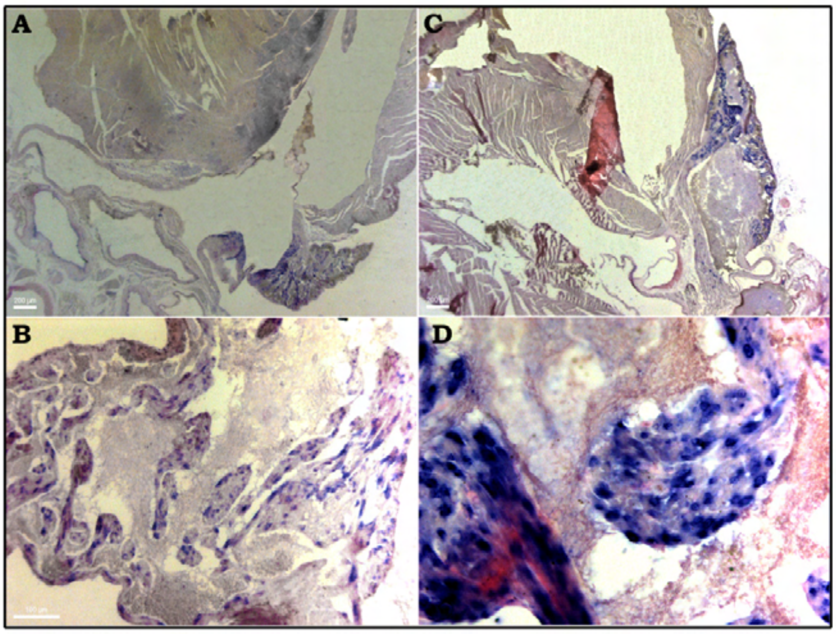

Fig. 3.30. Representative images of in situ hybridization with a BMP10 specific antisense probe in MnSOD heterozygous mice heart (A,B) and matched controls (C,D). B and D show higher magnification of right atrium of images A and C, respectively and illustrate decreased expression of BMP10 in MnSOD+/-. The signal is present in blue.

The deregulation of BMP10 transcription in the right atrium was confirmed by immunodetection of the protein. In transgenic mice, a heterogeneous pattern of BMP10 distribution was observed, as shown in Fig. 3.31. Three different types of BMP10 cellular localization were found:

1. Preserved membrane location, typical for wild type mice
2. Cytosolic accumulation of BMP10 granules
3. Absence of the signal

In ventricles, cells expressing BMP10 were detected in MnSOD heterozygous, but not WT mice. Clusters of BMP10 positive interstitial cells were found in the subepicardial layer and the myocardium (Fig. 3.31C and D).

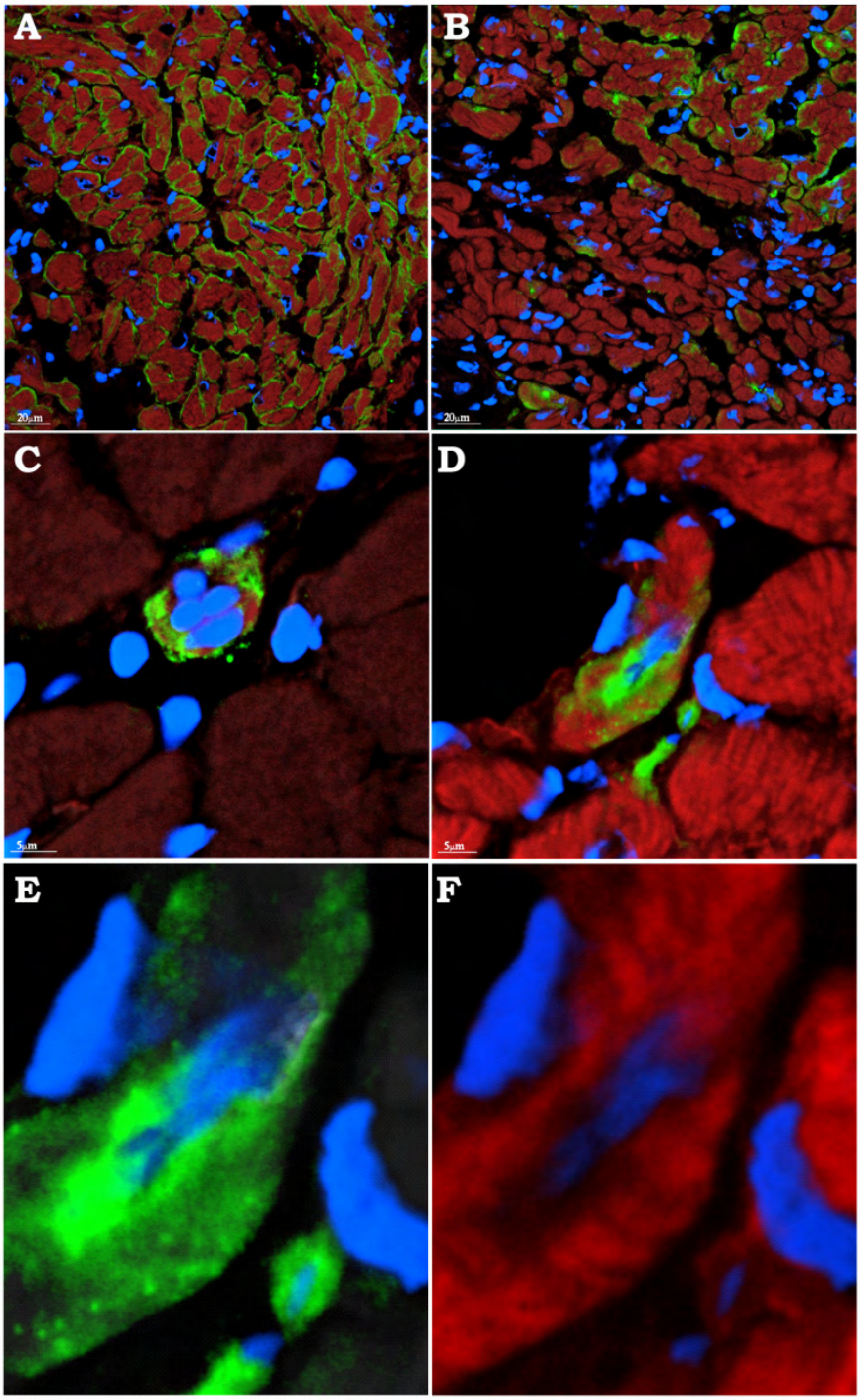

Fig. 3.31. Confocal images of BMP10 localization (green) in heterozygous MnSOD (B-D) and control (A) mice. Panels A and B- BMP10 distribution in the right atrium. Panels C,D- BMP10 positive cells were found in ventricles of the transgenic mouse. Sections were counterstained with phalloidin-TRITC (red). Panels E and F- higher magnification of (D) illustrating a BMP10 positive cell on an myocyte (E), F- counterstained with phalloidin-TRITC (red). Panels E and F represent different layers of confocal image to illustrate localization of BMP10 in the interstitial cell. Nuclei were visualized with Draq5 (blue).

The stained cell presented in Fig. 3.31D seems to resemble a small cardiomyocyte, but confocal analysis revealed that it is an interstitial cell situated on a myocyte.

The relative level of BMP10 transcription in transgenic mice was reduced in comparison to wild type control (Fig. 3.32A), as revealed by semi-quantitative RT-PCR. Analysis of BMP10 expression on the protein level also indicated a decreased amount of BMP10 (Fig. 3.32B) whereas ANF expression was upregulated in SOD2 heterozygous (Fig. 3.32C). In situ hybridization with an ANF probe revealed specific localization in the proximity of vessels of ANF transcripts in knock-outs (Fig. 3.33).

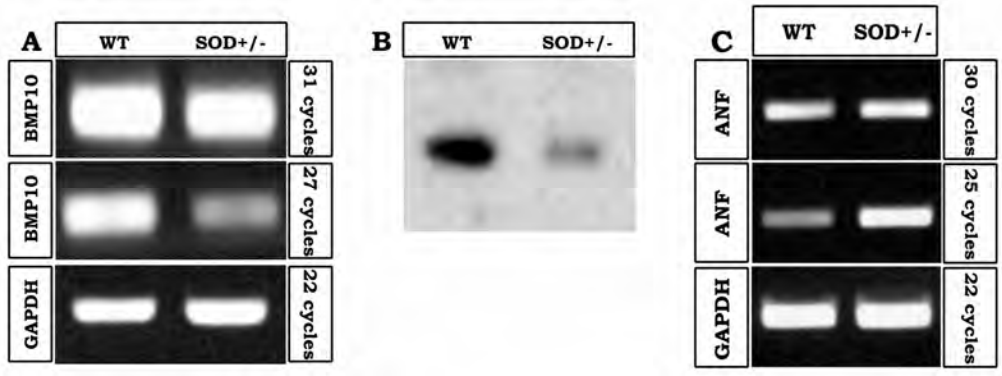

Fig. 3.32. Panel A- semi-quantitative RT-PCR analysis of BMP10 expression in MnSOD heterozygous and control mice. Panel B- Western Blot shows relative difference in BMP10 protein level in transgenic and control mice. Panel C- semi-quantitative analysis of ANF expression in WT and SOD2 heterozygous. An equal amount of RNA was monitored by the level of the GAPDH PCR product (22 cycles).

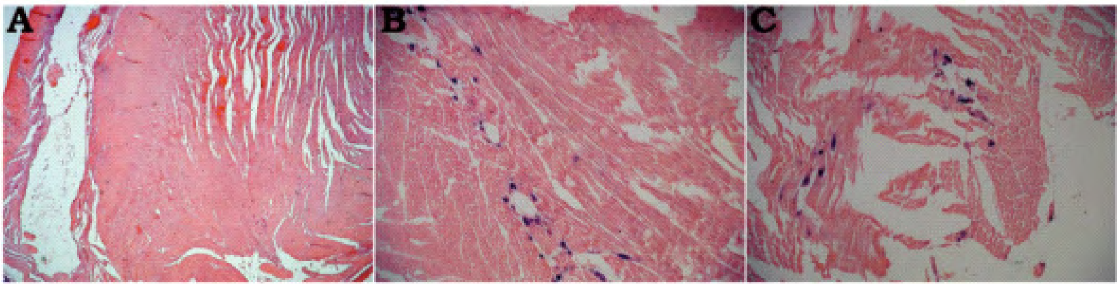

Fig. 3.33. In situ hybridization in paraffin embedded heart slices with an antisense ANF probe. ANF expression in ventricles in WT (A) is restricted to single cells, whereas in MnSOD heterozygous foci of interstitial cells surrounding vessels (B) and myocytes (C) ANF positive cells were detectable.

3.5.3. Redistribution and upregulation of BMP10 in doxorubicin induced CMP

Clear changes of the BMP10 expression pattern were found in Desmin knock-out and SOD2 heterozygous mice, which might be considered as models of chronic heart failure. On the other hand, drug induced cardiomyopathies might serve as models of acute cardiac disorder.

Mice treated with doxorubicin exhibited apparent changes in the BMP10 expression as revealed by in situ hybridization. BMP10 transcripts were detectable not only in the right atrium (Fig. 3.34A), but also in single, ventricular interstitial cells (Fig. 3.34B). The number of positive cells was not abundant, and definitely lower than in Desmin knock-out and MnSOD heterozygous. It should also be noted that the chamber dilation did not only affected ventricles but also the atria.

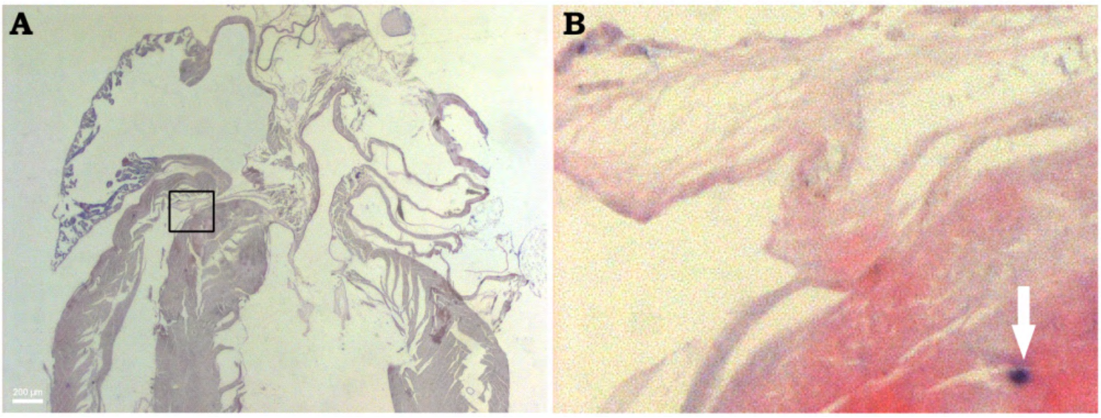

Fig. 3.34. In situ hybridization with an antisense BMP10 specific probe in doxorubicin treated mouse heart. Panel A- BMP10 expression in the right atrium (blue label), dilation of the left ventricle and the right atrium is also visible. Panel B- higher magnification of (A), the arrow indicates the BMP10 signal in the septum.

Using immunohistochemistry, an ectopic expression of BMP10 in the ventricular myocardium was confirmed (Fig. 3.35). Clusters of BMP10 positive cells, however, were not found in this model. Only single cells stained with BMP10 antibody were detected and, as was already mentioned, their number was lower than in genetic models.

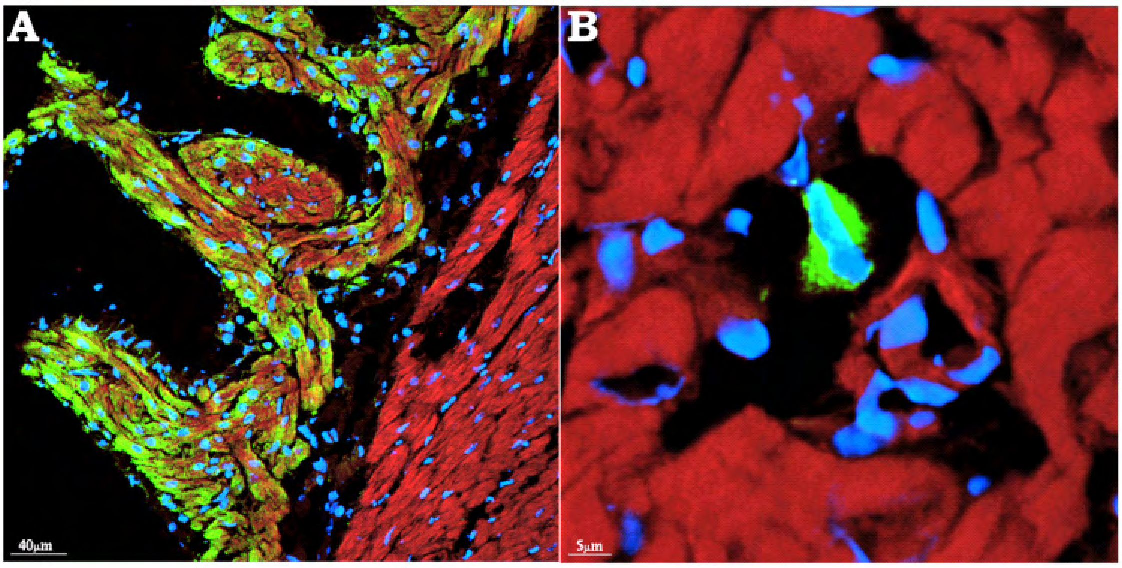

Fig. 3.35. Representative confocal images illustrating BMP10 (green) expression in the right atrium (A) and ventricles (B) in heart of doxorubicin treated mouse. Sections were counterstained with phalloidin-TRITC (red) and nuclei were visualized with Draq5 (blue).

Administration of doxorubicin resulted in redistribution of BMP10 protein in the atrium, as shown in Fig. 3.35A. BMP10 was accumulated in the cytoplasm and only a minor amount was localized at the membrane. Quantitative determination of BMP10 expression revealed an upregulation of BMP10 in adriamycin treated mice. Results of semi-quantitative RT-PCR and Western Blot analysis are presented in Fig. 3.36. Additionally, ANF expression was only slightly upregulated (Fig. 3.36C) and ANF transcripts were detectable in single, ventricular cells, as shown in Fig. 3.37.

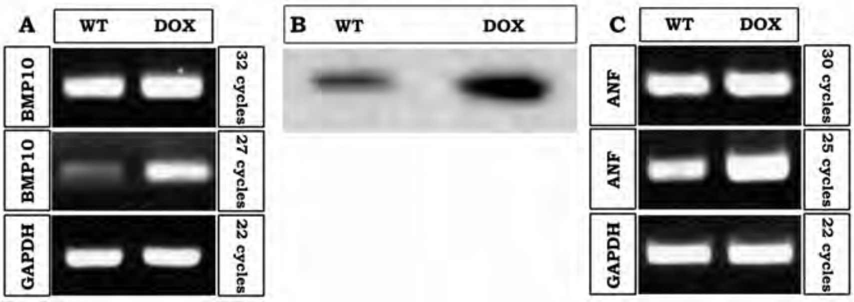

Fig. 3.36. Semi-quantitative RT-PCR of BMP10 (A) and ANF (C) in doxorubicin (right) and PBS (left-WT) treated mouse heart. B- Western Blot presenting up-regulation of BMP10 on the protein level.

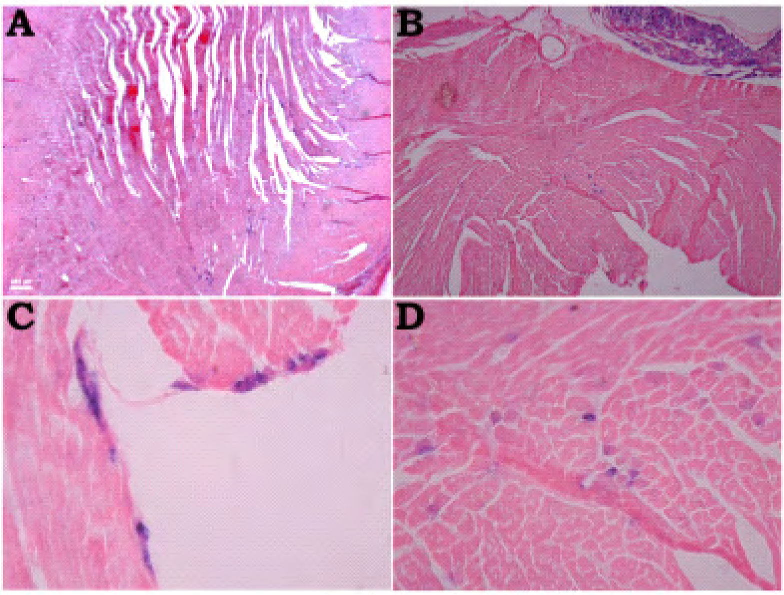

Fig. 3.37. In situ hybridization in paraffin embedded heart slides with an antisense ANF probe. ANF expression was not detectable in ventricles in PBS treated control (A,B). In doxorubicin induced cardiomyopathy (C,D) transcripts were detectable in single, ventricular cells (blue label) and indicated a slight upregulation of ANF expression in the pathological heart.

3.5.4. Downregulation of BMP10 in isoproterenol induced hypertrophic CMP

The previously described models represent the dilated type of cardiomyopathy (DCM). It was unclear, whether changes in BMP10 expression and localization were typical only for DCM or whether it is a common marker of heart failure. Hence, isoproterenol induction of hypertrophy was included in the study as a model of acute hypertrophic CMP.

In situ hybridization (Fig. 3.38) as well as immunolabeling (Fig. 3.39) revealed qualitative changes in BMP10 expression. In the right atrium, some cells did not express BMP10 anymore (Fig. 3.38B and C), while other strongly expressed BMP10.

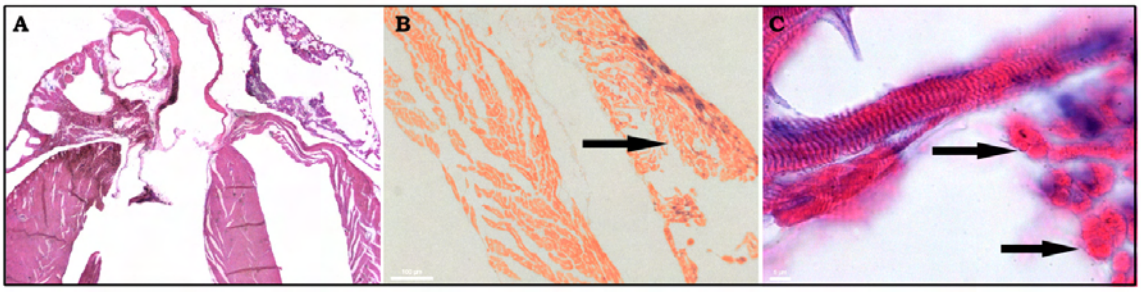

Fig. 3.38. In situ detection of BMP10 transcripts (blue label) in isoproterenol treated mouse heart. Panel A- shows an overview. Panel B- illustrates downregulation of BMP10 in the right atrium. Note lack of BMP10 expression in some areas of the right atrial appendage. Panel C- higher magnification of the BMP10 signal in cardiomyocytes and interstitial cells in the right atrium. Arrows indicate lack of BMP10 expression.

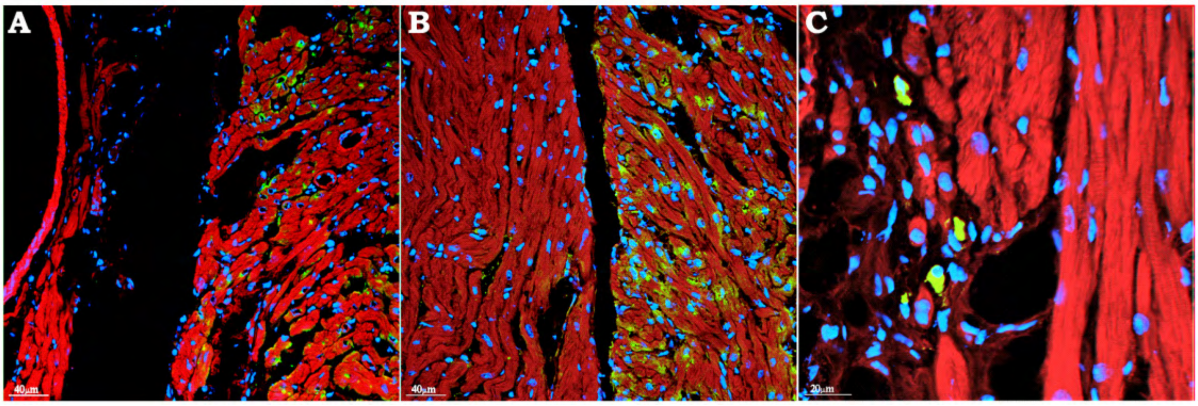

Fig. 3.39. Representative confocal images of BMP10 (green) localization in isoproterenol treated mouse heart. Panel A- homogeneous pattern of BMP10 downregulation. Panel B- heterogeneity of BMP10 distribution. Panel C- example of ectopic BMP10 expression in ventricles. Sections were counterstained with phalloidin-TRITC (red), nuclei with Draq5 (blue).

Similar results were obtained on the protein level. In the isoproterenol treated mice two distinct patterns were observed in the atrium:

1. Homogeneous downregulation (Fig. 3.39A)
2. Heterogeneous pattern (Fig. 3.39B), as already described for MnSOD heterozygous mice.

A number of cells expressing BMP10 were found in the ventricles, as shown above. Only single, separated BMP10 positive cells were detected. These cells did not form clusters as in genetic models, however pairs were sometimes found. It was difficult to determine the overall BMP10 expression level due to the heterogeneity of the expression and localization pattern. Hence, quantification by PCR and Western Blot analysis had to be performed (Fig. 3.40). Preliminary determination on RNA level revealed a decrease of BMP10 expression (Fig. 3.40A), while ANF (Fig. 3.40C,D), FHL2 and BNP (data not shown) were upregulated. To verify differences in BMP10 levels real-time quantitative RT-PCR was used (Fig. 3.40D). In hypertrophied hearts, the ANF level increased 4.5 fold, while BMP10 was down-regulated by a factor of 7.3.

Western Blot confirmed results obtained from RT-PCR analysis. FHL2 has been described as specific and reliable marker of hypertrophy (Kong et al., 2001), hence in situ hybridization with FHL2 specific riboprobe was performed. Transcript detection revealed expression of this gene in most of the ventricular cells of the treated heart (Fig. 3.41), while in control only a weak signal was detected.

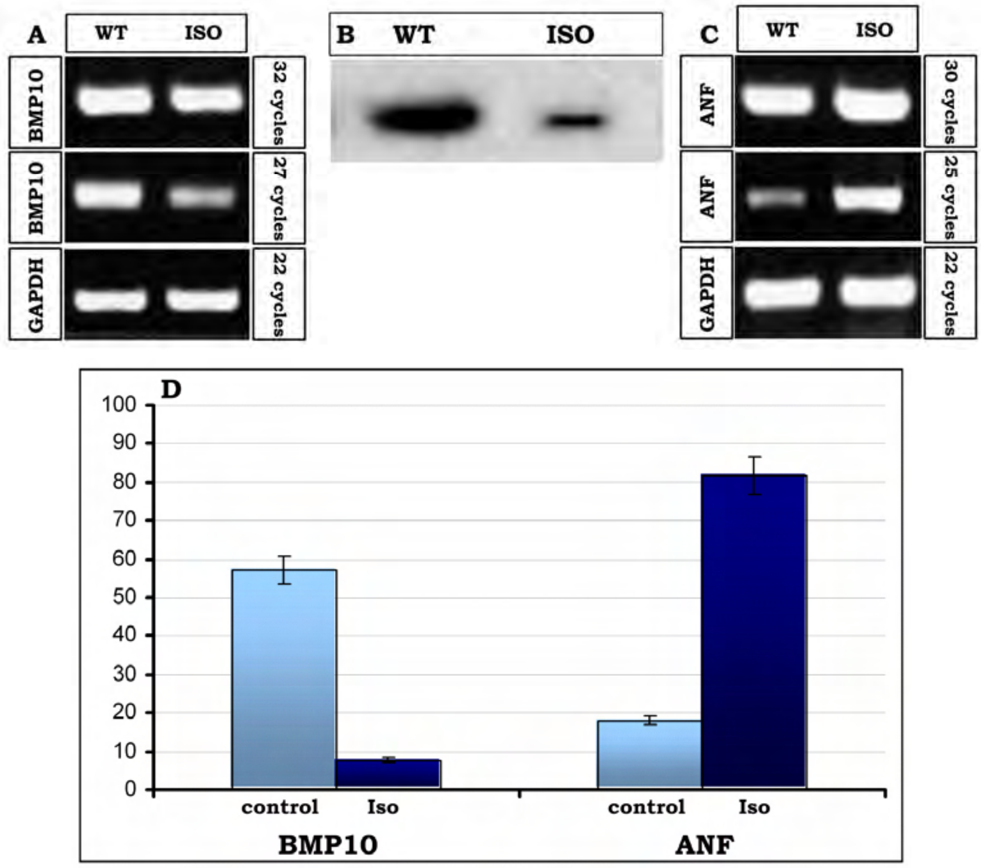

Fig. 3.40. Semi-quantitative RT-PCR of BMP10 (A) and ANF (C) in isoproterenol (right) and PBS (left-WT) treated mouse heart. B- Western Blot showing downregulation of BMP10 on protein level. Preliminary semi-quantitative RT-PCR was confirmed by real time PCR analysis (D). Results were normalized to GAPDH expression and are presented as copy number of gene of interest per 100 GAPDH copies.

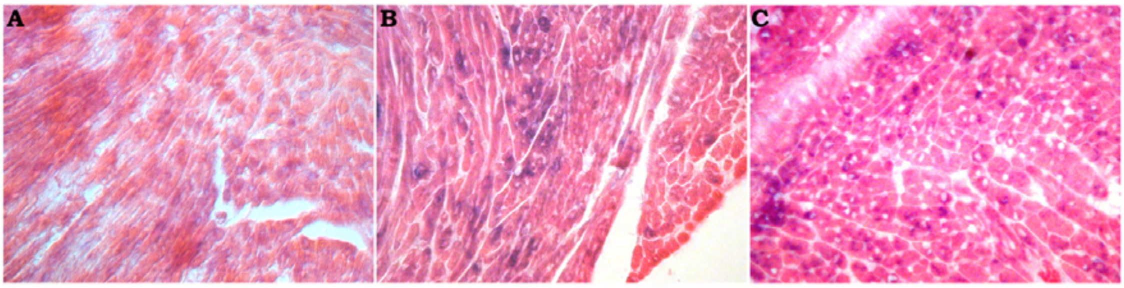

Fig. 3.41. FHL2 transcript detection (blue label) by in situ hybridization in control (A) and isoproterenol treated (B,C) hearts. Only a weak signal was detectable in control hearts (A). Strong induction of FHL2 expression in isoproterenol treated hearts was observed (B,C).

3.5.5. Deregulation of BMP10 expression in neonatal SOD2 knock-outs

Homozygous SOD2 knock-outs die shortly after the birth due to severe dilated cardiomyopathy (Li et al., 1996; Lebovitz et al., 1996). It was interesting therefore to check changes in BMP10 expression in this genetic model. Three days old MnSOD homozygous, heterozygous and WT mice from the same litter, on mixed C57Bl6/ICR background (generous gift from Dr. T. Loch) were used for the analysis. In situ hybridization in paraffin embedded hearts slides revealed striking differences in BMP10 transcription (Fig. 3.42). In knock-out mice, ectopic expression was detected in ventricles, while in the right atrium the signal intensity was apparently diminished. Neonatal heterozygous MnSOD mutant mice, which do not show impairment of cardiac function and which have a virtually normal lifespan, did not exhibit any apparent changes in BMP10 expression (data not shown).

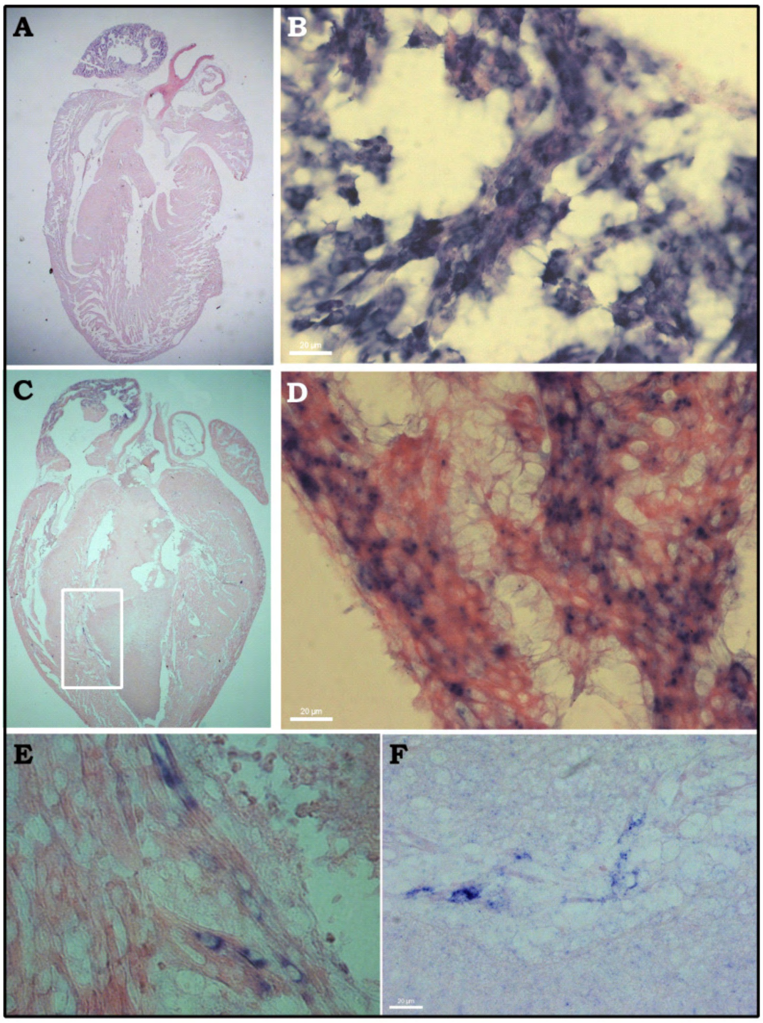

Fig. 3.42. Recapitulation of BMP10 expression in ventricles and downregulation of its atrial transcription in three day old MnSOD knock-out. In situ hybridization

with the BMP10 specific antisense riboprobe (blue label). Panels A and B- illustrate the BMP10 expression in three day old wild type control. Panels C,D- show decrease of BMP10 expression in the right atrium of SOD2 homozygotes. Panels B,D- represent higher magnification of the atria in wild type and knock-out, respectively. E,F- higher magnification of (C) illustrating the signal detected in the ventricles of neonatal SOD2 homozygous.

Immunostaining of BMP10 showed a striking decrease of protein expression in the right atria of knock-outs (Fig. 3.43), but not in heterozygous (data not shown) and wild type controls. Representative confocal images of BMP10 localization in two different SOD2 homozygous and in control mouse are shown in Fig. 3.43. As already mentioned, membrane location and cytoplasmic accumulation of BMP10 in the cells of right atrium is typical for wild type neonatal mouse. However, in neonatal MnSOD knock-outs the BMP10 signal in the cytoplasm was not detectable and only membrane bound BMP10 was found in the subset of atrial cells.

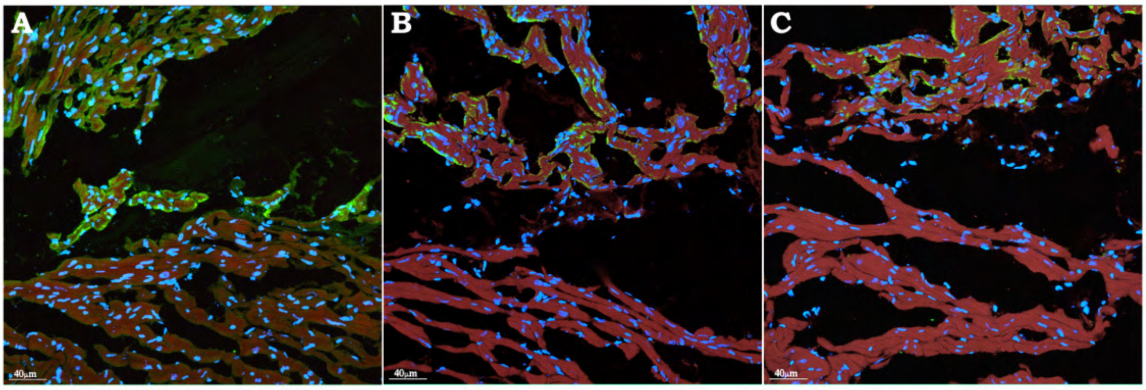

Fig. 3.43. The representative images of the BMP10 in situ immunodetection results. Downregulation of atrial BMP10 (green) expression in neonatal MnSOD homozygous (C,D) mice as compared to the control wild type (A). Sections were counterstained with phalloidin-TRITC (red) and nuclei were visualized with DAPI (blue).

The relative comparison of BMP10 expression level in MnSOD homozygous with heterozygous and wild type controls by semi-quantitative RT-PCR confirmed the overall downregulation of the gene in knock-out animals. Simultaneously, expression of known markers of cardiomyopathy, i.e. BNP and ANF was monitored and a strong increase was detected. As shown in Fig. 3.44, a decreased expression of BMP10 was detected only in MnSOD-/-, but not in heterozygous mice. An increase of ANF was observed exclusively in knock-outs.

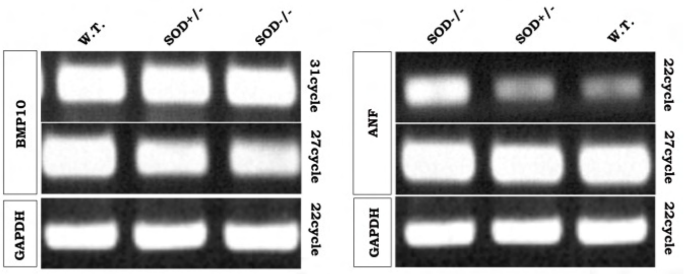

Fig. 3.44. Semi-quantitative RT-PCR analysis of BMP10 (left panel) and ANF expression (right panel) in three day old wild type, heterozygous and homozygous MnSOD knock-outs. Downregulation of BMP10 expression in SOD2-/- is correlated with an increase of ANF.

3.6. Characterization of ventricular BMP10 positive cells in pathological adult hearts

The induction of BMP10 expression in different regions of the failing ventricles suggested its role in an adaptive or pathological response. To determine its positive or negative action, it was necessary to characterize the ventricular BMP10 positive cells. Based on preliminary observations, i.e. localization in the close proximity to vessels and the presence of cell clusters- endothelial, smooth muscle and proliferation markers were chosen to unequivocally identify BMP10 expressing cells.

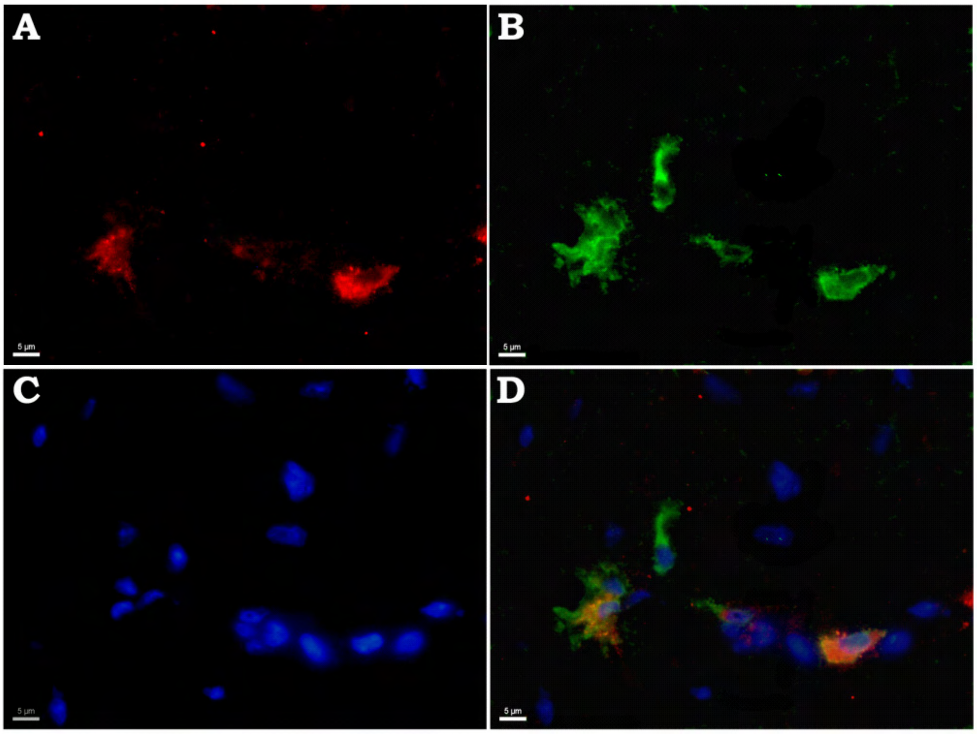

Fig. 3.45. A subpopulation of BMP10 positive cells express the endothelial marker PECAM. Double immunodetection of endothelial marker CD31/PECAM (A, red) and BMP10 (B, green) in the ventricles of Desmin knock-out mouse heart. Nuclei were visualized with DAPI (C, blue). Panel D shows merged images. For exact description see text.

As shown above, a subpopulation of BMP10 positive cells was positive for the endothelial marker- platelet endothelial cell adhesion molecule PECAM/CD31 (Fig. 3.45). It should be noted, that BMP10 was not found in all endothelial cells (data not shown). Similar results were obtained when smooth muscle actin was used as a marker (Fig. 3.46). Again, BMP10 was detected in a subpopulation of smooth muscles cells. Most of the BMP10 positive cells exhibited moderate expression of the smooth muscle marker, but only a minority of smooth muscles cells in the heart stained positive for BMP10.

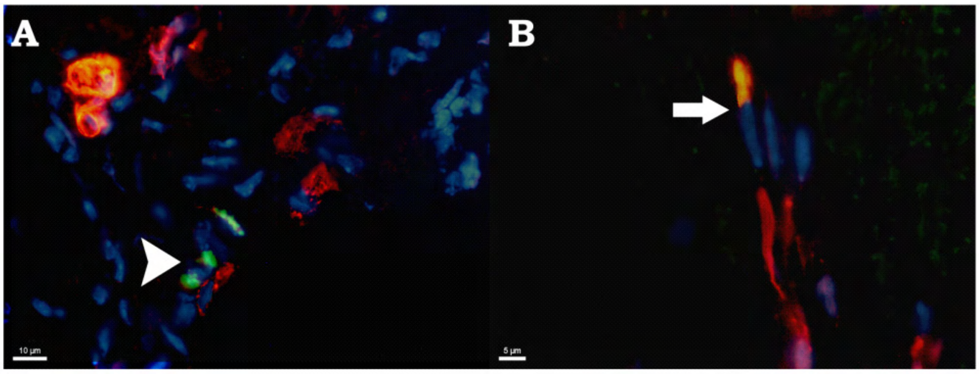

Fig. 3.46. A minority of SMA positive cells in ventricles of MnSOD heterozygous expressed BMP10. Merged images of double immunostaining (A-B) of smooth muscle actin- SMA (red) and BMP10 (green)- yellowish when co-localize. The arrow indicates the cell expressing both BMP10 and SMA, arrowhead- BMP10$^{pos.}$/SMA$^{neg.}$ cell. Nuclei were visualized with DAPI (blue).

Double immunolabeling of BMP10 and the proliferation markers phospo-histone H3 (Fig. 3.47) and Aurora B (Fig. 3.48), revealed that a major subpopulation of BMP10 positive cells underwent mitosis. Phospo-histone H3 marks cells in both G2 and mitosis (Fig. 3.47), while Aurora B marks those in anaphase, telophase and cytokinesis. On the basis of the Aurora B pattern, BMP10 positive cells in cytokinesis were found in the different genetic models of cardiomyopathy (Fig. 3.48) and isoprotererol induced (data not shown) models. Surprisingly, in doxorubicin treated mouse heart, an accumulation of Aurora B was detected in nuclei of BMP10 positive cells although these cells did not exhibit features of cytokinesis (Fig. 3.48).

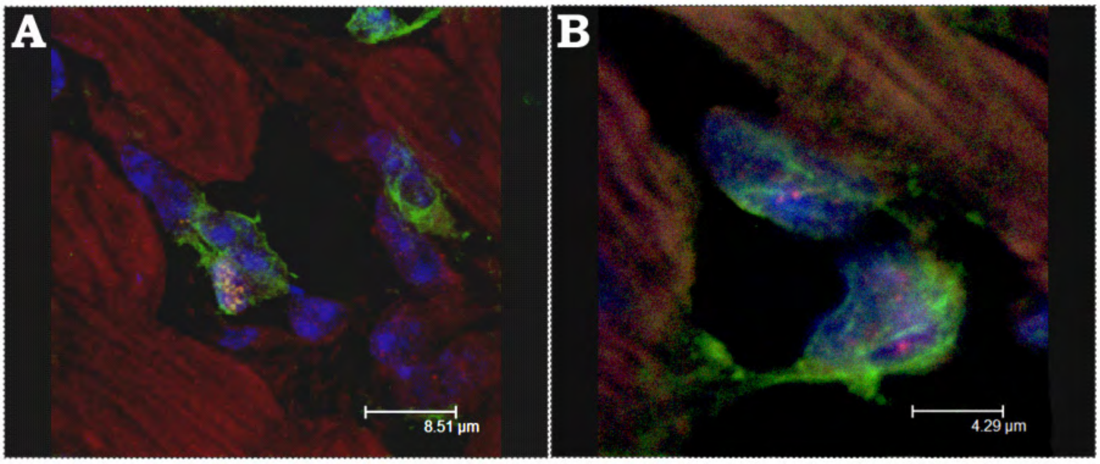

Fig. 3.47. In a subpopulation of BMP10 positive cells (green) phosphorylated histone H3 is detectable (pink, nuclear location). Nuclei were visualized with DAPI (blue) and sections were counterstained with phalloidin 633 (dark red).

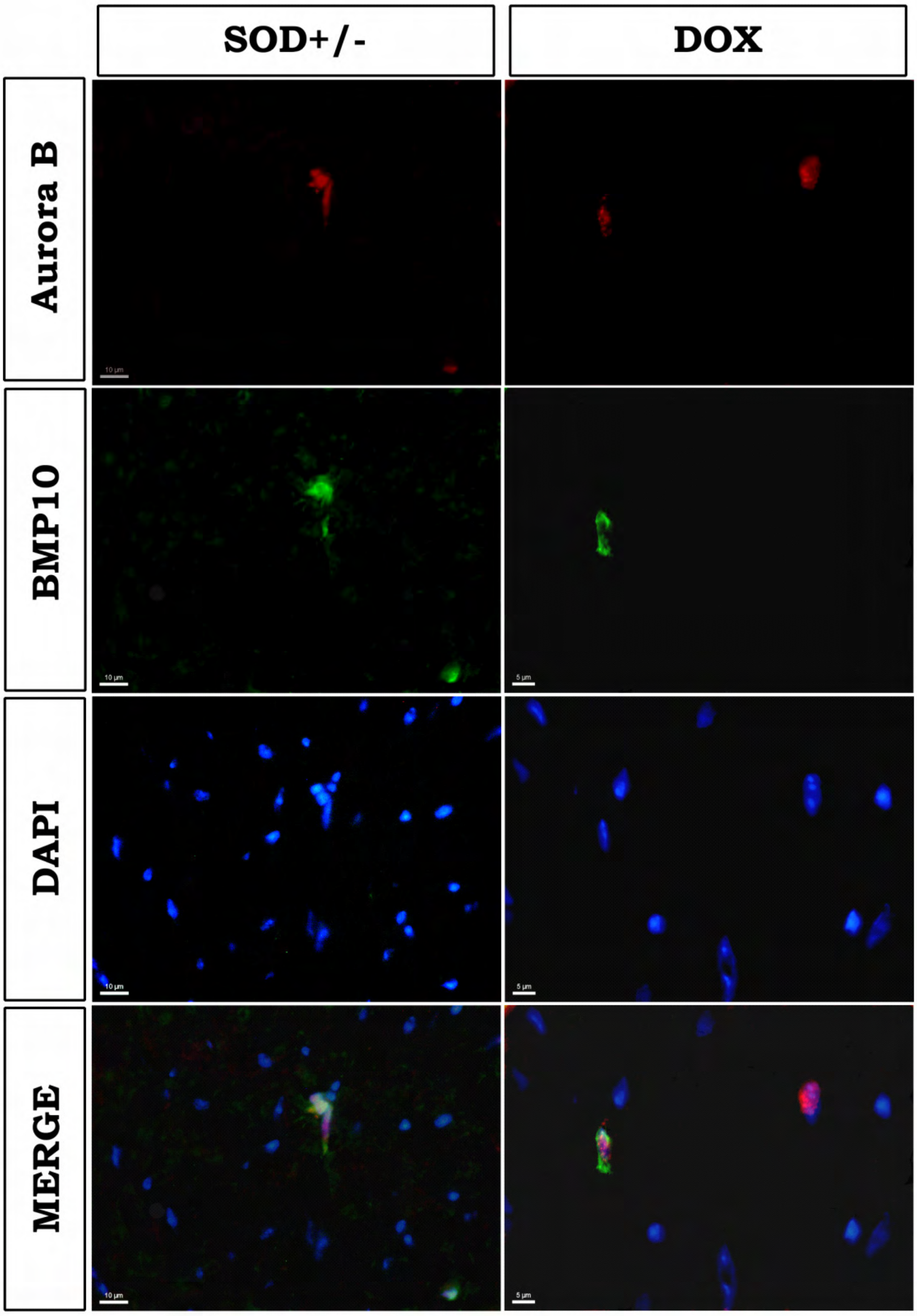

Fig. 3.48. BMP10 is detectable in proliferating cells. Proliferation marker- Aurora B (red) co-localizes with BMP10 (green) in ventricles of MnSOD heterozygous (SOD+/-) and doxorubicin (DOX) treated mice. Nuclei were stained with DAPI (blue). Note the accumulation of Aurora B in nuclei of BMP10 positive cells in doxorubicin treated heart, however, these cells did not exhibit features of cytokinesis.

During the analysis of BMP10 expression in different models of cardiomyopathies, the question arose whether BMP10 is present in ventricular cardiomyocytes. As already mentioned in the case of MnSOD heterozygous, due to the small size of BMP10 positive cells it was easy to confuse BMP10 positive cells as heart muscle cells. Sometimes even a careful confocal analysis did not give clear answer. Hence, two distinct cardiomyocyte specific markers, Nkx2.5 and MHC were selected and used in double labeling experiments.

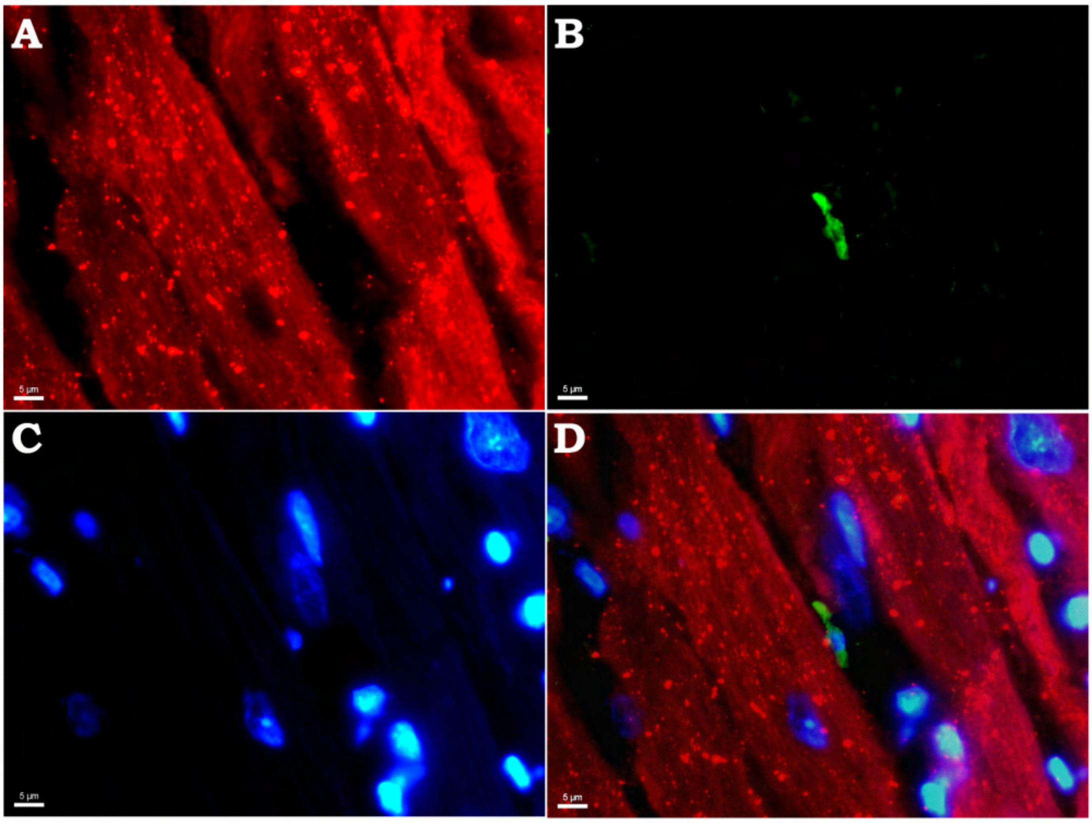

Fig. 3.49. Immunolabeling of Myosin Heavy Chain (red) with MF20 antibody (A) and BMP10 (B, green) in isoproterenol induced hypertrophy showed that BMP10 is expressed in interstitial cells but not in cardiomyocytes in ventricles of the failing heart. Nuclei are shown in blue by DAPI staining (C). Panel D- merged images.

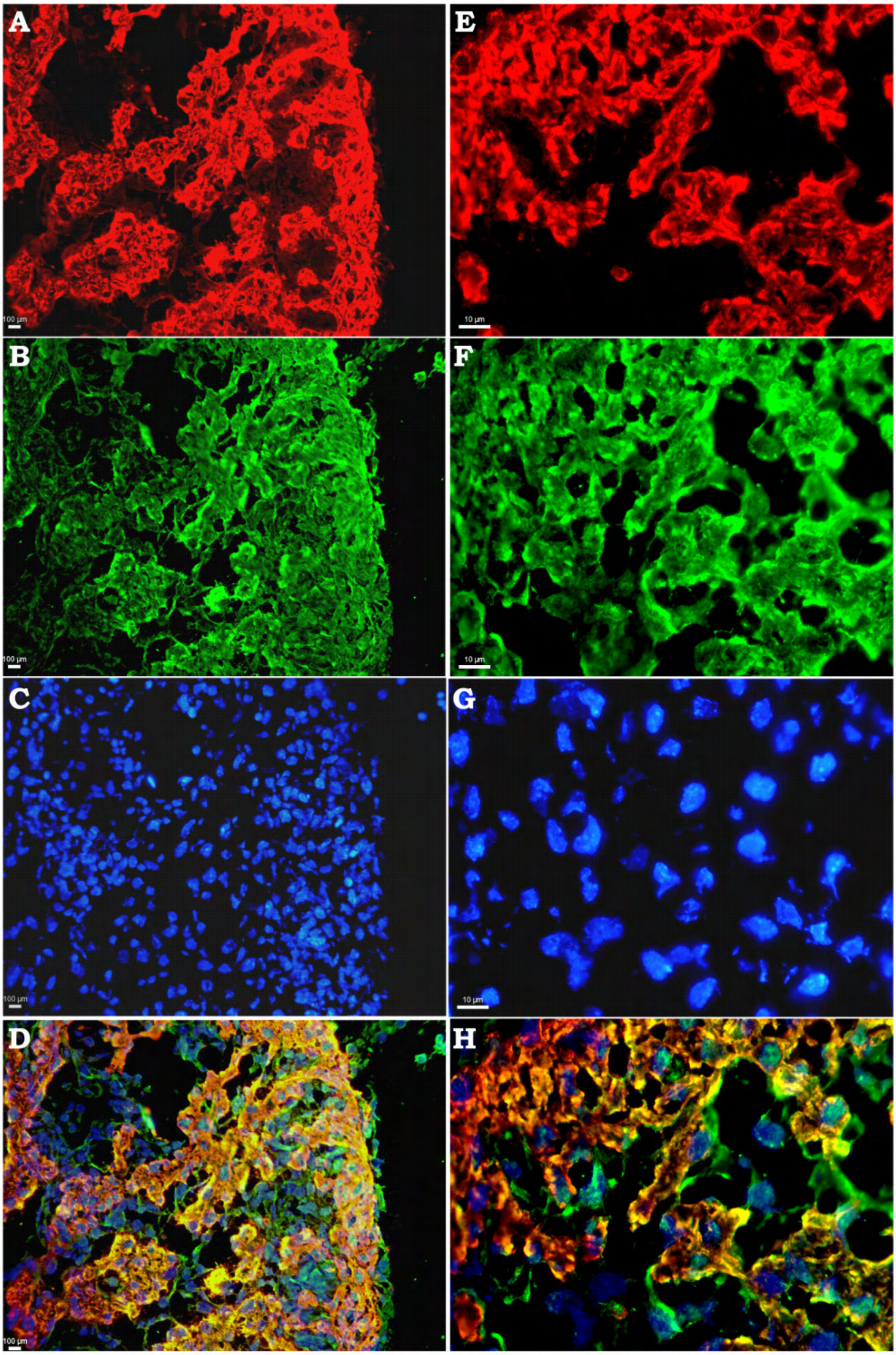

Fig. 3.50. Immunostaining of MF20 (A,E- red) and BMP10 (B,F- green) in the developing mouse heart at E11.5. BMP10 is detected not only in cardiomyocytes, but also in surrounding cells. Nuclei were visualized with DAPI (C,G- blue). D and H show merged images.

Representative results of MF20 and BMP10 double staining are shown in Fig. 3.49. Hypertrophied ventricular cardiomyocytes in isoproterenol treated mouse are negative for BMP10 and BMP10 positive cell do not express myosin. It should be emphasized however, that in the right atrium BMP10 staining was detected in myocytes (illustrated in Fig. 3.51 on the example of Nkx2.5).

In the developing mouse heart, BMP10 was detected by in situ hybridization (Neuhaus et al., 1999) and immunostaining (own results) in the trabeculated myocardium. Additionally, embryonic BMP10 deficiency (Chen et al., 2004) leads to defective outgrowth of these structures, hence it was interesting to analyze, whether BMP10 localization is restricted to cardiomyocytes in embryonic ventricles.

In trabeculae, centrally located MF20 and BMP10 positive cells were surrounded by non-cardiomyocytes which did also express BMP10. Hence both myocytes and non-cardiomyocytes express BMP10 in embryonic hearts (Fig. 3.50.)

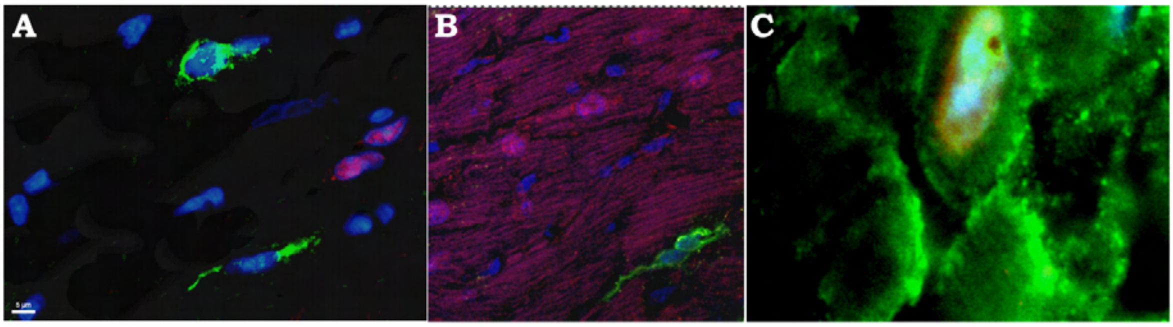

Fig. 3.51. A and B- ventricular BMP10 positive cells (green) do not express Nkx2.5 (purple in merge with blue DAPI). Section B was counterstained with phalloidin 633. C- High magnification of atrial cardiomyocytes with membrane location of BMP10 (green) and Nkx2.5 staining (red) in nucleus.

Since structural proteins label only relatively mature cardiomyocytes, the transcription factor Nkx2.5 was used as an additional marker for cardiomyocytes. The double immunostaining with BMP10 and Nkx2.5 specific antibody (Fig. 3.51) resolved my prior observations concerning a possible BMP10 expression in cardiomyocytes. Under pathological conditions BMP10 expression was not detected in ventricular myocytes, but only in interstitial cells.

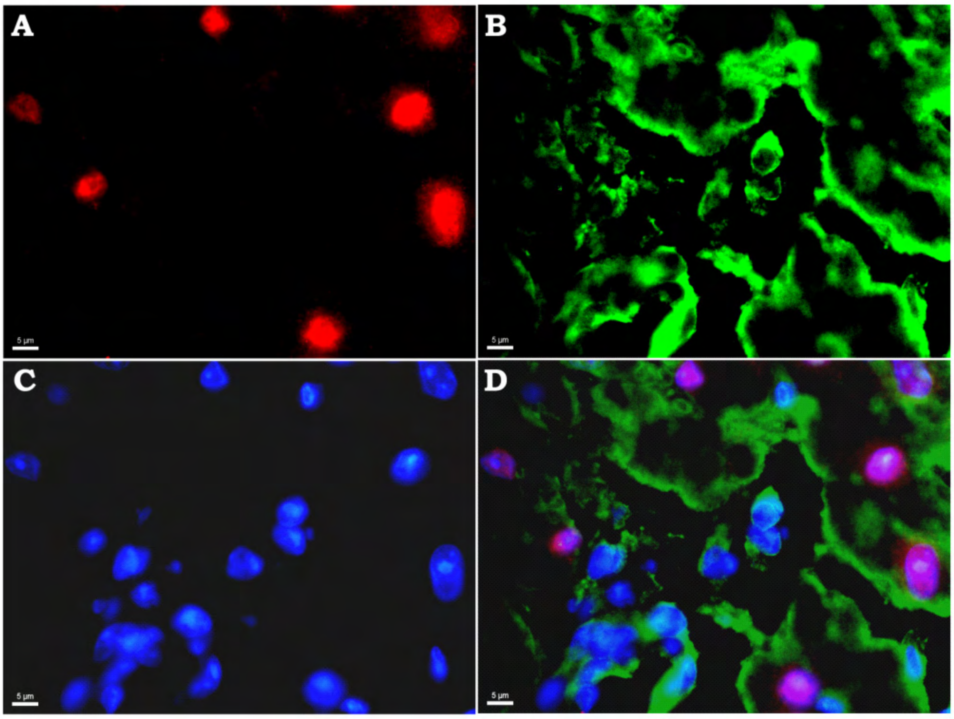

Fig. 3.52. Immunostaining of Nkx2.5 (A- red) and BMP10 (B- green) in developing mouse heart at E11.5. BMP10 is detected not only in cardiomyocytes, but also in other cells. Nuclei were visualized with DAPI (C- blue). D shows merged images.

Since BMP10 was detected only in pathologically altered ventricles, but not in healthy hearts I wanted to identify the origin of these BMP10 expressing cells. It is believed that pluripotent progenitor cells reside in the heart and can be characterized by stem cell antigen 1 (Sca1)/Ly6A expression (Oh, H., 2003). Additionally, resident Sca1 positive cells in the heart were further subdivided into two: CD31- and 31+ cardiac side populations (Pfister et al., 2005). For this reason I used transgenic mice overexpressing GFP under the control of a Sca1 promoter (generous gift from Prof. T. Braun). An additional advantage of using a transgenic strain is the amount and stability of the expressed GFP and the possibility to monitor Sca1 promoter induction changes on the basis of GFP intensity differences.

First, the number of progenitor cells in the heart was verified on the basis of green fluorescence. As shown in Fig. 3.53, an enormous number of cells expressing GFP were found in the heart, even without signal amplification with an anti-GFP antibody.

In addition it was analyzed whether PECAM/CD31 and Sca1-GFP were expressed in the same cells. CD31 positive cells incorporated in vessels did not express

Sca1 (data not shown), only a minority of Sca1-GFP positive cells outside of the vessel wall expressed platelet endothelial cell adhesion molecule (Fig. 3.54).

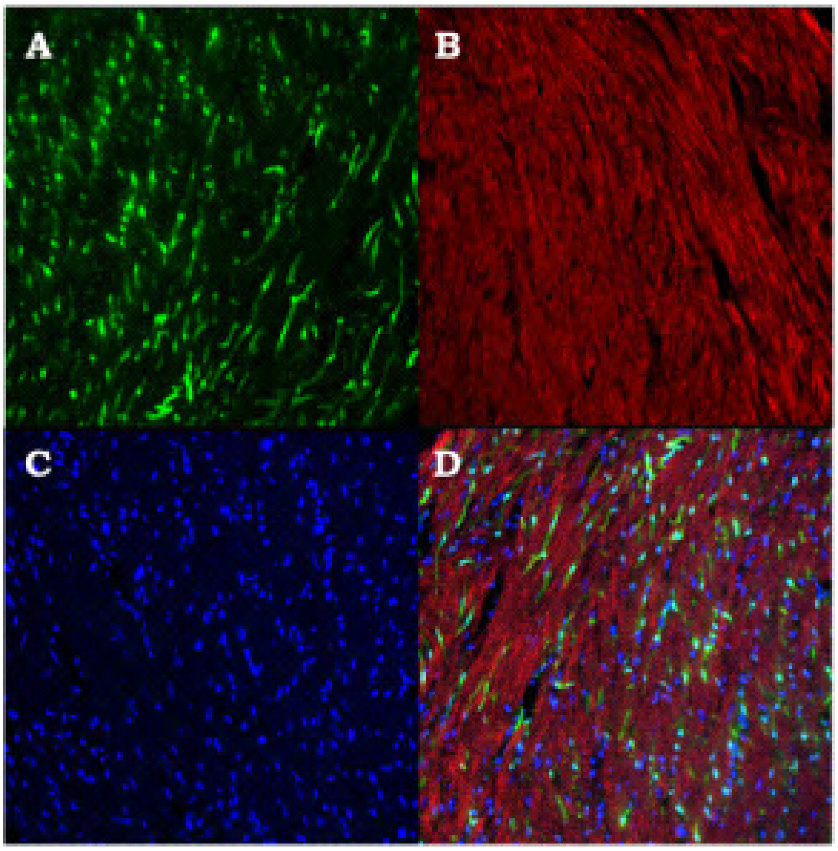

Fig. 3.53. A high number of stem cell antigen 1 positive cells reside in the heart as shown by visualization of GFP expression driven by Sca1 promoter (A). Panel B- the same section as in A counterstained with phalloidin-TRITC (red), C- nuclei were visualized with DAPI (blue) D-merged images.

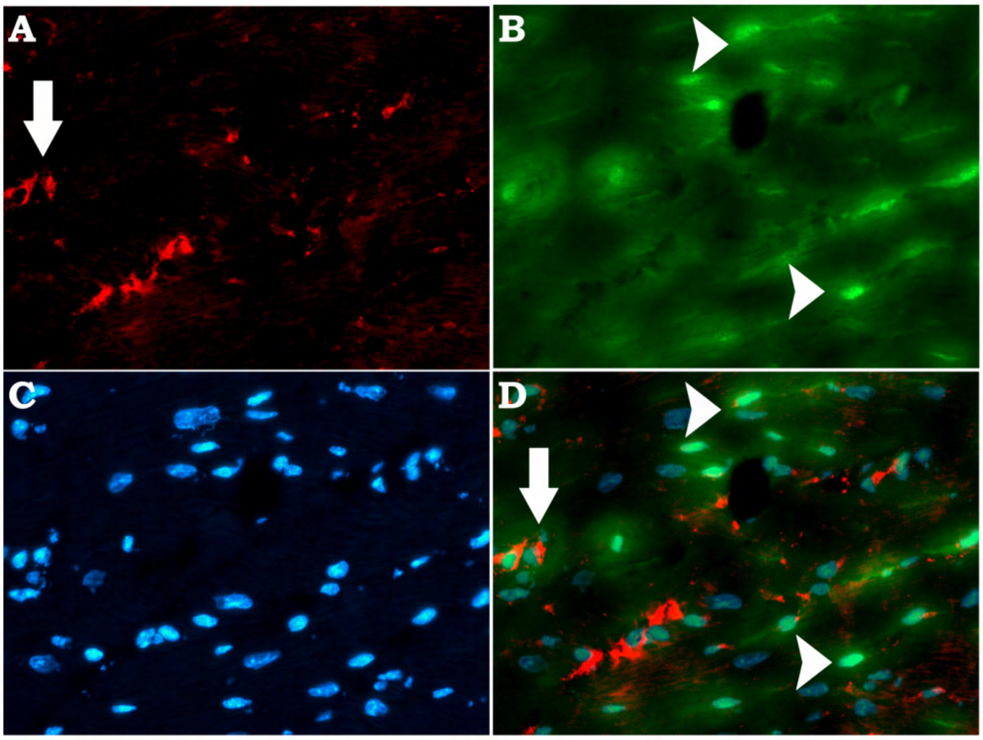

Fig. 3.54. Colocalization of CD31 (A-red) and Sca1-GFP (B-green) cells in Ly6A transgenic mouse heart. The arrow indicates colocalization of PECAM and Sca1 antigen, arrowheads PECAM$^{neg.}$/Sca1$^{pos.}$ cells. Nuclei were visualized in blue with DAPI (C). Panel D presents merged images.

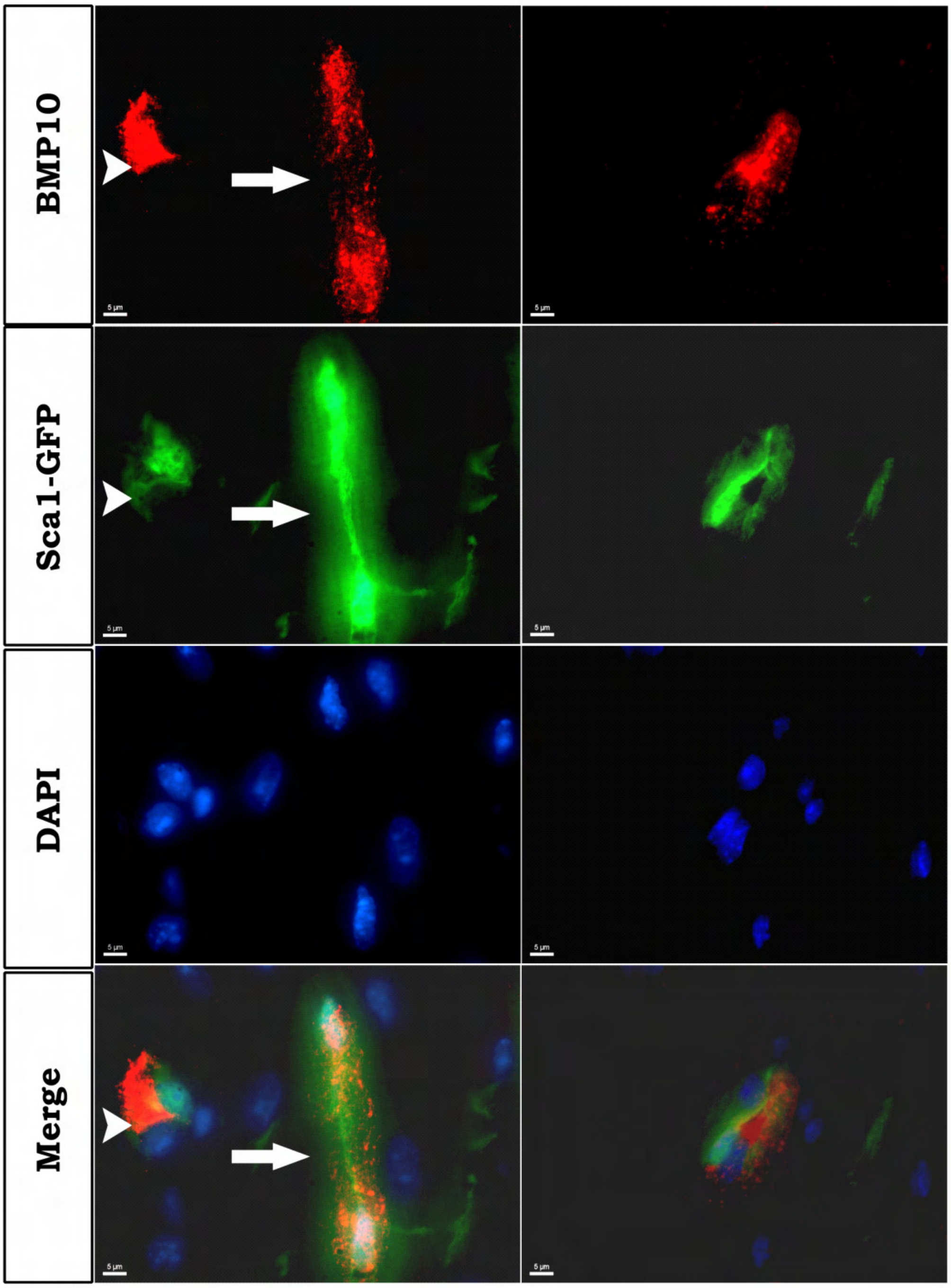

Fig. 3.55. BMP10 co-localizes with Sca1 antigen in the ventricles of isoproterenol treated Sca1-GFP transgenic mice. Membrane bound BMP10 (red) was found in Sca1 positive cells which underwent cytokinesis (arrow). BMP10 accumulated in cytoplasm correlated with the marginal GFP signal (arrowhead). GFP was not amplified by antibody staining. For nuclei visualization DAPI was used (blue).

To study BMP10 expression in Sca1-GFP mice, cardiac dilation or/and hypertrophy had to be induced by doxorubicin and isoproterenol administration, respectively, prior to immunohistochemical analysis. In mice treated with both drugs, BMP10 was found in Sca1$^{pos.}$, but also in cells negative or weakly expressing Sca1 (Fig. 3.55). As shown below, in a model of hypertrophic cardiomyopathy, BMP10 was detected in separating GFP positive cells (Fig. 3.55, left panel, arrow). Note the difference between BMP10 locations: in the left panel BMP10 is membrane bound in cells probably undergoing cytokinesis, , whereas in clustered cells on the left side of the image, a clear cytosolic accumulation is visible (Fig. 3.55, left panel, arrowhead). It should be mentioned that the presence of cytosolic BMP10 accumulation was most often but not always correlated with weak Sca1 expression, as shown in Fig. 3.55. The right panel shows a rare example of cell strongly positive for BMP10 with a preserved Sca1 signal. From two BMP10$^{pos.}$ cells, one exhibits strong GFP fluorescence, while the second has diminished, marginal GFP expression (limited to the disappearing signal in nucleus). On this image a Sca1$^{pos.}$ cell with membrane location of BMP10 is also shown.

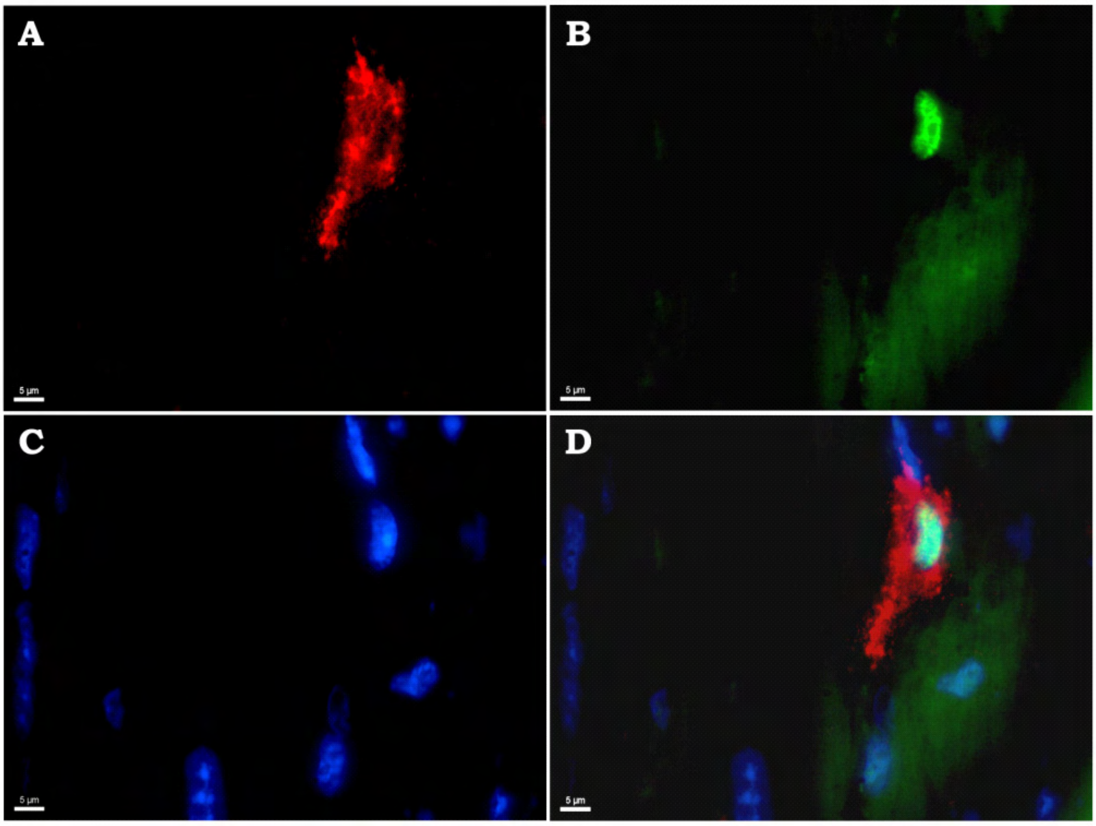

Fig. 3.56. BMP10 (A- red) was detected in single ventricular Sca1 positive cells (B-green) in doxorubicin treated Sca1-GFP transgenic mice. For nuclei visualization DAPI was used (C- blue). Panel D shows merged images.

Induction of BMP10 with doxorubicin yielded similar results. BMP10 was localized in both Sca1$^{pos.}$ and Sca1$^{neg.}$ cells and a correlation of GFP intensity and BMP10 accumulation was noticed. As already mentioned, ventricular cells, which ectopically expressed BMP10 due to doxorubicin administration, did not show the tendency to cluster and only single BMP10 positive cells were found. When Sca1$^{pos.}$ cells were marked with GFP, very often pairs or even clusters of Sca1$^{pos.}$ cells were present, but in contrast to isoproterenol there was only single BMP10$^{pos.}$ cell among them (Fig. 3.56).

3.7. Growth and differentiation function of BMP10- *in vitro* studies

3.7.1. The BMP10-IRES-GFP construct produces functional BMP10 protein

To test the function of BMP10 in vitro, a BMP10 expression construct was generated. 293T cells were transiently transfected with the BMP10-IRES2-GFP construct or pEGFP empty vector (control). Twenty-four hours after transfection, when the GFP reporter molecule expression was apparent and transfection efficiency was estimated to comprise a minimum level of 80% (based on GFP fluorescence), the growth medium containing 10% FCS was replaced with serum free DMEM medium. Forty-eight hours later, medium and cells were collected to test whether BMP10 and GFP proteins overexpressed in mammalian cells show the following properities:

1. Detection of BMP10 by Western Blot in cells as well in medium due to the leader secretion sequence included in BMP10 cDNA. GFP should be detectable only in transfected cell lysates.
2. Induction of alkaline phosphatase (ALP) in C2C12 cells by BMP10 containig supernatant from transfected cells.

As shown in Fig. 3.57 293T cells were efficiently transfected with the BMP10-IRES-GFP plasmid (Fig. 3.57A) and the pEGFP control vector (data not shown). Using Western Blot analysis GFP was detected with the anti-GFP antibody in the lysate of cells transfected with either the BMP10-IRES2-GFP expression construct or the control vector.

A weak signal was also visible in both control and conditioned serum free media; which is probably derived from dying transfected cells. In case of BMP10, Western Blot revealed the expression of the full length protein in 293T cells transfected with the plasmid, but not with the empty vector. A stronger band of appropriate size was also detectable in BMP10 conditioned medium, which indicates efficient secretion and accumulation of full length protein in this medium. The band was not present in control serum free medium after pEGFP transfection (Fig. 3.57B).

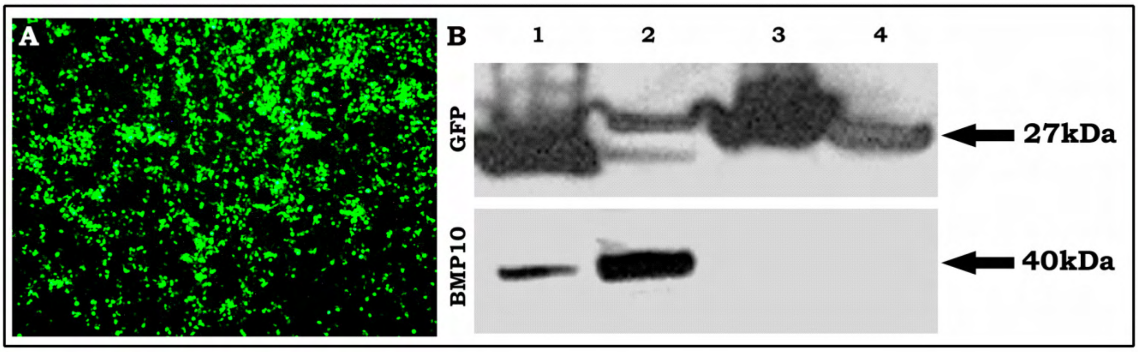

Fig. 3.57. Panel A- Typical transfection efficiency of 293T cells necessary for enrichment of the medium with BMP10. Panel B- Western Blot analysis of cell lysates (lanes 1 and 3) and serum free medium (lanes 2 and 4) 72 hours after transfection with BMP10-IRES-GFP (lanes 1 and 2) or control pEGFP (lanes 3 and 4).

Since the protein of the expected size was efficiently synthesized, secreted and accumulated in the medium, the most important was to verify the biological activity of the overexpressed BMP10. All members of the Bone Morphogenetic Proteins family are known to induce osteoblast differentiation of myoblastic cells, such as C2C12 cells (Katagiri et al., 1994; Aoki et al., 2001).

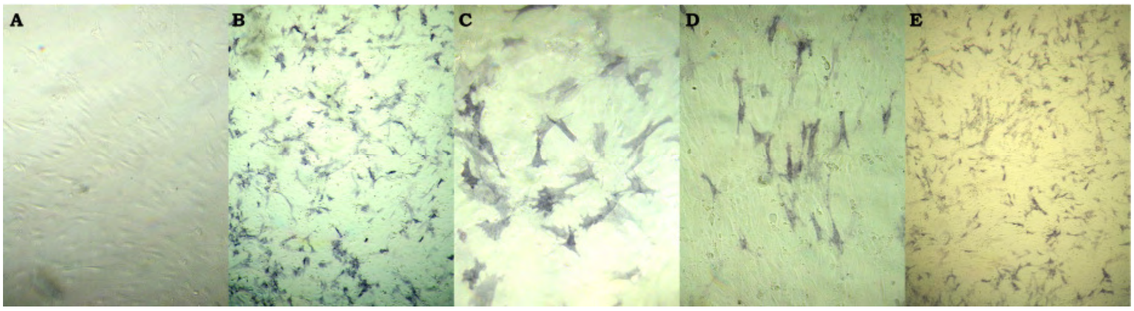

Fig. 3.58. BMP10 induces differentiation of C2C12 cells into osteoblasts. Alkaline phosphatase activity detection (blue) in C2C12 cells treated with SF control (A), BMP10 enriched medium (B-D) and BMP2 (E- positive control). Panel A- 100% of control serum free medium medium; B and C (high magnification)- 100% of

BMP10 conditioned medium, D-5% of BMP10 conditioned medium; E- positive control 200ng/ml BMP2.

Osteoblasts exhibit high levels of alkaline phosphatase (ALP) activity (Katagiri et al., 1994). Thus, induction of ALP by BMP10 would prove the biological activity of BMP10. Hence, C2C12 cells were plated in 96-well dishes in regular growth medium and 24 hours later the medium was replaced with serum free medium enriched in BMP10 or with control medium of different concentrations. Medium collected from pEGFP transfected 293T cells was prepared in parallel and used as a negative control. Commercially available BMP2 (Sigma) was used as a positive control. Cells were cultured for further 48 hours followed by detection of alkaline phosphatase (ALP) activity as described in Experimental Procedures.

The BMP10-IRES-GFP expression construct produced a functional BMP10 protein which is capable of activating ALP at a level comparable to BMP2. BMP10 is efficiently overexpressed and secreted since only 5% of BMP10 conditioned medium was sufficient to induce alkaline phosphatase activity in C2C12 cells (Fig. 3.58). ALP was neither induced in control conditioned medium (Fig. 3.58A) nor in DMEM serum free medium (data not shown).

A similar set of experiments was also carried using 10T1/2 and 293T cells. In both cell lines alkaline phosphatase expression/activity was not induced by BMP10 conditioned medium.

3.7.2. Cell line selection for *in vitro* studies

On the basis of immunohistochemistry BMP10 positive cells in pathological murine hearts exhibited the following features:

1. They reside in the vicinity or are incorporated in vessels
2. They express proliferation markers
3. A subpopulation coexpresses the smooth muscle marker- SM actin
4. A subpopulation coexpresses the endothelial marker -PECAM
5. They can originate from Sca1 positive cells

Based on these observations, which suggest that BMP10 might exert effects on vessel-associated cells 3 different cell lines were chosen to test the function of BMP10:

1. mBM-MASC1- mouse bone marrow derived mesenchymal stem cells- because of their pluripotency and high expression of the Sca1 antigene (Belema Bedada et al., 2005).
2. The multipotent mouse embryonic fibroblastic 10T1/2 cell line because of its ability to differentiate into pericytes/vascular smooth muscle cells (vSMCs) (Hirschi et al., 1998), a process stimulated by TGFβ1.
3. Mouse adult non-cardiomyocytes (mANCM) isolated from adult wild type murine hearts. For this particular experiment cells were also isolated from the transgenic strain with GFP expression under control of the stem cell antigen 1 promoter- Sca1 (Ly6A)-GFP. The heterogeneity of the mANCM culture was checked by immunocytochemistry on the basis of the expression of various markers: fibroblasts (vimentin), myofibroblasts (vimentin and SMA), smooth muscle cells (SMA) and endothelial cells (PECAM and AcLDL uptake).

Serum free medium collected from 293T cells transfected with empty vector and prepared identical to BMP10 conditioned medium served as a negative control in each cell culture experiment.

As BMP10 exerts its function via receptor binding, the expression profile of BMPs/TGFβ type I receptors in all cell lines used in the project was analyzed by RT-PCRs (Tab. 3.2). 10T1/2, C2C12 and bm-MASCs express all type I receptors. In 293T cells ALK1 is not present, while COS1 cells lack ALK1, ALK5 and ALK6, described already as the least responsive cell line to BMP10 (Mazerbourg et al., 2005).

Expression profile of BMPs/TGFβ receptors in cell lines used in this study

	ALK1	**ALK3**	**ALK5**	**ALK6**
Cos1	-	+	-	-
10T1/2	+	+	+	+
C2C12	+	+	+	+
293T	-	+	+	+
BM-MASC1	+	+	+	+

Tab. 3.2. Collective representation of TGFβ type I receptor expression profile in cell lines used in this study (RT-PCRs results).

3.7.3. BMP10 induces proliferation

As mentioned before, the only consistent feature of all ventricular BMP10 positive cells in pathological murine hearts was the co-expression of proliferation markers. Since BMP10 knock-out embryos display a complete loss of ventricular cell proliferation (Chen et al., 2004), and overexpression of BMP10 in the embryonic myocardium results in increased cellular mitosis (Pashmforoush et al., 2004) the effects of BMP10 on growth of non-cardiomyocytes as well of various cell lines of embryonic and adult was investigated.

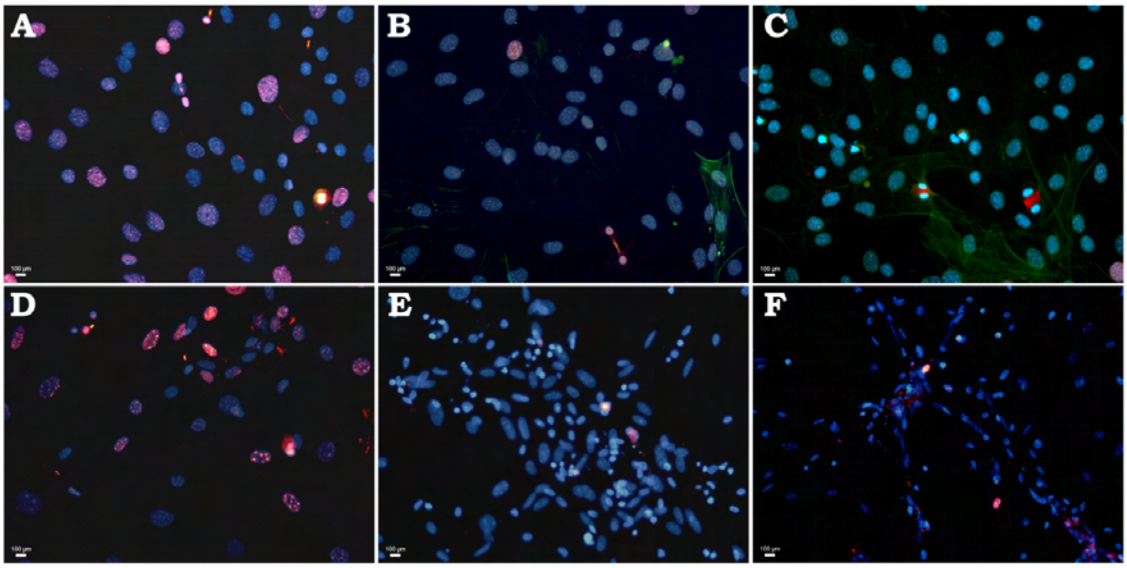

Fig. 3.59. BMP10 induced proliferation of 10T1/2 cells and mANCM isolated from the heart. Panels A-C- 10T1/2 cell line. Panels D-F- mANCM. Mitosis and cytokinesis marker- Aurora-B immunostaining (red) of cultured in standard growth medium containing 10% FCS (A and D), control serum free medium (B and E) and BMP10 conditioned medium (C and F) indicated the higher number of proliferating cells in BMP10 enriched medium compared to control SF medium, but lower than in growth medium. Nuclei are visualized in blue by DAPI.

Non-cardiomyocytes isolated from adult mouse heart (Fig. 3.59), 10T1/2 (Fig. 3.59) and mBM-MASC1 (Fig. 3.61) were plated at equal density. Cells were grown in standard growth medium containing 10% FCS or serum free control or BMP10 conditioned medium for 48 hours. Aurora-B staining was used to visualize cells undergoing mitosis and cytokinesis. Proliferating cells in late stages of mitosis and cytokinesis were counted and the relative ratio of proliferation was calculated with the number of dividing cells in control serum free medium was taken as 1. The summarized results are shown in Fig. 3.60. BMP10 induced proliferation in all tested cell lines compared to serum free control medium. In mBM-MASCs the number of mitotic cells increased 3.3 fold while in 10T1/2 and mANCM 2.4 and 2.2 fold more proliferating cells were noted, respectively in BMP10 conditioned than control medium.

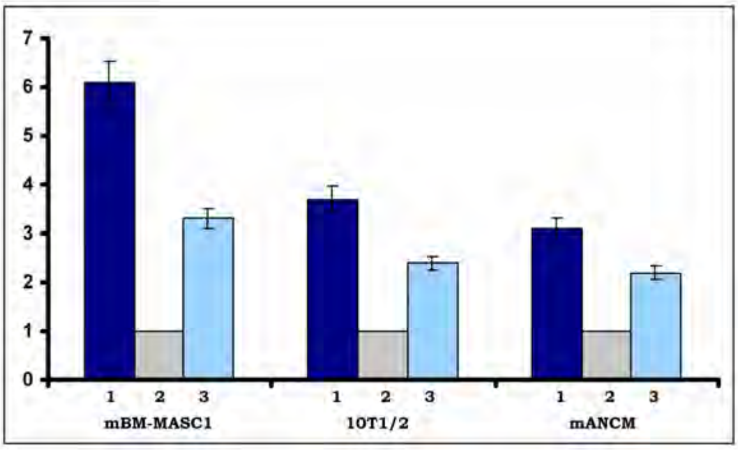

Fig. 3.60. BMP10 induces proliferation of cells in serum free medium. Relative proliferation ratio of mBM-MASCs, 10T1/2 and mANCM cells grown in standard growth medium supplemented with 10% FCS (bars 1) serum free control medium (bars 2)- reference value calculated as1 and serum free BMP10 enriched medium (bars 3).

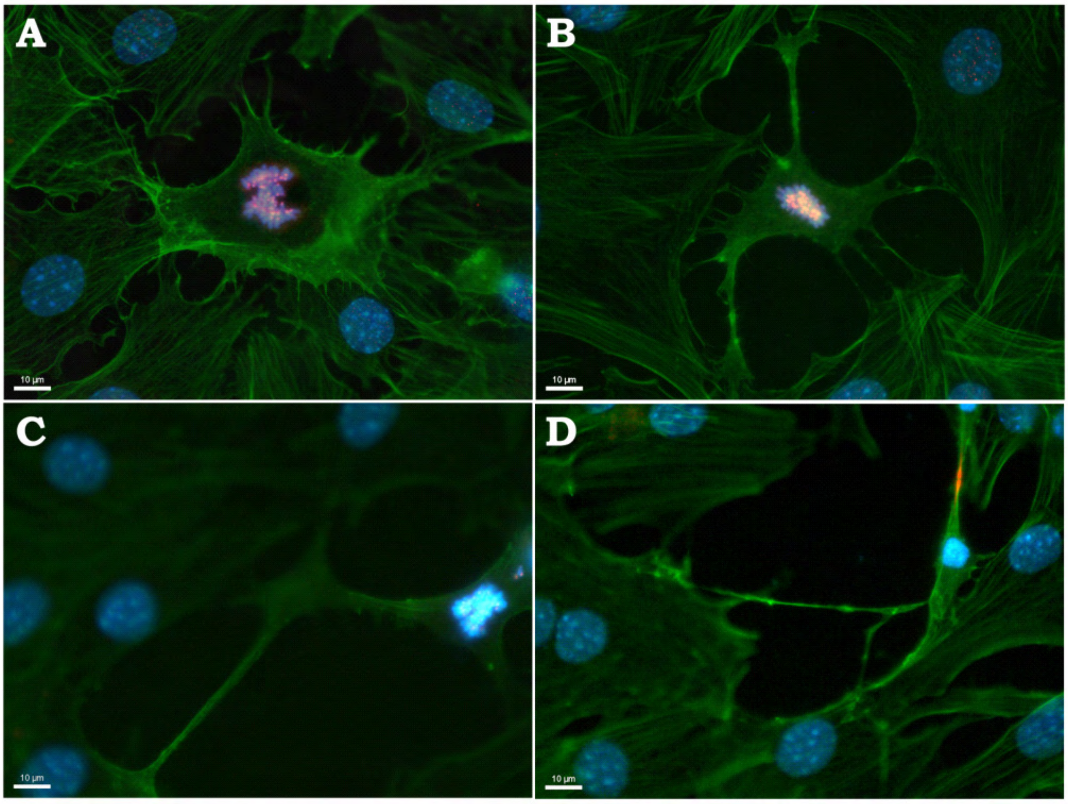

Fig. 3.61. BMP10 induces proliferation of mBM-MASCs. Note, that proliferating BMP10 treated mBM-MASCs cells (B-D) are morphologically distinct from control (A). Aurora-B immunostaining (red) of mBM-MASCs cultured in control

serum free medium (A) and BMP10 conditioned medium (B-D). Nuclei are visualized in blue by DAPI. F-actin was stained with phalloidin-FITC (green).

3.7.4. BMP10 induces morphological changes of various cell types

During the studies that addressed the effects of BMP10 on proliferation, not only the induction of mitosis, but also changes in the morphology of treated cells were noted. Forty-eight hours after replacing the growth medium to conditioned or control medium, BMP10 addition caused an intensive proliferation of smaller cells than in control medium as illustrated in mBM-MASCs (Fig. 3.61) and this morphology was preserved after cell division (Fig. 3.62).

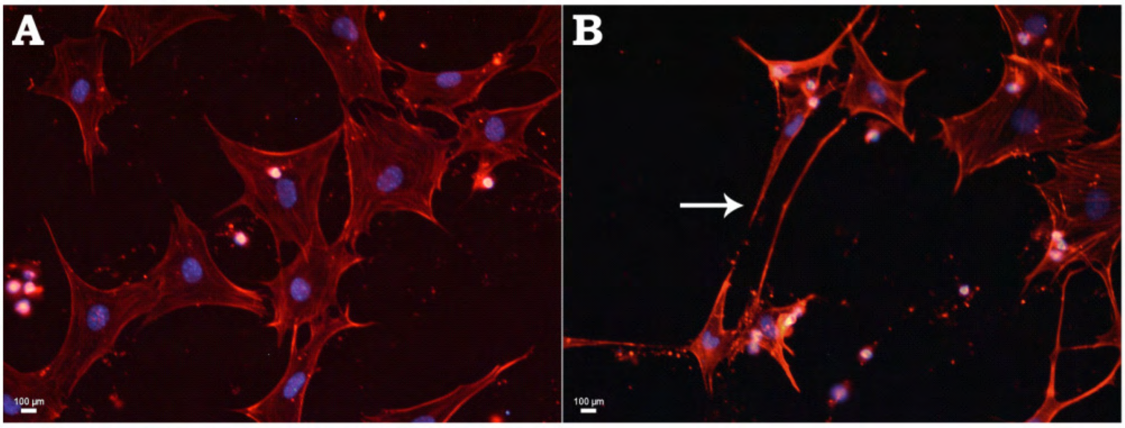

Fig. 3.62. mBM-MASCs grown in control serum free (A) and BMP10 enriched (B) medium were counterstained with phalloidin-TRITC (red). Nuclei are visualized in blue by DAPI. Note that the BMP10 treated cells formed far-reaching cell-cell contacts (arrow).

These cells created long processes enabling far-reaching cell-cell contacts (Figs. 3.62B, 3.63B,C). Most of them exhibited a spindle-like shape with centrally located nuclei and elongated cytoplasm. The nuclei of the newly appeared subpopulation of cells upon BMP10 addition in mBM-MASCs as well as in 10T1/2 were much smaller than in control cultures (Fig. 3.59C and 3.61B-D, respectively for both cell lines). It should be mentioned that in control medium serum deprivation also caused induction of a sub-population of smaller cells; however, to a much lower degree and they failed to form long distance cell-cell contacts.

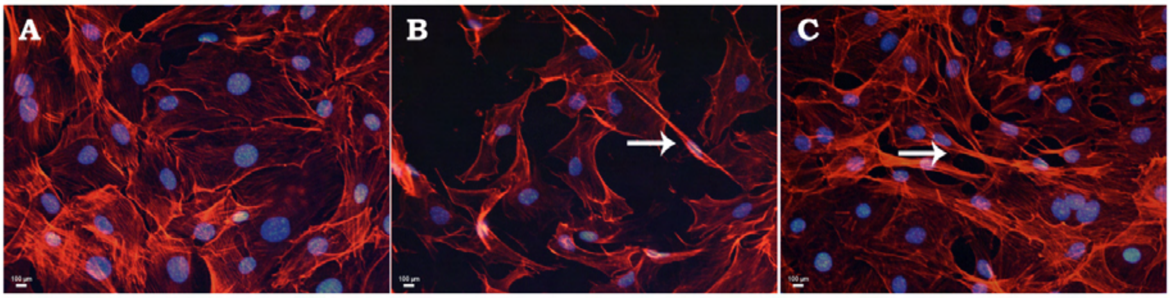

Fig. 3.63. 10T1/2 grown in control serum free (A) and BMP10 enriched (B,C) medium show distinct morphology. Arrows indicate created cell-cell contacts in BMP10 treated culture. Cells were counterstained with phalloidin-TRITC (red) and nuclei are visualized in blue by DAPI.

It is a well known phenomenon that serum deprivation induces SM-actin expression of 10T1/2 cells and differentiation to pericytes is strongly amplified by TGFβ-1 addition as judged by the expression of others pericyte markers (Hirshi et al., 1998). Kale et al., noted maximal SM-actin expression after 48 hours of 10T1/2 induction with TGFβ-1 (Kale et al., 2004). On the basis of this observation smooth muscle actin was firstly analyzed in the cell lines after 2 days of BMP10 addition. In 10T1/2 cells a robust expression of SM-actin was detected in BMP10 treated cultures, while only single cells in the control culture expressed this marker. No signal was detectable in cells grown in medium supplemented with 10% FCS. BMP10 induced SM-actin expression also in mesenchymal stem cells but in this case the expression was limited to a morphologically distinct subpopulation (Fig. 3.64).

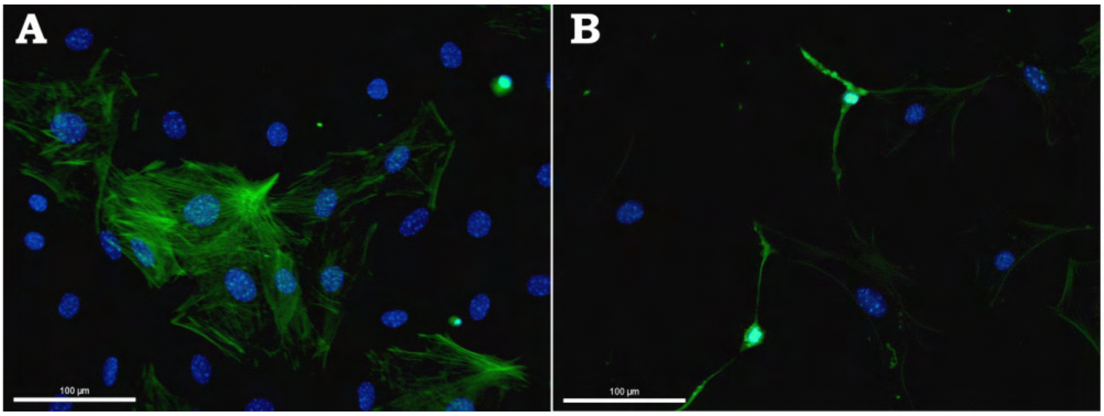

Fig. 3.64. SM-actin immunodetection in mBM-MASCs. Panel A- SMA expression (green) was induced by serum deprivation in control SF medium in cells with fibroblast-like morphology. Note the highly organized pattern of actin filaments. Panel B- SM-actin positive mBM-MASCs cells (green) grown in BMP10 enriched serum free medium for 48h showed a different morphology and accumulation of disorganized actin filaments. Nuclei were visualized by DAPI staining (blue).

In mBM-MASCs cells growing in control SF medium an expression of SM-actin was found in some larger cells with fibroblast-like morphology and the actin filaments showed a high degree of organization (Fig. 3.64A) opposite to the BMP10 treated cells where disorganized SMA was accumulated in the cytoplasm (Fig. 3.64).

3.7.5. BMP10 induces a distinct subset of mBM-MASC-derived cells and tube-like formation

Since 48 hours treatment of mesenchymal cells with BMP10 caused induction of a morphologically distinguishable cell population, the effect of this factor during later time-points was further studied.

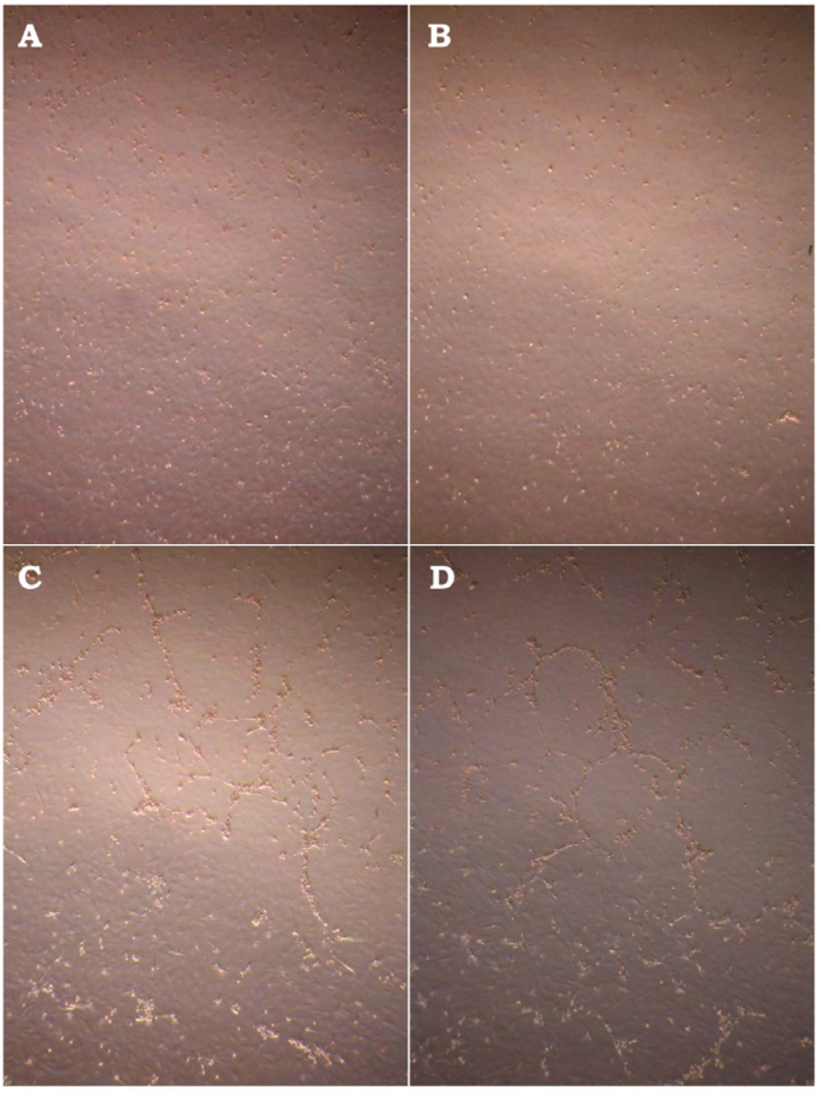

Fig. 3.65. Phase-contrast micrographs of mBM-MASCs after 96 hours of culture in serum free control (A,B) and BMP10 conditioned medium (C,D).

Fig. 3.65 illustrates the difference between mBM-MASCs cultured in control and BMP10 enriched serum free medium for 4 days. Cells stimulated with BMP10 failed to form a monolayer and recruited neighboring cells to create characteristic line or ring-shaped patterns. This observation indicated stem cell differentiation into endothelial (EC) or pericytes/vSM cells. Hence the expression of EC markers (PECAM and Capsulin/POD/Epicardin as well Ac-LDL uptake), pericyte specific markers (PDGFRβ, SMA) and smooth muscle specific molecule (Calponin) were tested.

As mentioned in the previous chapter, SM-actin expression was first noted 48h after BMP10 stimulation. Forty-eight hours later (96 hours in conditioned or control medium) SMA expression was analyzed again and was found mostly in "line-like" structures composed of a population of small cells with disorganized actin filaments.

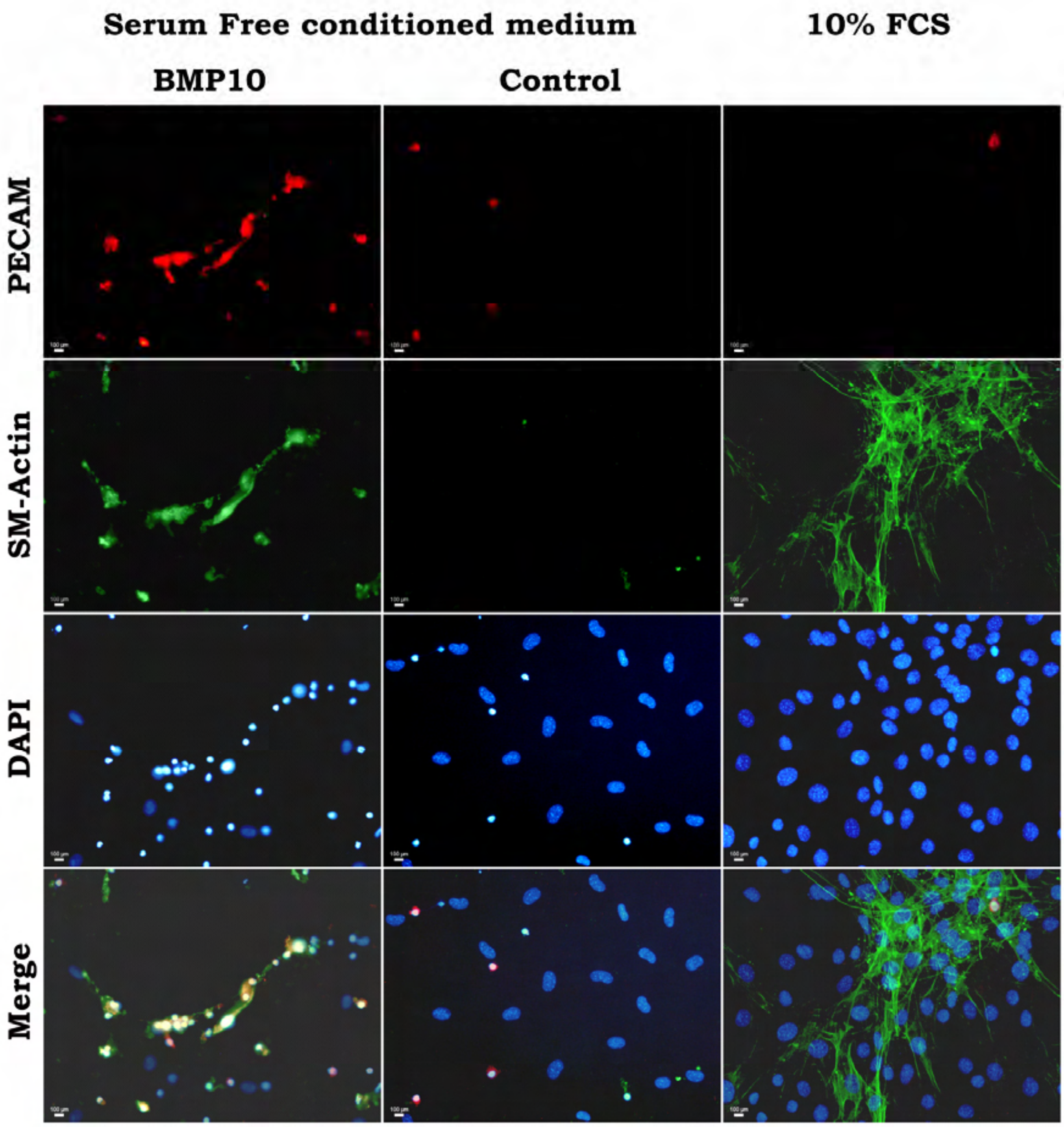

Fig. 3.66. BMP10 induced PECAM (red) and SM-actin (green) expression in mBM-MASCs (left panel). Note the co-localization of endothelial and smooth muscle cell markers upon BMP10 treatment. In mBM-MASCs grown in control SF medium (middle panel) and standard growth medium (right panel) expression of CD31 and SMA was also noted, but co-localization of signals was never observed. Nuclei were stained with DAPI (blue).

Surprisingly, PECAM was also detectable in some SMA positive cells (Fig. 3.66), although some cells were found that expressed only a single marker. mBM-MASCs cultured in control serum free generatedmedium single cells positive for one marker were also found. However, co-localization of signals was never observed. SMA expression was detected in some of the cells with highly organized actin filaments when mBM-MASCs reached confluence in standard growth medium supplemented with 10% FCS.

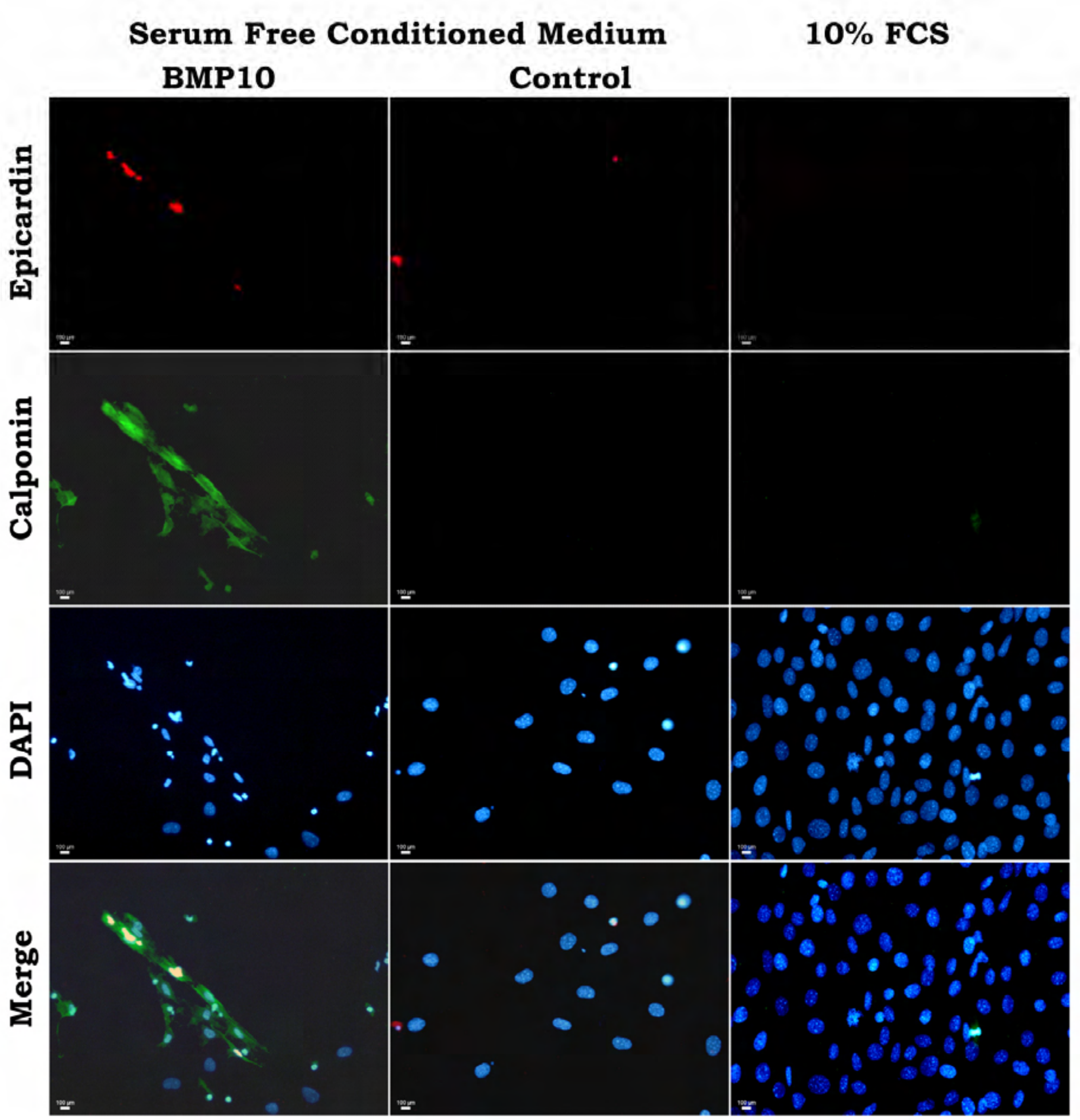

Fig. 3.67. The endothelial marker– epicardin (red) co-localizes with calponin expression (green) in a subpopulation of BMP10 treated cells (left panel). Both markers were only occasionally found in control SF medium (middle panel) or growth medium (right panel). Nuclei were stained with DAPI (blue).

This might be explained by spontaneous differentiation of stem cells in all types of cells due to their pluripotency when they are confluent (data kindly provided by Dr. F. Belema Bedada, personal communication). Similar results were observed in the case of serum deprivation.

Unexpectedly PECAM and SMA co-localized in some BMP10 treated cells. To further investigate the identity of these cells another set of smooth muscle and endothelial cell markers - calponin and epicardin, was studied.

A specific nuclear localization of epicardin was found in "line-like structures", but not in other cells, and the majority of capsulin positive cells expressed also calponin (Fig. 3.67). On the other hand, in approximately of 70% cells positive for calponin the endothelial marker was not detectable. Only a minor amount of cells grown in control serum free or standard growth medium (GM) was calponin positive, as it is a more specific marker and expressed later than SM-actin.

The most specific method to identify an endothelial cells subpopulation is their ability to take up Ac-LDL (Acetylated Low Density Lipoprotein). Some mBM-MASCs induced with BMP10 were positive for Ac-LDL uptake as presented above (Fig. 3.68). Red fluorescence, specifically indicating the endothelial character of labeled cells partially overlapped with diminished SM-actin staining, but most of the ECs were not expressing smooth muscle actin. Neither cells from the control culture nor stem cells grown in standard GM were positive for Ac-LDL uptake.

As mentioned previously, TGFβ is known to induce differentiation of 10T1/2 cells to pericytes/vSMCs. Several markers are commonly used to identify pericytes, e.g. SM-actin and platelet-derived growth factor receptor β (PDGFRβ). There is evidence that pericytes may also give rise to other types of cells, including fibroblasts, osteoblasts, chondrocytes and adipocytes (Collet et al., 2005, Armulik et al., 2005). To address the question whether BMP10 induced expression of other pericyte markers in MASC mesenchymal stem cells I also investigated the presence of PDGFRβ (Fig. 3.69).

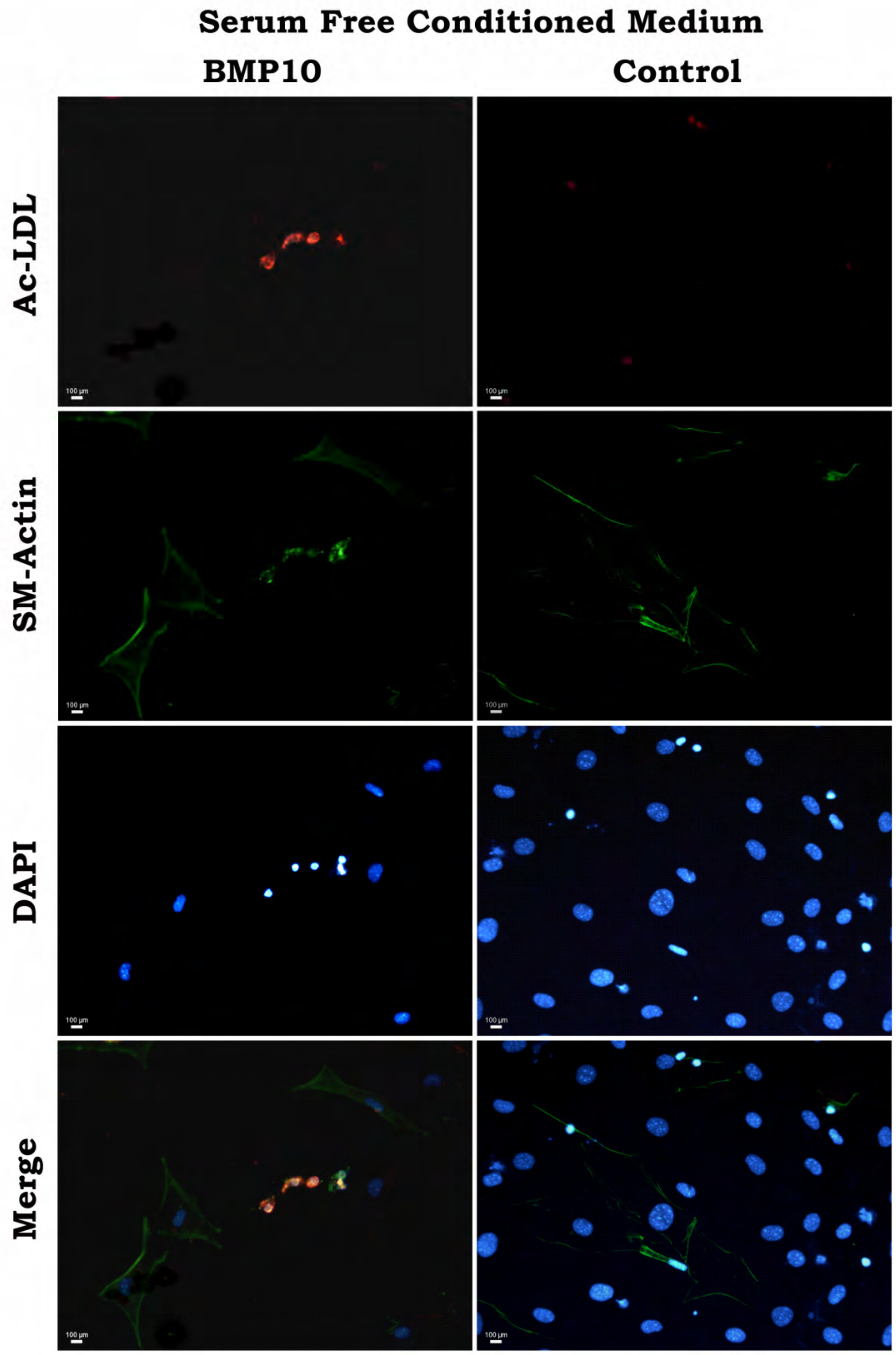

Fig. 3.68. Representative images of Dil- labeled Ac-LDL (red) uptake by mBM-MASCs grown in the presence of BMP10 (left panel). The drug was not detectable in mBM-MASCs grown in control SF medium (right panel). Cells were stained with anti-SM actin (green) and nuclei were visualized with DAPI.

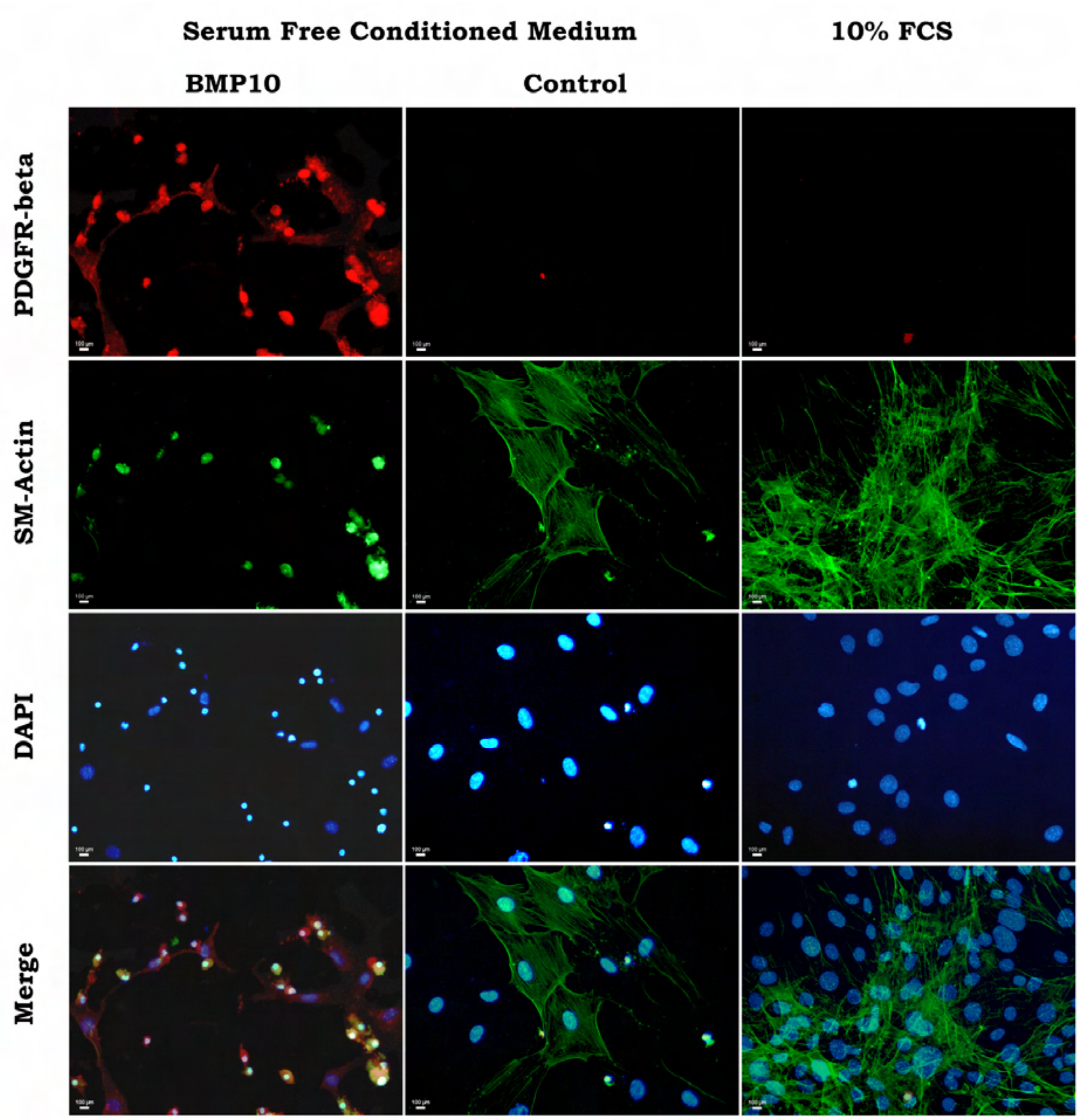

Fig. 3.69. Immunostaining of PDGFRβ receptor (red) and SMA (green) in mBM-MASCs. PDGFRβ is specifically detected in BMP10 treated cells (left panel), but not in control cells (middle panel- control SF medium; right panel- standard GM). DAPI stains nuclei in blue.

PDGFRβ expression was specifically induced by BMP10 addition, but not by serum deprivation in a control culture of bone marrow derived mesenchymal stem cells. Approximately 50% of PDGFRβ positive cells express SM-actin as well. In addition I also detected cells with only one of the two tested markers. As before, SMA was detected in both serum free control medium and 10%FCS supplemented growth medium. Moreover, SMA co-localized in some BMP10 treated cells with vimentin expression (Fig. 3.70). Vimentin was not found in control untreated cells and BM-MASCs grown in growth medium.

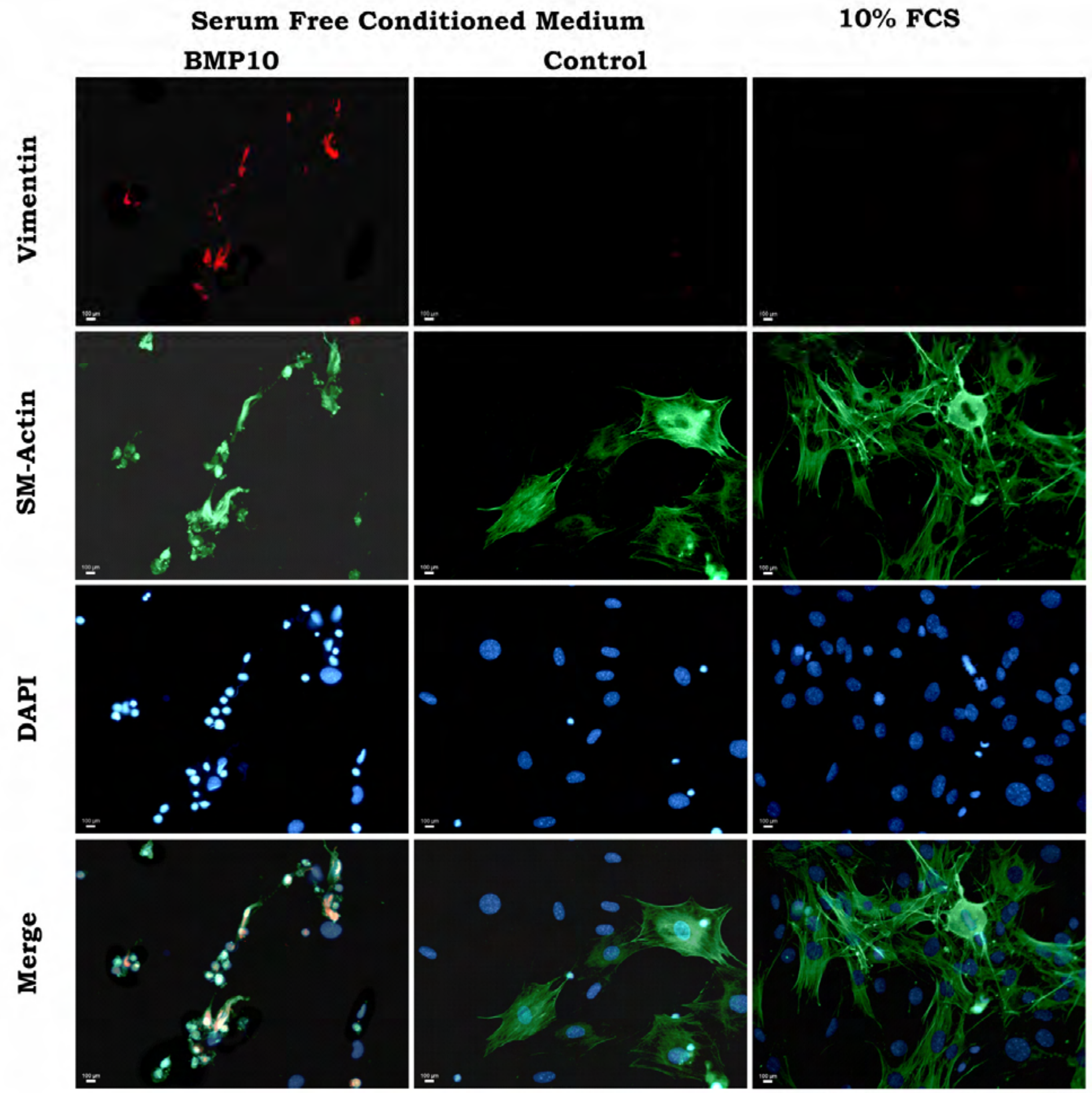

Fig. 3.70. Immunostaining of EMT marker - vimentin expression is induced by BMP10 (left panel, red) and co-localizes with SMA (green). Vimentin was not detectable in both control cultures. Nuclei are visualized in blue by DAPI.

3.7.6. Differentiation of 10T1/2 cells is stimulated by BMP10 addition

Multipotent mesenchymal 10T1/2 cells are known to differentiate into various cell types. MyoD induces fibroblast conversion to muscle cells (Braun et al., 1989), whereas their stimulation with TGFβ results in expression of pericyte/vSMC markers (Hirshi et al., 1998). Preliminary results indicated that treatment of 10T1/2 with BMP10 might induce differentiation into a new sub-population of morphologically distinct cells. 10T1/2 fibroblasts were grown in serum free BMP10 conditioned or control medium followed by immunocytochemical analysis as in the case of mBM-MASCs. In BMP10 enriched medium 10T1/2 cells created cord-like structures, as shown below (Fig. 3.71).

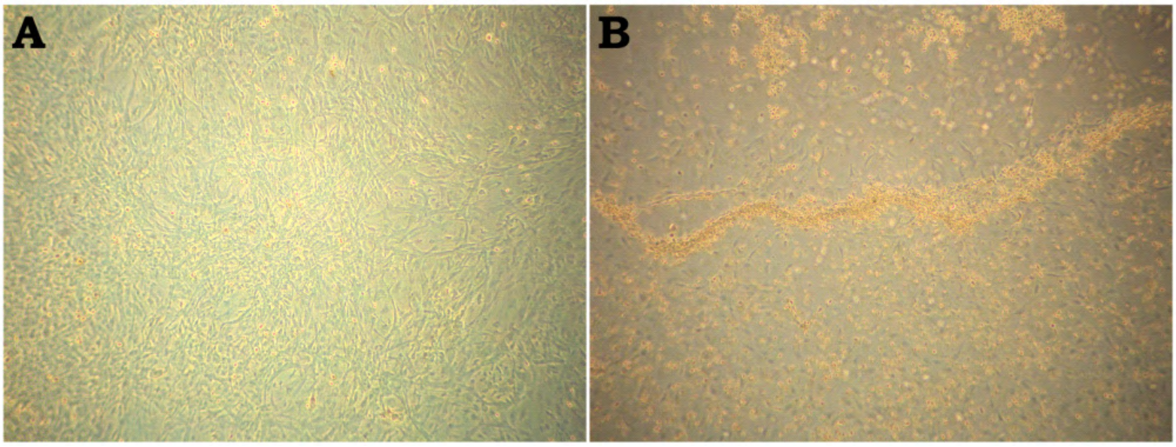

Fig. 3.71. Phase contrast microphotography of 10T1/2 cells grown in control (A) and BMP10 enriched (B) serum free medium for 7 days. The BMP10 but not the control serum free medium stimulateed cord-like structure formation.

The first and obvious question was whether the effect of BMP10 on 10T1/2 differentiation was similar to the TGFβ effect, hence immunodetection of PDGFRβ and SM-actin, which serve as pericyte/vSMC markers, was performed.

Strong induction of PDGFRβ expression was observed in BMP10 treated cultures. In cord-like structures SMA co-localized with the PDGF-BB receptor (Fig. 3.72 middle panel). In a sub-population of small cells, which did not show the this line-like pattern, PDGFRβ positive cells mostly did not express SM-actin and an overlapping signal was found only occasionally. To further investigate the induction of smooth muscle markers, the expression of calponin- a late SMCs marker- was examined (Fig. 3.73).

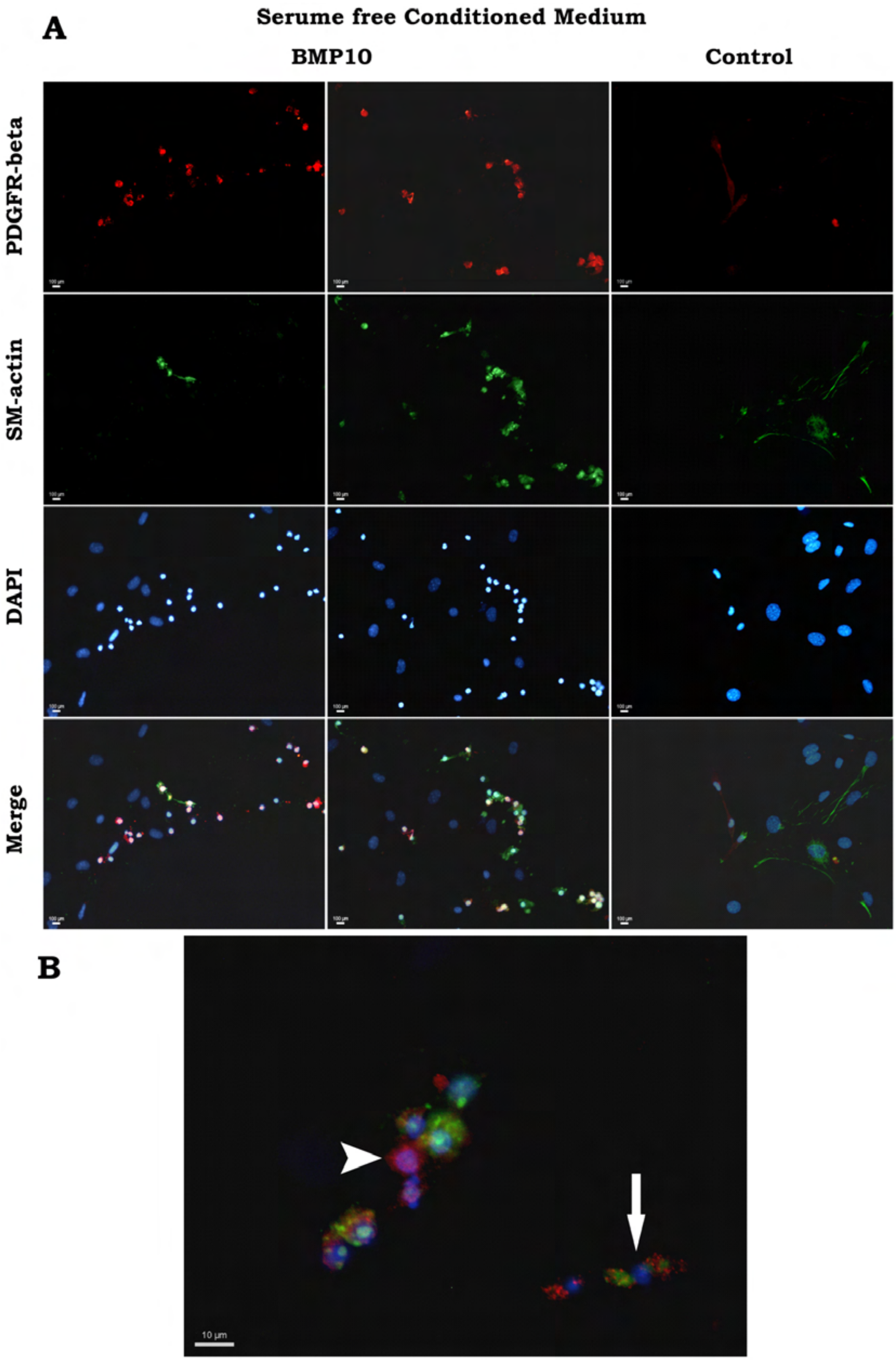

Fig. 3.72. (A) Low power magnification of PDGFRβ (red) and SMA (green) immunodetection in 10T1/2 cells treated with BMP10 (left and middle panel), or control SF medium (right panel). Nuclei were stained with DAPI (blue). (B) Higher magnification of BMP10 treated cells stained as in A. Note the partially overlapping signal of PDGFRβ and SMA (arrow) or the lack of their co-localization (arrowhead) in BMP10 treated cells

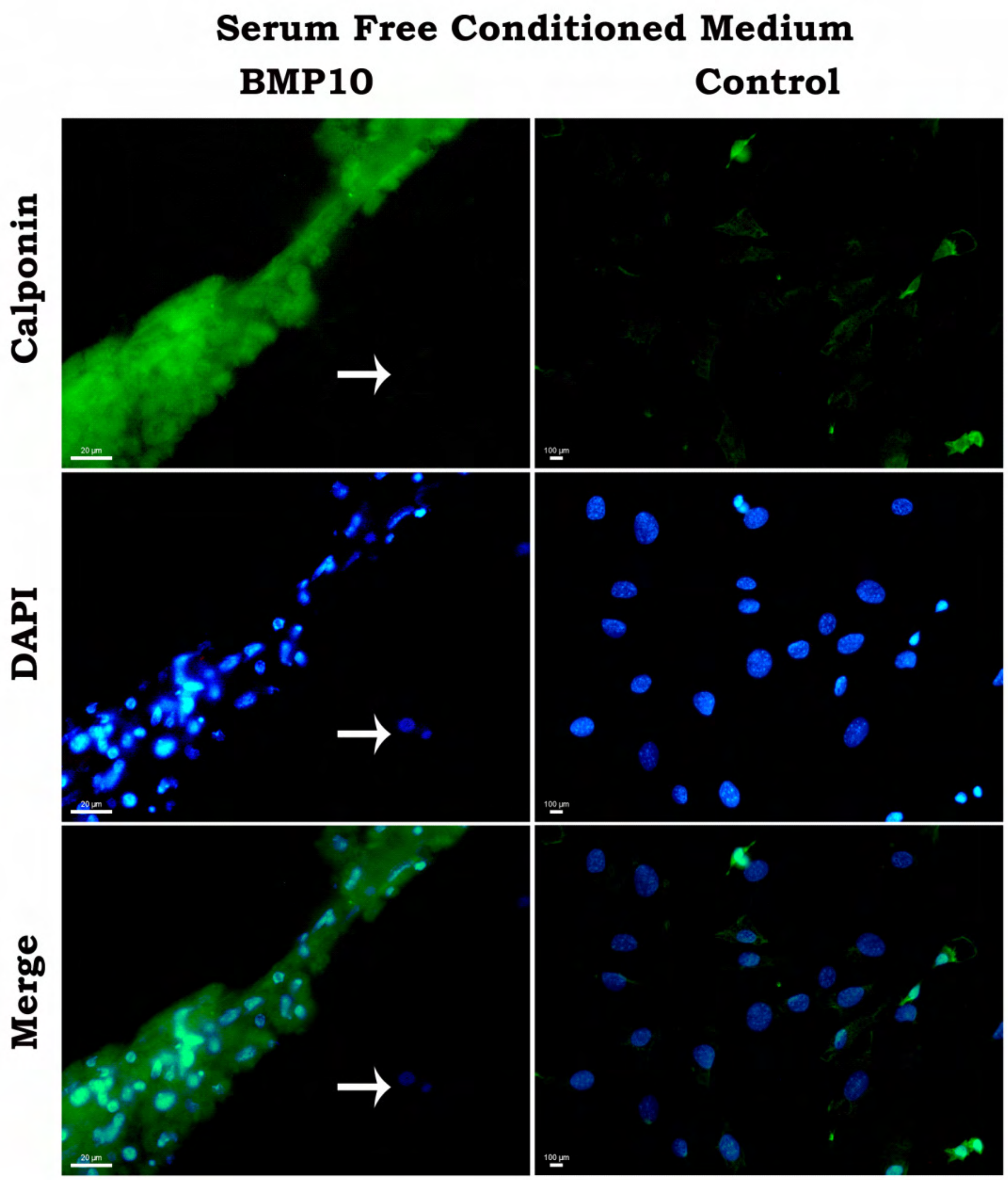

Fig. 3.73. Immunodetection of calponin (green) in 10T1/2 cells grown in BMP10 conditioned (left panel) or control (right panel) serum free medium. Arrows indicate a monolayer cell negative for calponin. Nuclei are visualized in blue by DAPI.

Fig 3.73 shows the results of calponin detection in 10T1/2 cells cultured in BMP10 enriched and control medium. Strong calponin expression was found after BMP10 treatment in highly organized tube-like structures, but not in other cells. Only a minor back-ground signal was noted in control cultures.

Addition of BMP10 to stem cell cultures induced expression of endothelial markers. Therefore CD31 and Ac-LDL uptake was also examined in 10T1/2 cells.

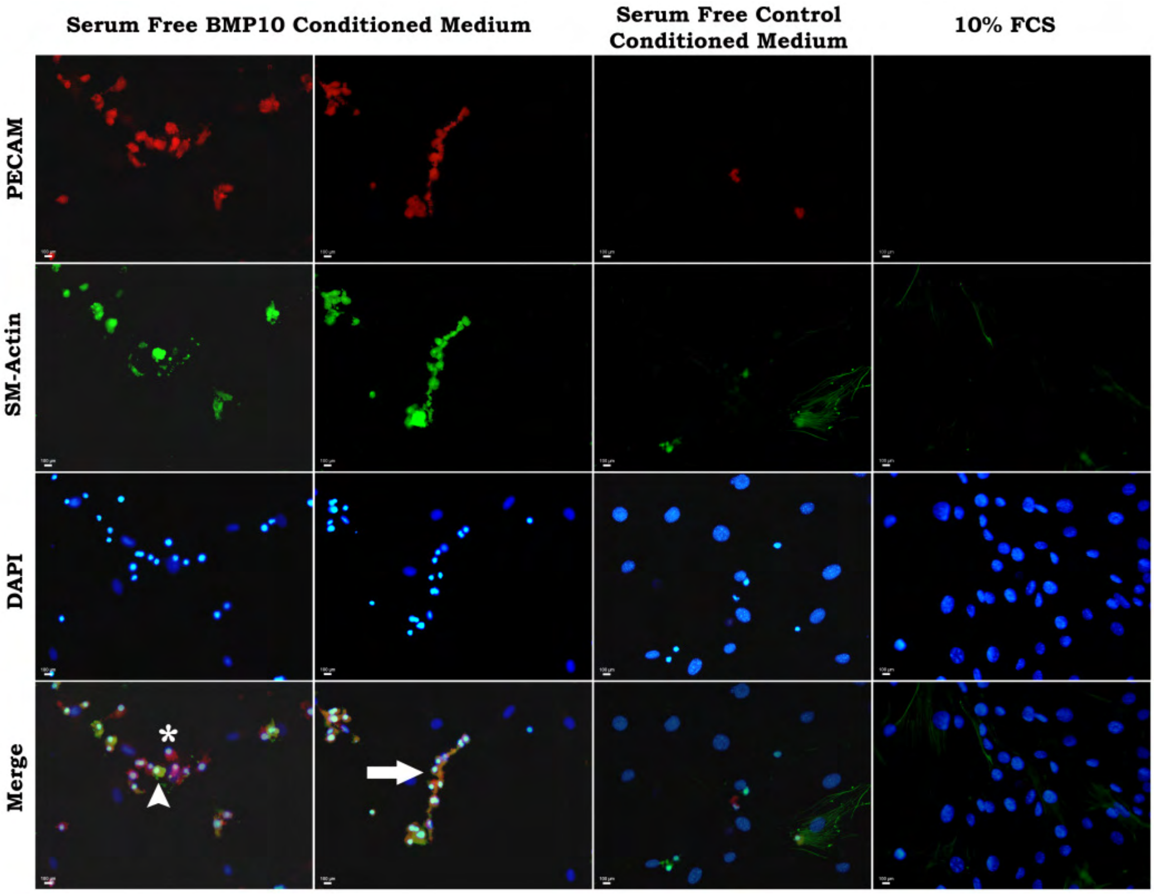

Fig. 3.74. A. Low magnification images of PECAM/CD31 (red) and SMA (green) immunodetection of 10T1/2 cultured in BMP10 conditioned and control SF medium, as well in standard growth medium supplemented with 10% FCS. Nuclei are shown in blue. Note three populations of cells in BMP10 treated culture: PECAM$^{pos.}$/SMA$^{pos.}$ (arrow); PECAM$^{pos.}$/SMA$^{neg.}$ (asterisk) and PECAM$^{neg.}$/SMA$^{pos.}$ (arrowhead). PECAM and SMA were detected in single cells in control cultures at marginal background level.

Two distinct patterns of PECAM/SM-actin expression were found (Fig. 3.74). In cord-like structures induced by BMP10, most of the cells expressed both proteins, while in areas where theses structures were not yet obvious three phenotypes were noted: PECAM$^{pos.}$/SMA$^{pos.}$; PECAM$^{pos.}$/SMA$^{neg.}$ and PECAM$^{neg.}$/SMA$^{pos.}$. It should be emphasised that most of cells in this case were PECAM$^{pos.}$/SMA$^{neg.}$. When cells were positive for both antigens, one signal was usually stronger and the other weaker. Ac-LDL uptake (Fig. 3.75) followed by SM-actin staining confirmed this observation.

Red fluorescence indicating endothelial cells were only found in 10T1/2 cells grown in serum free BMP10 conditioned medium, but not in the control culture (Fig. 3.75).

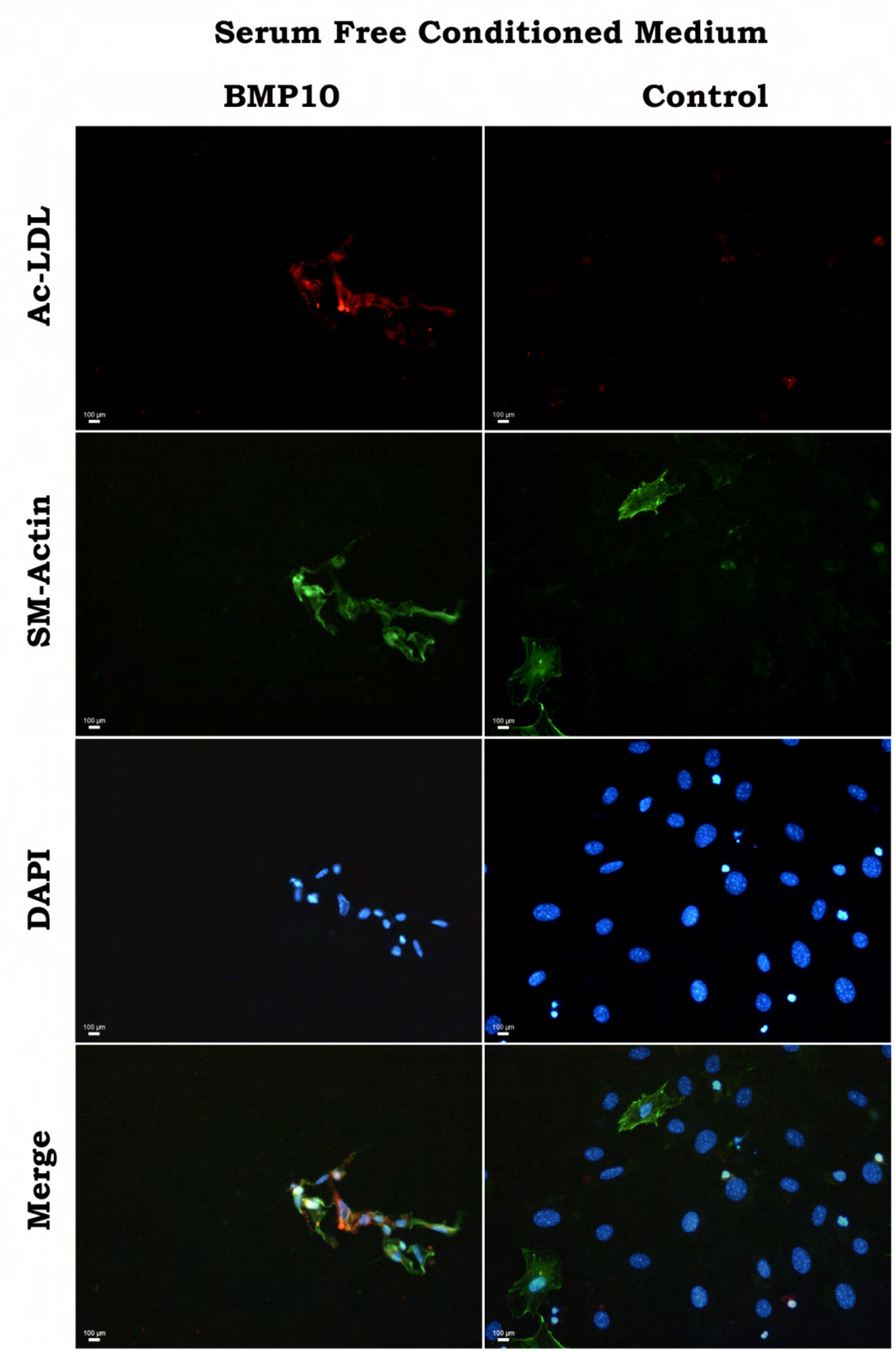

Fig. 3. 75. Identification of endothelial cells on the basis of DiI-Ac-LDL uptake (red), followed by SM-actin staining (green) in BMP10 treated (left panel) and control cultures (right panel). Nuclei were stained with DAPI (blue).

Cells strongly positive for Ac-LDL uptake had only a weak, marginal SMA signal and vice versa. Approximately 40% of the cord-like forming cells were AcLDL positive, 40% exhibited smooth muscle phenotype and 20% were negative or weakly positive for both. Because of the unexpected induction of either smooth muscle or endothelial markers by BMP10 addition, their expression was also analyzed at the RNA level.

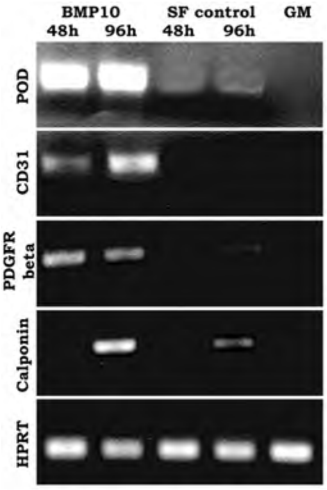

Fig. 3.76. BMP10 induces expression of endothelial markers (POD, CD31), the pericyte-specific marker PDGFRβ and the smooth muscles marker calponin in 10T1/2 cells. Semi-quantitative RT-PCR analysis of BMP10 treated and control 10T1/2 cells 48 and 96 hours in culture as well as in confluent culture in growth medium. The endothelial specific transcription factor- POD is highly expressed after 48 hours of BMP10 treatment, whereas cell-surface CD31 is upregulated after 4 days. Note the induction of calponin expression by serum deprivation. Equal loading of RNA was assured by monitoring expression of the housekeeping gene HPRT.

Semi-quantitative RT-PCR analysis confirmed the results of immunocytochemistry (Fig. 3.76). Strong induction of the endothelial specific transcription factor POD was detectable in 10T1/2 cells already 48 hours after BMP10 addition and was sustained at the same level 48 hours later. The other cell surface endothelial marker- CD31 was weakly expressed after 2 days in conditioned medium but its level increased after 96 hours of treatment. Calponin was not detectable at an earlier time-point, but on the fourth day of BMP10 treatment its transcription was strongly induced. It should be mentioned that serum deprivation also caused an expression of calponin albeit at a much lower level. PDGFRβ was also detected in treated cells after 48 and 96 hours.

Vimentin, a mesenchymal marker, is known to be up-regulated during endothelial-to-mesenchymal transition (EMT). Vimentin was highly expressed in

10T1/2 cells growing in medium containing 10% FCS (Fig. 3.77). Serum deprivation resulted in down-regulation of vimentin expression. In fibroblasts grown in serum free BMP10 supplemented medium vimentin was also downregulated, but its expression level was preserved in a small subpopulaion of cells in cord-like structures. A strong signal of vimentin was observed mostly in cells weakly positive or negative for SMA.

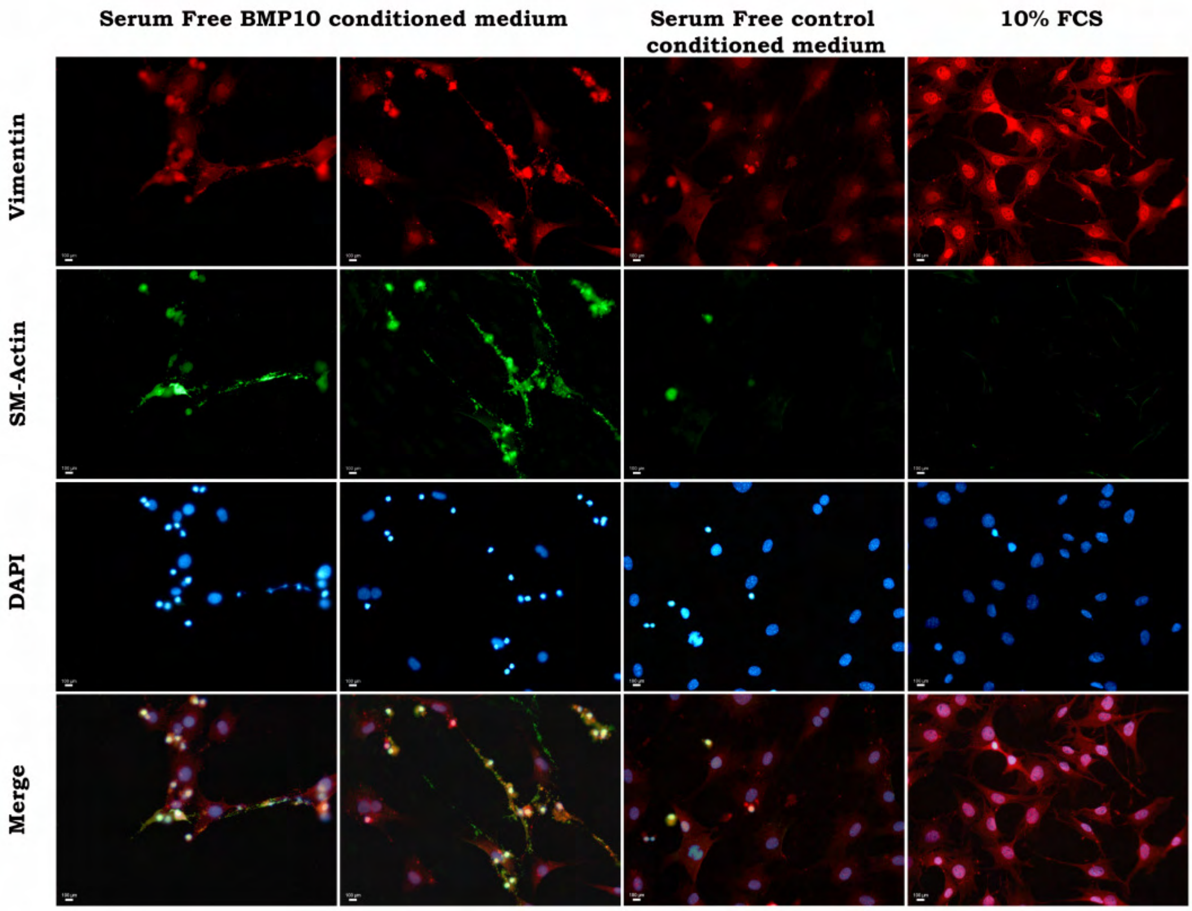

Fig. 3.77. Downregulation of vimentin expression (red) correlated with SMA (green) upregulation in BMP10 treated 10T1/2 cells in cord-like structures. Decreased vimentin staining without significant SMA induction was observed in control serum free medium in 10T1/2 cells. The right panel represents 10T1/2 cells grown in standard GM, stained with the same set of markers. Note the strong and homogeneous vimentin pattern. Nuclei are visualized in blue by DAPI staining.

3.7.6.1. Overexpression of BMP10 induces differentiation of 10T1/2 cells

Since addition of BMP10 to the medium induced differentiation of 10T1/2 cells, I investigated whether it is possible to achieve the same effect by direct overexpression of the growth factor. This experiment allowed me to confirm that induction of proliferation and differentiation of fibroblasts are direct downstream effects caused by BMP10, but not a result of other proteins secreted from 293T cells to the conditioned medium. 10T1/2 cells were seeded at equal density and transfected with BMP10-IRES-GFP plasmid or a pEGFP empty vector as a control. After transfection cells were grown in standard growth medium supplemented with 10% FCS to avoid the differentiation in response to serum deprivation. It should be emphasized that transfection efficiency was comparable for both pEGFP and BMP10-IRES-GFP after 24 hours, when GFP expression was clearly visible. Figure 3.78 illustrates the difference in cell morphology between control and BMP10 transfected 10T1/2 cells 24 hours after transfection. An obvious proliferative effect as well a morphologically distinct shape of BMP10 transfected cells was noted after 48 hours as shown in Fig. 3.79. Control cells expressing GFP remained morphologically indistinguishable from surrounding fibroblasts and did not exhibit a high rate of mitosis since only single cells, not clusters of green cells were found 48 hours after transfection. Clusters of elongated green cells creating network –like structures became visible at the same time point after transfection with BMP10-IRES-GFP construct.

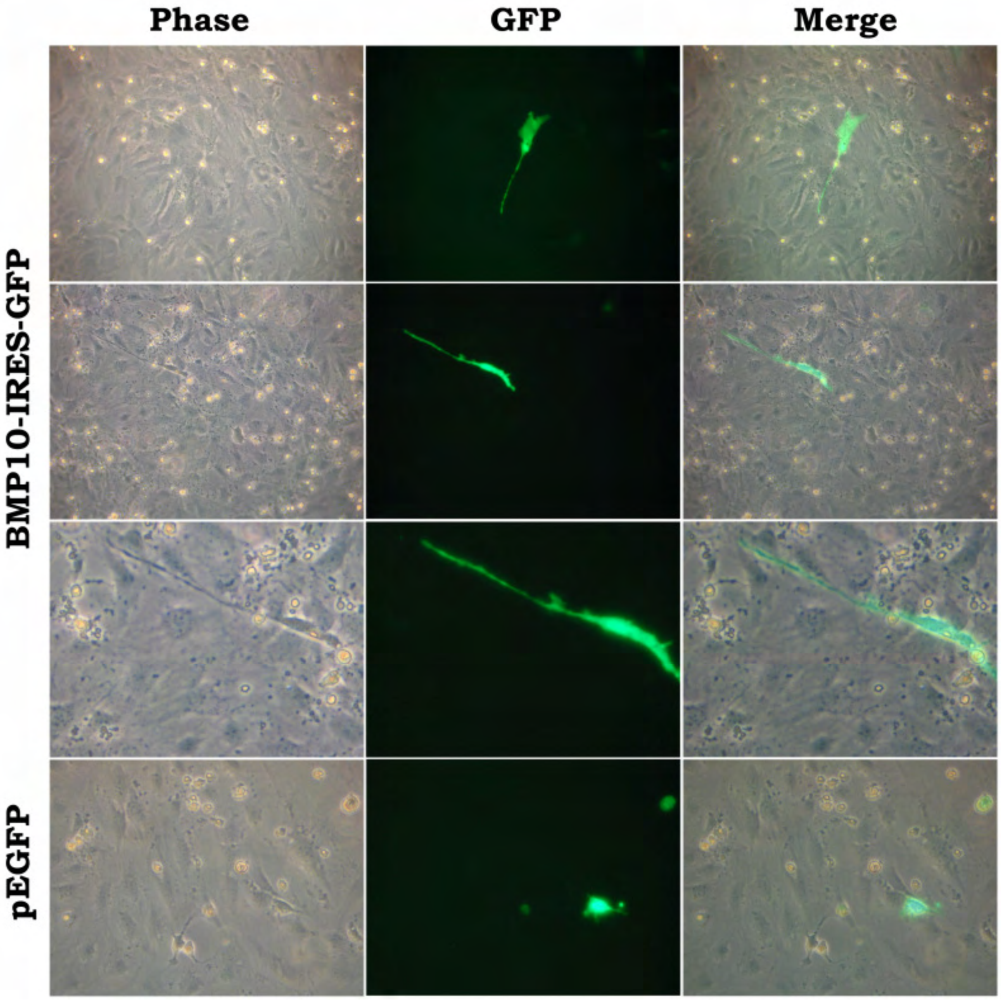

Fig. 3.78. 10T1/2 cells 24 hours after transfection with BMP10-IRES-GFP and control pEGFP vector. GFP positive cells indicating on BMP10 expression (BMP10-IRES-GFP transfected) are morphologically distinct from cells transfected with the empty vector.

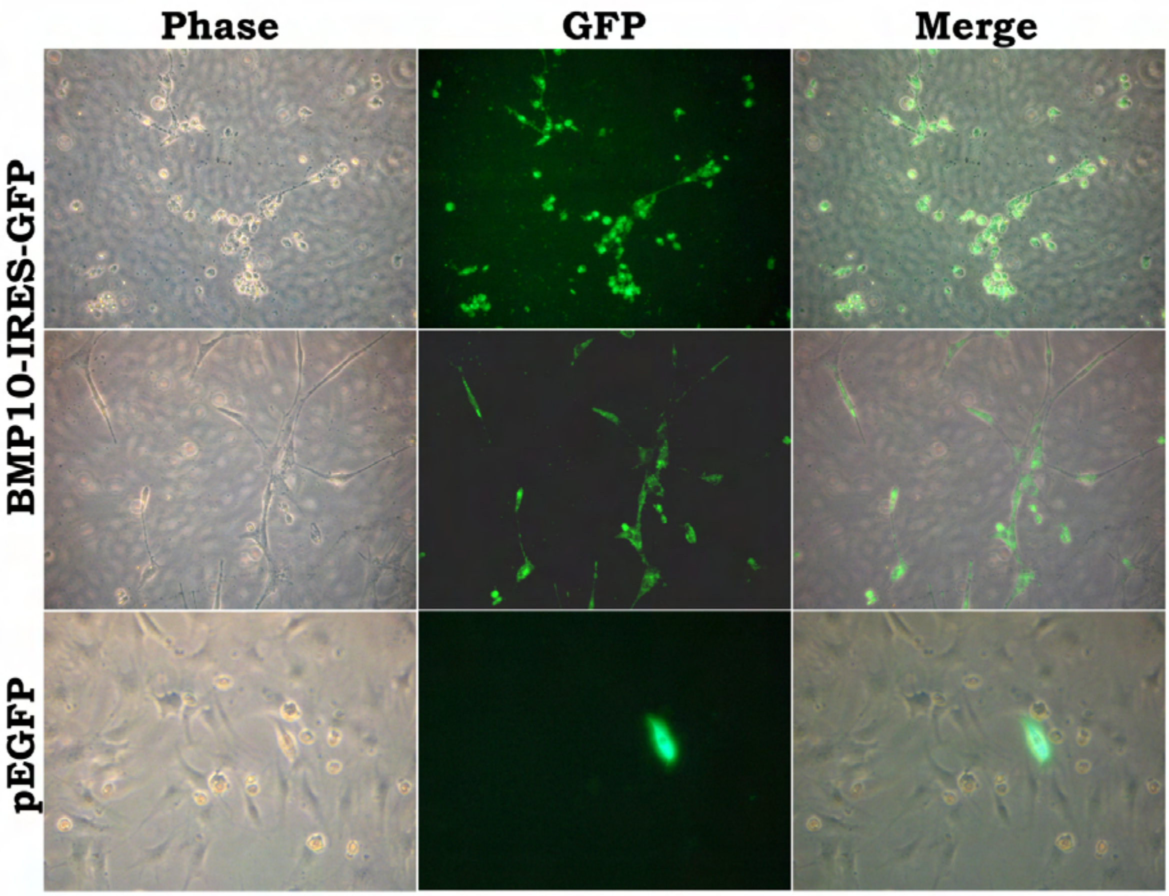

Fig. 3.79. 10T1/2 cells 48 hours after transfection with BMP10-IRES-GFP and control pEGFP vector. GFP positive cells indicating BMP10 expression (BMP10-IRES-GFP transfected) are morphologically distinct from cells transfected with the empty vector. Note the increased number of green cells in the 10T1/2 cell line transfected with the BMP10 expression construct indicating a pro-mitotic effect of BMP10.

The effects of BMP10 overexpression in 10T1/2 cells was more pronounced 72 hours after transfection. In contrast to control cultures (data not shown), where only single or pairs of GFP positive cells were found, a large number of BMP10 expressing cell clusters was visible (Fig. 3.80). In addition to long-shaped cells, a sub-population of smaller cells expressing GFP appeared in the culture, as shown in Fig. 3.80. The new type of cells was comparable with those induced by BMP10 conditioned medium in both 10T1/2 and BM-MASC cell lines. These cells remained connected with elongated cells creating “nodes” and formed clusters with each other. The pro-mitotic effect was maintained even 72 hours after transfection.

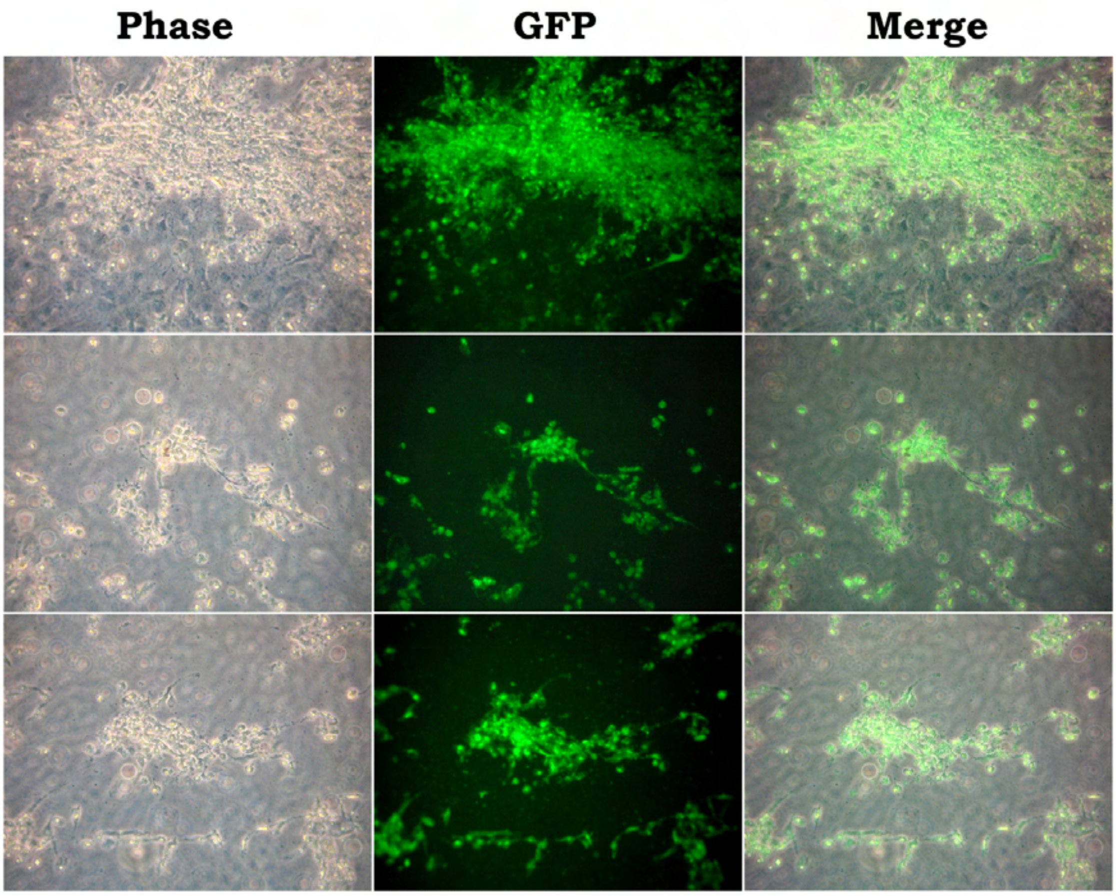

Fig. 3.80. 10T1/2 cells 72 hours after transfection with BMP10-IRES-GFP. Green cells expressing BMP10 were highly proliferative. In addition to long-shaped cells, a sub-population of smaller BMP10-IRES-GFP expressing cells appeared in the culture.

The use of the BMP10-IRES2-GFP expression construct for transfection allows to monitor cells, which express BMP10. I asked the question whether in such cells are able to create cord/tube-like structures and to take up acetylated low density lipoprotein (Ac-LDL), the most reliable and specific method to distinguish endothelial cells.

As shown below, GFP positive cells expressing BMP10 form three dimensional tubes as visualized by phalloidin counterstaining (Fig. 3.81). Cells transfected with the control pEGFP vector did not exhibit this feature and were not able to take up Ac-LDL (data not shown). In Fig. 3.82 representative images illustrating Ac-LDL uptake by BMP10 expressing cells (as estimated by green fluorescence) are shown. All 10T1/2 cells that express BMP10 were also positive for red fluorescence, indicating the presence of LDL in these cells. It should be mentioned that also in some of the cells neighbouring GFP positive red fluorescence was noted.

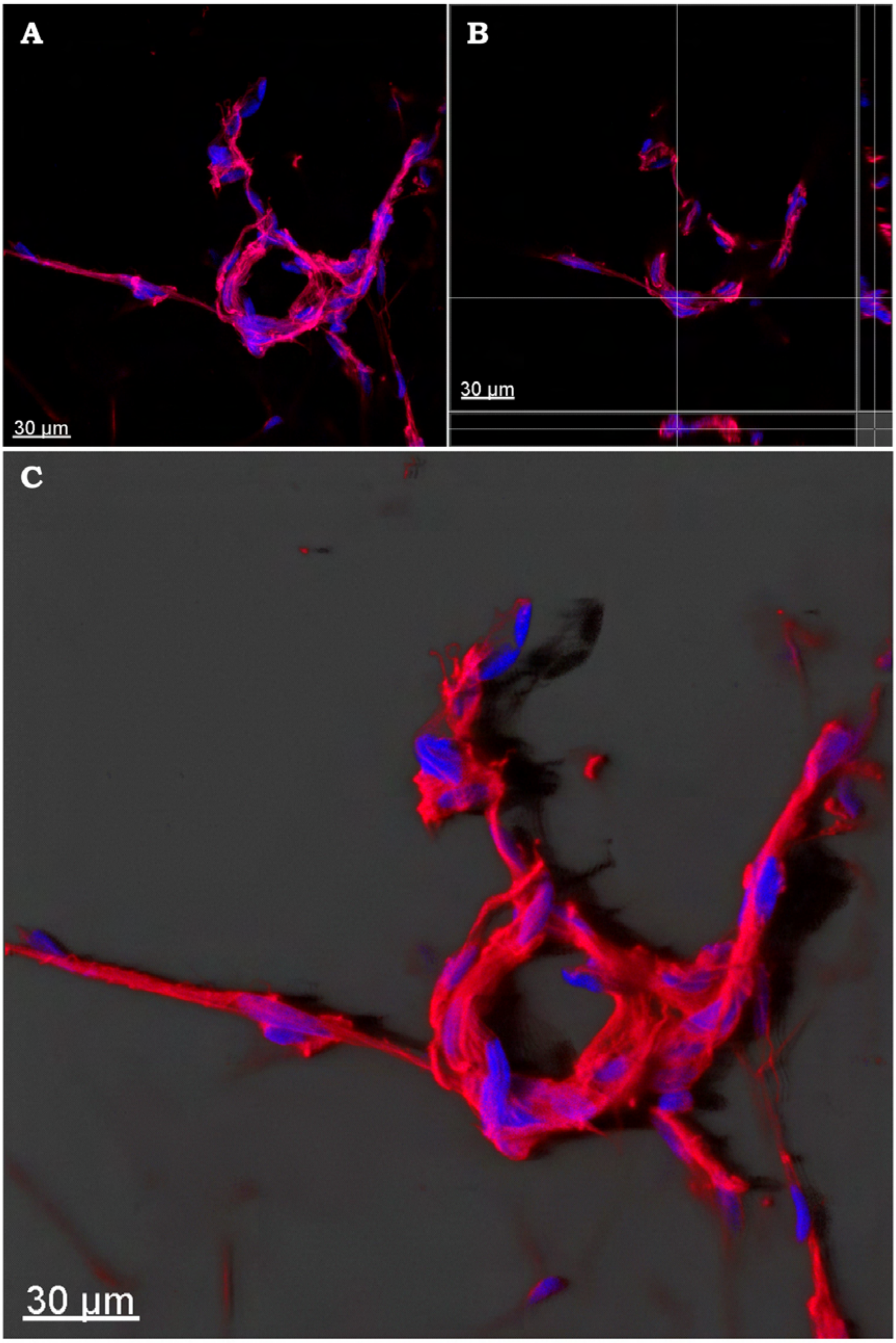

Fig. 3.81. Tube-like formation of BMP10-IRES-GFP transfected 10T1/2 cells. Panel A- confocal image of cells stained with phalloidin-TRITC (red). Panel B- Z-position illustrates 3D structure created by transfected cells as illustrated on selected confocal sections; C- 3D reconstruction of the confocal images shown in A and B. Nuclei were visualized with DAPI (blue).

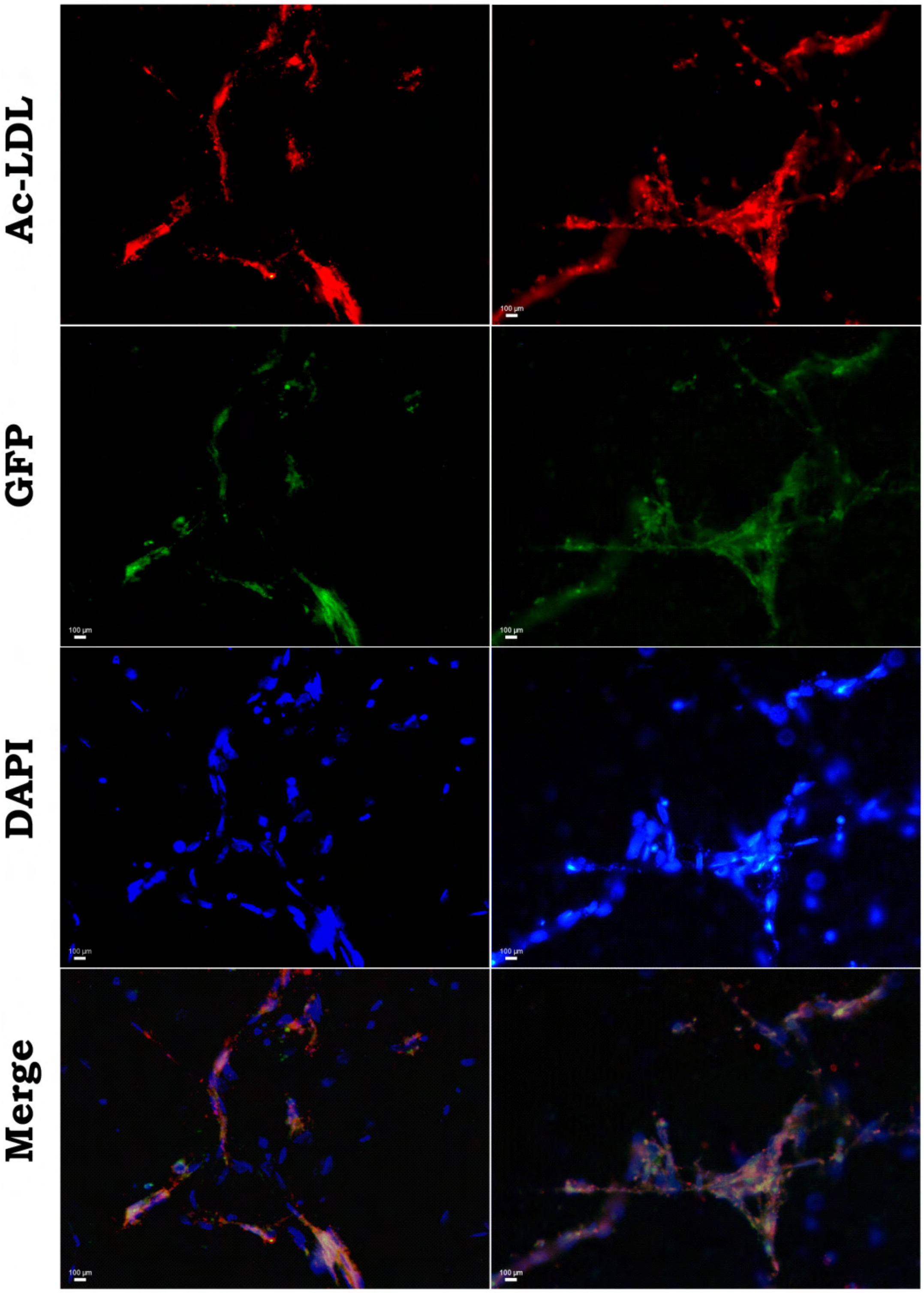

Fig. 3.82. BMP10-IRES-GFP transfected 10T1/2 cells (green) were able to take up DiI conjugated acetylated LDL (Ac-LDL) (red). Nuclei were visualized with DAPI (blue).

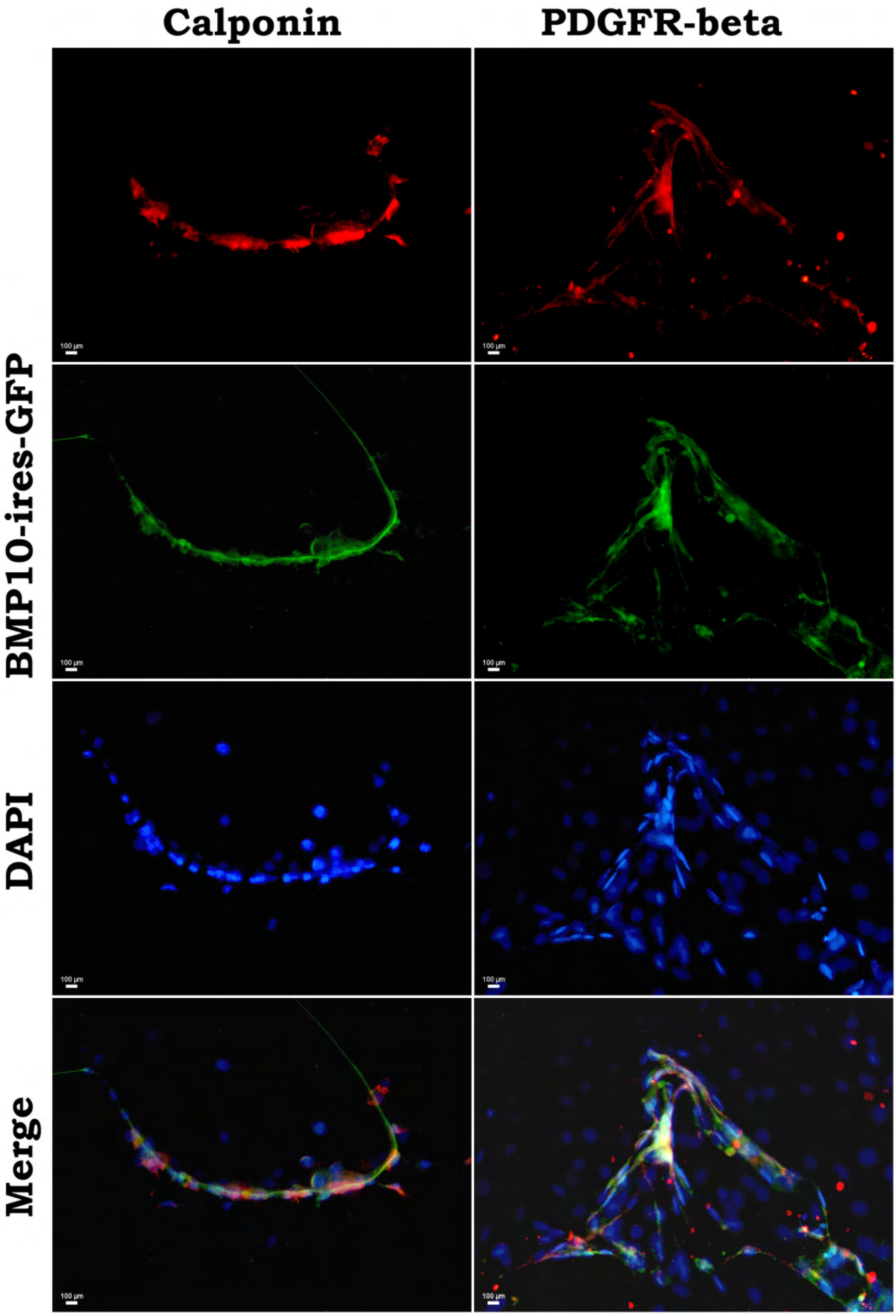

Fig. 3.83. 10T1/2 cells transfected with BMP10-IRES-GFP (green) expressed calponin (left panel, red) and PDGFRβ (right panel, red). Note that in some of the

cells neighbouring transfected cells both markers are detectable. Nuclei were visualized with DAPI (blue).

This experiment proved that BMP10 is able to promote differentiation of mesenchymal, fibroblastic 10T1/2 cells into endothelial-like cells. As already mentioned, the activity of alkaline phosphatase was not detectable in this cell line upon BMP10 induction, both by conditioned medium or transfection with BMP10-IRES-GFP plasmid. This might indicate a specific and selective induction of differentiation by BMP10.

Since addition of BMP10 to the medium induced expression of smooth muscle specific gene expression, for example calponin, I checked whether cells transfected with BMP10 express calponin as well. Another question was, if the PDGFRβ receptor is detectable in these cells.

Calponin was detected in transfected, but also in some cells adjacent to BMP10 expressing cells, as shown in Fig. 3.83. Staining was noted in cord-like, GFP marked structures and in the cells that seemed to be recruiting to them. Similar resulst was obtained with BMP10 conditioned medium. The expression of the pericyte specific gene- PDGFRβ was found to be stimulated by BMP10 (Fig. 3.83). The results of BMP10 treatment and transfections of 10T1/2 cells are summarized in Tab. 3.3.

The BMP10effects on 10T1/2 cells

Cell line	**Effects/Markers**	**Control**	**BMP10 treated**	**BMP10 transfected**	**Remarks**
10T1/2					
	Proliferation	+	upregulated	upregulated	
	Cord-like structures	-	induced	induced	
	Smooth muscle cell markers	+	+	+	10T1/2 cells adopt pericytes/vSMC phenotype in SF medium
	PDGFRβ	+	+	+	
	Endothelial cell markers	-	+	+	In cells forming cord-like structures
	Vimentin	downreguleted	+	+	Expression was preserved in cord-like structures

Tab. 3.3. Summary of BMP10 influence on 10T1/2 cells.

3.7.7. BMP10 induces formation of cord-like structures in primary cultures of mouse adult non-cardiomyocytes

3.7.7.1. Characterisation of isolated cells

Since BMP10 was found to be expressed in ventricular cells that do not express cardiomyocyte-specific markers, the total population of non-cardiomyocytes was isolated from adult mouse heart. These cells were grown in 10% FCS medium and early passages (1-3) were used for the experiments. For each experiment, the heterogeneity of culture was analyzed by immunocytochemistry on the basis of the following markers: fibroblasts (vimentin), myofibroblasts (vimentin and SMA), smooth muscle cells (SMA, calponin), pericytes (PDGFRβ) and endothelial cells (PECAM and AcLDL uptake) (Fig. 3.84).

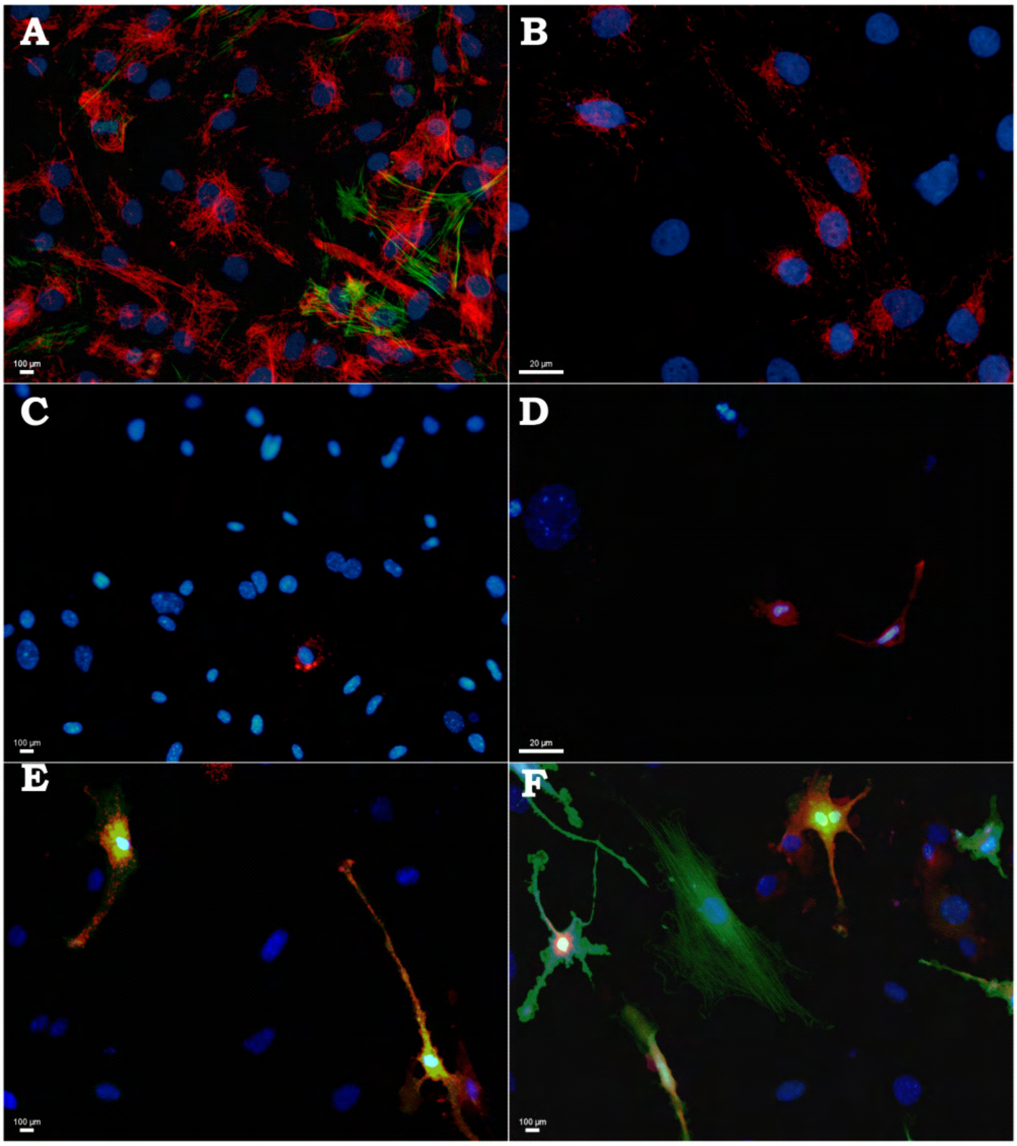

Fig. 3.84. Characterisation of mANCM isolated from WT mouse heart (A-E) and Sca1(Ly6A)-GFP transgenic strain (F). The following antibodies were used to estimate the content of different sub-populations of cells in the heterogeneous culture: (A)- anti-Vimentin (red)/anti-SMA (green) (fibroblasts, smooth muscle cells and myofibroblasts, when co-localize); (B)- anti-CD31 (red- endothelial cells); (C)- anti-PDGFRβ (red, pericytes); (D)- anti-Calponin (red, smooth muscle cells), and Ac-LDL uptake (E,F- endothelial cells). See text for details.

The average content of fibroblasts, characterised by vimentin but not SMA expression, was estimated to be in the range of 90%-95%, depending on the isolation. The number of myofibroblasts- cells positive for both, vimentin and SMA, never exceeded 3%, and smooth muscle cells judged by the calponin and SMA signal were 7%-10%. Only a few single cells expressing PDGFRβ were found in the cultures. The quantity of endothelial cells as estimated by CD31 immunodetection was at the level of 30%, whereas 20% of cells were able to take up Ac-LDL. In 50% of Sca1^{pos} cells, identified by GFP expression, DiI-Ac-LDL was detected. However, cells that did not express the Sca1 antigen did also take up Ac-LDL, as shown in Fig. 3.84F.

3.7.7.2. Some mANCM cells express BMP10 in culture

After isolation of mANCM from the whole heart, cells were grown to reach confluence in 10%FCS DMEM medium, trypsinised and plated at two different densities: 1x10^6 and 1x10^5 per 6 cm plate. The next day the growth medium was replaced with serum free BMP10 conditioned or control medium.

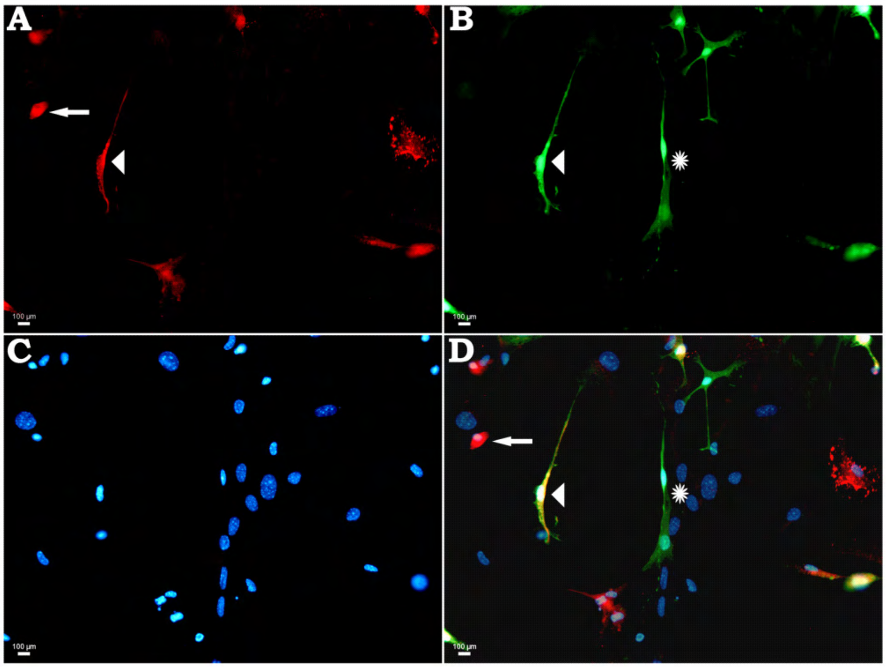

Fig. 3.85. BMP10 in primary mANCM culture isolated from the Sca1-GFP transgenic strain was detected with anti-matBMP10 antibody (red). GFP signal was not amplified (green). Arrows indicate the small subpopulation of BMP10^{pos}/Sca1^{neg} cells, arrowhead BMP10^{pos}/Sca1^{pos}, asterisk BMP10^{neg}/Sca1^{pos}. Nuclei were stained with DAPI (blue).

A proliferative effect of BMP10 was apparent in low-density cell cultures while no induction of mitosis by BMP10 was observed in more confluent cultures. Therefore, it had to be verified whether BMP10 expression is induced in the high-density cell cultures growing in the standard growth medium not supplemented with BMP10. BMP10 expression was tested by immunocytochemistry and on the RNA level by RT-PCR analysis. Since mANCM were isolated from the whole heart, cells expressing BMP10 were found in all cultures, independent of cell density (Figs. 3.85 and 3.86). In mANCM isolated from Sca1-GFP mouse heart, BMP10$^{pos.}$/Sca1$^{neg.}$ and BMP10$^{pos.}$/Sca1$^{pos.}$ were found. Most of the cells BMP10$^{pos.}$/Sca1$^{neg.}$ were smaller than those expressing both genes (Fig. 3.85). When cells were plated with lower density, only single BMP10$^{pos.}$ cells were found in the culture and BMP10 expression on mRNA was also low. In more confluent cultures, the number of cells expressing BMP10 rapidly increased, as shown in Fig. 3.86. Induction of BMP10 expression was further confirmed by RT-PCR analysis (Fig. 3.86).

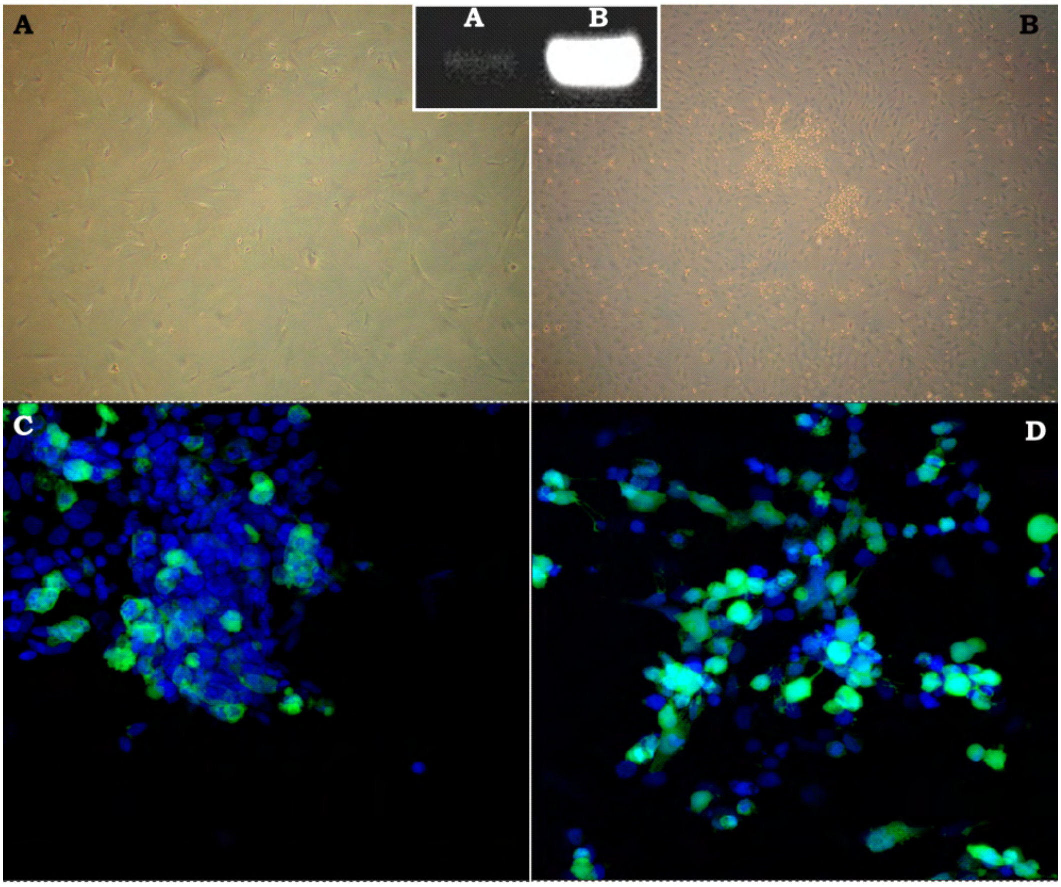

Fig. 3.86. Low power magnification phase contrast microphotograph of mANCM cells 1 day (A) and 7 days (B) in culture and semi-quantitative RT-PCR analysis of BMP10 expression level (box). RNA for RT-PCRs was isolated from the presented cells (A,B). Confocal images (C,D) of BMP10 immunostaining (green) in confluent maNCM. Nuclei were stained with DAPI (blue).

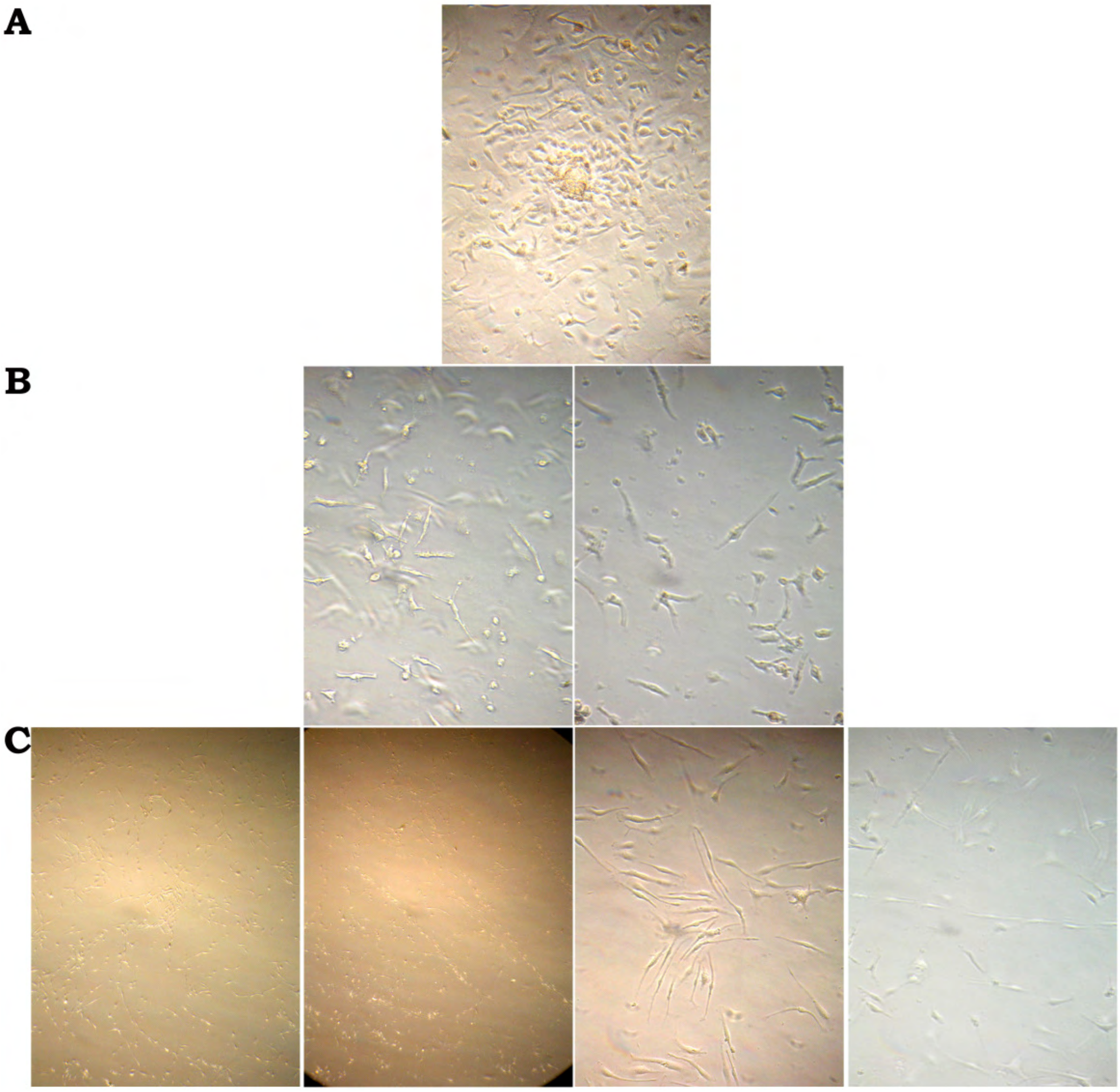

Fig. 3.87. A highly proliferative sub-population of confluent mANCMs (A) was picked and cultured separately in growth medium containing 10%FCS. B- 24 hours later the cells had fibroblast-like morphology. C- 72 hours in culture, cord-like structures were noted.

When mANCMs were confluent, either in serum free or FCS supplemented medium, highly proliferative cells, which did not form a monolayer appeared in the cultures. These cells were BMP10 positive. This might explain the lack of the effect of exogenous BMP10 to confluent cultures as the gene is already efficiently expressed in many cells. Clusters of these cells (Fig. 3.87A) were isolated and cultured further in growth medium (Fig. 3.87B-C). On day 1, cells exhibited a typical fibroblast-like morphology (Fig. 3.87B). Two days later, structures resembling a cord-like pattern were visible in the culture (Fig. 3.87C) and although this pattern was conserved later on the cord-like structures had an immature apperence. However, when as a result of picking cell-cell contacts were disturbed (cells were not confluent), proliferation of this sub-population of mANCM was significantly diminished, which will be described in detail in the next chapter.

3.7.7.3. Characterisation of the mANCM subpopulation containing BMP10 positive cells.

The tendency to form cord-like structures by a subpopulation of BMP10 positive mANCM cells, resembled the effect of BMP10 in all cell lines tested. The structures formed by the isolated subpopulation of mANCMs were not “fully developed” and did not exhibit the ability to create protrusions allowing long-distance cell-cell contact. However, the cells spontaneously were arranged in parallel forming longitudinal chains. To characterize the type of cells that create these chains, after isolation clones containing BMP10 positive cells, the same set of antibodies as for 10T1/2 and BM-MASCs was used (Fig. 3.88).

Aurora B staining showed the disturbed proliferation of the cells growing in standard growth medium supplemented in 10% FCS (Fig. 3.88A,B). SM actin was detected in contaminating cells, but not in cells building chain-like structures (Fig. 3.88A,C). Strong vimentin expression indicating a mesenchymal origin was observed. PECAM expression was also found (Fig 3.88B), although not so strong as in HUVEC cells, that served as positive control and no signal was noted in the negative control (data not shown). Only a weak signal for PDGFRβ staining was found in single cells.

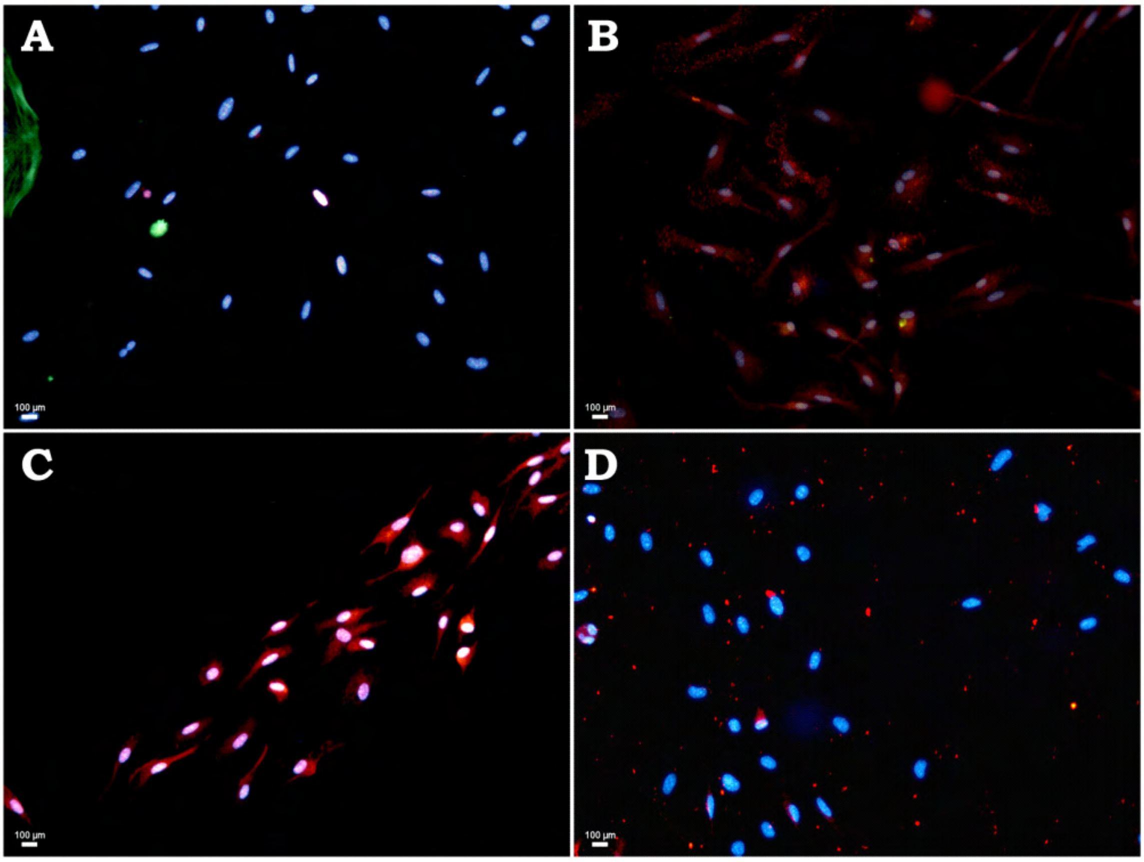

Fig. 3.88. Characterization of picked subpopulation of mANCMs. Note: (A) Impaired proliferation and lack of smooth muscle markers (SMA- green and Aurora-B- red). (B) Weak expression of PECAM (red) and single Aurora-B positive cells (green). (C) Strong vimentin staining (red) and lack of SMA expression (green) indicate the mesenchymal origin. (D) PDGFRβ was found only in single cells (red). Nuclei were stained with DAPI (blue).

3.7.7.4. Effects of BMP10 on mANCM cells

BMP10 expression is strongly induced in confluent cultures of maNCM, but downregulated after trypsinization when the cell density is lower. To investigate the effects of BMP10 on heterogeneous mANCM cells, but avoid induction of endogenous BMP10 expression, only low density cultures were used. $1x10^5$ cells were plated on a 6 cm dish to examine the effects of BMP10. The next day, the growth medium was replaced with serum free BMP10 conditioned or control medium and cells were further incubated for 96 hours with medium changes every 48 hours. Cells treated with BMP10 started to create similar structures as observed in the case of mBM-MASCs and 10T1/2 cells. An identical set of antibodies was used for characterisation of BMP10 induced changes.

Figure 3.89 illustrates the results of SM actin and Aurora B double staining. In BMP10 treated cultures, the highly proliferative cells forming cord-like structures are mostly negative for the smooth muscle marker, in contrast to previously described cell lines. The overall number of smooth muscle actin positive cells seemed to be reduced. Comparable results concerning induction of mitosis were obtained as already mentioned. Since cells forming tube-like structures were negative for SM actin it was likely that they are endothelial cells. This assumption was confirmed by immunostaining, as presented below (Fig. 3.90).

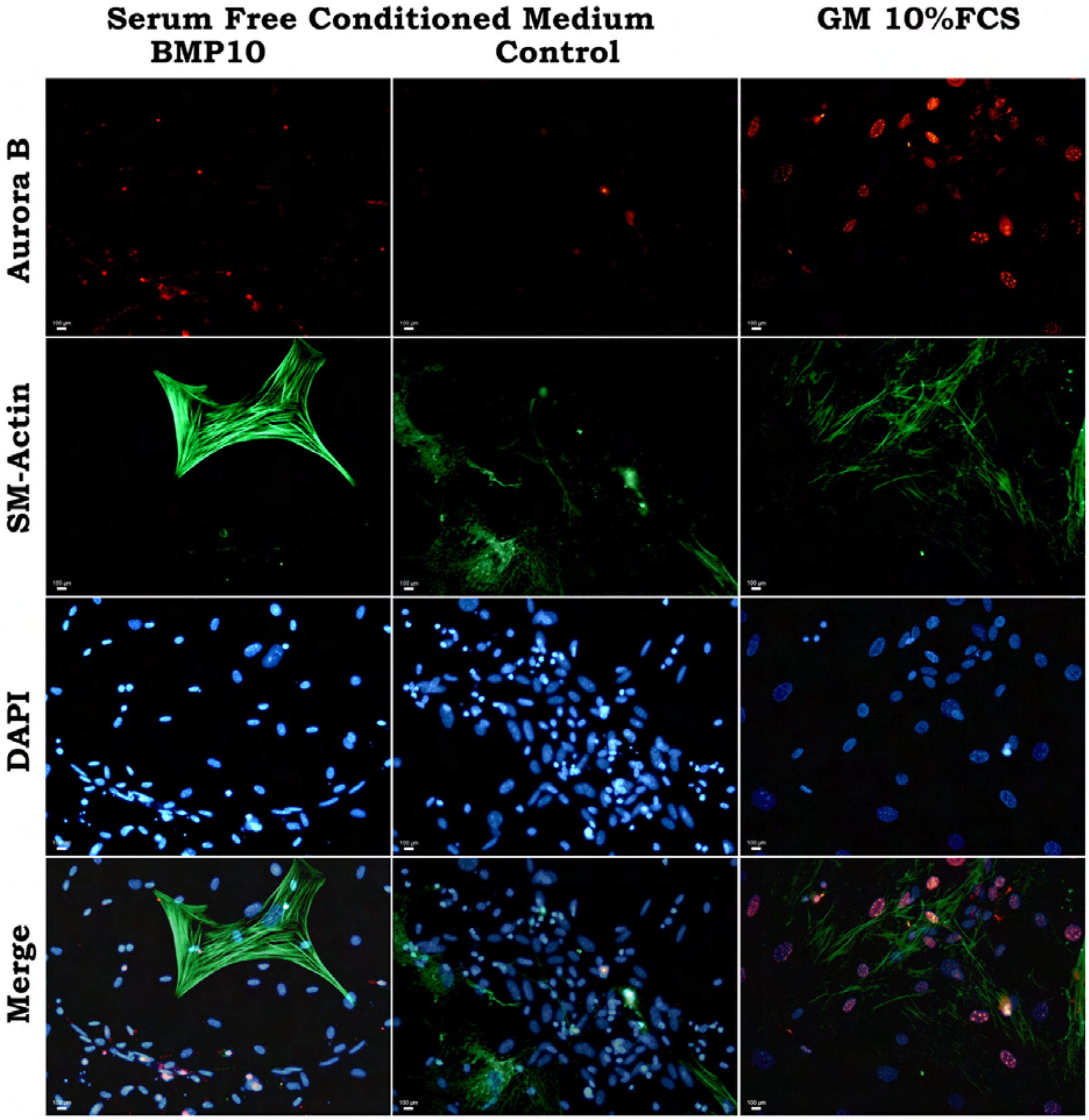

Fig. 3.89. BMP10 induced proliferation of SMA$^{neg.}$ cells in the mANCM culture. Immunodetection of SM actin (green) and Aurora B (red) in BMP10 treated (left panel) and control cultures of mANCM. Nuclei are visualized in blue by DAPI.

Structures induced by BMP10 addition to the medium were strongly positive for PECAM. In control serum free and in growth medium cells expressing PECAM were forming incomplete line-like structures.

Since BMP10 forced the expression of PDGFRβ in 10T1/2 and BM-MASC cells, the induction of this gene in maNCM was also investigated. In mANCMs cultured in standard growth medium only single cells positive for PDGFRβ were found as described in chapter 3.7.7.1. Comparable results were obtained when cells were grown in serum free control medium. After stimulation with BMP10 most of the cells in cord-like structures expressed PDGFRβ indicating the acquisition of a pericyte identity (Fig. 3.91).

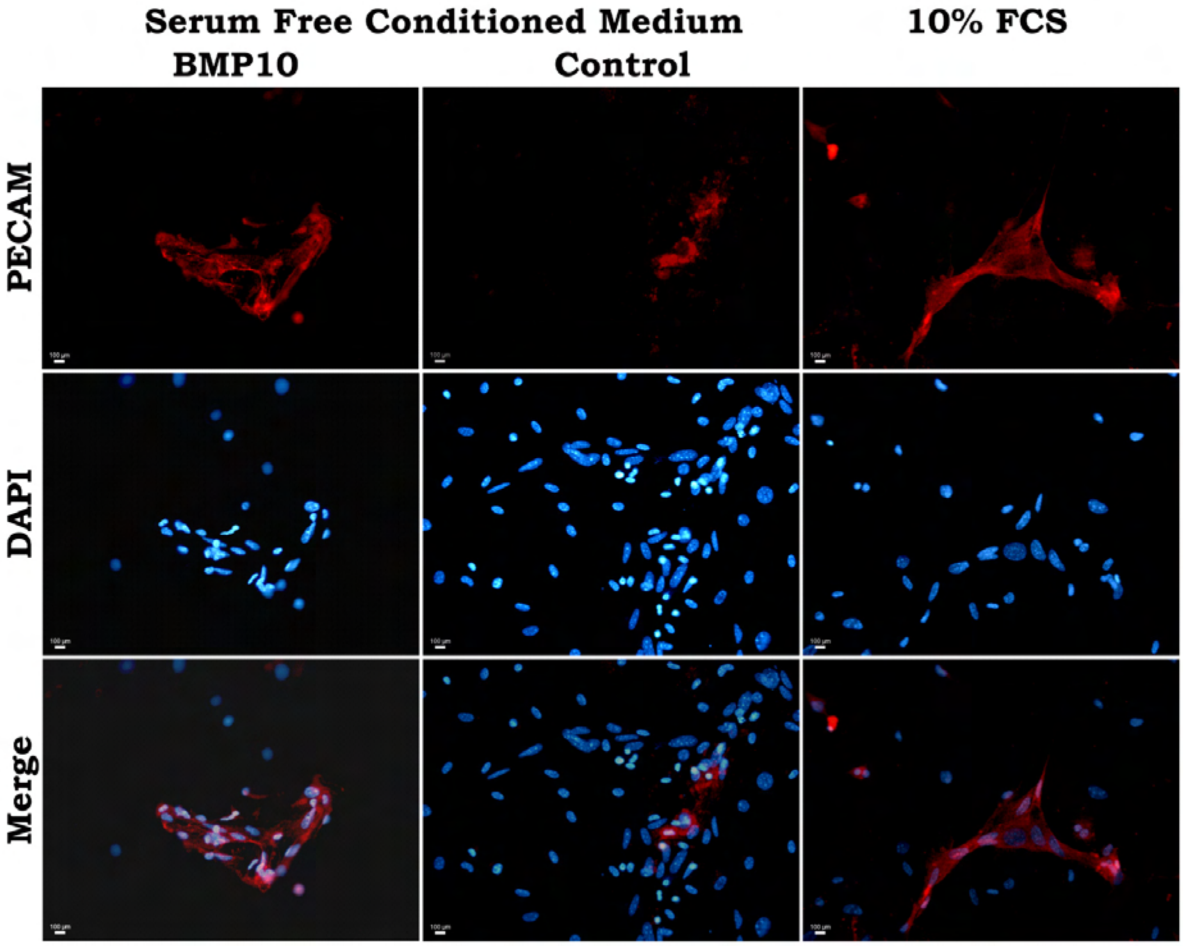

Fig. 3.90. BMP10 stimulated PECAM expression in a subpopulation of mANCM. CD31 (PECAM) immunodetection in BMP10 treated (left panel) and control

(middle-serum free control medium, right panel- growth medium) mANCM. Note that CD31$^{pos.}$ cells in BMP10 treated cultures are smaller than in controls and formed ring-like structures. Nuclei were counterstained with DAPI (blue).

It is interesting to note, that some cells which express PDGFRβ as a result of BMP10 addition did not express SM actin. Often strong PDGFRβ staining was observed in cells adjacent to SMA$^{pos.}$ cells. Smooth muscle actin was found in bigger, morphologically distinct cells outside of the cords and rings. In control cultures co-localization of SMA and PDGFRβ was visible.

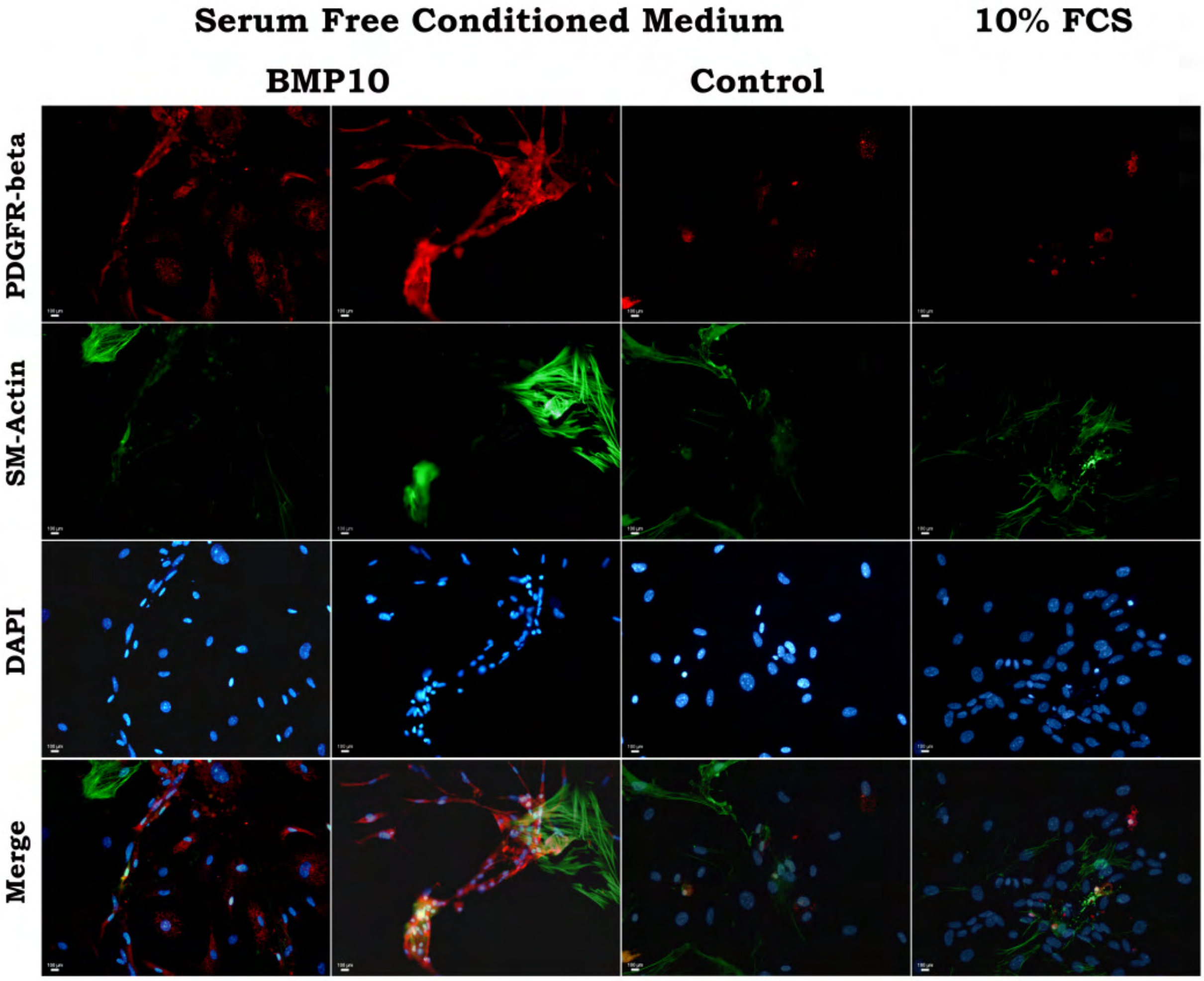

Fig. 3.91. BMP10 induced PDGFRβ expression in cord-like structures. Immunodetection of PDGFRβ (red) and SM actin (green) in mANCM cultured in serum free BMP10 enriched and control medium as well as in standard growth medium. Note that upon BMP10 stimulation the strongest PDGFRβ signal was in smaller cells creating ring-like structures and weaker staining was in larger cells in cords. Highly organized smooth muscle actin filaments were detected in morphologically distinct cells. In tube-like structures SMA showed a disorganized pattern. Nuclei are visualized in blue by DAPI staining.

The preliminary characterization of mANCM revealed that more than 90% of the cells in this heterogeneous culture were positive for vimentin, comparable to the changes in vimentin expression observed in 10T1/2 and BM-NCMs upon BMP10 treatment. The influence of BMP10 addition on vimentin expression in cells of heart origin was worth to be examined. Representative images of double vimentin and SMA immunodetection in mANCM cultures are shown in Fig. 3.92.

Vimentin expression was preserved upon BMP10 treatment, although its cellular organisation was disrupted. It did not co-localize with smooth muscle actin. Figure 3.92 clearly illustrates the smaller size of cells forming ring-like structures, in mANCM grown in serum free BMP10 enriched medium in comparison to control serum free and growth medium.

The effects of BMP10 treatment on mANCM and bm-MASC cells are displayed in Tab. 3.4, whereas Tab. 3.5 summarizes the results observed after BMP10 treatment of all cell lines used in this study in comparison to the expression of various BMP receptors

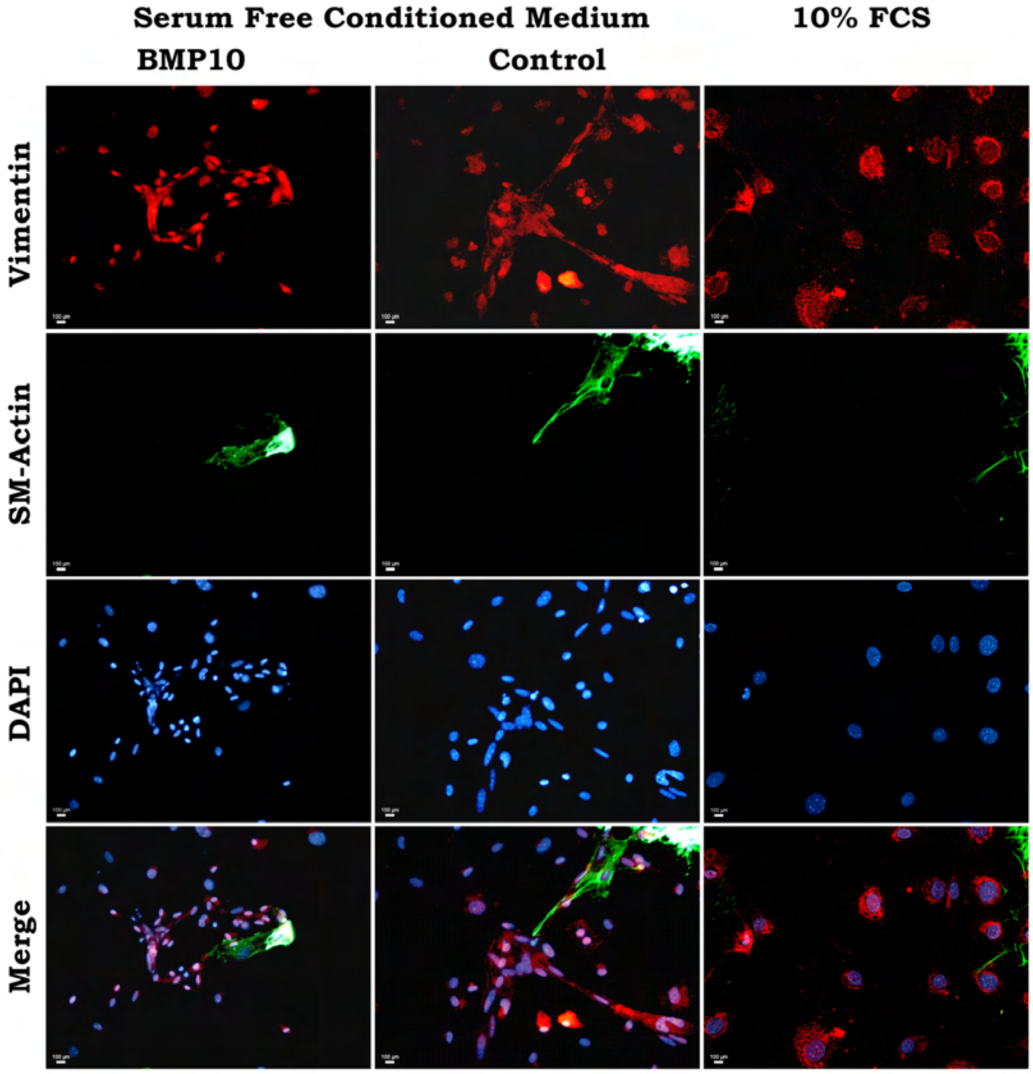

Fig. 3.92. BMP10 did not influence the expression levels of vimentin (red) but its cellular organization in cord-like structures in mANCM. Note that SMA (green) filaments were disorganized in ring-like structures as well. Double immunodetection of vimentin (red) and SMA (green) in mANCM cultured in serum free BMP10 enriched (left panel) and control (middle panel) medium. Right panel illustrates the same staining in cells grown in 10% FCS containing medium. All images represent the same magnification. Nuclei were stained with DAPI (blue).

BMP10 effects on mANCM and bm-MASC1 cells

Cell line	Effects/Markers	Control	BMP10 treated	Remarks
mBM-MASC1				
	Proliferation	+	upregulated	
	Cord-like structures	-	induced	
	Smooth muscle cell markers	+	++	SMA expression is induced by serum deprivation and in confluent culture
	PDGFRβ	-	+	
	Endothelial cell markers	-	+	Co-localization of EC and SMC markers in BMP10 treated, but not in control culture
	Vimentin	-	+	
mANCM				
	Proliferation	+	upregulated	
	Cord-like structures	-	induced	In control culture not completely formed structures were observed
	Smooth muscle cell markers	+	+	
	PDGFRβ	Single cells	+	Expressed in cord-like structures in BMP10 treated culture
	Endothelial cell markers	+	expressed in cord-like structures	Expressed in morphologically distinct cells
	Vimentin	+	+	BMP10 did not affect the expression levels of vimentin but its cellular organisation.

Tab. 3.4. Summary of BMP10 effects on mANCM and bm-MASC1 cells.

Cell line	**Effects of BMP10**	**Type I Receptors**	
		Present	**Absent**
COS1	Lack of induction of ALP activity Lack of cord-like structures	ALK3	ALK1 ALK5 ALK6
293T	Lack of ALP activity Lack of cord-like structures	ALK3 ALK5 ALK6	ALK1
C2C12	Induction of ALP activity	ALK1 ALK3 ALK5 ALK6	
10T1/2	Lack of ALP activity Induction of tube-like structures formation	ALK1 ALK3 ALK5 ALK6	
mBM-MASC	Lack of ALP activity Induction of tube-like structures formation	ALK1 ALK3 ALK5 ALK6	
mANCM	Lack of ALP activity Induction of tube-like structures formation	N.D*	N.D*

Tab. 3.5. Summary of BMP10 effects on various cell lines in comparison to expressed type I receptors. N.D.- not done because of heterogeneity of culture (*).

4. Discussion

4.1. BMP10 expression and localization in healthy murine hearts

At the beginning of this project only the expression of BMP10 during mouse embryonic development was known. Whole mount in situ hybridization and northern blot results had also indicated that the expression of BMP10 was restricted to the right atrium in adult human tissues (Neuhaus et al., 1999). To investigate more closely the expression of BMP10 in adult murine tissues, this study started with the RT-PCR analysis of BMP10 expression. The results revealed that BMP10 expression is confined to the heart. Within the heart the BMP10 specific PCR product is present only in the right atrium confirming previously published expression patterns (Neuhaus et al., 1999). By in situ hybridization it was possible to detect BMP10 expression in the majority of atrial cells, both interstitial and atrial cardiomyocytes. Transcripts were also found in the trabeculated atrial wall of the right atrial appendage and the interatrial septum. However, the compact layer of the wall as well as the pericardium do not express BMP10. BMP10 transcripts are absent in both ventricular chambers and in the left atrium or the left atrial appendage.

BMP10 is a cytokine that belongs to the TGFβ family. The leader secretion sequence indicates that expression might, but not necessarily has to overlap with the localization of BMP10 after secretion. Partially overlapping expression and localization domains have been noticed in the case of BMP2 (Sugi et al., 2004). That was the reason to generate the antibody specifically recognizing the mature, processed form of BMP10, i.e. the active ligand interacting with receptors. After confirmation of the specificity of the BMP10 antibody by western blot, immunocyto- and immunohistochemistry, it was possible to examine BMP10 protein localization during embryonic development and in the adult mouse heart. By in situ hybridization BMP10 during embryogenesis was found to be expressed in the heart in the trabeculated, non-compacted myocardium only (Neuhaus et al., 1999). Immunodetection of BMP10 at E11.5 revealed that the extent of protein localization is significantly broader than the expression domains. Surprisingly, accumulation of BMP10 positive cells was found in the walls of the outflow tract. Moreover, the mature ligand of BMP10 was found not only in the trabecular layer of the developing heart, but also in the compact wall of the ventricles. In ventricular chambers

BMP10 localizes in a subpopulation of trabecular cells with a gradual decrease of staining intensity in the non-compacted myocardium, where BMP10 transcripts are not detectable. Cells that constitute a fine epicardial layer are positive for BMP10 as well. Double immunodetection of the myosin heavy chain (MHC), Nkx2.5 and BMP10 revealed localization of the cytokine in cardiomyocytes, but additionally in interstitial cells surrounding muscles.

Based on the expression and localization profile it seemed likely that BMP10 might probably act both in an autocrine fashion and in a paracrine way. A cardiomyocyte restricted effect of BMP10 action was postulated by Chen (Chen et al., 2004) but not investigated further since BMP10 deficient embryos die between E9.5 and E10.5. Mutant embryos displayed "cardiac dysgenesis with profound hypoplastic ventricular walls and absence of trabeculae" (Chen et al., 2004). Based on in situ hybridization experiments the authors found that BMP10 expression is restricted to muscles cells and postulated that the defective trabeculation and hypoplastic ventricular walls in mutants were caused by marked reduction of cardiomyocytes proliferation. It was suggested therefore that BMP10 provides a positive growth signal for cardiomyocytes. Although the authors recognized abnormal development of the endocardial cushion in both outflow tract (OFT) and atrioventricular canal (AVC), and found that this phenotype in BMP10 deficient hearts is rescued by BMP10 protein supplementation, they could not exclude that this effect was secondary to a severely impaired cardiac growth. Since immunodetection with the generated antibody proves that BMP10 localizes to the OFT, it is likely that OFT abnormalities in embryos lacking BMP10 represent direct effects of this growth factor deficiency. The authors however, did not characterize the nature of abnormalities in the OFT (Chen et al., 2004).

Expression of BMP10 in the neonatal mouse was found to be restricted to the right atrium, with transcripts limited by the annulus fibrosus. In contrast to the embryonic heart the protein localization predominantly overlapped with in situ transcripts detected in infants. However, a vestigial amount of BMP10 protein was found in the right ventricle. In the right atrium, two distinct localization patterns of the mature ligand were observed. Some cells exhibit cytosolic accumulation of the protein, while other cells show BMP10 bound to the membrane.

In the adult murine hearts BMP10 localizes predominantly to cells of the atrium resulting in a homogenous, cell-membrane localization pattern with marginal cytosolic staining. Detailed examination shows that additional structures in the heart are able to bind or express BMP10. Immunohistochemistry showed binding of BMP10 by cells of the tricuspid valve. Careful in situ transcript detection analysis confirmed the results of protein immunodetection, and expression of BMP10 in some cells in the valve was found. Moreover, single cells adjacent to the big veins and arteries in the upper atrial area of the heart demonstrate BMP10 transcription. The detailed knowledge of BMP10 expression and localization in the healthy murine heart was required to analyze pathological changes of BMP10 expression in different models of cardiomyopathies.

4.2. Phenotypic differences and similarities of the mouse models of CMP

One of the primary aims of the present work was the characterization of BMP10 expression in various models of cardiomyopathies (CMP). In this study both genetic and drug induced models resembling dilated and hypertrophic cardiomyopathies were used. I took advantage of the accessible and well characterized Desmin knock-out (Milner et al., 1996; Thornell et al., 1997, Li et al., 1996) (generous gift from Prof. T. Braun). As the second genetic model, 10 months old heterozygous mice deficient in the manganese superoxide dismutase gene (MnSOD/SOD2), generated by Dr. T. Loch were used (laboratory collection). These models represent examples of desmin related cardiomyopathy (Gard et al., 2005; Sanbe et al., 2004; Olivé et al., 2004) and mitochondropathy, respectively (Finster, 2004; Russell et al., 2005). Induction of dilated cardiomyopathy by doxorubicin administration (Gille et al., 1997; Zhou et al., 2001; Childs et al., 2002; Green et al., 2002; Wallace, 2003) was also utilized. Treatment of mice with isoproterenol resulting in heart hypertrophy (Boluyt et al., 1995) served as a second drug induced model. A detailed pathological description of all models, including MRI analysis and characterization of the nature and degree of pathomorphological changes were a prerequisite of this study. Parameters for the histopathological analysis included the degree of fibrosis and cardiomyocyte hypertrophy, presence or absence of myofiber disarray and two types of cell death, namely apoptosis and necrosis. Additionally, the levels of ANF, BNP and FHL2 as indicators of heart disorder were monitored.

Desmin deficient mice are the best characterized among the tested models (Milner et al., 1996; Milner et al., 1999) and on the basis of published data as well as own results exhibit the most severe degree of cardiomyopathy. The desmin protein is an intermediate filament expressed in all types of muscles. The null mutation causes the most severe phenotype in cardiac muscles (Milner et al., 1996; Li et al., 1996; Thornell 1997), which correlates with a higher content of this protein in the myocardium (2%) than in skeletal muscles (0.35%) (Price, 1984). Selective microvascular dysfunction was also observed in desmin null mice (Loufrani et al., 2001). Desmin mutations resulting in dilated cardiomyopathy have been described in humans and the term “desminopathies” has been proposed (Li et al, 1999).

In this study, magnetic resonance analysis of Desmin knock-out mice revealed hypertrophy of the heart, confirmed by measurements of myocardial volume. In addition impairement of systolic function and chamber dilation was observed, as already reported by Milner (Milner, DJ et al., 1999). However, the authors claimed, that dilatation of the chambers was accompanied by thinning of the ventricular free walls, which is in contrast to our results. An obvious increase in thickness visible in MRI images was further confirmed by histological examination. Histological inspection revealed advanced calcification, which was visible at a first glance in most of the desmin deficient mice, however at different degrees dependent on the genetic background. An elevated heart weight to body weight index as compared to WT corroborates previously published results (Milner et al., 1999). The histopathological analysis confirmed most of the published data (Mavroidis et al., 2002; Milner et al., 1996). Hearts of mice lacking desmin demonstrate numerous muscle architectural defects, with loss of alignment of myofibrils. Fibrous scar tissue develops throughout the myocardium and foci of abundantly accumulated collagen VI deposits were found. Cardiomyocytes are hypertrophied and the increase in myocyte size among all the tested models is the most pronounced in Desmin knock-out mice. Surprisingly, transgenic hearts did not contain significant number of apoptotic or necrotic cells as detected by TUNEL and Complement9 staining, respectively. Previous publications claimed that fibrosis and calcification found in desmin knock-out hearts were the result of high incidences of programmed cell death of myocytes (reviewed by Capetanaki, 2002; Weisleder et al., 2002) and necrosis (Li et al., 1996). However, this observation was not confirmed in the present study. One of the reasons might be that both groups examined young animals whereas in the present work older animals (6-8 months) were used, because we did not observe striking features of cardiomyopathy in younger knock-out mice. This was caused probably by the use of a different genetic background. Moreover, the expression level of the marker of cardiac disorders- ANF is significantly upregulated with accumulation in apex, septum and ventricular free wall. ANF is a peptide hormone with diuretic, natriuretic and vasorelaxant properties (Rosenzweig et al., 1991; de Bold et al., 1996) and its ventricular expression is often correlated with an increase in ventricular mass in pathological hearts (Calderone et al., 1995; Matsubara et al., 1990). ANF was also shown to be specifically expressed in the regions of hearts with the highest degree of tissue pathology (Vikstrom et al., 1998).

Superoxide dismutase (SOD) catalyzes the dismutation reaction of superoxide anion to hydrogen peroxide (Halliwell et al., 1995). Three different SODs are known in mammals: cytosolic copper/zinc SOD (Cu/ZnSOD or SOD1), mitochondrial manganese SOD (MnSOD or SOD2) and extracellular copper/zinc SOD (EC-SOD or SOD3) (van Remmen et al., 2001; reviewed by Bartosz, 2003). Among these three homologues only MnSOD exhibits a modulated expression induced by a variety of physiological factors suggesting that SOD2 plays a role in other processes than the antioxidant defense system (Li et al., 1995; Sato et al., 1995; Nogae et al., 1995).

Not many data are available concerning cardiomyopathy caused by manganese superoxide dismutase deficiency. Two independent groups generated mutant strains lacking MnSOD (Li et al., 1995; Lebovitz et al., 1996; Huang et al., 2001). Both observed neonatal lethality, although at different time points, dependent on the genetic background. In both mutant strains dilated cardiomyopathy was a common finding. Neonatal MnSOD homozygous generated in our laboratory by Dr. T. Loch exhibit DCM manifested by ventricular cavity enlargement and free wall thinning (data provided by Dr. T. Loch, personal communication). Upregulation of ANF expression in 3 days old neonatal SOD2-/-, but not in heterozygous further confirmed pathological changes of the heart.

Several reports describe the cardiac phenotype in MnSOD deficient homozygous mice, but apart for some biochemical reports, not many data are available concerning old heterozygous MnSOD mice. An average reduction of enzyme activity in heterozygous MnSOD mutants was estimated at the level of 50% (Li et al., 1995), whereas the strain generated in our laboratory exhibits only 30% of MnSOD activity reduction in the heart (Dr. T. Loch, personal communication). This decrease in the level of the enzyme influences the physiological function of the heart as shown in 6 months old MnSOD$^{+/-}$ mutants characterized by impaired systolic function and reduced ejection fraction (unpublished data, kindly provided by Dr. T. Loch, personal communication). It has been assumed that pathological changes will proceed with the age of the animals.

During this study a detailed histopathological analysis of 10 months old heterozygous MnSOD mice heart was performed. A moderate increase of the degree of fibrosis and slight cardiomyocyte hypertrophy was observed in mutants compared to age and strain matched controls. A disarrangement of the myocardial architecture, typical for desmin knock-outs was not present in MnSOD$^{+/-}$ mice. In heterozygotic MnSOD, only necrotic but not apoptotic cells are detected in the myocardium. It has been reported that isolated cardiomyocytes from knock-out mice heterozygous for MnSOD are more sensitive to apoptosis than heart muscle cells from WT, or untreated MnSOD$^{+/-}$ myocytes (Van Remmen et al., 2001). Moreover, another group found induction of the apoptotic pathway in vivo, as detected by enhanced staining of the poly(ADP-ribose)polymerase (PARP) and activated caspase-3 in heterodeficient SOD2 mice, as soon as 6 to 10 days after birth (Strassburger et al., 2005). Both methods are based on detection of cleaved forms of PARP (24kDa and 89kDa) and activated caspase-3 (17kDa) and are reliable when used in Western Blot (reviewed by Rodriguez et al., 2005). In this study, the TUNEL method indicating DNA fragmentation was used for detection of apoptotic cells but in contrast to published reports, programmed cell death was not observed in MnSOD heterodeficient mice.

Doxorubicin (adriamycin), an anthracycline, is a potent anti-cancer drug and has a wide spectrum of activity (Blum et al., 1974). Doxorubicin has a very high affinity to the nucleus (60% of the total intracellular amount of the drug was found in the nucleus) and was recognized as a potent DNA modifier inhibiting DNA polymerase and nucleic acid synthesis. In addition, anthracyclines are known to stabilize the complex of topoisomerase and DNA which leads to protein bound double strand DNA breaks (reviewed by DeBeer et al., 2001). In this respect, the primary effect of the adriamycin anti-tumor action is the inhibition of proliferation and induction of apoptosis. However, the therapeutical potential of doxorubicin is limited by the development of dose-dependent cardiomyopathy (Unverferth et al., 1982). Both, acute and chronic cardiovascular changes have been described in patients undergoing adriamycin chemotherapy (reviewed by De Beer et al., 2001). Acute side-effects are usually transient and clinically manageable, but chronic effects may develop several weeks or even months after repetitive doxorubicin administration in humans. In the 1970s and the beginning of the 80s, when doxorubicin was commonly used as a chemotherapeutic agent, the mortality rate, due to developed congestive heart failure, has been described to vary from 30%-60% (Haq et al., 1985). Signs indicating a cardiotoxic effect include hypotension, tachycardia, cardiac dilation and ventricular failure (Singal et al., 1987; De Beer et al., 2001). Several mechanisms leading to adriamycin induced cardiotoxic effects have been proposed. These include the free radical hypothesis, Ca^{2+} overload, doxorubicin metabolite- doxorubicinol toxicity, as well direct interactions with the contractile system and some other cardiac-restricted targets (Jeyaseelan et al., 1997; Lewis et al., 1986; De Beer et al., 2001).

In the present study, doxorubicin was administrated to 6-8 weeks old ICR mice for 14 days. The empirically established dosage (15µg/g of body weight) did not cause premature lethality and MRI analysis indicated a moderate degree of heart failure. An increase of adriamycin concentration results in a high mortality rate during the drug administration period, making further examination impossible. However, even when the pathological changes or cardiac dysfunction caused by doxorubicin are not obvious, the results revealed significant changes of BMP10 expression in treated hearts. Therefore the same drug dosage, time etc, was applied for the experimental groups.

On the basis of MRI analysis a moderate decrease of ejection fraction in comparison to the placebo group was found, and the myocardial volume was slightly, but significantly reduced in doxorubicin treated mice. These MRI parameters indicate modest chamber dilation. Cardiomyocyte hypertrophy is absent but the “beginning” of myofiber disarrangement is clearly visible. Upon doxorubicin administration an increase of collagen deposition in the extracellular space resulting in replacement fibrosis is evident. Two distinct types of cardiomyocyte death were detected in doxorubicine induced cardiomyopathy: necrosis commonly induced by toxic agents and apoptosis because doxorubicin exhibits a pro-apoptotic function (De Beer et al., 2001).

Many studies indicate that dystrophin cleavage is a common pathway to advanced heart failure and some link dystrophin loss with cardiomyocyte death (Kawada et al., 2005; Kaprielian et al., 2000). Interestingly, cells lacking this membrane associated protein are found only in doxorubicin treated mice hearts, but not in other models.

Cardiomyopathies caused by homozygous and heterozygous SOD2 deficiency or induced by doxorubicin are considered as mitochondria-related CMPs and the term mitochondropathies was proposed by several authors (Finster, 2004; Russell et al., 2005). Adriamycin was shown to induce activity of MnSOD (Childs et al., 2001) and vice versa, MnSOD overexpression modifies early oxidative events of doxorubicin’s acute side effects in the heart (Chaiswing et al., 2005). Despite these physiological correlations and independent of the elevated levels of reactive oxygen species which lead to heart dysfunction in both models a distinct pathological changes were found in both groups.

Cardiac hypertrophy is observed in various cardiovascular diseases, including hypertension, myocardial infarction and cardiomyopathy. In end-stage human heart failure elevated levels of plasma catecholamines have been found (Daly et al., 1990) and it has been suggested that prolonged β-adrenergic stimulation plays a role not only in modulation of cardiac function but also in the development of the hypertrophic response (Mueller et al., 1995; Zou et al., 2001). This hypothesis was supported by the finding that β-blocker treatment is able to restore cardiac function (Motomura et al., 1990). Moreover, continuous infusion of a synthetic catecholamine in rats, namely isoproterenol (ISO), acting as β-adrenergic receptor agonist, elicits typical hypertrophy associated cardiac gene expression (Boluyt et al., 1995; Morisco et al., 2001). For this reason, isoproterenol induced hypertrophic cardiomyopathy was included in the study. Like doxorubicin, isoproterenol (225µg/g of body weight) was administrated to 6-8 weeks old ICR mice for 14 days, followed by NMR examination. The applied dosage of ISO induced severe heart hypertrophy with impaired systolic function, as clearly visible from the end-systolic MRI image at the level of the papillary muscles. This observation, together with a significant decrease of ejection fraction, indicates ventricular chamber dilation. The elevated myocardial volume, as well the significantly increased heart to body weight ratio in comparison to placebo treated controls further confirm the diagnosis of cardiac hypertrophy. Histological analysis revealed cardiomyocyte enlargement. Modest fibrosis, characterized by collagen accumulation, similar in its extent to that observed in doxorubicin induced cardiomyopathy is present as a result of isoproterenol administration. Moreover, both types of myocyte death (apoptosis and necrosis) were found in the myocardium of this model. However, β-adrenergic stimulation does not cause other pathological changes, e.g. myofiber disarray and dystrophin disruption. These results are consistent with previously published findings (Stanton et al., 1969; Shizukuda et al., 1998).

4.3. BMP10 as a novel marker of pathological changes in the heart

In all models tested two types of changes of the localization and expression of BMP10 were noted. First, a drastic redistribution of BMP10 correlating with quantitative changes of the protein in the right atrium was observed. Second, ventricular cells ectopically expressing the BMP10 protein were detected. For example, in Desmin knock-outs an ectopic BMP10 expression was found in both right and left ventricle, with a higher number of stained cells in the left chamber. In situ immunodetection of BMP10 protein further confirmed this observation. Surprisingly, BMP10 positive cells mostly localize in the proximity of cardiac vessels and their incorporation in the coronary vasculature was also noted. Similar results were obtained in doxorubicin and isoproterenol treated hearts as well as in MnSOD heterozygous mice. Moreover, stained cells often form clusters, although isolated single cells were also detected in doxorubicin treated mice. In cardiomyopathy induced by isopreterenol administration, ventricular BMP10 positive cells are not located in tightly packed clusters but still close to each other.

High levels of ectopic BMP10 expression in ventricular myocardium were also found in ventricular cardiomyocytes restricted Nkx2.5 knock-out (Pashmforoush et al., 2004). Inactivation of Nkx2.5 by Cre-recombinase under the control of a myosin light chain-2V (MLC2V) promoter, thus preserving transcription factor expression in atrial myocytes, leads to marked cardiac enlargement with trabeculae filling the left ventricular cavity in both neonatal and adult mutants, due to the persistence of trabecular cardiomyocyte proliferation after birth. A similar phenotype was observed in human patients with Nkx2.5 mutation. Myocardial overgrowth was also found in embryos of transgenic strains overexpressing BMP10 controlled by an ANF promoter (Pashmforoush et al., 2004). These data indicate that BMP10 might stimulate cardiomyocyte proliferation. However, it indicates two distinct pathways of ectopic induction of BMP10 expression, i.e. Nkx2.5 dependent and independent pathways. While the former might be restricted to cardiomyocytes and direct negative looping BMP10-Nkx2.5 was proposed by the authors (Pashmforoush et al., 2004), there seems to be another pathway of BMP10 induction by pathological stimuli which is restricted to non-cardiomyocytes. On the other hand the upregulation and ectopic expression of BMP10 in Nkx2.5 knock-out mice might also occur by an indirect pathway. The absence of Nkx2.5 might trigger pathological changes that stimulate BMP10 expression.

Besides the ectopic ventricular expression of BMP10, deregulation of gene expression in the right atrium is observed in all models, as described in chapter 3.5. Since these changes are very strong, it is highly probable, that changes in expression of atrial BMP10 levels result in overall quantitative deregulation of gene expression in pathological murine hearts. These data are summarized in Table 4.1.

Summary of BMP10 expression and localization changes

	Qualitative changes		**Quantitative changes**
	Ventricles	**Right Atrium**	
WT	Absent	Homogenous Membrane location	-
Desmin knock-out	Clusters of BMP10$^{pos.}$ cells	Membrane location Cytosolic accumulation	Upregulated
SOD heterozygous	Clusters of BMP10$^{pos.}$ cells	Heterogeneous pattern: 1.Lack of BMP10 2. Membrane location 3. Cytosolic accumulation	Downregulated
Doxorubicin	Single BMP10$^{pos.}$ cells	Cytosolic accumulation Loss of membrane location	Upregulated
Isoproterenol	Single BMP10$^{pos.}$ cells Closely located to each other	Two types of changes: 1.Homogenous downregulation 2. Heterogeneous pattern, as in SOD$^{+/-}$	Downregulated
Nkx2.5 knock-out (Pashmforoush et al., 2004)	Expressed in trabeculae of adult myocardium (in situ hybridization data)		Upregulated

Tab. 4.1. Characterization of qualitative and quantitative BMP10 expression changes in models of cardiomyopathy of adult mouse. An exact description of the observed changes is included in chapter 3.5.

Qualitative and quantitative changes of BMP10 expression in the right atrium and ectopic expression of BMP10 in ventricles in models of cardiomyopathies are evident. It should also be mentioned that the number of ventricular cells, which ectopically express BMP10 varies significantly between the different models. Desmin knock-out displays the most severe pathological phenotype and the number of ventricular BMP10 positive cells is the highest among all adult models examined. A lower number of cells ectopically expressing BMP10 are present in MnSOD$^{+/-}$, while both drug induced models of cardiomyopathy exhibit the lowest numbers of ventricular BMP10$^{pos.}$ cells. Since the number of cells ectopically expressing BMP10 in ventricles is low, the general quantitative changes of BMP10 in pathological hearts most probably reflect a deregulation of BMP10 in the right atrium.

4.4. BMP10 positive cells constitute a subpopulation of cardiac progenitors

Characterization of ventricular cells expressing BMP10 was carried out using a double immunolabeling method. Since BMP10 was found in ventricular cells of failing, but not of healthy hearts, I became interested in the origin of these cells. It has been reported that progenitor cells reside in the heart and that they can be characterized by stem cell antigen 1 (Sca1) expression (Oh et al., 2003; Matsuura et al., 2004). Moreover, Sca1 positive cells in skeletal muscle were described as small interstitial cells adjacent to the basal lamina, typically co-expressing PECAM (CD31) and localized in proximity of endothelial cells i.e. Sca1$^{neg.}$/CD31$^{pos.}$ (Oh et al., 2003). In the heart Sca1$^{pos.}$ cells were further subdivided into two groups: CD31$^{pos.}$ and CD31$^{neg.}$ the latter exhibiting a distinct differentiation potential (Pfister et al., 2005). It was proposed that CD31$^{neg.}$ but not CD31$^{pos.}$ cells can differentiate into cardiomyocytes. While Sca1$^{pos.}$/CD31$^{neg.}$ express cardiomyocyte specific transcription factors, Sca1$^{pos.}$/CD31$^{pos.}$ exhibit both endothelial (based on Tie2 expression) and smooth muscle (as judged by SM-actin expression) phenotypes (Pfister et al., 2005). Moreover, circulating Sca1$^{pos.}$ cells are also considered by some authors as endothelial progenitor cells (EPCs) and were shown to incorporate into vascular sprouts and capillaries *in vivo* (Takahashi et al., 1999). Hence, in this study a Sca1-GFP transgenic mouse strain was used and cardiomyopathy was induced with doxorubicin and isoproterenol leading to induction of ectopic BMP10 expression. Results of characterization of ventricular BMP10 positive cells are summarized in table 4.2.

Characterization of BMP10 positive cells

Cell type/ Process	**Marker**	**Characteristic- cellular labeling**
Endothelial Cells	PECAM (CD31)	BMP10$^{pos.}$/CD31$^{pos.}$ BMP10$^{neg.}$/CD31$^{pos.}$ BMP10$^{pos.}$/CD31$^{neg.}$
Smooth Muscle Cells	Smooth Muscle Actin (SMA)	BMP10$^{pos.}$/SMA$^{pos.}$ BMP10$^{neg.}$/SMA$^{pos.}$ BMP10$^{pos.}$/SMA$^{neg.}$
Cardiomyocytes	Myosin Heavy Chain (MF20) Nkx2.5	BMP10$^{pos.}$/MF20$^{neg.}$ BMP10$^{pos.}$/Nkx2.5$^{neg.}$ **Atrium and embryonic heart** BMP10$^{pos.}$/MF20$^{neg.}$ BMP10$^{pos.}$/Nkx2.5$^{pos.}$ BMP10$^{pos.}$/MF20$^{neg.}$ BMP10$^{pos.}$/Nkx2.5$^{pos.}$
Proliferation	Phospho-Histone H3 (pH3) Aurora B	BMP10$^{pos.}$/pH3$^{pos.}$ BMP10$^{neg.}$/pH3$^{pos.}$ BMP10$^{pos.}$/Aurora B$^{pos.}$ BMP10$^{neg.}$/Aurora B$^{pos.}$
Sca1 progenitors	Reporter gene expression (GFP)	BMP10$^{neg.}$/Sca1$^{pos.}$ BMP10$^{pos.}$/Sca1$^{pos.}$ BMP10$^{pos.}$/Sca1$^{neg.}$

Tab. 4.2. Characterization of cells ectopically expressing BMP10 in ventricles of diseased hearts.

The only persistent and common feature of all BMP10$^{pos.}$ cells in ventricular chambers was co-expression of proliferation markers (Aurora B and phophorylated histone H3) and lack of cardiomyocyte specific gene expression. Ventricular cells ectopically expressing BMP10 in failing hearts exhibit both smooth muscle and endothelial marker expression. Moreover, co-expression of Sca1 antigen in most of the BMP10 positive cells was observed with a correlation of the gradient increase/decrease of BMP10/Sca1 signal intensity, respectively. These results might indicate that BMP10 induced proliferation of Sca1$^{pos.}$/CD31$^{pos.}$ followed by their differentiation. Similar to skeletal muscle (Oh et al., 2003), CD31$^{pos.}$, i.e. endothelial cells incorporated in the vessels did not express Sca1 antigen and circulating EPCs which originally expressed Sca1 adopted the endothelial phenotype upon incorporation (Takahashi et al., 1999).

Thus, from this observation it is evident that cells expressing BMP10 constitute a subpopulation of cardiac progenitor cells that contribute to remodeling process in the heart.

4.5. Pro-mitotic function of BMP10

Published data clearly indicate that BMP10 stimulates of cardiomyocytes during embryogenesis (Chen et al., 2004). In the adult pathological heart a re-expression of BMP10 was found in ventricles and seemed to be restricted to muscle cells (Pashmforoush et al., 2004). My own results which were obtained using a specific antibody against BMP10 clearly exclude that BMP10 is re-expressed in ventricular cardiomyocytes in adult hearts. It seems most likely that the poor resolution of the in situ hybridization technique used by Pashmforoush led to an incorrect identification of BMP10 expressing cells. Furthermore it seems likely that the function of BMP10 can differs between adult and embryonic heart as well in case of cardiomyocytes and interstitial cells. Recently, overexpression of BMP10 in postnatal myocardium was shown to disrupt hypertrophic growth of cardiomyocytes and to induce proliferation of non-muscle cells (Chen et al., 2006). Transgenic mice have smaller hearts due to smaller cardiomyocyte size, resembling the atrial phenotype, whereas the number of myocytes in the heart remains constant. The authors found an increase in ejection fraction in mutants (Chen et al., 2006) which supports the hypothesis that inhibition of hypertrophic response has a beneficial effect on heart function (Jeong et al., 2006).

Chen and colleagues used the embryonic heart culture system to prove that BMP10 addition can completely rescue the phenotype of hearts isolated from embryos with BMP10 null mutation (Chen et al., 2004). BMP10 enriched medium was able to restore proliferation in knock-out hearts *in vitro*. In the present study a BMP10 conditioned medium was used to investigate the effect of BMP10 on non-muscle cells. One could argue that conditioned medium contains also factors secreted by transfected cells and the achieved effect results from the action of these growth factors. Hence, to monitor the function of BMP10, 10T1/2 cells were directly transfected with a BMP10-IRES-GFP expression construct.

The main objective which was addressed using biologically active BMP10 was whether ectopic expression of BMP10 in failing heart affected the survival of cardiomyocytes and/or stimulated the proliferation and differentiation of non-cardiomyocytes in the heart. Basically it is believed that members of the TGFβ/activin family exhibit a "destructive" function in pathological hearts (reviewed by Euler-Taimor et al., 2006). Enhanced expression of these factors is generally related with ventricular hypertrophy (Ikeuchi et al., 2004), interstitial fibrosis (Hao et al., 2000; Wang et al., 2002) and induction of apoptosis (Francis et al., 2000; Chipuk et al., 2001). Even though BMPs belong to the TGFβ superfamily they exert beneficial effects on the heart, primarily during heart development (Mozen et al., 2001; Chen et al., 2004). They also inhibit apoptosis in adult cardiomyocytes (Izumi et al., 2001). Based on the localization of BMP10$^{pos.}$ cells in cardiomyopathic hearts and their phenotype as judged by double immunolabeling, the effects of BMP10 was analyzed using various non-muscle cells such 10T1/2 fibroblasts and adult bone marrow pluripotent mesenchymal stem cells (bm-MASCs) (Belema Bedada et al., 2005). Moreover, primary cultures of a heterogeneous population of non-cardiomyocytes isolated from adult mouse heart were used to study the BMP10 effect on potential target cells.

10T1/2 cells are known to differentiate into pericytes/vascular smooth muscle cells (vSMCs) in response to TGFβ1 (Karen et al., 1998; Darlan et al., 2001; Kale et al., 2004; Kurzen et al., 2001). *In vitro* studies using different cell lines of various origins and cells isolated from the heart confirmed that the effect of BMP10 is not limited to cardiomyocytes. As described in chapter 3.7.3 a strong induction of proliferation was observed. Another proof of the pro-mitotic effects of BMP10 was the finding that BMP10 expression in mANCM primary cultures correlated with the proliferation of certain subpopulation of cells exhibiting great colony forming activity. The ability of non-cardiomyocyte cells to give rise to distinct cell populations was described by three independent groups. In particular it was demonstrated that Sca1 progenitors of cardiac origin which also expressed the CD31 molecule are present in a large number in the heart and exhibit great colony forming activity (Oh et al., 2003; Matsuura et al., 2004; Pfister et al., 2005). However, the authors ignored the highly proliferative subpopulation and concentrated on examination of the differentiation potential of Sca1$^{pos.}$ into cardiomyocytes (Oh et al., 2003; Matsuura et al., 2004) or more specifically Sca1$^{pos.}$/CD31$^{neg.}$ cells (Pfister et al., 2005). Pro-mitotic function of BMP10 was expected and easy to predict as BMP10 during heart development has been also implicated in proliferation of cells forming trabeculae (Chen et al., 2004) and BMP10 overexpression leads to trabecular overgrowth (Pashmforoush et al., 2004). Moreover, ventricular BMP10$^{pos.}$ cells co-express proliferation markers. Cell culture experiments showed that BMP10 induces proliferation in all tested cell lines and as mANCMs were used, this effect can be also achieved in adult cardiomyopathic hearts further confirming observations in heart failure models.

4.6. BMP10 is a potent regulator of vasculogenesis/angiogenesis

Besides the increased proliferation rate, addition of BMP10 did also stimulate cell differentiation, recruitment and development of three dimensional structures as shown below.

While the proliferative function of BMP10 was expected, the of induction of cord/tube-like structure formation by this cardiac restricted cytokine was suprising. Even TGFβ1, a known potent factor inducing 10T1/2 fibroblast differentiation to pericytes/vSMCs was not able to induce the formation of a 3D structure (Karen et al., 1998; Kurzen et al., 2004). This effect was achieved only in co-culture systems of endothelial cells (ECs) with smooth muscle like 10T1/2 cells using Matrigel™ as a frame (Darland et al., 2001). In the present study vessel-like structures expressing both endothelial and smooth muscle markers were obtained using BMP10 alone without gel support. The same effect was obtained when 10T1/2 cells were directly transfected with a BMP10-IRES-GFP expression construct (see chapter 3.7.6.1). BMP10 transfected cells exhibit higher rate of proliferation than control, i.e. pEGFP transfected cells. BMP10 expressing 10T1/2 cells were also able to recruit each other and neighboring cells to form cord-like structures. Furthermore a new subpopulation of small cells (GFP positive i.e expressing BMP10) appeared in the culture similar to the conditioned medium.

In MASCs and 10T1/2 cells treated with BMP10 co-localization of SMC and EC markers were observed, as described in chapters 3.7.5 and 3.7.6 respectively, for both cell lines. In isolated Sca1$^{pos.}$ cells a co-localization of SMC and EC markers was also noted (Pfister et al., 2005), similar to the models of CMP where BMP10$^{pos.}$/Sca1$^{pos.}$, BMP10$^{pos.}$/CD31$^{pos.}$, BMP10$^{pos.}$/SMA$^{pos.}$ cells were found in ventricles. Therefore it is likely that cells with this phenotype and differentiation potential reside in the heart and might contribute to reverse remodeling processes. This is further supported by the results obtained with mANCM cells that are also able to develop 3D cord-like structures in response to BMP10.

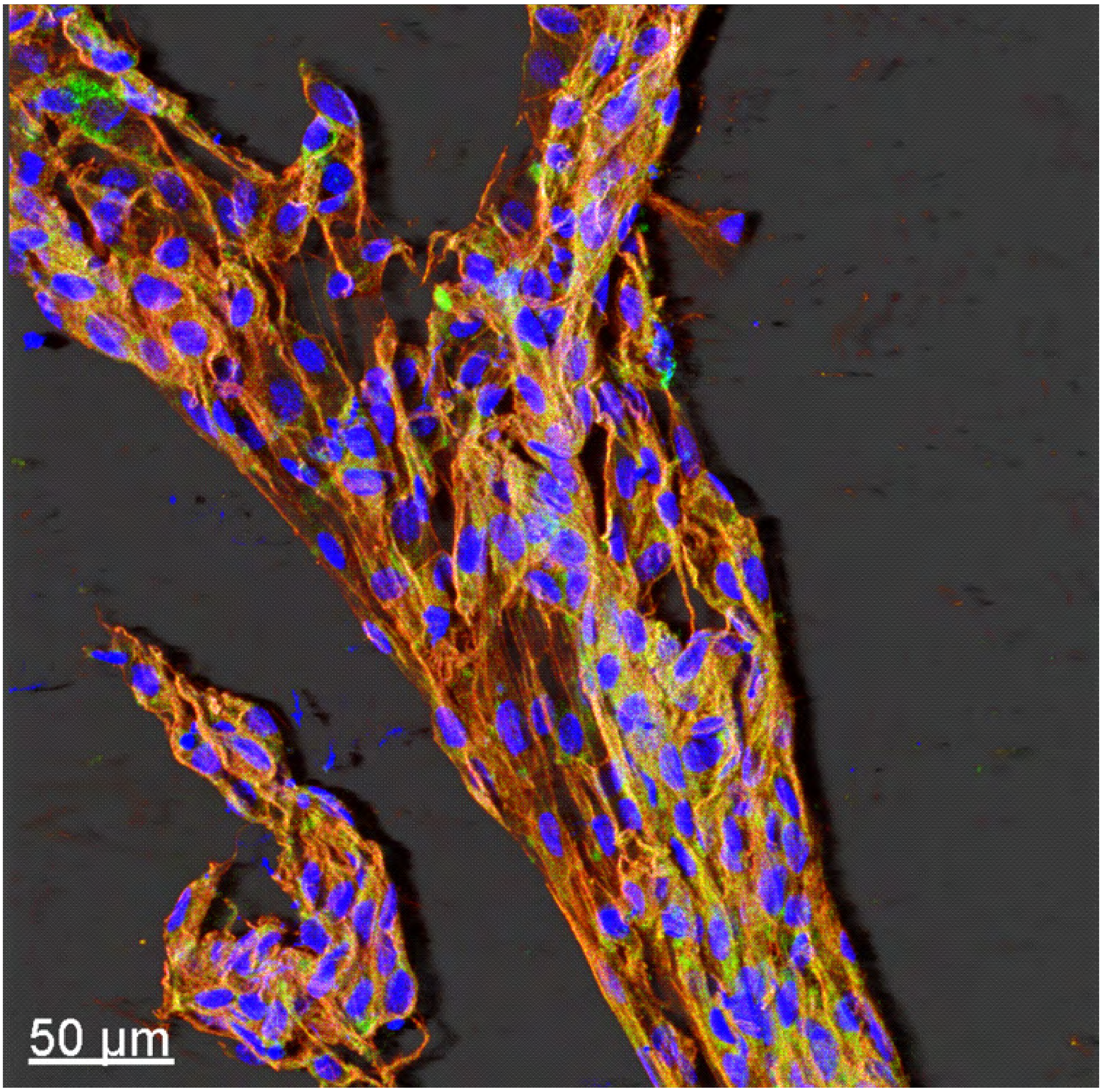

Fig. 4.1. Confocal image illustrating the 3-dimensional structure created by differentiated 10T1/2 cells as a result of transfection with BMP10 expression construct (green). Cells were counterstained with phalloidin-TRITC (red). GFP marks transfected cells. Nuclei were visualized with DAPI (blue).

4.7. Distinct functions of BMP10- interaction with different receptors

BMP10 exerts it function via interaction with specific receptors. It was not a main aim of this study to analyze interactions of BMP10 with specific receptor. However it was possible postulate putative BMP10-Receptor interactions based on BMP10 expression, localization in combination with published data and the expression profile of the BMPs receptors in different cell lines. Moreover, in the case of proteins that are secreted and act via receptors it is not possible to consider the functional implication separately from the receptor. It is generally assumed that BMPs can interact with three different type I receptors, i.e. ALK2, ALK3, ALK6. ALK-6 is absent in the developing heart from midgestation on (Dewulf et al., 1995). In the healthy murine heart ALK3 is abundantly expressed in the right atrium with lower expression levels in the ventricles and the left atrium, whereas ALK1 is almost absent in regions where BMP10 is normally expressed. As ALK6 is not expressed in the adult heart one could expect BMP10 to act via the ALK3 receptor. Interaction of BMP10 with this receptor was shown by another group (Mazerbourg et al., 2005). The same report indicates the possibility of BMP10 binding to ALK6. However, ALK1 was excluded from the study, due to the high background activation of the reporter gene. Strong activation of the BRE promoter by BMP10 upon binding to ALK1 was ignired by the authors due to the background activation (Mazerbourg et al., 2005). Moreover, BMP10 signaling through the ALK3 receptor has been proposed to have an anti-hypertrophic action on cardiomyocytes, as judged by the expression level of the ALK3 receptor in the heart (Chen et al., 2006). My own results show that ALK3 expression in the heart is highest in the right atrium, which overlaps with BMP10 expression while the level of ALK1, which is very low in the right atrium. Since atrial cardiomyocytes are smaller than ventricular cells, the anti-hypertrophic function of BMP10 (Chen et al., 2006) is probably achieved by signaling through ALK3. However, even if BMP10 in the right atrium or in a transgenic strain (Chen et al., 2006) acts via the ALK3 receptor, it might interact with a different receptor in ventricular cells where it is ectopically expressed upon pathological stimuli. This possibility is supported by the absence of ALK3 expression in Sca1$^{pos.}$ heart resident cells (Oh et al., 2003). Additionally, the disruption of ALK3 expression in Sca1$^{pos.}$ cells followed by their differentiation revealed an unchanged induction of Nkx2.5 expression while induction of other cardiomyocyte specific markers, i.e. MEF2C and MHC, were severely impaired (Oh et al., 2003). In the proposed negative regulatory loop which employs BMP10-Nkx2.5 (Pashmforoush et al., 2004) a cardiac myocyte specific ALK3 deletion had very little effect on trabeculation and did not cause an alteration of Nkx2.5 expression (Gaussin et al., 2002; Chen et al., 2004). Hence, it is not clear whether BMP10 signaling through the ALK3 receptor during embryogenic induces myocytes proliferation and differentiation. Interestingly, in ALK3 mutant embryos, BMP10 expression in the trabeculae was unchanged, but BMP10 expression was induced in embryonic atria much earlier than in wild type (Gaussin et al., 2002), indicating that BMP10 may be downstream of ALK3 in atrial myocytes.

The expression profile of type I receptors in cell lines used in cell culture experiments revealed that proliferative and angiogenic effects of BMP10 was observed in cells expressing ALK1, ALK3 and ALK5. Cos1 cells have been described as the least responsive to BMP10 (Mazerbourg et al., 2005) and express neither ALK1 nor ALK5. Overexpression of BMP10 in 293T cells did not cause an effect as in 10T1/2 or MASCs. Since the only missing receptor in the 293T cell line is ALK1, it is possible that BMP10 binding to ALK1 promotes the angiogenic signaling pathway, however further experiments are necessary to support this hypothesis.

The BMP10 antibody which was generated in the course of the project allowed detection of the secreted protein. In mouse embryos, the mature ligand was found in the outflow tract in addition to the developing heart chambers. Moreover, BMP10 was shown to induce both endothelial and smooth muscle cell phenotypes *in vitro* followed by 3D tube-like structures formation. Cells expressing BMP10 and SMC and/or EC markers were also found in various models of cardiomyopathies. TGFβ signaling is known to play an important role during vascular remodeling (Oh et al., 2000; Goumans et al., 2002) and two type I receptors are implicated in these processes, namely ALK1 and ALK5. As already mentioned expression levels of ALK1 in right atrium is extremely low. So it is unlikely that BMP10 acts via this receptor in the right atrium of the healthy heart. However, ALK1 is believed to modulate TGFβ1 signaling during angiogenesis (Oh et al., 2000, Seki et al., 2003) and it is specifically expressed in the arterial endothelium during embryogenesis with a significant decrease in adult blood vessels (Seki et al., 2003). ALK5 was also shown to transmit TGFβ1 signals and its expression is restricted to the vascular smooth muscles of vessels (Seki et al., 2006). Interestingly, ALK5 expression in the developing heart is confined to trabecular muscles, and is not found in the compact wall. Additionally, some mesenchymal cells surrounding the aorta expressed ALK5. In the adult heart, expression was found in the pulmonary artery valve and some ventricular, but not endothelial cells (Seki et al., 2006). Surprisingly, null mutation of ALK1 leads to defective differentiation and recruitment of smooth muscle cells, while disruption of the ALK5 gene to impaired endothelial cells migration and proliferation (Oh et al., 2000; Urness et al., 2000; Larsson et al., 2001; Goumans et al., 2003). These data suggest that there is a link between ECs and SMCs dependent on the ALK1/ALK5 pathway. This role was assigned to platelet derived growth factor BB (PDGF-BB) released by ECs during the resolution phase of angiogenesis. This potent chemoattractant is bound by vSMCs/pericytes expressing the PDGFβ receptor (Hellstrom et al., 1999). Additionally, PDGF induces TGFβ expression in vSMCs/pericytes (Nishishita et al., 2003). BMP10 induces expression of EC, vSMC/pericyte markers *in vitro*, and *in vivo* BMP10 is expressed in Sca1 progenitors which are also known to express these genes (Pfister et al., 2005). It is likely that ectopic BMP10 expression induces differentiation of common endothelial and smooth muscle progenitors from Sca1$^{pos.}$ resident cells, thus inducing angiogenic events in a tissue specific manner. The simultaneous expression of EC, vSMC and pericyte markers is already known and was described *in vivo* (DeRuiter et al., 1997). It can be induced *in vitro* by TGFβ in epicardial explants, in an ALK5 dependent pathway (Compton et al., 2005). As already mentioned, BMPs are known to bind to ALK2, -3 and -6, however, the closest homolog of BMP10, i.e. BMP9 (GDF2) has been shown to interact with ALK1 in combination with BMPR II (Brown et al., 2005). This finding further supports the possible BMP10 action via ALK1 receptor, which is known to play a role during angiogenesis. A postulated mechanism is presented below (Fig. 4.2).

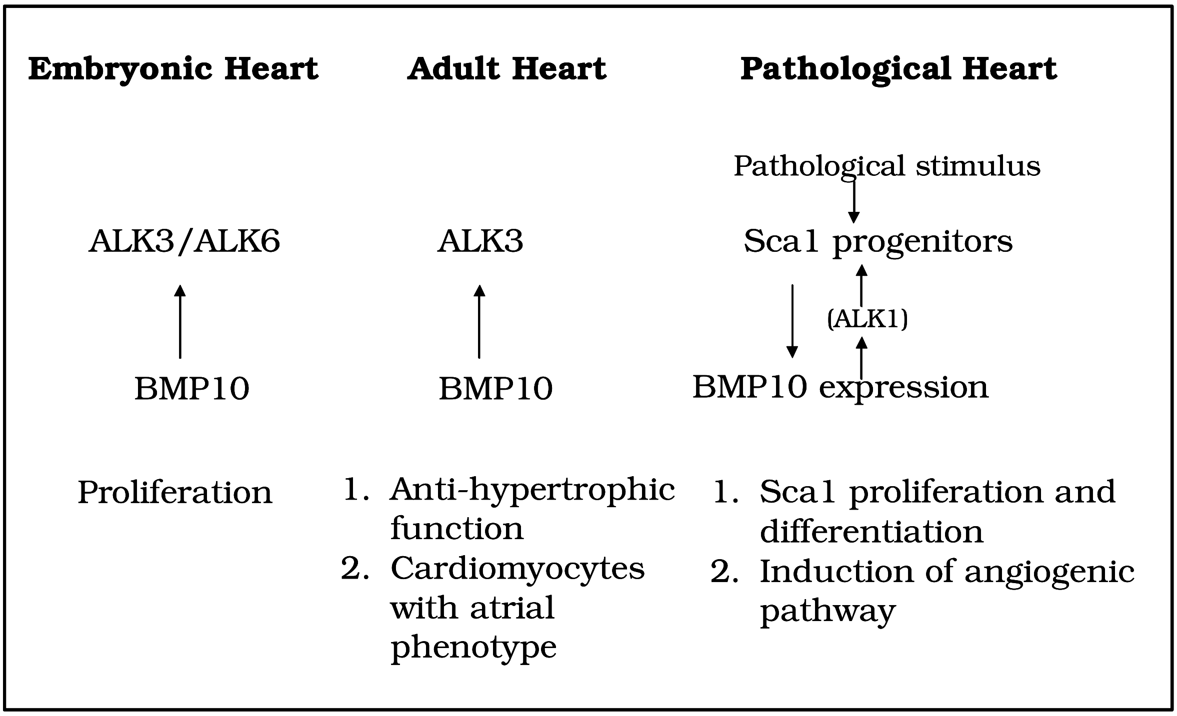

Fig. 4.2. Schematic representation of distinct BMP10 functions dependent on the interaction with specific receptor.

4.8. Functional implications of BMP10 expression in diseased hearts

The purpose of this study was to clarify the possible role of BMP10 in cardiac diseases. I investigated, therefore, cardiac tissue from different models of cardiomyopathic mice. Data on BMP10 in myocardium is scarce even though BMP10 is the only cardiac restricted member of the BMP protein family. Much information can be found on the role of BMPs in bone development, pathology and regeneration. In the past decade the role of BMPs expressed in heart on the cardiac development was also intensively studied. This information, discussed extensively in the Introduction, formed the basis of my present work.

BMPs are known to play an important role during bone repair (Lee et al., 2006). The effects include induction of proliferation, migration and differentiation of mesenchymal progenitor as well as vascular invasion (Redi, 1997; Okubo et al., 2002; Lind et al., 1996; Bostrom et al., 1995). Similar functions were uncovered for BMP10 in functional studies which I performed using various cells culture models. The most important observation in this context was the induction of morphogenetic events leading to the formation of vessel-like, tubular structures.

The unusual variety of ventricular cells expressing BMP10, the induction of EC, vSMC markers and tube formation by BMP10 *in vitro* allowed to draw the following conclusions and to formulate a hypothesis:

1. As a result of pathological stimuli a new subpopulation of proliferating cells appears in the ventricles of the adult heart, which is characterized by ectopic BMP10 expression (BMP10$^{pos.}$ cells).
2. BMP10 is a sensitive marker of heart dysfunction and drastic expression changes and redistribution of protein can be found even when the pathological phenotype is modest.
3. A possible function in vasculogenesis or angiogenesis of ventricular BMP10$^{pos.}$ cells might be deduced based on their localization and characterization. BMP10 can induce proliferation in resident cardiac progenitors followed by differentiation into ECs and/or vSMCs. These results were further confirmed *in vitro* using different cell lines.
4. BMP10 exhibits various functions dependent on the target cells. The physiological effect of BMP10 probably differs between the embryonic heart and the adult right atrium in the healthy adult heart.

Different functions might be assumed for embryonic and atrial cardiomyocytes as well as for interstitial cells. It can be hypothesized that this effect is achieved by differentially expressed BMP10 receptors.

5. The function of BMP10 in the pathological heart is distinct from that of the healthy organ.
6. Ventricular BMP10 positive cells originate from Sca1$^{pos.}$ cells and BMP10 signaling can modulate proliferation followed by differentiation of Sca1 cardiac progenitors in the failing heart. Cell culture experiments together with published data confirm this possibility.

Taken together, these findings allow the conclusion that BMP10 in diseased hearts plays a significant role in cardiac remodeling.

Cardiac remodeling is a determinant of the clinical course of heart disorders. It implies that cardiac structure and function slowly deteriorate in response to pathological stimuli acting on the heart such as hypertension, pressure or volume overload or genetic factors such as in primary or secondary cardiomyopathies. Often, the term “adverse” remodeling is used to indicate an aggravation of structure and function until heart failure occurs. The most widely used definition of remodeling was given by Cohn in 2000:

> Cardiac remodeling is defined as gene expression resulting in molecular, cellular and interstitial changes and manifested clinically as changes in size, shape and function of the heart (Cohn et al., 2000).

This applies also to the models of cardiomyopathy used in this study. Experimental animals similar to human patients show adverse remodeling processes, which involve myocytes, the extracellular matrix and the microvasculature. The term reverse remodeling definies reversal of the negative effects, i.e. improvement of cardiac structure and function.

It can be hypothesized that BMP10 expression in cardiac ventricles as observed in this study might be important for remodeling during the course of the cardiomyopathies studied here by allowing a certain adaptation to negative effects of the disease. It might be assumed that BMP10 is involved in the remodeling process by acting as a protecting factor, i.e. by provoking either, to certain extent, reverse remodeling or at least a delay in the occurrence of the heart failure as endpoint of remodeling. Probably the protective effects of BMP10 counteracting adverse remodeling processes are twofold: (i) a positive influence on the cardiac microvasculature including capillaries and arterioles-arteries based on the results presented here, and (ii) BMP10 might have an antihypertrophic effect as shown by Chen (Chen et al., 2006).

The scheme of fig. 4.3 shows the possible action of BMP10 on the cardiac microvasculature.

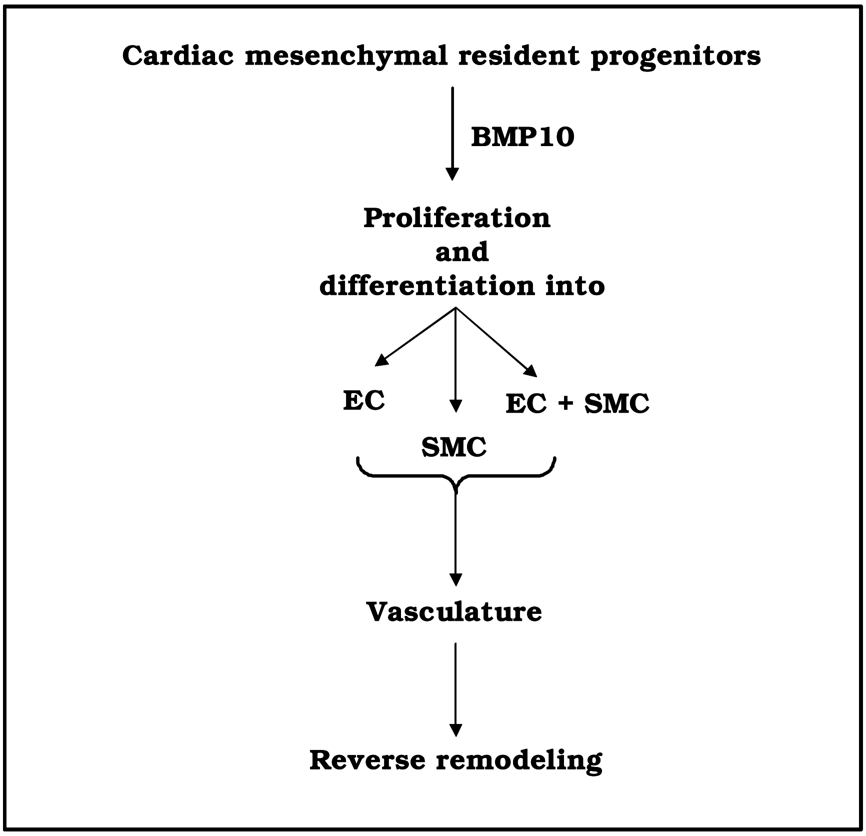

Fig. 4.3. Schematic drawing of the role of BMP10 as a compensatory factor in cardiac remodeling.

It is known that proliferation of interstitial cells and activation of endothelial cells play a role in cardiac reverse remodeling (Cohn et al., 2000). Induction of the proliferation and differentiation by BMP10 of resident cardiac progenitors into endothelial and vascular smooth muscle cells - the components of capillaries and arteries together with induced migration of these cells might lead to an enhanced cardiac vascular development. This may improve the oxygen supply of the hypertrophied and/or diseased heart. Therefore, recapitulation of BMP10 expression in pathological ventricles may be a key component of the complex compensatory machinery that is initiated by various pathological conditions.

Even though cardiomyocytes represent the major proportion of the protein mass of the heart (approximately 75%) they constitute only a minor part of the cell number (around 25%) in the heart (reviewed by Shapiro et al., 1996). Although there is sometimes the tendency to consider only the response of myocytes in the development of cardiomyopathy, the integration of other cell types should not be ignored. Non-cardiomyocytes such as vascular smooth muscle, vascular and endocardial endothelial cells, fibroblasts and components of the nervous system play an important role in the development of the pathological as well as physiological responses.

In the current work I proved that BMP10 is a cardiac specific factor able to induce proliferation and differentiation of mesenchymal progenitors to endothelial and vascular smooth muscle cells followed by tube-like structure assembly. Therefore it is highly probable that ectopic expression of BMP10 in pathological hearts has a beneficial pro-angiogenic function.

5. Summary

PURPOSE:

BMP10 is a cardiac specific member of the TGFβ superfamily and the expression of this cytokine is limited to the right atrium of the healthy heart. In the work presented here, I attempted to unveil the function of BMP10 in the pathological adult heart.

MATERIAL AND METHODS:

The expression and localization of BMP10 was studied in embryonic, neonatal and adult mouse hearts. Two genetic (heterozygous MnSOD and Desmin knock-out strains) and two drug induced (doxorubicin and isoproterenol) murine models of cardiomyopathies were used to investigate the changes of BMP10 expression and localization. MRI analysis was used to determine alterations of cardiac function and histopathological examination to identify changes of myocytes and the interstitium was carried out in the hearts of all models tested. The TUNEL method (apoptosis) and Complement9 staining (necrosis) were used for determination of cell death. Quantitative changes of BMP10 in the pathological murine hearts were monitored on the RNA level by semi-quantitative and real-time RT-PCR as well on the protein level by western blot. The levels of ANF, BNP and FHL2 as indicator of heart disorder were examined. Redistribution of BMP10 mRNA expression in diseased hearts was shown by in situ hybridization. By overexpression of the His-tagged mature region of the BMP10 in *E.coli* and its purification it was possible to generate an antibody specifically recognizing the mature secreted domain of the BMP10. Therefore, BMP10 localization in the healthy and cardiomyopathic murine hearts was investigated. The generation of expression construct producing functional BMP10 protein allowed to conduct *in vitro* experiments. Cell culture experiments using medium enriched in active BMP10 protein allowed evaluation of the BMP10 action on the primary culture of isolated non-cardiomyocytes as well as multipotent mesenchymal 10T1/2 fibroblasts and the bone marrow derived stem cell line bm-MASCs. Immunocytochemistry and RT-PCR analysis of treated cells wereused to analyze the effects of BMP10 *in vitro.*

RESULTS:

1. During embryonic heart development BMP10 expression was found in the trabeculated myocardial layer, and BMP10 protein was observed additionally in the outflow tract, the compacted heart wall and the epicardial layer.
2. BMP10 in the healthy adult heart is expressed in the right atrium and after secretion binds to the membrane of both atrial cardiomyocytes and interstitial cells. Moreover, expression and binding of this protein was observed in the tricuspid valve and cells adjacent to the arteries in the upper atrial area of the heart.
3. The murine models used in this study represent the dilated and hypertrophic type of cardiomyopathy and exhibit different degrees of cardiac dysfunction characterized by changes in myocardial volume and reduced ejection fraction. Interstitial and replacement fibrosis, cardiomyocyte hypertrophy, myofiber disarray and cell death in respect to necrosis and apoptosis were detected but the degree of structural changes was different in all models. The number of apoptotic or necrotic cells was very low.
4. In diseased hearts two types of qualitative BMP10 distribution changes were found. The subcellular localization of BMP10 in cells of the right atrium was changed. In addition, BMP10 was re-expressed in ventricular cells.
5. In Desmin knock-out and in doxorubicin induced dilated cardiomyopathy upregulation of the BMP10 expression was found, while quantification of BMP10 in MnSOD heterozygous and isoproterenol treated mouse heart revealed its downregulation. These variations in BMP10 quantity were monitored at the RNA and protein level. The number of BMP10 positive cells in the ventricles of pathological hearts is low, and therefore quantitative changes represent most probably the deregulation of BMP10 expression in the right atrium.
6. Ventricular cells ectopically expressing BMP10 in pathological hearts are $\text{Sca1}^{\text{pos.}}$ and show signs of proliferation. Characterization of the ventricular $\text{BMP10}^{\text{pos.}}$ cells revealed that they constitute a heterogeneous population of cells often expressing endothelial and smooth muscle cell markers, but never cardiomyocyte specific genes. BMP10 is expressed, however, by embryonic and atrial cardiomyocytes.
7. BMP10 effects are dependent on the differentially expressed receptors in various cell lines. The effect of BMP10 in C2C12 cells is limited to the induction of osteoblast differentiation. In contrast, BMP10 induced multipotent mesenchymal 10T1/2 embryonic fibroblasts, adult bone marrow mesenchymal stem cells and in

non-cardiomyocytes isolated from the adult mouse heart to express smooth muscle, endothelial and pericyte markers. Moreover, cells expressing these markers are able to form 3D tube-like structures indicating a possible role of BMP10 in angiogenesis.

CONCLUSION:

On the basis of these results it can be concluded that BMP10 acts in an autocrine and paracrine fashion. As expression and localization of BMP10 changes dramatically even when the pathological changes are still moderate, BMP10 may play an important role in the disease process of dilated and hypertrophic cardiomyopathy. In cardiomyopathic hearts ventricular BMP10$^{pos.}$ cells seem to originate from cardiac Sca1 progenitors and it might be concluded that BMP10 induces their proliferation and differentiation. In addition, cell culture experiments show that BMP10 induced differentiation of mesenchymal cells to endothelial, smooth muscle cells and pericytes leading to the assembly of tube-like structures. BMP10 may play a protective role in the cardiomyopathies studied here by stimulating the development of the cardiac microvasculature including capillaries, arterioles and small arteries. This process might result in an inhibition or at least a delay of adverse remodeling of the heart, which is part of an important adaptive process to cardiac diseases. Further studies including the inactivation of BMP10 in the adult heart are necessary to investigate the BMP10 function *in vivo*.

6. Zusammenfassung

ZIEL DER STUDIEN:

BMP10 ist ein herzspezifisches Mitglied der TGFβ-Superfamilie. Die Expression dieses Zytokins ist auf das rechte Atrium des gesunden Herzens begrenzt. In der vorliegenden Arbeit bemühte ich mich, die Funktion von BMP10 im pathologischen adulten Herzen aufzudecken.

MATERIAL & METHODEN:

Die Expression und Lokalisation von BMP10 wurde im embryonalen, neonatalen und adulten Mausherzen untersucht. Zwei genetisch (heterozgote MnSOD und Desmin knock-out Stämme) und zwei Drogen induzierte (Doxorubizin und Isoproterenol) murine Kardiomyopathiemodelle wurden genutzt, um Veränderungen der BMP10 Expression und Lokalisation zu prüfen. An den Herzen aller getesteten Modelle wurden MRI-Analysen durchgeführt, um kardiale Funktionsänderungen zu bestimmen, und histopathologische Betrachtungen unternommen, um Veränderungen der Myozyten und des Interstitiums aufzudecken. Die TUNEL Methode (Apoptose) und die Complement9-Färbung (Nekrose) dienten der Feststellung von Zelltod. In den pathologischen Mäuseherzen wurden die quantitative Veränderungen von BMP10 auf RNS-Ebene durch semi-quantitative und „real-time" RT-PCR kontrolliert, indessen auf Proteinebene durch die Methode des Western Blots. Die ANF-, BNP- und FHL2-Level als Indikatoren für Herzstörungen wurden ebenfalls analysiert. Die Neuverteilung der BMP10 mRNS-Expression in geschädigten Herzen wurde durch *in situ* Hybridisierungen gezeigt. Die Lokalisation des BMP10 Proteins in gesunden und pathologischen Herzen wurde mit einem Antikörper untersucht, der spezifisch die aktive Domäne von BMP10 erkennt. Für die Generierung des Antikörperes wurde zuvor das reife, mit einem His-Schwanz versehene Protein in *E. coli* überexprimiert und aufgereinigt. Die Herstellung eines Expressionskonstrukts, das ein funktionsfähiges BMP10 Protein produziert, ermöglichte die Durchführung von *in vitro* Experimenten. Zellkulturexperimente mit aktivem BMP10 Protein angereichertem Medium, ermöglichte die Aufklärung der BMP10-Aktivität im Primärkulturen von nicht-Kardiomyozyten, in multipotenten mesenchymalen 10T1/2 Fibroblasten und einer Knochenmark abstammenden Stammzelllinie bm-MASC (*engl.:* „bone marrow derived mesenchymal adult stem cells“). Immunozytochemische und RT-PCR Analysen an den behandelten Zellen dienten der Aufklärung der BMP10-Effekte *in vitro*.

ERGEBNISSE:

1. Während der embryonalen kardialen Entwicklung konnte die Bmp10 Expression im trabekulierten Myokard detektiert werden. Das BMP10 Protein wurde außerdem im Ausflusstrakt, der kompaktierten Herzwand und im Epikard nachgewiesen.
2. Bmp10 wird im gesunden adulten Herzen im rechten Atrium exprimiert. Nach der Sekretion bindet das Protein an die Membranen beider atrialen Kardiomyozyten und die interstitialen Zellen. Des Weiteren wurden die Expression und die Bindung des Proteins in den Trikuspidalklappen und den benachbarten Zellen der Arterien in der oberen atrialen Region des Herzen beobachtet.
3. Die murinen Modelle, die in dieser Studie verwendet wurden, repräsentieren die dilative und die hypertrophe Form der Kardiomyopathie. Sie weisen verschiedene Grade der kardialen Dysfunktion auf, die charkaterisiert sind durch Veränderungen im myokardialen Volumen und eine reduzierte Ejektionsfraktion. Interstitiale und reparative Fibrose, kardiomyozytäre Hyperthrophie, Fehlanordnung der Herzmuskelfasern und Zelltod in Bezug auf Apoptose und Nekrose konnte in allen Modellen festgestellt werden. Jedoch der Grad der jeweiligen strukturellen Veränderung war different. Die Anzahl der apoptotischen und nekrotischen Zellen war sehr gering.
4. In den geschädigten Herzen konnten zwei Typen einer qualitativen Veränderung der BMP10 Verteilung gefunden werden. Zum einen war die subzelluläre Lokalisation von BMP10 im rechten Atrium verändert, und zum anderen wurde BMP10 in ventrikulären Zellen re-exprimiert.
5. In der Desmin-defizitären Maus und in Doxorubizin-induzierten dilativen Kardiomyopathien konnte eine Hochregulation der BMP10 Expression gefunden werden, während die Quantifizierung von BMP10 in MnSOD heterozygoten und Isoproterenol behandelten Mäusenherzen eine Runterregulation aufdeckte. Diese Variationen der BMP10 Quantität wurden auf RNS- und Proteinebene kontrolliert. Die Anzahl der BMP10 positiven Zellen in den Ventrikeln der pathologischen Herzen ist gering. Folglich repräsentieren die quantitativen Veränderungen höchstwahrscheinlich die Deregulierung der BMP10 Expression im rechten Atrium.

6. Ventrikuläre Zellen, die ektopisch BMP10 im pathologischen Herz exprimieren, sind Sca1^{pos} und weisen Anzeichen der Proliferation auf. Die Charakterisierung dieser BMP10^{pos} Zellen enthüllte, dass sie eine heterogene Population von Zellen darstellen, die oftmals endotheliale Marker und solcher glatter Muskulatur exprimieren, aber niemals Kardiomyozyten-spezifische Gene. Dennoch wird BMP10 von embryonalen und atrialen Kardiomyozyten exprimiert.
7. Die BMP10-Effekte sind abhängig von differentiell exprimierten Rezeptoren in den verschiedenen Zelllinien. Die Effekte von BMP10 auf C2C12 Zellen sind limitiert auf die Induktion der Osteoblastendifferenzierung. Im Gegensatz dazu induziert BMP10 in multipotenten mesenchymalen 10T1/2 Fibroblasten, adulten Knochenmark abstammenden mesenchymalen Stammzellen und in nicht-Kardiomyozyten, die aus dem adulten Mausherzen isoliert wurden, endotheliale, perikardiale und für glatte Muskulatur typische Marker. Darüber hinaus sind die Zellen, die diese Marker exprimieren, in der Lage, dreideimensionale röhrenartige Strukturen zu bilden. Dies weist auf eine mögliche Rolle von BMP10 während der Angiogenese hin.

SCHLUSSFOLGERUNGEN:

Basierend auf den dargestellten Ergebnissen kann geschlussfolgert werden, dass BMP10 auf eine autokrine und parakrine Art und Weise wirkt. Da die BMP10 Expression und Lokalisation sich dramatisch verändern, auch wenn die pathologischen Veränderungen noch moderat sind, ist es möglich, dass BMP10 eine wichtige Rolle im Krankheitsverlauf der dilativen und hypertrophen Kardiomyopathien spielt. In kardiomyopathischen Herzen scheinen die ventrikulären BMP10^{pos} Zellen aus kardialen Sca1 Vorläufern hervorzugehen. Es könnte gefolgert werden, dass BMP10 ihre Proliferation und Differenzierung induziert. Des Weitern haben Zellkulturexperimente gezeigt, dass BMP10 die Differenzierung von mesenchymalen Zellen zu endothelialen Zellen, Zellen der glatten Muskulatur und Perizyten induziert, was schließlich zur Bildung von röhrenähnlichen Strukturen führt. In den untersuchten Kardiomyopathien spielt BMP10 eine protektive Rolle, indem es die Entwicklung der kardialen Mikrovaskulatur inklusive der Kapillaren, Arteriolen und kleinen Atrierien stimuliert. Dieser Prozess resultiert möglicherweise in einer Inhibition oder zumindest einer Verzögerung der nachteiligen Umgestaltung des Herzens, welche Teil des wichtigen adaptiven Prozess an Herzerkrankungen ist. Weitere Studien, inklusive der

Inaktivierung von BMP10 im adulten Herzen sind notwendig, um die BMP10 Funktion *in vivo* zu untersuchen.

7. ABBREVIATIONS

3D	three-dimensional
A	Adenine
ActR	activin receptor
ALK	activin receptor-like kinases
ALP	Alkaline phosphatase
ANF	Atrial Natiuretic Factor
Ao	aorta
AVC	Atrioventricular Canal
AVCD	Atrioventricular canal defects
BAMBI	BMP and activin membrane bound inhibitor
BLAST	Basic Local Alignment Search Tool
BMP	Bone Morphogenetic Protein
BMP10	Bone Morphogenetic Protein 10
BMPR	BMP receptor
BNP	Brain Natiuretic protein
bp	base pairs
BRAM1	BMP receptor associated molecule 1
BrdU	Bromo-deoxy-Uridine
BSA	Bovine Serum Albumine
C	Cytosine
cDNA	DNA complementary to mRNA
CMP	cardiomyopathy
Co-Smads	Common-partner Smads
DOX	doxorubicin
E	Embryonic day
EC	Endothelial cells
ECG	Electrocardiogram
EF	Ejection fraction
EMT	Endothelial to mesenchymal transition
EPI	Epicardial layer
ERK	Extra-cellular signal regulated kinase

ES	embryonic cells
EST	expressed sequence tag
EtOH	ethanol
FCS	Fetal Calf Serum
FHL	Four and half LIM protein
FKBP12	FK506-binding protein 12
FOV	Field of view
FRT	Flp recombinase recognition site
g	gram
G	Guanine
GDF	growth/differentiation factor
GDNF	glial cell line-derived neurotrophic factor
GFP	Green Fluorescence Protein
GM	Growth medium
H	hour
IAS	Interatrial septum
IRES	internal ribosome entry site
I-Smads	Inhibitory Smads
ISO	Isoproterenol
kbp	kilo base pairs
kDa	kilo Daltons
KO	Knock-out
LA	Left atrium
LAA	Left atrium appendage
LV	Left ventricle
M	mol
mANCM	mouse adult non-cardiomyocytes
MAPK	Mitogen activated protein kinase
matBMP10	mature region of the Bone Morphogenetic Protein 10
mBM-MASC1	mouse bone marrow mesenchymal adult stem cell line 1
MeOH	Methanol
mg	milligram
MHC	Myosin heavy chain
min.	minute

ml	milliliter
mM	mili Mol
MRI	Magnetic Resonance Imaging
mRNA	messenger RNA
neg.	negative
ng	nanogram
nm	nanometer
NMR	Nuclear magnetic resonance
o.n.	over night
OFT	Outflow tract
P	Phosphorylation site
PBS	Phosphate Buffered Saline
PBT	PBS+Tween20
PCR	Polymerase Chain Reaction
PDGFRß	platelet-derived growth factor receptor ß
PFA	Paraformaldehyde
PGK	phosphoglycerol kinase
pmol	piko mol
pos.	positive
RA	Right atrium
RAA	Right atrium appendage
RNA	ribonucleic acid
R-Smads	Receptor-regulated Smads
RT	Repetition time
RT-PCR	Reverse Transcriptase Polymerase Chain Reaction
RV	Right ventricle
Sca1	stem cell antigen 1
SDS-PAGE	SDS polyacrylamide gel electrophoresis
SF	Serum Free medium
SMA	Smooth muscle actin
SOD	superoxide dismutase
T	Tesla
TE	echo time
TGFß	Transforming Growth Factor ß

TR	Trabeculae
TUNEL	Terminal dUTP deoxynucleotidyl transferase nick end-labeling
DCM	dilated cardiomyopathy
U	unit
v/v	volume/volume
vSMC	vascular smooth muscle cell
wt	wild type
μg	microgram

8. Appendix

8.1. Curriculum Vitae

DATE OF BIRTH: 13 August 1977
STATUS: married
NATIONALITY: Polish

EDUCATION:

1996 -2001	Student of Agricultural University of Poznań, Faculty of Biotechnology (G.P.A: 4.6/5.0), Engineer and Master of Science Diploma made at the Institute of Bioorganic Chemistry Polish Laboratory of tRNA, Team of Protein Biosynthesis. Master Thesis Diploma defended on June 2001 (5.0/5.0). Rector's prize for achievements during studies.

RESEARCH EXPERIENCE:

1999-2000	volunteer work in Protein Biosynthesis Laboratory in Institute of Bioorganic Chemistry Polish Academy of Sciences
2000-2001	Engineer and Master of Science Diploma at Institute of Bioorganic Chemistry Polish Academy of Sciences. Thesis: "Investigating of conformational changes of eukariotic ribosome using antisense oligonucleotides hybridisation method"
11.2001-4.2005	Marie Curie fellow, Probiodrug, Halle, Germany
1.05.2002-01.2005	Ph.D. student at the Marthin-Luther University Halle-Wittenberg, Germany; Institute for Physiological Chemistry, involved in two projects belonging to one grant: "Functional Genomics of the ageing heart: Affected genes and their mode of action"
02.2005 – 06.2005	PhD student at the Martin Luther University Halle -Wittenberg, Medicine Faculty, Institute of Physiological Chemistry; Max-Planck Institute of Heart and Lung Research –Bad Nauheim.

07.2005 -	to present, PhD student at the University Klinik Giessen – Marburg, Max-Planck Institute of Heart and Lung Research –Bad Nauheim.

CONFERENCES AND COURSES

1. Polish American Conference Physico-Chemical Methods in Biotechnology and Material Science; 5-7 June 2000, Poznan, Poland

2. International Conference " Molecular Architecture of Evolution: Primary and Secondary Determinants" Poznan, Poland, (2000)

3. Theoretical Course “RNA Structure and Function” International Centre for Genetic Engineering and Biotechnology; 9-12 April 2001, Trieste, Italy

PUBLICATIONS:

Piotrowska, I., Dudzinska, B., Twardowski, T., (2002) Structure and function of prokaryotic ribosome (in Polish). Advances in Biochemistry 48(1), 2-19

8.2. Publications and scientific activity in congresses during PhD studies

8.2.1. Publications

Presented results have not been published.

8.3.2. Presentation

Results have not been presented during scientific congresses.

8.3.4. Courses

RNAi Myores Workshop, Villie-Morgon, 2006

9. Acknowledgments

This study was carried out at the Martin Luther University Halle-Wittenberg, Institute of Physiological Chemistry and Max-Planck Institute for Heart and Lung Research in Bad Nauheim.

I would like to express my thanks to **Prof. Thomas Braun**, my direct scientific supervisor for the scientific liberty and trust that I received.

I am greatly indebted to many people at Institute of Physiological Chemistry in Halle for collaboration and support:

Dr. Herbert Neuhaus for the possibility of continuing his project, theoretical and practical introduction, plasmids that he gave me and for the time he spent teaching me.

Dr. Petra Neuhaus for introduction and help with Real-Time PCR and many other things.

Gabrile Liebert-Hoang and Dr. Cuong Hoang-Vu for their friendship, constant support and helping hand whenever I need it. For advises how to live and survive in exceptionally bureaucratic Germany.

Dr. Weber for helping advices with protein purification.

Dr. Tomasz Loch, currently at the Medical University, Sosnowiec, Poland for MnSOD mice and help in many situations.

Robert Kramek, currently somewhere in Warsaw, for his support and friendship.

Dr. Helmut Sauter and **Prof. Metchild Hatzfeld** for introducing me in the complicated and unpredictable “protein world”.

Sincere thanks are given to **all people** at the Institute of Physiological Chemistry for their willingness to help in various situations and introducing me to techniques and equipment.

I would like to express my warmest thanks to **all people from Max Planck Institute in Bad Nauheim:** Dr. Andre Schneider, Veronika Handzik, Steffi Bachman, Monika Euler, Ram Ayyaswamy, Dr. Thomas Bottger and his PhD students, Dr. Rene Zimmerman, Silvia Lindlar, Claudia Ullmann, Frank Voss, Helmuth Busch, Gerhard Stammler, Helmut Kreuzer, Sigrum Fahrland, Tamara Grigat, Renate Nordgren, Elke Conradi, Burkhard Scheibner, Elvira Albrecht for the relaxed and friendly working atmosphere, generous help in many situations and for the possibility to work with them. I owe special thanks to people who participated in my thesis studies and experiments:

Dr. Sawa Kostin deserves my warmest thanks. Everything I know about immunohistochemistry, confocal microscopy, cardiomyopathies, and pathology I know from you Sawa. He is wonderful teacher and mentor. He also performed 3D reconstructions presented in this work, some confocal images and helped in many other ways. I want all readers of this thesis to acknowledge the crucial role of Dr. Kostin and his ideas and effort in the pathological analysis and confocal imaging.

I am deeply grateful to **Dr. Astrid Wietelmann** for MRI analysis, data evaluation and helping hand in other situations. I also owe special thanks to **Ursula Hofmann**, who also did MRI and created together with Astrid friendly atmosphere.

I owe special thanks to Master of cardiomyocytes and non-cardiomyocytes isolation **Marion Wiesnet.**

I am thankful to **Dr. Thomas Kubin and Kerstin Richter** for helping with Western Blots and many other things.

I want to thank **Susane Martin** for her invaluable secretarial work and **Dr. Judith Scheaffer** for organizational framework.

I am grateful to **Fikru Belema Bedada,** who provided bm-MASCs.

Angela Bachmann is acknowledged for valuable advises concerning rules at Justus Liebieg University

I want to express my deepest gratitude to **Sandra Buecker** for translation of the Summary into German Zusammenfassung.

I owe special thanks to **Beate Grohmann,** who helped me a lot with immunohistochemistry**.** Thank you, Beate for your friendship, support and many, many other things. I am really honored to be your friend.

I wish to thank my husband **Michal Mielcarek** for his patience and support throughout these years we worked together.

Finally, I wish to express my gratitude to my scientific (and not only) authority **Prof. Jutta Schaper** for her faith in me, support and help in many situations. Dear Prof. Schaper! It is difficult to express how grateful I am for everything you did for me. Thank you! I am really honored that I had opportunity to meet you. I wish to be like you.

This work is dedicated:

In memory of my father
Kazimierz Piotrowski (1942-2006).
Thank you Dad! - For encouragement when I wanted to give up.
Żałuję Tato, ze nie zobaczyłeś mojego doktoratu

And

My mother
Teresa Piotrowska
Za poświęcenie mi całego swojego życia

10. REFERENCES

Aoki, H., Fujii, M., Imamura, T., Yagi, K., Takehara, K., Kato, M., Miyazono, K., (2001) Synergistic effects of different bone morphogenetic protein type I receptors on alkaline phosphatase induction. *J. Cell Science,* **114**, 1483-1489.

Armulik, A., Abramsson, A., Betsholtz, Ch., (2005) Endothelial/pericyte interactions. *Circ. Res.,* **97**, 512-523.

Asakura, A., Seale, P., Girgis-Gabardo, A., Rudnicki, M.A., (2002) Myogenic specification of side population cells in skeletal muscle. *J. Cell Biol.*, **159**, 123-134.

Ausubel, F.M., Brent, R., Kingston, R.E., Moore, D.D., Seidman, J.G., Smith, J.A., Struhl, K., (1992) Current Protocols in Molecular Biology, Looseleaf Service, Wiley-Liss, New York, USA.

Bartosz, G., (1995) The second face of oxygen. Eds.: Bartosz, G., PWN, Warsaw, Poland.

Bassing, C.H., Yingling, J.M., Howe, D.J., Wang, T., He, W.W., Gustafson, M.L., Shah, P., Donahoe, P.K., Wang, X.F., (1994) A transforming growth factor beta type I receptor that signals to activate gene expression. *Science,* **263**, 87-89.

Belema Bedada, F., Technau, A., Ebelt, H., Schulze, M., Braun, T., (2005) Activation of myogenic differentiation pathways in adult bone marrow-derived stem cells. *Mol. Cell. Biol.,* **25**, 9509-9519.

Bhatia, M., Bonnet, D., Wu, D., Murdoch, B., Wrana, J., Gallacher, L., Dick, J.E., (1999) Bone morphogenetic proteins regulate the developmental program of human hematopoietic stem cells. *J. Exp. Med.*, **189**, 1139-1148.

Blum, R.H., Carter, S.K., (1974) Adriamycin. A new anticancer drug with significant clinical activity. *Ann. Intern. Med.,* **80**, 249-259.

Boluyt, M.O., Long, X., Eschenhagen, T., Mende, U., Schmitz, W., Crow, M.T., Lakatta, E.G., (1995) Isoproterenol infusion induces alterations in expression of hypertrophy-associated genes in rat heart. *Am. J. Physiol.*, **269**, H638-H647.

Bone Morphogenetic proteins (BMPs) - www.rndsystems.com

Bostrom, M.P., Lane, J.M., Berberian, W.S., Misri, A.A., Tomin, E., Weiland, A., Doty, S.B., Glaser, D., Rosen, V.M., (1995) Immunolocalization and expression of bone morphogenetic proteins 2 and 4 in facture healing. *J. Orthop. Res.,* **13,** 357-367

Boucek, R.J. Jr, Miracle, A., Anderson, M., Engelman, R., Atkinson, J., Dodd, D.A., (1999) Persistent effects of doxorubicin on cardiac gene expression. *J. Mol. Cell Cardiol.*, **31,** 1435-1446.

Brown, M.A., Zhao, Q., Baker, K.A., Naik, C., Chen, C., Pukac, L., Singh, M., Tsareva, T., Parice, Y., Mahoney, A., Roschke, V., Sanyal, I., Choe, S., (2005) Crystal structure of BMP-9 and functional interactions with pro-region and receptors. *J. Biol. Chem.,* **280**, 25111-25118.

Calderone, A., Takahashi, N., Izzo, N., Thaik, C.M., Colucci, W.S., (1995) Pressure- and volume-induced left ventricular hypertrophies are associated with distinct myocyte phenotypes and differential induction of peptide growth factor mRNAs. *Circulation*, **92**, 2385-2390.

Capetanaki, Y., (1999) The absence of Desmin leads to cardiomyocyte hypertrophy and cardiac dilation with compromised systolic function. *J. Mol. Cell Cardiol.,* **31**, 2063-2076.

Capetanaki, Y., (2002) Desmin cytoskeleton: a potential regulator of muscle mitochondrial behaviour and function. *TCM*, **12**, 339-348.

Chaiswing, L., Cole, M.P., Ittarat, W., Szweda, L.I., St. Clair, D.K., Oberley, T.D., (2005) Manganese superoxide dismutase and inducible nitric oxide synthase modify early oxidative events in acute Adriamycin-induced mitochondrial toxicity. *Mol. Cancer Ther.,* **4**, 1056-1064.

Cheifetz, S., Like, B., Massague, J., (1986) Cellular distribution of type I and type II receptors for transforming growth factor- beta. *J. Biol. Chem.*, **261**, 9972-9978.

Chen, H., Shi, S., Acosta, L., Li, W., Lu, J., Bao, S., Chen, Z., Yang, Z., Schneider, M.D., Chien, K.R., Conway, S.J., Yoder, M.C., Haneline, L.S., Franco, D., Shou, W., (2004) BMP10 is essential for maintaining cardiac growth during murine cardiogenesis. *Development*, **131**, 2219-2231.

Chen, H., Yong, W., Ren, W., Shen, W., He, Y., Cox, K.A., Zhu, W., Li, W., Soonpaa, M., Payne, R.M., Franco, D., Field, L.J., Rosen, V., Wang, Y., Shou, W., (2006) Overexpression of bone morphogenetic protein 10 in myocardium disrupts cardiac postnatal hypertrophic growth. *J. Biol. Chem.,* in press.

Chen, Y.G., Hata, A., Lo, R.S., Wooton, D., (1998) Determinants of specificity in TGF-ß signal transduction. *Genes Dev.,* **12,** 2144-2152.

Chen, Y.G., Liu, F., Massague, J., (1997) Mechanism of TGFbeta receptor inhibition by FKBP12. *EMBO J.*, **16**, 3866-3876.

Chien, D., Zhao, M., Mundy, G.R., (2004) Bone Morphogenetic Proteins. *Growth Factors*, **22**, 233-241.

Childs, A.C., Phaneuf, S.L., Dirks, A.J., Philips T., Leeuwenburgh, C., (2002) Doxorubicin treatment in vivo causes cytochrome c release and cardiomyocyte apoptosis, as well as increased mitochondrial efficiency, superoxide dismutase activity, and Bcl-2:Bax ratio. *Cancer Res.,* **62**, 4592-4598.

Chipuk, J.E., Bhat, M., Hsing, A.Y., Ma, J., Danielpour, D., (2001) Bcl-xL blocks transforming growth factor-ß1-induced apoptosis by inhibiting cytochrome c release and not by directly antagonizing apaf-1 dependent caspase activation in prostate epithelial cells. *J. Biol. Chem.,* **276**, 26614-26621.

Christian, J.L., Nakayama, T., (1999) Can not get no Smadisfaction: Smad proteins as positive and negative regulators of TGF-ß family genes. *BioEssays,* **21**, 382-390.

Cohn, J.N., Ferrari, R., Sharpe, N., (2000) Cardiac remodeling – concepts and clinical implication: a consensus paper from an International Forum on Cardiac Remodeling. *J. Am. Coll. Cardiol.,* **35**, 569-582

Collet, G.D.M., Canfield, A.E., (2005) Angiogenesis and pericytes in the initiation of ectopic calcification. *Circ. Res.,* **96,** 930-938.

Compton, L.A., Potash, D.A., Mundell, N.A., Barnett, J.V., (2006) Transforming growth factor-ß induces loss of epithelial character and smooth muscle cell differentiation in epicardial cells. *Dev. Dyn.,* **235**, 82-93.

Daly, P.A., Sole, M.J., (1990) Myocardial catecholamines and the pathophysiology of heart failure. *Circulation*, **82**(2 Suppl), I35-I43.

Darland, D.C., D`Amore, P.A., (2001) TGFß is required for the formation of capillary-like structures in three-dimensional cocultures of 10T1/2 and endothelial cells. *Angiogenesis*, **4**, 11-20.

De Beer, E.L., Bottone, A.E., Voest, E.E., (2001) Doxorubicin and mechanical performance of cardiac trabeculae after acute and chronic treatment: a review. *Eur. J. Pharmacol.,* **415**, 1-11.

De Bold, A.J., Bruneau, B.G., Kuroski de Bold, M.L., (1996) Mechanical and neuroendocrine regulation of the endocrine heart. *Cardiovasc. Res.,* **31**, 7-18.

Delot, E.C., Bahamonde, M.E., Zhao, M., Lyons, K.M., (2003) BMP signaling is required for septation of the outflow tract of the mammalian heart. *Development,* **130**, 209-220.

DeRuiter, M.C., Poelmann, R.E., Van Munsteren, J.C., Mironov, V., Markwald, R.R., Gittenberger-de Groot, A.C., (1997) Embryonic endothelial cells transdifferentiate into mesenchymal cells expressing smooth muscle actins in vivo and in vitro. *Circ. Res.*, **80**, 444-451.

Dewulf, N., Verschueren, K., Lonnoy, O., Moren, A., Grimsby, S., Vande Spiegle, K., Miyazono, K., Huylebroeck, D., Ten Dijke, P., (1995) Distinct spatial and temporal expression patterns of two type I receptors for bone morphogenetic proteins during mouse embryogenesis. *Endocrinology,* **136**, 2652-2663.

Di Somma, S., Di Benedetto, M.P., Salvatore, G., Agozzino, L., Ferranti, F., Esposito, S., La Dogana, P., Scarano, M.I., Caputo, G., Cotrufo, M., Santo, L.D., de Divitiis, O., (2004) Desmin-free cardiomyocytes and myocardial dysfunction in end stage heart failure. *Eur. J. Heart Fail.*, **6**, 389-398.

Dickson, M.C., Martin, J.S., Cousins, F.M., Kulkarni, A.B., Karlsson, S., Akhurst, R.J., Defective haematopoiesis and vasculogenesis in transforming growth factor-beta 1 knock out mice. *Development,* **121**, 1845-1854.

Dudley, A.T., Lyons, K.M., Robertson, E.J., (1995) A requirement for bone morphogenetic protein-7 during development of the mammalian kidney and eye. *Genes Dev.,* **9**, 2795-2807.

Dudley, A.T., Robertson, E.J., (1997) Overlapping expression domains of bone morphogenetic protein family members potentially account for limited tissue defects in BMP7 deficient embryos. *Dev. Dyn.,* **208**, 349-362.

Euler-Taimor, G., Heger, J., (2006) The complex pattern of SMAD signaling in the cardiovascular system. *Cardiovasc. Res.,* **69**, 15-25.

Finsterer, J., (2004) Mitochondriopathies. *Eur. J. Neurol.,* **11**, 163-186.

Francis, J.M., Heyworth, C.M., Spooncer E., Pierce, A., Dexter, T.M., Whetton, A.D., (2000) Transforming growth factor-ß1 induces apoptosis independently of p53 and selectively reduces expression of Bcl-2 in multipotent hematopoietic cells. *J. Biol. Chem.,* **275**, 39137-39145.

Gard, J.J., Yamada, K., Green, K.G., Eloff, B.C., Rosenbaum, D.S., Wang, X., Robbins, J., Schuessler, R.B., Yamada, K.A., Saffitz, J.E., (2005) Remodeling of gap junctions and slow conduction in a mouse model of desmin-related cardiomyopathy. *Cardiovasc. Res.,* **67**, 539-547.

Gaussin, V., Morley, G.E., Cox, L., Zwijsen, A., Vance, K.M., Emile, L., Tian, Y., Liu, J., Hong, C., Myers, D., Conway, S.J., Depre, C., Mishina, Y., Behringer, R.R., Hanks, M.C., Schneider, M.D., Huylebroeck, D., Fishman, G.I., Burch, J.B., Vatner, S.F., (2005) Alk3/Bmpr1a receptor is required for development of the atrioventricular canal into valves and annulus fibrosus. *Circ. Res.,* **97**, 219-226.

Gaussin, V., Van de Putte, T., Mishina, Y., Hanks, M.C., Zwijsen, A., Huylebroeck, D., Behringer, R.R., Schneider, M.D., (2002) Endocardial cushion and myocardial defects after cardiac myocyte-specific conditional deletion of the bone morphogenetic protein receptor ALK3. *Proc. Natl. Acad. Sci. USA,* **99**, 2878-2883.

Gentry, L.E., Lioubin, M.N., Purchio, A.F., Marquardt, H., (1988) Molecular events in the processing of recombinant type I pre-pro- transforming growth factor beta to the mature polypeptide . *Moll Cell Biol., 8*, 4162-4168.

Gilboa, L., Nohe, A., Geissendorfer, T., Sebald, W., Henis, Y.I., Knaus, P., (2000) Bone morphogenetic protein receptor complexes on the surface of live cells: a new oligomerization mode for serine/threonine kinase receptors. *Mol. Biol. Cell*, **11**, 1023-1035.

Gille, L., Nohl, H., (1997) Analyses of the molecular mechanism of adriamycin-induced cardiotoxicity. *Free Rad. Biol. & Med.*, **23**, 775-782.

Goumans, M.J., Lebrin, F., Valdimarsdottir, G., (2003) Controlling the angiogenic switch: a balance between two distinct TGF-b receptor signaling pathways. *Trends Cardiovasc Med.,* **13**, 301-307.

Goumans, M.J., Mummery, C., (2000) Functional analysis of the TGFß receptor/Smad pathway through gene ablation in mice. *Int. J. Dev. Biol.*, **44**, 253-265.

Goumans, M.J., Valdimarsdottir, G., Itoh, S., Rosendahl, A., Sideras, P., ten Dijke, P., (2002) Balancing the activation of the endothelium via two distinct TGF-ß type I receptors. *EMBO J.,* **21**, 1743-1753.

Green, P.S., Leeuwenburgh, C., (2002) Mitochondrial dysfunction is an early indicator of doxorubicin-induced apoptosis. *Biochem. Biophys. Acta*, **1588**, 94-101.

Halliwell, B., Gutteridge, J.M.C., (1995) Protection against oxidants in biological systems: the superoxide theory of oxygen toxicity. In Free Radicals in Biology and Medicine, Eds.: Halliwell, B. and Gutteridge, J.M.C., Oxford, UK: Clarendon, 86-187.

Hao, J., Wang, B., Jones, S.C., Jassal, D.S., Dixon, I.M., (2000) Interaction between angiotensin II and Smad proteins in fibroblasts in failing heart and in vitro. *Am. J. Physiol. Heart Circ. Physiol.,* **279**, H3020-H3030.

Haq, M.M., Legha, S.S., Choksi, J., Hortobagyi, G.N., Benjamin, R.S., Ewer, M., Ali, M., (1985) Doxorubicin-induced congestive heart failure in adults. *Cancer*, **56**, 1361-1365.

Hassel, S., Schmitt, S., Hartung, A., Roth, M., Nohe, A., Petersen, N., Ehrlich, M., Henis, Y.I., Sebald, W., Knaus, P., (2003) Initiation of Smad-dependent and Smad-independent signaling via distinct BMP-receptor complexes. *J. Bone Joint Surg. Am.,* **85**, 44-51.

Hay, E., Lemonnier, J., Fromigue, O., Marie, P.J., (2001) Bone morphogenetic protein-2 promotes osteoblast apoptosis through a Smad-independent, protein kinase C-dependent signaling pathway. *J. Biol. Chem.,* **276**, 29028-29036.

Heldin, C.H., Miyazono, K., ten Dijke, P., TGF-ß signalling from cell membrane to nucleus through SMAD proteins. *Nature*, **390**, 465-471.

Hellstrom, M., Kalen, M., Lindahl, P., Abramsson, A., Betsholtz, C., (1999) Role of PDGF-B and PDGFR-ß in recruitment of vascular smooth muscle cells and pericytes during embryonic blood vessel formation in the mouse. *Development*, **126**, 3047-3055.

Hirschi, K.K., Rohovsky, S.A., D'Amore, P.A., (1998) PDGF, TGF-β, and heterotypic cell-cell interactions mediate endothelial cell-induced recruitment of 10T1/2 cells and their differentiation to smooth muscle fate. *J. Cell Biol.,* **141**, 805-814.

Homeister, J.W., Satoh, P.S., Lucchesi, B.R., (1992) Effect of complement activation in the isolated hearts. Role of terminal complement components. *Circ. Res.,* **71**, 303-319.

Huang, T.T., Carlson, E.J., Kozy, H.M., Mantha, S., Goodman, S.I., Ursell, P.C., Epstein, C.J., (2001) Genetic modification of prenatal lethality and dilated cardiomyopathy in Mn superoxide dismutase mutant mice. *Free Rad. Biol. & Med.,* **31**, 1101-1110.

Ikeuchi, M., Tsutsui, H., Shiomi, T., Matsusaka, H., Matsushima, S., Wen, J., Kubota, T., Takeshita, A., (2004) Inhibition of TGF-h signaling exacerbates early cardiac dysfunction but prevents late remodeling after infarction. *Cardiovasc. Res.,* **64**, 526-535.

Iwasaki, S., Iguchi, M., Watanabe, K., Hoshino, R., Tsujimoto, M., Kohno, M., (1999) Specific activation of the p38 mitogen-activated protein kinase signaling pathway and induction of neurite outgrowth in PC12 cells by bone morphogenetic protein-2. *J. Biol. Chem.,* **274**, 26503-26510.

Izumi, M., Fujio, Y., Kunisada, K., Negoro, S., Tone, E., Funamoto, M., Osugi, T., Oshima, Y., Nakaoka, Y., Kishimoto, T., Yamauchi-Takihara, K., Hirota, H., (2001) Bone morphogenetic protein – 2 inhibits serum deprivation-induced apoptosis of neonatal cardiac myocytes through activation of the Smad1 pathway. *J. Biol. Chem.,* **276**, 31133-31141.

Jeyaseelan, R., Poizat, C., Baker, R.K., Abdishoo, S., Isterabadi, L.B., Lyons, G.E., Kedes, L., (2002) A novel cardiac-restricted target for doxorubicin. CARP, a nuclear modulator of gene expression in cardiac progenitor cells and cardiomyocytes. *J. Biol. Chem.*, **272**, 22800-22808.

Jeong, D., Cha, H., Kim, E., Kang, M., Yang, D.K., Kim, J.M., Yoon, P.O., Oh, J.G., Bernecker, O.Y., Sakata, S., Thu, L.T., Cui, L., Lee, Y-H., Kim, D.H., Woo, S-H., Liao, R., Hajjar, R.J., Park, W.J., (2006) PICOT inhibits cardiac hypertrophy and enhances ventricular function and cardiomyocyte contractility. *Circ. Res.,* in press.

Jiao, K., Kulessa, H., Tompkins, K., Zhou, Y., Batts, L., Baldwin, H.S., Hogan, B.L.M., (2003) An essential role of BMP4 in the atrioventricular septation of the mouse heart. *Gen. Dev.*, **17**, 2362-2367.

Kale, S., Hanai, J., Chan, B., Karihaloo, A., Grotendorst, G., Cantley, L., Sukhatme, V.P., (2005) Microarray analysis of in vitro pericyte differentiation reveals an angiogenic program of gene expression. *FASEB J.,* **19**, 270-271.

Katagiri, T., Yamaguchi, A., Komaki, M., Abe, E., Takahashi, N., Ikeda, T., Rosen, V., Wozney, J.M., Fujisawa-Sehara, A., Suda, T., (1994) Bone morphogenetic protein-2 converts the differentiation pathway of C2C12 myoblasts into the osteoblast lineage. J. *Cell Biol.*, **127**, 1755-1766.

Kaprielian, R.R., Severs, N.J., (2000) Dystrophin and the cardiomyocyte membrane cytoskeleton in the healthy and failing heart. *Heart Fail. Rev.,* **5**, 221-238.

Katagiri, T., Yamaguchi, A., Komaki, M., Abe, E., Takahashi, N., Ikeda, T., Rosen V., Wozney, J.M., Fujisawa-Sehara, A., Suda, T. (1994) Bone Morphogenetic Protein-2 converts the differentiation pathway of C2C12 myoblasts into osteoblast lineage. *J. Cell Biol.,* **127**, 1755-1766.

Kawada, T., Masui, F., Tezuka, A., Ebisawa, T., Kumagai, H., Nakazawa, M., Toyo-Oka, T., (2005) A novel scheme of dystrophin disruption for the progression of advanced heart failure. *Biochim. Biophys. Acta.,* **1751**, 73-81.

Kim, R.Y., Robertson, E.J., Solloway, M.J., (2001) Bmp6 and Bmp7 are required for cushion formation and septation in the developing mouse heart. *Dev. Biol.*, **235**, 449-466.

King, L.A., Possee, R.D., (1992) The Baculovirus Expression System. Chapman & Hall, London, UK.

Kingsley, D.M., Bland, A.E., Grubber, J.M., Marker, P.C., Russell, L.B., Copeland, N.G., Jenkins, N.A., (1992) The mouse short ear skeletal morphogenesis locus is associated with defects in a bone morphogenetic member of the TGF beta superfamily. *Cell*, **71**, 399-410.

Knaus, P., Sebald, W., (2001) Cooperativity of binding epitopes and receptor chains in the BMP/TGFbeta superfamily. *J. Biol. Chem.,* **382**, 1189-1195.

Kong, Y., Shelton, J.M., Rothermel, B., Li, X., Richardson, J.A., Bassel-Duby, R., Williams, R.S., (2001) Cardiac-specific LIM protein FHL2 modifies the hypertrophic response to ß-adrenergic stimulation. *Circulation*, **103**, 2731-2738.

Kostin, S., (2005) Pathways of myocyte death: implications for development of clinical laboratory biomarkers. *Adv. Clin. Chem.,* **40**, 37-98.

Kostin, S., Hein, S., Bauer, E.P., Schaper, J., (1999) Spatiotemporal development and distribution of intercellular junctions in adult rat cardiomyocytes in culture. *Circ. Res.,* **85**, 154-167.

Kretzschmar, M., Massague, J., (1998) SMADs: mediators and regulators of TGF-beta signaling. *Curr. Opin. Genet. Dev.,* **8**, 103-111.

Kurzen, H., Manns, S., Dandekar, G., Schmidt, T., Pratzel, S., Kraling, B.M., (2002) Tightening of endothelial cell contacts: a physiologic response to cocultures with smooth-muscle-like 10T1/2 cells. *J. Invest. Dermat.,* **119**, 143-153.

Lebovitz, R.M., Zhang, H., Vogel, H., Cartwright Jr., J., Dionne, L., Lu, N., Huang, S., Matzuk, M.M., (1996) Neurodegeneration, myocardial injury and perinatal death in mitochondrial superoxidase dismutase-deficient mice. *Proc. Natl. Acad. Sci. USA*, **93**, 9782-9787.

Lebrin, F., Deckers,M., Bertolino, P., Ten Dijke, P., (2005) TGF-beta receptor function in the endothelium. *Cardiovasc Res.,* **65**, 599-608.

Lee, D.H., Park, B.J., Lee, M-S., Lee, J.W., Kim, J.K., Yang, H.C., Park, J.C., (2006) Chemotactic migration of human mesenchymal stem cells and MC3T3-E1 osteoblast-like cells induced by COS-7 cell line expressing rhBMP-7. *Tissue Eng.,* **12**, 1577-1586.

Lewis, W., Gonzalez, B., (1986) Anthracycline effects on actin and actin-containing thin filaments in cultured neonatal rat myocardial cells. *Lab. Invest.,* **54**, 416-423.

Li, D., Tapscoft, T., Gonzalez, O., Burch, P.E., Quinones, M.A., Zoghbi, W.A., Hill, R., Bachinski, L.L., Mann, D.L., Roberts, R., (1999) Desmin mutation responsible for idiopathic dilated cardiomyopathy. *Circulation,* **100**, 461-464.

Li, D.Y., Sorensen, L.K., Brooke, B.S., Urness, L.D., Davis, E.C., Taylor, D.G., Boak, B.B., Wendel, D.P., (1999) Defective angiogenesis in mice lacking endoglin. *Science,* **284**, 1534-1537.

Li, J.J., Oberley, L.W., St. Clair, D.K., Ridnour, L.A., Oberley, T.D., (1995) Phenotypic changes induced in human breast cancer cells by overexpression of manganese-containing superoxide dismutase. *Oncogene*, **10**, 1989-2000.

Li, Y., Huang, T.T., Carlson, E.J., Melov, S., Ursell, P.C., Olson, J.L., Noble, L.J., Yoshimura, M.P., Berger, C., Chan, P.H., Wallace, D.C., Epstein, C.J., (1995) Dilated cardiomyopathy and neonatal lethality in mutant mice lacking manganese superoxide dismutase. *Nature Genet.*, **11**, 376-381.

Li, Z., Colucci-Guyon, E., Pincon-Raymond, M., Mericskay, M., Pournin, S., Paulin, D., Babinet, C., (1996) Cardiovascular lesions and skeletal myopathy in mice lacking desmin. *Dev. Biol.,* **175**, 362-366.

Lin, H.Y., Wang, X.F., Ng-Eaton, Weinberg, R.A., Lodish, H.F., (1992) Expression clonning of the TGF-beta type II receptor, a functional transmembrane serine/threonine kinase. *Cell*, **68**, 775-785.

Lind, M., Eriksen, E.F., Bunger, C., (1996) Bone morphogenetic protein-2 but not bone morphogenetic protein-4 and -6 stimulates chemotactic migration of human osteoblasts, human marrow osteoblasts and U2-OS cells. *Bone*, **18**, 53-57

Liu, F., Ventura, F., Doody, J., Massagué, J., (1995) Human type II receptor for bone morphogenic proteins (BMPs): extension of the two kinase receptor model to the BMPs. *Mol. Cell. Biol.,* **15**, 3479-3486.

Loufrani, L., Matrougui, K., Li, Z., Levy, B.I., Lacolley, P., Paulin, D., Henrion, D., (2002) Selective microvascular dysfunction in mice lacking the gene encoding for desmin. *FASEB J.,* **16**, 117-119.

Lyons, K.M., Pelton, R.W., Hogan, B.L., (1989) Patterns of expression of murine Vgr-1 and BMP-2a RNA suggest that transforming growth factor-beta-like genes coordinately regulate aspects of embryonic development. *Genes Dev.*, **3**, 1657-1668.

Lyons, K.M., Pelton, R.W., Hogan, B.L., (1990) Organogenesis and pattern formation in the mouse: RNA distribution patterns suggest a role for bone morphogenetic protein-2A (BMP-2A). *Development,* **109**, 833-844.

Ma, L., Lu, M.F., Schwartz, R.J., Martin, J.F., (2005) Bmp2 is essential for cardiac cushion epithelial-mesenchymal transition and myocardial pattering. *Development,* **132**, 5601-5611.

Macías-Silva, M., Hoodless, P.A., Tang, S.J., Buchwald, M., Wrana, J.L., (1998) Specific activation of smad1 signaling pathways by the BMP7 type I receptor, ALK2. *J. Biol. Chem.,* **273**, 25628-25636.

Massague, J., Wotton, D., (2000) Transcriptional control by the TGFß/Smad signalling system. *EMBO J.,* **19**, 1745-1754.

Masuyama, N., Hanafusa, H., Kusakabe, M., Shibuya, H., Nishida, E., (1999) Identification of two Smad4 proteins in Xenopus. Theit common and distinct properties. *J. Biol. Chem.*, **274**, 12163-12170.

Matsubara, H., Yamamoto, J., Hirata, Y., Mori, Y., Oikawa, S., Inada, M., (1990) Changes in atrial natriuretic peptide and its messenger RNA with development and regression of cardiac hypertrophy in renovascular hypertensive rats. *Circ. Res.*, **66**, 176-184.

Matsuura, K., Nagai, T., Nishigaki, N., Oyama, T., Nishi, J., Wada, H., Sano, M., Toko, H., Akazawa, H., Sato, T., Nakaya, H., Kasanuki, H., Komuro, I., (2004) Adult cardiac Sca-1-positive cells differentiate into beating cardiomyocytes. *J. Biol. Chem.*, **279**, 11384-11391.

Matthews, D.J., Goodman, L.J., Gorman, C.M., Wells, J.A., (1994) A survey of furin substrate specificity using substrate phage display. *Protein Sci.,* 3, 1197-1205.
Matthews, L.S., Vale, W.W., (1991) Expression cloning of an activin receptor, a predicted transmembrane serine kinase. *Cell*, **65**, 973-982.

Matthews, L.S., Vale, W.W., Kintner, C.R., (1992) Cloning of a second type of activin receptor and functional characterization in Xenopus embryos. *Science*, **255**, 1702-1705.

Mavroidis, M., Capetanaki, Y., (2002) Extensive induction of important mediators of fibrosis and dystrophic calcification in desmin-deficient cardiomyopathy. *Am. J. Pathol.*, **160**, 943-952.

Mazerbourg, S., Sangkuhl, K., Luo, C.W., Sudo, S., Klein, C., Hsueh, A.J., (2005) Identification of receptors and signaling pathways for orphan bone morphogenetic protein/growth differentiation factor ligands based on genomic analyses. *J. Biol. Chem.*, **280**, 32122-32132.

McKenna, W.J., (1996) Hypertrophic cardiomyopathy. In: Diseases of the heart., Eds.: Julian, D.G., Camm, A.J., Fox, K.M., Hall, R.J.C., Poole-Wilson, P.A., W.B. Saunders Company Ltd., London, UK.

Mehra, A., Wrana, J.L., (2002) TGF-beta and the Smad signal transduction pathway. Biochem. *Cell Biol.*, **80**, 605-622

Mellman, I., (1996) Endocytosis and molecular sorting. *Annu. Rev. Cell Dev. Biol.,* **12**, 575-625.

Michael, L.H., Behringer, B.R., Garry, D.J., Entmann, M.L., Schneider, M.D., (2003) Cardiac progenitor cells from adult myocardium: Homing, differentiation, and fusion after infarction. *Proc. Natl. Acad. Sci. USA,* **100**, 12313-12318.

Milner, D.J., Taffet, G.E., Wang, X., Pham, T., Tamura, T., Hartley, C., Gerdes, A.M., Capetanaki, Y., (1999) The absence of desmin leads to cardiomyocyte hypertrophy and cardiac dilation with compromised systolic function. *J. Mol. Cell Cardiol.,* **31**, 2063-2076.

Milner, D.J., Weitzer, G., Tran, D., Bradley, A., Capetanaki, Y. (1996) Disruption of muscle architecture and myocardial degeneration in mice lacking desmin. *J. Cell Biol.,* **134**, 1255-1270.

Miyazono, K., Maeda, S., Imamura, T., (2005) BMP receptor signaling: transcriptional targets, regulation of signals, and signalling cross-talk. *Cyt. & Growth Factors Rev.,* **16**, 251-263.

Miyazono, K., ten Dijke, P., Heldin, C.H., (2000) TGF-ß signalling by Smad proteins. *Adv. Immunol.*, **75**, 115-157.

Monzen, K., Hiroi, Y., Kudoh, S., Akazawa, H., Oka, T., Takimoto, E., Hayashi, D., Hosoda, T., Kawabata, M., Miyazono, K., Ishii, S., Yazaki, Y., Nagai, R., Komuro, I., (2001) Smads, TAK1, and their common target ATF-2 play a critical role in cardiomyocyte differentiation. *J. Cell Biol.,* **153**, 687-698.

Monzen, K., Shiojima, I., Hiroi, Y., Kudoh, S., Oka, T., Takimoto, E., Hayashi, D., Hosoda, T., Habara-Ohkubo, A., Nakaoka, T., Fujita, T., Yazaki, Y., Komuro, I., (1999) Bone morphogenetic proteins induce cardiomyocyte differentiation through the mitogen-activated protein kinase kinase kinase TAK1 and cardiac transcription factors Csx/Nkx-2.5 and GATA-4. *Mol Cell Biol.,* **19**, 7096-7105.

Morisco, C., Zebrowski, D.C., Vatner, D.E., Vatner, S.F., Sadoshima, J., (2001) Beta-adrenergic cardiac hypertrophy is mediated primarily by the beta(1)-subtype in the rat heart. *J. Mol. Cell Cardiol.,* **33**, 561-573.

Motomura, S., Deighton, N.M., Zerkowski, H.R., Doetsch, N., Michel, M.C., Brodde, O.E., (1990) Chronic beta 1-adrenoceptor antagonist treatment sensitizes beta 2-adrenoceptors, but desensitizes M2-muscarinic receptors in the human right atrium. *Br. J. Pharmacol.*, **101**, 363-369.

Muller, F.U., Boknik, P., Horst, A., Knapp, J., Linck, B., Schmitz, W., Vahlensieck, U., Walter, A., (1995) In vivo isoproterenol treatment leads to downregulation of the mRNA encoding the cAMP response element binding protein in the rat heart. *Biochem. Biophys. Res. Commun.,* **215**,1043-1049.

Muller, W., Scharffetter-Kochanek, K., (2005) Heterozygous deficiency of manganese superoxide dismutase results in severe lipid peroxidation and spontaneous apoptosis in murine myocardium in vivo. *Free Radic. Biol. Med.*, **38**, 1458-1470.

Neuhaus, H., Rosen, V., Thies, R.S., (1999) Heart specific expression of mouse BMP-10 a novel member of the TGF-ß superfamily. *Mech. Dev.,* **80**, 181-184.

Nishishita, T., Lin, P.C., (2004) Angiopoietin 1, PDGF-B, TGF-ß gene regulation in endothelial cell and smooth muscle cell interaction. *J. Cell. Biochem.*, **91,** 584-593.

Nogae, C., Makino, N., Hata, T., Nogae, I., Takahashi, S., Suzuki, K., Taniguchi, N., Yanaga, T., (1995) Interleukin 1α-induced expression of manganous superoxide dismutase reduces myocardial reperfusion injury in the rat. *J. Mol. Cell Cardiol.*, **27**, 2091-2099.

O´Reily, D.R., Miller, L.K., Luckov, V.A., (1992) Baculovirus expression vectors. A laboratory manual. W.H. Freeman & Company, New York, USA.

Oh, H., Bradfute, S.B., Gallardo, T., Nakamura, T., Gaussin, V., Mishina, Y., Pocius, J., Oh, S.P., Seki, T., Goss, K.A., Imamura, T., Yi, Y., Danahoe, P., Li, L., Miyazono, K., ten Dijke, P., Kim, S., Li, E., (2000) Activin receptor-like kinase 1 modulates transforming growth factor-ß1 signaling in the regulation of angiogenesis. *Proc. Natl. Acad. Sci. USA*, **97**, 2626-2631.

Okubo, Y., Bessho, K., Fajimura, K., Kusomoto, K., Ogawa, Y., Iizuka, T., (2002) Expression of bone morphogenetic protein in the course of osteoinduciton by recombinant human bone morphogenetic protein-2. *Clin. Oral. Implants Res.*, **13**, 80-85

Olive, M., Goldfarb, L., Moreno, D., Laforet, E., Dagvadorj, A., Sambuughin, N., Martinez-Matos, J.A., Martinez, F., Alio, J., Farrero, E., Vicart, P., Ferrer, I., (2004) Desmin-related myopathy: clinical, electrophysiological, radiological, neuropathological and genetic studies. *J. Neurol. Sci.,* **219,** 125-137.

Oshima, M., Oshima, H., Taketo, M.M., (1996) TGF-beta receptor type II deficiency results in defects of yolk sac hematopoiesis and vasculogenesis. *Dev. Biol.*, **179**, 297-302.

Panchenko, M.P., Williams, M.C., Brody, J.S., Yu, Q., (1996) Type I receptor serine-threonine kinase preferentially expressed in pulmonary blood vessels. *Am. J. Physiol.,* **270**, L547-L558.

Pashmforoush, M., Lu, J.T., Chen, H., Amand, T.S., Kondo, R., Pradervand, S., Evans, S.M., Clark, B., Feramisco, J.R., Giles, W., Ho, S.Y., Benson, D.W., Silberbach, M., Shou, W., Chien, K.R., (2004) Nkx2-5 pathways and congenital heart disease; loss of ventricular myocyte lineage specification leads to progressive cardiomyopathy and complete heart block. *Cell,* **117**, 373-386.

Price, M.G., (1984) Molecular analysis of intermediate filament cytoskeleton--a putative load-bearing structure. *Am. J. Physiol.,* **246**(4 Pt 2), H566-H572.

Raida, M., Clement, J.H., Leek, R.D., Ameri, K., Bicknell, R., Niederwiesser, D., Harris, A.L., (2005) Bone morphogenetic protein 2 (BMP-2) and induction of tumor angiogenesis. *J. Cancer Res. Clin. Oncol.,* **131**, 741-750.

Ramsdell, A.F., Yost, H.J., (1999) Cardiac looping and the vertebrate left-right axis: antagonism of left-sided Vg1 activity by a right-sided ALK2-dependent BMP pathway. *Development,* **126**, 5195-5205.

Reddi, A.H., (1997) Bone morphogenetic proteins: an unconventional approach to isolation of first mammalian morphogens. *Cytokine Growth Factor Rev*., **8**, 11-20

Rodriguez, M., Schaper, J., (2005) Apoptosis: measurement and technical issues. *J. Mol. Cell. Cardiol.,* 38, 15-20.

Roelen, B.A., van Rooijen, M.A., Mummery, C.L., (1997) Expression of ALK-1, a type 1 serine/threonine kinase receptor, coincides with sites of vasculogenesis and angiogenesis in early mouse development. *Dev. Dyn.,* **209**, 418-430.

Rosenzweig, A., Seidman, C.E., (1991) Atrial natriuretic factor and related peptide hormones. *Ann. Rev. Biochem.*, **60**, 229-255.

Russell, L.K., Finck, B.N., Kelly, D.P., (2005) Mouse models of mitochondrial dysfunction and heart failure. *J. Mo. Cell Cardiol.,* **38**, 81-91.

Sambrook, J., Fritsch, E.F., Maniatis, T., (1999) Molecular cloning: A laboratory manual. Cold Spring Harbor laboratory Press, Cold Spring Harbor, New York.

Sanbe, A., Osinska, H., Saffitz, J.E., Glabe, C.G., Kayed, R., Maloyan, A., Robbins, J., (2004) Desmin-related cardiomyopathy in transgenic mice: a cardiac amyloidosis. *Proc. Natl. Acad. Sci. USA*, **101**, 10132-10136.

Sankar, S., Mahooti-Brooks, N., Bensen, L., McCarthy, T.L., Centrella, M., Madri, J.A., (1996) Modulation of transforming growth factor beta receptor levels on microvascular endothelial cells during in vitro angiogenesis. *J. Clin. Invest.,* **97**, 1436-1446.

Sato, M., Sasaki, M., Hojo, H., (1995) Antioxidative roles of metallothionein and manganese superoxide dismutase induced by tumor necrosis factor- α and interleukin-6. *Arch. Biochem. Biophys.,* **316**, 738-744.

Seki, T., Hong, K.H., Oh, S.P., (2006) Nonoverlapping expression patterns of ALK1 and ALK5 reveal distinct roles of each receptor in vascular development. *Lab Invest.,* **86**, 116-129.

Seki, T., Yun, J., Oh, S.P., (2003) Arterial endothelium-specific activin receptor-like kinase 1 expression suggests its role in arterialization and vascular remodeling. *Circ.Res*., **93**, 682-689.

Shapiro, L.M., Sugden, P.H., (1996) Left ventricular hypertrophy. In: Diseases of the heart., Eds.: Julian, D.G., Camm, A.J., Fox, K.M., Hall, R.J.C., Poole-Wilson, P.A., W.B. Saunders Company Ltd., London, UK.

Shizukuda, Y., Buttrick, P.M., Geenen, D.L., Borczuk, A.C., Kitsis, R.N., Sonnenblick, E.H., (1998) Beta-adrenergic stimulation causes cardiocyte apoptosis: influence of tachycardia and hypertrophy. *Am. J. Physiol.,* **275**(3 Pt 2), H961-H968.

Shou, W., Aghdasi, B., Armstrong, D.L., Guo, Q., Bao, S., Charng, M.J., Mathews, L.M., Schneider, M.D., Hamilton, S.L., Matzuk, M.M., (1998) Cardiac defects and altered ryanodine receptor function in mice lacking FKBP12. *Nature*, **391**, 489-492.

Singal, P.K., Deally, C.M., Weinberg, L.E., (1987) Subcellular effects of adriamycin in the heart: a concise review. *J. Mol. Cell Cardiol.,* **19**, 817-828.

Solloway, M.J., Dudley, A.T., Bikoff, E.K., Lyons, K.M., Hogan, B.L., Robertson, E.J., (1998) Mice lacking Bmp6 function. *Dev. Genet*., **22**, 321-339.

Solloway, M.J., Robertson, E.J., (1999) Early embryonic lethality in Bmp5;Bmp7 double mutant mice suggests functional redundancy within the 60A subgroup. *Development,* **126**, 1753-1768.

Stanton, H.C., Brenner, G., Mayfield, E.D., Jr., (1969) Studies on isoproterenol-induced cardiomegaly in rats. *Am. Heart J.,* **77**, 72-80.

Stottmann, R.W., Choi, M., Mishina, Y., Meyers, E.N., Klingensmith, J., (2004) BMP receptor IA is required in mammalian neural crest cells for development of the cardiac outflow tract and ventricular myocardium. *Development,* **131**, 2205-2218.

Strassburger, M., Bloch, W., Sulyok, S., Schuller, J., Keist, A.F., Schmidt, A., Wenk, J., Peters, T., Wlaschek, M., Lenart, J., Krieg, T., Hafner, M., Lenart, J., Kumin, A., Werner, S. (2005) Heterozygous deficiency of manganese superoxide dismutase results in severe lipid peroxidation and spontaneous apoptosis in murine myocardium in vivo. Free Radic Biol Med., **38**(11),1458-70.

Sugi, Y., Yamamura, H., Okagawa, H., Markwald, R.R., (2004) Bone morphogenetic protein-2 can mediate myocardial regulation of atrioventricular cushion mesenchymal cell formation in mice. *Dev. Biol.,* **269**, 505-518.

Sun, P.D., Davies, D.R., (1995) The cystine-knot growth-factor superfamily. *Annu. Rev. Biophys. Biomol. Struct.,* **24**, 269-291.

Takahashi, T., Kalka, C., Masuda, H., Chen, D., Silver, M., Kearney, M., Magner, M., Isner, J.M., Asahara, T., (1999) Ishemia- and cytokine-induced mobilization of bone marrow-derived endothelial progenitor cells for neovascularization. *Nature Med.,* **5**, 434-438.

ten Dijke, P., Ichijo, H., Franzen, P., Schulz, P., Saras, J., Toyoshima, H., Heldin, C.H., Miyazono, K., (1993) Activin receptor-like kinases: a novel subclass of cell-surface receptors with predicted serine/threonine kinase activity. *Oncogene*, **8**, 2879-2887.

ten Dijke, P., Yamashita, H., Sampas, T.K., Reddi, A.H., Estevez, M., Riddle, D.L., Ichijo, H., Heldin, C.H., Miyazono, K., (1994) Identification of type I receptors for osteogenic protein-1 and bone morphogenetic protein-4. *J. Biol. Chem.,* **269**, 16985-16988.

ten Dijke., Miyazono, K., Heldin, C.H., (2000) Signalling inputs converge on nuclear effectors in TGFß signalling. *Trends Biochem. Sci.,* **25**, 64-70.

Thornell, L., Carlsson, L., Li, Z., Mericskay, M., Paulin, D., (1997) Null mutation in the desmin gene gives rise to a cardiomyopathy. *J. Mol. Cell Cardiol.,* **29**, 2107-2124.

Toyo-Oka, T., Kawada, T., Nakata, J., Xie, H., Urabe, M., Masui, F., Ebisawa, T., Tezuka, A., Iwasawa, K., Nakajima, T., Uehara, Y., Kumagai, H., Kostin, S., Schaper, J., Nakazawa, M., Ozawa, K., (2004) Translocation and cleavage of myocardial dystrophin as a common pathway to advanced heart failure: a scheme for the progression of cardiac dysfunction. *Proc. Natl. Acad. Sci. USA*, **101**, 7381-7385.

Unverferth, D.V., Magorien, R.D., Leier, C.V., Balcerzak, S.P., (1982) Doxorubicin cardiotoxicity. *Cancer Treat. Rev.,* **9**, 149-164.

Urist, M.R., (1965) Bone formation by autoinduction. *Science*, **150**, 893-899.

Van Remmen, H., Williams, M.D., Guo, Z., Estlack, L., Yang, H., Carlson, E.J., Epstein, C.J., Huang, T.T., Richardson, A., (2001) Knockout mice heterozygous for Sod2 show alterations in cardiac mitochondrial function and apoptosis. *Am. J. Physiol. Heart Circ. Physiol.,* **281**, H1422-H1432.

Vikstrom, K.L., Bohlmeyer, T., Factor, S.M., Leinwand, L.A., (1998) Hypertrophy, pathology, and molecular markers of cardiac pathogenesis. *Circ. Res.,* **82**, 773-778.

Wagner, S., Helisch, A., Ziegelhoeffer, T., Bachmann, G., Shaper, W., (2004) Magnetic resonance angiography of collateral vessels in a murine femoral artery ligation model. *NMR Biomed.*, **17**, 21-27.

Wallace, K.B., (2003) Doxorubicin-induced cardiac mitochondrionopathy. *Pharmacol. Toxicol.,* **93**, 105-115.

Wang, B., Hao, J., Jones, S.C., Yee, M.S., Roth, J.C., Dixon, I.M., (2002) Decreased Smad7 expression contributes to cardiac fibrosis in the infracted rat heart. *Am. J. Physiol. Heart Circ. Physiol.,* **282**, H1685-H1696.

Wang, J., Sridurongrit, S., Dudas, M., Thomas, P., Nagy, A., Schneider, M.D., Epstein, J.A., Kaartinen, V., (2005) Atrioventricular cushion transformation is mediated by ALK2 in the developing mouse heart. *Dev. Biol.,* **286**, 299-310.

Weisleder, N., Soumaka, E., Abbasi, S., Taegtmeyer, H., Capetanaki, Y., (2004) Cardiomyocyte-specific desmin rescue of desmin null cardiomyopathy excludes vascular involvement. *J. Mol. Cell Cardiol.*, **36**, 121-128.

Yang, L., Cai, C.L., Lin, L., Qyang, Y., Chung, C., Monteiro, R.M., Mummery, C.L., Fishman, G,I., Cogen, A., Evans, S., (2006) Isl1Cre reveals a common Bmp pathway in heart and limb development. *Development*, **133**, 1575-1585.

Yokouchi, Y., Sakiyama, J., Kameda, T., Iba, H., Suzuki, A., Ueno, N., Kuroiwa, A., (1996) BMP-2/-4 mediate programmed cell death in chicken limb buds. *Development*, **122**, 3725-3734.

Zhang, H., Bradley, A., (1996) Mice deficient for BMP2 are nonviable and have defects in amnion/chorion and cardiac development. *Development*, **122**, 2977-2986.

Zhao, Z., Rivkees, S.A., (2000) Programmed cell death in the developing heart: regulation by BMP4 and FGF2. *Dev. Dyn.,* **217**, 388-400.

Zhou, S., Starkov, A., Froberg, M.K., Leino, R.L., Wallace, K.B., (2001) Cumulative and irreversible cardiac mitochondrial dysfunction induced by doxorubicin. *Cancer Res*., **61**, 771-777.

Zhoung, W., Oberley, L.W., Oberley, T.D., St. Clair, D.K., (1997) Suppression of the malignant phenotype of human glioma cells by overexpression of manganese superoxide dismutase. *Oncogene*, **14**, 481-490.

Zou, Y., Yao, A., Zhu, W., Kudoh, S., Hiroi, Y., Shimoyama, M., Uozumi, H., Kohmoto, O., Takahashi, T., Shibasaki, F., Nagai, R., Yazaki, Y., Komuro, I., (2001) Isoproterenol activates extracellular signal-regulated protein kinases in cardiomyocytes through calcineurin. *Circulation*, **104**, 102-108.